AN ABSTRACT OF THE THESIS OF

Christopher W. Sinton for the degree of Doctor of Philosophy in Oceanography presented on May 17, 1996

Title: A Tale of Two Large Igneous Provinces: Geochronological and Geochemical Studies of the North Atlantic Volcanic Province and the Caribbean Oceanic Plateau

Abstract approved: Redacted for privacy

Robert A. Duncan

A significant portion of lavas associated with the North Atlantic Volcanic Province (NAVP) lie submerged along the continental margins of the North Atlantic. ^{40}Ar-^{39}Ar radiometric dating of continentally-contaminated lavas from the southeast Greenland margin drilled during ODP Leg 152 shows that magmatism began in this area by at least 62 Ma. Stratigraphically younger, MORB-like lavas are constrained to be 56-53 Ma based on magnetic anomaly identification. A late-stage sill from the most seaward site is bounded by early Eocene sediments and has an age of 52 Ma. The age of initial magmatism is similar to such widely distributed locations regions as West Greenland and the British province. Compiled ages from the NAVP indicate that the bulk of the lavas erupted during two magmatic episodes: the first occurred prior to 60 Ma, probably associated with the arrival of the Iceland mantle plume and the second phase began at ~57 Ma with voluminous basaltic eruptions centralized along the eventual line of continental separation. Magmatism at this stage was associated with continental breakup and massive decompression melting of the hot upper mantle.

The thick oceanic crust of the Caribbean plate is the remnant of an oceanic plateau wedged between the North and South American plates. Uplifted margins of the plateau allow examination of its volcanic stratigraphy, structure, and composition. ^{40}Ar-^{39}Ar ages and compositional data from an exposure of the plateau in the Nicoya Peninsula of Costa Rica indicate that all of the igneous rocks belong to a single suite that began erupting at ~90 Ma. ^{40}Ar-^{39}Ar ages from other exposures at Curaçao, Haiti, Gorgona Island, and Western Colombia indicate that the bulk of the plateau formed at 91-88 Ma with a second widespread but probably smaller volume magmatic event at 76 Ma.

The coincidence of catastrophic volcanism and global ocean anoxia and the extinction of marine organisms at about 91 Ma (Cenomanian-Turonian boundary) suggests a genetic relationship. It is possible that massive, short-lived pulses of submarine magmatism produced hydrothermal plumes that may have consumed the dissolved oxygen in seawater and contributed to anoxia.

A Tale of Two Large Igneous Provinces: Geochronological and Geochemical Studies of the North Atlantic Volcanic Province and the Caribbean Oceanic Plateau

by

Christopher W. Sinton

A THESIS
submitted to
Oregon State University

in partial fulfillment of
the requirements for the
degree of

Doctor of Philosophy

Presented May 17, 1996
Commencement June 1997

Doctor of Philosophy thesis of Christopher W. Sinton presented on May 17, 1996

APPROVED:

Redacted for privacy

Major Professor, representing Oceanography

Redacted for privacy

Dean of College of Oceanic and Atmospheric Sciences

Redacted for privacy

Dean of Graduate School

I understand that my thesis will become part of the permanent collection of Oregon State University libraries. My signature below authorizes release of my thesis to any reader upon request.

Redacted for privacy

Christopher W. Sinton, Author

Acknowledgements

I would like to thank Bob Duncan for his steady support and encouragement throughout my research. I also would like to acknowledge Lew Hogan, Dave Christie, Dave Graham, Anita Grunder, Michael Storey, Marty Fisk, and Roger Nielsen for teaching me about rocks and machines. Fellow students who bought me beer and laughed at my jokes are: Randy Keller, Doug Pyle, Lance Forsythe, Chris Guay, Karen Harpp, Bill Gallahan, Kipp Shearman..... I think a few others chuckled. I thank Matt Gorring for spending a great deal of time to get good isotopic data. Thanks to Sue Pullen for always helping when a problem reared its ugly head. This research was supported by NSF and USSAC.

Most of all, thanks to my family, who make it all worthwhile. In particular, the incredible Diana, the fabulous Emily, and all future wee ones.

Contribution of Authors

Dr. Robert Duncan was involved in the design and execution of the research reported herein and is a coauthor on two of the manuscripts.

Table of Contents

Table of Contents, Continued

List of Figures

List of Figures, Continued

List of Tables

A Tale of Two Large Igneous Provinces: Geochronological and Geochemical Studies of the North Atlantic Volcanic Province and the Caribbean Oceanic Plateau

Chapter I: Introduction

The Earth is a dynamic planet, a thermally driven engine that is capable of moving massive lithospheric plates at phenomenally slow speeds or of blowing off the side of a mountain in seconds. The movement of the Earth produces a constantly changing surface (and interior) of which our current view represents the accumulation of 4.6 billion years of motion. It is our challenge as geologists to try to recreate not only the processes involved in shaping the earth, but when and at what rate they occurred. In a sense we are detectives with a still warm body in front of us. We have a variety of tools to make observations which we then synthesize to solve the mystery or, in reality, to constrain it. I say this because in the process of creating new surface features, there is a resulting destruction of other features and, consequently, as we delve farther into the past, there are fewer surviving clues. In the end, we often state that observations are "consistent" with a given hypothesis or model and rarely reach unequivocal conclusions. In this thesis, I use geochronological and geochemical methods to try to recreate the formation history of two large igneous provinces (LIPs): the North Atlantic Volcanic Province (NAVP) and the Caribbean oceanic plateau. The fundamental questions I address include: When did magmatism occur? How long did it last? Are the erupted rocks similar in composition or were they derived by different processes or from different sources in the mantle? Did magmatism have any affect on the biosphere? While I cannot absolutely answer all these questions, my research was designed to at least partially illuminate them.

The thermal energy in the earth is derived in small part from residual heat that was produced during the initial accretion of the earth, but mainly from the decay of radioactive elements in the mantle and crust. The heat within the earth diffuses from the hot interior to the cool surface by conduction and convection (and possibly radiation if parts of the mantle are translucent). Conduction is the only way heat transfers through opaque solids, but it is a relatively slow process. Heat transfer via convection is much faster than conduction and is accomplished by the upward movement of thermally or chemically buoyant mantle material. Convective transfer of heat also occurs when the mantle partially melts and low viscosity magmas ascend quickly to the surface and are erupted. Magmas that intrude the crust or lithosphere help transfer heat to the earth's surface either by conduction or by

hydrothermal convection of water. Thus igneous eruptions and intrusions are the most effective way for the earth to release heat. The existence of LIPs (continental flood basalts and their submarine equivalents, oceanic plateaus) indicate that at discrete, short-lived intervals, large volumes of heat and energy were released at rates far above what we would consider steady state. Such catastrophic volcanism must have entailed great disturbances in the mantle and may have resulted in massive perturbations within the biosphere. For these reasons, the study of LIPs is important.

Continental flood basalt provinces are the best studied type of LIP as they are subaerially exposed and accessible, and often deeply dissected by erosion. The remnants of flood basalts can be found on all of the continents and they are as old as Archean (now represented by greenstone belts; Campbell et al., 1989) and as young as ~16 Ma (the Columbia River basalts). Continental flood basalts are found in intra-continental settings (e.g., the Siberian traps) and, perhaps more often, along continental rifted margins (e.g., the Parana-Etendeka flood basalts). The latter observation suggests a causal relationship between continental rifting and flood basalt volcanism (Richards et al., 1989; White and McKenzie, 1989). Field observations indicate that flood basalt provinces erupted rapidly, but it was not until the development of precise radiometric dating techniques that it was realized that the bulk of flood basalt provinces were erupted over geologically short time spans (~1 m.y.; e.g., Deccan traps; Duncan and Pyle, 1988) .

Another type of LIP, oceanic plateaus, are poorly understood because of their enormous size and relative inaccessibility, i.e., they are submerged in intraplate locations at considerable depth and are usually covered with thick sedimentary sequences. Our current understanding of them is a result of geophysical surveys (seismic, gravity, magnetic) and ODP drilling of plateaus (e.g., the Ontong Java Plateau, Leg 130; Mahoney et al, 1993). The Ontong-Java plateau is the largest of the oceanic plateaus and, based on the age of overlying sediments and radiometric ages of the lavas, formed during discrete, short-lived magmatic pulses beginning in the Aptian (Tarduno et al., 1991; Mahoney et al., 1993; Tejada et al., in press). Thickened oceanic crust of the nearby Manihiki Plateau and the Nauru, East Mariana, and Pigafetta Basins may also be part of the Ontong-Java LIP (Coffin and Eldholm, 1994), covering almost 1% of the earth's surface. Unfortunately, there is still a paucity of sampling from these regions, prohibiting a thorough study of the province.

Several flood basalt provinces (e.g., the Deccan Traps, the Parana/Etendeka basalts, and Kerguelen Plateau) can be unequivocally traced back to active hotspots by chains of seamounts and aseismic ridges (e.g., Duncan and Hargraves, 1990), suggesting that some LIPs are intimately related to mantle plumes. One hypothesis for the formation of LIPs proposes that they are the initial eruptive phase of mantle plumes (Courtillot and Besse, 1987; Richards and Griffiths, 1989; Campbell and Griffiths, 1990). In this scenario, thermally buoyant material rises from the lower mantle (possibly from the core-mantle boundary) and, as it rises, the leading edge of the diapir forms a large head that can entrain large amounts the middle to upper mantle material. Upon reaching the base of the lithosphere, the plume head flattens and widespread, large-scale mantle melting occurs, resulting in flood basalt volcanism. The trailing conduit continues to feed material to the surface as steady state hotspot volcanism.

The chemical and isotopic compositions of volcanic rocks provides one of the primary means of obtaining information about mantle evolution and structure (geodynamics; Allegre, 1982; Zindler and Hart, 1986). Therefore, geochemical data can be used to test the plume head hypothesis as it predicts that the erupted lavas should be derived from a mix of upper (depleted) mantle and a more enriched (plume source?) mantle. Isotopic ratios of Sr, Nd, and Pb of magmas, which retain the ratios of the mantle source, are indispensable in assessing mantle sources and mixing. Furthermore, they can provide information on the timing of the formation of mantle source domains. Because continental flood basalts have erupted through continental lithosphere, the potential for contamination of the magma by a lithospheric component may obscure the geochemical signals of the plume and upper mantle components, particularly for elements more concentrated in continental lithosphere (such as P and Sr). Oceanic plateaus are much less affected by such a continental component, although there is the potential for addition of an oceanic crustal contaminant. Nevertheless, the study of oceanic plateaus provides a more straightforward test of the plume/asthenosphere mixing relations in LIP formation. The general geochemistry of western Pacific oceanic plateaus indicate that they are derived from a mantle source which is distinct (less depleted) from that which produces normal mid-ocean ridge basalts (e.g., Castillo et al., 1986; Floyd, 1989; Mahoney et al., 1993). This observation is consistent with the mixing of depleted upper asthenospheric material with a more enriched mantle plume.

While geochemistry can provide information on mantle source characteristics, precise radiometric ages of lavas are crucial in constructing accurate magmatic histories of

LIPs and for determining eruption rates. Moreover, precise ages coupled with geochemistry may elucidate the relative timing of input from different mantle sources. In the following chapters, I present new ^{40}Ar-^{39}Ar ages and some compositional and isotopic data from two LIPs, the North Atlantic Volcanic Province (a volcanic rifted margin) and Caribbean oceanic plateau.

I served as a petrologist on Ocean Drilling Program Leg 152 that drilled into the continental margin of southeast Greenland. The primary purpose of the cruise was to drill into the submerged lava flows (referred to as seaward dipping reflector sequences [SDRS] because they are seismically imaged as sub-parallel reflectors) that are found on both margins of the North Atlantic. The SDRS encompass a large proportion of the North Atlantic Volcanic Province that had not previously been sampled from the western margin of the North Atlantic. My post-cruise work involved dating the recovered igneous rocks using ^{40}Ar-^{39}Ar incremental heating methods. The second chapter is my contribution to the scientific results volume.

In the third and fourth chapters, I present a study of the Caribbean oceanic plateau. The thick oceanic crust that forms the core of the Caribbean plate has been interpreted to be an oceanic plateau that has been wedged between North and South America (Burke et al., 1978; Duncan and Hargraves, 1984). Subduction around the edges of the Caribbean plate has resulted in the on-land emplacement of numerous fragments of the plateau and these can be used to investigate the anatomy of the plateau. The research plan was to look at a single locality in detail (Costa Rica) in which previous studies have suggested that there is older, normal oceanic crust over which the plateau lavas were erupted. I have used ^{40}Ar-^{39}Ar dating and petrological and geochemical data to test this hypothesis. The samples in this study were collected by myself in March 1993 with the guidance of Percy Denyer of the Universidad de Costa Rica and with field assistance from Martin Streck. The fourth chapter is a broader study of the whole Caribbean plateau. I report ^{40}Ar-^{39}Ar ages from other on-land sections (samples obtained from previous researchers) as well as drill cores from Leg 15 of the Deep Sea Drilling Project to test whether or not the plateau formed over a short time period *à la* flood basalt volcanism. I use new and existing geochemical data to compare the similarities and differences between the different sections, to discuss the possible relationship of the plateau to the Galapagos hotspot, and speculate on the mantle dynamics of oceanic plateau formation.

Chapter V is a foray into the possible effects of oceanic plateau formation on the submarine environment and its relationship to marine species extinction. The age of Caribbean volcanism (~90 Ma) coincides with the Cenomanian-Turonian boundary which is marked by a significant extinction of certain marine organisms (Raup and Sepkoski, 1986), the deposition of organic carbon-rich sediments (e.g., Schlanger and Jenkyns, 1976; Wignall, 1994), and an apparent increase in hydrothermal activity (Orth et al., 1993; Ingram et al., 1994). I consider the possibility that Caribbean volcanism directly contributed to seawater anoxia (evident from the increased preservation of organic material) by depleting oxygen dissolved in seawater during hydrothermal processes.

Chapter II: ^{40}Ar-^{39}Ar Ages of Lavas from the SoutheastGreenland Margin, ODP Leg 152, and the Rockall Plateau, DSDP Leg 81

Christopher W. Sinton and Robert A. Duncan

Abstract

^{40}Ar-^{39}Ar incremental heating experiments were performed on volcanic rocks recovered by drilling during Ocean Drilling Program Leg 152, southeast Greenland margin (63°N), and Deep Sea Drilling Project Leg 81, southwest Rockall Plateau (56°N). Both of these legs drilled into thick sections of submerged lava flows, known as seaward-dipping reflector sequences, that are part of the Tertiary North Atlantic Volcanic Province. Results show that subaerial volcanism began at the southeast Greenland margin as early as 61-62 Ma with the eruption of continentally-contaminated lavas. After an apparent hiatus, volcanism continued with the subaerial eruption of non-contaminated, MORB-like lavas. A sill or flow was emplaced at 52 Ma into the sediments overlying the basement lavas at the most seaward site (918). The MORB-like lavas of the Rockall Plateau gave poor results, though the data suggest that they erupted at 57-58 Ma and may be contemporaneous with the compositionally similar oceanic lavas of Leg 152.

Compiled ages from the North Atlantic Volcanic Province indicate that most of the lavas were erupted in two distinct magmatic episodes. The first occurred prior to 60 Ma with volcanism at the southeast Greenland margin, in West Greenland, and northwest British Isles. This early stage of widespread volcanism most likely records the arrival of the Iceland mantle plume. The second phase of magmatism began about 57 Ma with voluminous basaltic eruptions centralized along the eventual line of continental separation. Magmatism at this stage was associated with continental breakup and asthenospheric upwelling with probable thermal input from the mantle plume.

Introduction

The early Tertiary opening of the North Atlantic ocean was accompanied by voluminous, predominantly mafic, magmatism. The remnants of lava flows and sills associated with this event, collectively known as the North Atlantic Volcanic Province (NAVP), are preserved on Greenland, the Faeroe Islands, northwestern Britain and Ireland, and on the submerged margins of the North Atlantic. The submerged lavas were originally imaged as wedges of seaward-dipping reflector sequences (SDRS) that were correlated with subaerial lava flows (Hinz, 1981). Identified SDRS have been sampled by drilling at the Vøring Plateau (Deep Sea Drilling Project [DSDP] Leg 38 and Ocean Drilling Program [ODP] Leg 104), the SW Rockall Plateau (DSDP Leg 81) and more recently from the southeast Greenland margin (ODP Leg 152) (Fig. II.1). These studies have confirmed that the North Atlantic SDRS are composed predominantly of subaerially erupted lava flows and tuffs.

Precise crystallization ages of the North Atlantic SDRS are essential to understanding the interplay of magmatism and continental rifting, as well as the history of formation of oceanic lithosphere in the early opening of the North Atlantic. Until now, age control on the SDRS has been determined primarily by interpretation of seafloor magnetic anomaly sequences and fossil ages from sediments overlying or between lava flows. Magnetic anomaly data (Talwani and Eldholm, 1977) indicate that the Vøring Plateau SDRS are at least anomaly 24R age (53.3-55.9 Ma, Berggren et al., in press), consistent with the early Eocene age of the sediments overlying the lavas (Talwani and Udintsev, 1976; Eldholm, Thiede, Taylor, et al., 1987). Because the biostratigraphic data can place only a minimum age on the Vøring Plateau lavas, radiometric dating of recovered lavas or examination of the fossil assemblages of any inter-lava sediment layers must be used to determine a more precise age of volcanism.

The deepest penetration of the Vøring Plateau lavas was at Hole 642E (Leg 104) where 914 m of lavas (121 flows) and volcaniclastic sediments were drilled. The lava sequence was divided into two distinct series, a reversely magnetized upper series composed of subaerially erupted, MORB-like tholeiitic lavas and a lower, normally-magnetized series of mixed basaltic and peraluminous andesitic lavas (Eldholm, Thiede, Taylor, et al., 1987; Schönharting and Abrahamsen, 1989). The two series are separated by a 13-m-thick horizon of finely laminated mudstones and volcaniclastic sediments.

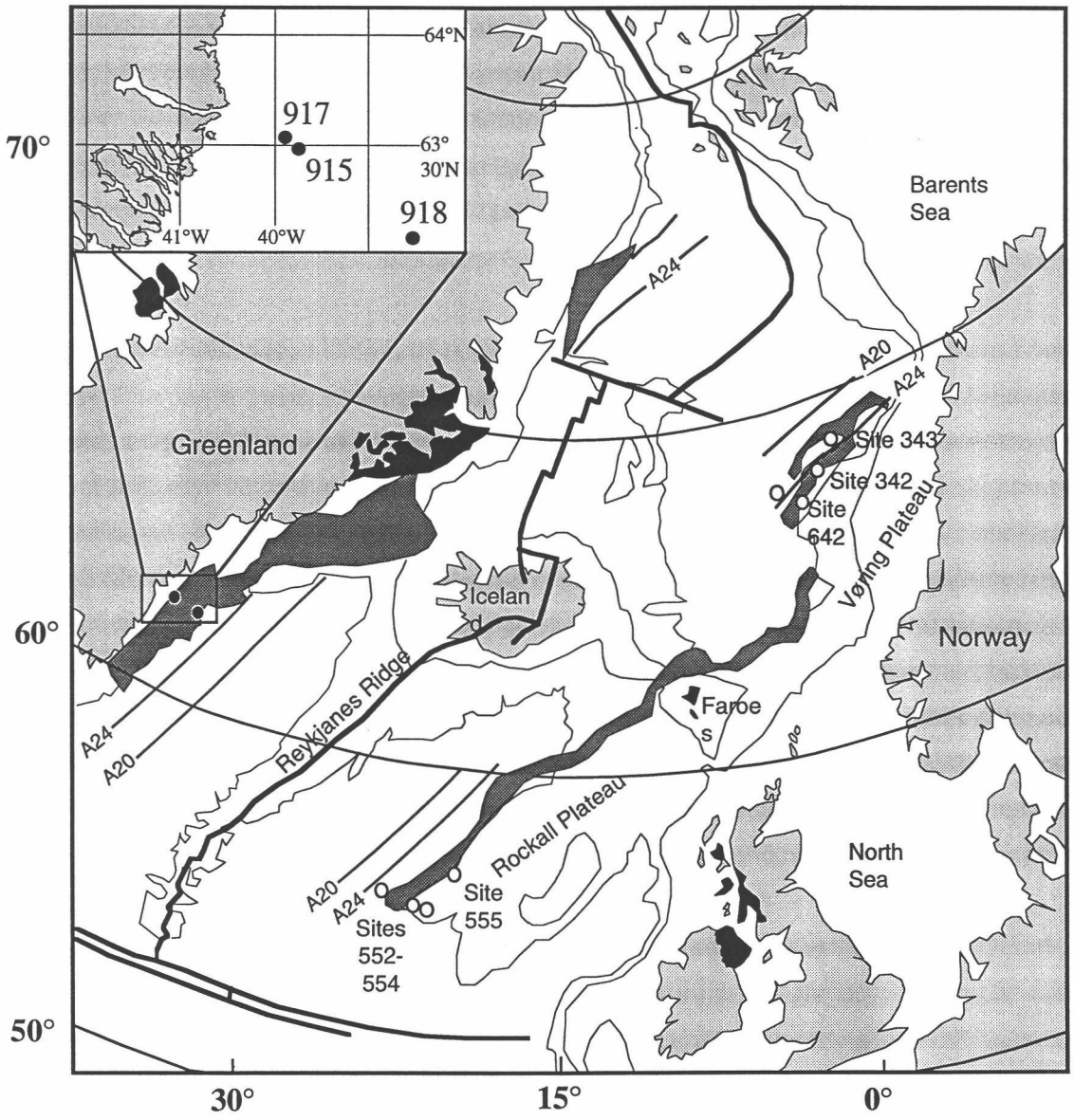

Figure II.1: Map of the North Atlantic region. Shown are subaerial lava outcrops of the North Atlantic Volcanic Province in black, seaward-dipping reflector sequences (in gray) (Eldholm and Grue, 1995; Larsen and Jakobsdóttir, 1988; White and McKenzie, 1989) , magnetic anomaly lineations, and DSDP and ODP drilling sites. Previous drill sites on the Vøring margin (Legs 38 and 104) and southwest Rockall Plateau (Leg 81) are shown as open circles. The filled circles are the sites from ODP Leg 152. The inset shows detail of the Leg 152 sites.

Although there is no reported fossil age for this sediment horizon, volcaniclastic sediments within the lower series lavas contain a dinoflagellate cyst assemblage that Boulter and Mancum (1989) correlated with nannoplankton zone NP9. This stage coincides with the Paleocene/Eocene boundary (Berggren et al., 1985), assigned an age of 55 Ma by the Berggren et al. (in press) timescale. However, Boulter and Mancum (1989) noted that the dinocyst assemblage is similar to that seen in coal layers between the Plateau lavas on the Isle of Mull and these have been radiometrically dated at 60.0 ± 0.5 Ma (average of four ages; Mussett, 1986). Thus, the dinocyst information may not place a precise absolute age on the lavas.

Attempts to radiometrically date the Vøring Plateau lavas have provided variable and imprecise data. K-Ar dating of DSDP Leg 38 lavas gave ages ~46 Ma (Kharin et al., 1976), much younger than the oldest overlying sediments. Rb-Sr isochrons of the lower lava series at Hole 642E are reported from two separate groups. LeHuray and Johnson (1989) used three unleached samples to produce an isochron of 57.8 ± 1.0 Ma. Taylor and Morton (1989) used five leached samples (three of which were used by LeHuray and Johnson, 1989) to calculate a five-point Rb-Sr isochron of 63 ± 19 Ma. The differing results from these two studies and the possibility that the linear array of data represent a mixing line rather than an isochron casts doubt on the accuracy and utility of the ages, although the results of LeHuray and Johnson (1989) generally agree with the fossil ages. ^{40}Ar-^{39}Ar analysis of the Hole 642E lavas is in progress and should provide more precise age constraints on the magmatic history of the Vøring Plateau .

The SDRS of the southern Rockall Plateau/Hatton Bank, which lies to the west of the British Isles, were sampled at three sites (553, 554, and 555) during DSDP Leg 81. The lavas at these sites are all consistently MORB-like in composition (Harrison and Merriman, 1984; Macintyre and Hamilton, 1984). The age of the lavas is at least late Paleocene/early Eocene based on the fossil age of the overlying sediments (Roberts and Schnitker, 1984) and identification of oceanic magnetic anomalies (Vogt and Avery, 1974). A more direct method of dating the lavas was attempted by interpreting the dinoflagellate cyst assemblages in sediments intercalated with lava flows at site 555. These sediments, like those associated with the Vøring lavas, are correlated to zone NP9 (Brown and Downie, 1984). K-Ar dating of the DSDP Leg 81 lavas gave a range of ages, although two from Site 555, which yielded 52.3 ± 1.7 and 54.5 ± 2.0, are the most reliable according to Macintyre and Hamilton (1984).

The results from previous drilling of the North Atlantic SDRS indicate a minimum age of late Paleocene/early Eocene for the lavas of the SDRS from the eastern margin of the North Atlantic. Because the complete volcanic succession was not penetrated at any of these sites, the maximum age of the SDRS is unknown, as is the total duration of volcanism that produced the SDRS. Recently, ODP Leg 152 drilled the landward feather-edge of the SDRS at the southeast Greenland margin, penetrating the lowermost portion of the volcanic stratigraphy at one of the sites, thus allowing the possibility of determining the age of initial volcanism at this part of the western North Atlantic margin.

Here, we present results from ^{40}Ar-^{39}Ar incremental heating experiments on lavas recovered during ODP Leg 152 and DSDP Leg 81. The Rockall Plateau is a few hundred kilometers to the south of the margin conjugate to the southeast Greenland margin and it is possible that the Tertiary lavas from these two regions are complementary. The purpose of this project was to constrain the age and duration of volcanism that formed the southern North Atlantic SDRS. The age determinations indicate that subaerial volcanism at the southeast Greenland margin began no later than 61-62 Ma and persisted at least until a small flow or sill penetrated Eocene marine sediments at 52 Ma. A significant hiatus is evident between the initial eruption of continentally-contaminated lavas and the later eruption of lavas with more oceanic affinities. The age determinations from the Rockall Plateau/Leg 81 samples are poorly constrain, yet suggest an eruption age of 57-58 Ma.

Sample Descriptions

Leg 152 drilled into the volcanic basement of the southeast Greenland margin at three sites along a transect close to 63°N (Larsen, Saunders, Clift, et al., 1995) (Fig. II.1). Two sites (915 and 917) were drilled on the landward, feather-edge of the SDRS. Here, the basement is overlain by sediments that are probably late Paleocene-early Eocene age (Larsen et al., 1995). Only 10 m of MORB-like tholeiitic basalt were drilled at Hole 915A, but drilling at nearby Hole 917A penetrated a succession of subaerial lavas and rare tuffs (779 m; 92 flow units) and into steeply inclined, low-grade metamorphic sediments.

The volcanic stratigraphy at Hole 917A was divided into three series: a lower series of basalts and rare picrites, a middle series of more evolved basalts and rare dacites and ash tuffs, and an upper series of thin olivine basaltic and picritic flows. Geochemical and petrographic data for the lower and middle series lavas indicate that they have been variably contaminated by the continental crust and/or lithospheric mantle (Fitton et al., this volume; Demant, this volume). The upper series shows evidence of only minor addition from the crust (Larsen, Saunders, Clift, et al., 1995; Fitton et al., this volume). The boundary between the upper and middle series is marked by a sandstone unit (67 cm) while the middle to lower series boundary is based on a change in lava compositions.

At Hole 918D, located about 80 km seaward of Site 917, 122 m of subaerial lava flows (18 flow units) were cored. The lavas are all uniformly aphyric tholeiitic basalts with MORB-like compositions (Larsen, Saunders, Clift, et al., 1995). A 12-m-thick alkalic sill or flow lies within the early Eocene sediments 9 m above the basement lavas and is the youngest volcanic unit drilled. All of the Leg 152 lavas are reversely magnetized and had been assigned to magnetic anomaly 24R or older (Larsen and Jakobsdóttir, 1988; Larsen, Saunders, Clift, et al., 1995)

Lavas from the southwest Rockall Plateau were recovered during Leg 81 at sites 553, 554, and 555. All are aphyric tholeiitic basalts geochemically similar to MORB (Roberts and Schnitker, 1984). Sites 553 and 554 are located on the western flank of the Rockall Plateau in the Edoras Basin, while Site 555 is more landward, between the Hatton Bank and the Edoras Bank. Site 553 basalts were subaerially erupted and are reversely magnetized. Site 554 lavas are normally magnetized and were erupted under shallow submarine conditions. Site 555 samples are reversely magnetized and were erupted in a shallow submarine environment (Roberts and Schnitker, 1984).

Samples for ^{40}Ar-^{39}Ar radiometric analysis were selected from each of the Leg 152 sites (Table II.1). Where possible, selected samples were the freshest, free of vesicles and cracks, highest in primary K_2O, and the best crystallized. Because of the low K_2O and fine-grained to glassy groundmass of the Site 917A upper series lavas, they are poor candidates for dating. This problem is exacerbated by the extensive zeolite-facies alteration of these rocks (Demant, this volume). Similar problems were encountered with the basement lavas from Hole 918D. The one lava unit from Site 915 is also low in K_2O, although it is relatively fresh compared with the other low-K_2O lavas from Leg 152.

The lavas from the middle and lower series of Hole 917A are generally the freshest and have the highest K_2O contents of all the Leg 152 lavas. The unit 35B (Sample 152-917A-23R-3, 35-39 cm) ash tuff is obviously altered: the matrix is heavily weathered and the plagioclase crystals are cloudy and variable in composition (Demant, this volume). On the other hand, the unit 35D (Sample 152-917A-24R-1, 8-10 cm) tuff unit still contains vitric glass shards, and the plagioclase crystals from this layer are clear and have a consistent andesine composition (Demant, this volume). A dacite flow (unit 55; Sample 152-917A-52R-1, 46-49 cm) near the base of the middle series was analyzed because it was the best-crystallized of the recovered dacites. The two plagioclase-phyric lavas from the 917 lower series (units 60 and 68; Samples 152-917A-55R-4, 4-9 cm and 64R-2, 29-35 cm) and Site 915 (unit 3; Sample 152-915A-24R-2, 78-84 cm) have 2-5 mm plagioclase phenocrysts containing abundant 10-20 μ melt inclusions. The stratigraphically lowest analyzed samples from Site 917 (units 82 and 84; Samples 152-917A-83R-2, 113-118 cm, and 88R-8, 46-50 cm) come from thick (15 m and 45 m, respectively) aphyric olivine basalt flows. The Site 918 sill (section 152-918D-94R-2) is a very fresh, holocrystalline rock with relatively high K_2O (0.57%).

Samples from Leg 81 (Rockall Plateau) were examined in thin section and selection was based on texture and degree of alteration. All are aphyric tholeiitic basalts with <0.10% K_2O. Brief petrographic descriptions and K_2O content of the analyzed samples are listed in Table II.1.

Analytical Methods

Both whole rock mini-cores, drilled from the freshest part of the sample, and feldspar separates were analyzed by ^{40}Ar-^{39}Ar incremental heating methods. Feldspars from the two ash tuffs were hand-picked after crushing. To obtain phenocryst and groundmass plagioclase separates from the basalts, samples were crushed and sieved to 0.1-0.5 mm, concentrated using a Franz magnetic separator, and checked for purity under a binocular microscope. The plagioclase separates were briefly washed with 5% HF to remove surficial alteration. The groundmass (composed of clinopyroxene, plagioclase, and Fe-Ti oxides) from a coarsely crushed (0.3-0.1 mm) fraction of Sample 152-915A-24R-2, 78-84 cm was separated from the non-magnetic phenocrysts in an effort to avoid inclusion-bearing plagioclase phenocrysts. All samples were ultrasonically washed in

Table II.1. Samples from the southeast Greenland margin analyzed by ^{40}Ar-^{39}Ar incremental heating experiments.

Core and sample interval	Unit	Series	Description	% K_2O	Material
152 915A-					
24R-2, 78-84	3		plag-px-ol basalt	0.21	phenocryst plagioclase, plagioclase-free groundmass
25R-1, 9-12	3		plag-px-ol basalt	0.15	whole-rock
152 917A-					
17R-4, 68-73	24	upper	aphyric ol basalt	0.16	whole-rock, groundmass plagioclase
23R-1, 31-36	34B	middle	aphyric basalt	0.4	whole-rock
23R-3, 35-39	35B	middle	tuff	?	feldspar
24R-1, 8-10	35D	middle	tuff	?	feldspar
40R-4, 15-20	52	middle	aphyric basalt	0.39-0.69	whole-rock
52R-1, 46-49	55	middle	plag-px dacite	2.89	whole-rock
55R-4, 4-9	60	lower	ol-plag-px basalt	0.12	phenocryst and groundmass plagioclase
64R-2, 29-35	68	lower	ol-plag basalt	0.29	phenocryst and groundmass plagioclase
69R-2, 48-53	71	lower	aphyric ol basalt	0.49	groundmass plagioclase
83R-2, 113-118	82	lower	ophitic ol diabase	0.25	whole-rock
	84	lower	ophitic ol diabase	0.29	whole-rock
88R-8, 46-50					
152 918D-					
94R-2, 42-47	1		plag-cpx basalt	0.57	whole-rock
106R-2, 15-19	11B		aphyric basalt	0.07	whole-rock, groundmass plagioclase
110R-4, 67-71	14		aphyric basalt	0.09	whole-rock, groundmass plagioclase
81 553A-					
46-3, 116-123			aphyric basalt	0.06	whole-rock
49-3, 65-72			aphyric basalt	0.06	whole-rock
81 554A-					
7-3, 77-85			aphyric basalt	0.19	whole-rock
7-4, 11-18			aphyric basalt	0.15-0.16	whole-rock
14-1, 33-40			aphyric basalt	0.36	whole-rock
81 555-					
69-3, 121-129			aphyric basalt	0.04-0.11	whole-rock
90-2, 102-109			aphyric basalt	0.07	whole-rock
95-2, 16-23			aphyric diabase	0.09	whole-rock
96-2, 30-37			aphyric diabase	0.09	whole-rock

K_2O values reported for each unit are from Larsen, Saunders, Clift, et al. (1995), Harrison and Merriman (1984), Joron et al. (1984), and Richardson et al. (1984).

distilled water and dried. Mineral separates, wrapped in high-purity Cu-foil, and the whole-rock mini-cores were then sealed in evacuated quartz tubes and irradiated for 6 hours at 1 MW power in the Oregon State University TRIGA reactor. The neutron flux was monitored by samples of the biotite standard FCT-3 (27.55 ± 0.12 Ma; Lanphere et al., 1990) placed at regular intervals between the samples. Calculated errors for J were between 1% and 1.5%.

Ar isotopic compositions were determined using the MAP 215-50 and AEI MS-10S mass spectrometers at Oregon State University using standard methods (Duncan and Hargraves, 1990; Duncan and Hogan, 1994). Samples were incrementally heated either by radio-frequency induction heating (MS-10S) or in a low-blank, double-vacuum resistance furnace (MAP 215-50). After corrections for background, isotopic interferences, and mass fractionation, an age for each heating step was calculated. The data for each sample were then reduced as age spectra (step age vs. % ^{39}Ar released). Heating step ages were integrated for plateau ages if they formed a well-defined succession of contiguous steps that are concordant within 2σ error and comprised at least 50% of the ^{39}Ar released from the sample. We calculated plateau ages in two ways. The first follows the method of Dalrymple et al. (1988), in which step ages are weighted by the inverse of the variance. In this way, the calculated mean more closely reflects the more precisely determined step ages. A more conservative method weights each step by the proportion of the total ^{39}Ar released in that step. In the discussion, we use the results from the first method. However, there was no statistical difference (at the 2σ confidence level) of the ages determined by these two methods.

The age of each step was calculated under the assumption that the original argon composition was atmospheric ($^{40}Ar/^{36}Ar = 295.5$). However, it is possible that the magmas did not completely equilibrate with the atmosphere upon crystallization. For each ^{40}Ar-^{39}Ar sample, isochrons were calculated, in which a linear correlation of the step isotopic compositions ($^{36}Ar/^{40}Ar$ vs. $^{39}Ar/^{40}Ar$) provide an age (related to the slope of the regression line) and an initial isotopic composition (from the $^{36}Ar/^{40}Ar$ intercept). Weighted linear regressions were fitted to the data from the steps included in the age plateau, except where noted. Replicates of Sample 917A-23R-1, 31-36 cm, were analyzed by both mass spectrometers to examine the reproducibility of the analyses and ensure that there are no systematic differences between the two instruments. The plateau and isochron ages from both samples are nearly identical and well within the 2σ standard deviation.

Results

Conventional K-Ar or ^{40}Ar-^{39}Ar total fusion ages may be inaccurate because of the effects of post-crystallization alteration (radiogenic ^{40}Ar loss) and/or incomplete equilibration of the rock with an atmospheric Ar composition at crystallization ("excess" ^{40}Ar). ^{40}Ar-^{39}Ar incremental heating methods allow internal checks on assumptions of closed system behavior and initial atmospheric Ar composition through age spectrum (plateau) and isotope correlation diagrams. If a sample yields concordant plateau and isochron ages and a near-atmospheric intercept, such ages are likely to represent reliable crystallization ages (Lanphere and Dalrymple, 1978). A sample that contains excess radiogenic ^{40}Ar may yield an age plateau that is older than external constraints allow, yet have a younger isochron age and an elevated $^{40}Ar/^{36}Ar$. In this case, the isochron age may be geologically meaningful, while the plateau is not. Other samples fail to provide a reliable plateau or isochron age for geological and analytical reasons.

Southeast Greenland Margin

Hole 917A

The results of the incremental heating experiments on lavas from Site 917A yield variable results, as expected from petrographic and compositional data. From the upper series, an aphyric olivine basalt flow (unit 24; Sample 152-917A-17R-4, 68-73 cm) was considered the best sample for analysis based on thin-section observations. However, an analysis of the groundmass plagioclase from this unit yielded no age plateau and an isochron (using the linearly arrayed data points) with an age (29.4 Ma) too young given the fossil and magnetic age constraints (Fig. II.2). Fortunately, the analyses from the middle and lower series lavas were much more successful.

Five samples from the middle and lower series provided concordant plateau and isochron ages and near-atmospheric initial Ar compositions (Table II.1). The plateau ages range from 60.1 to 62.2 Ma, but all ages lie within 2σ analytical error. Other analyzed samples showed disturbed age spectra. The whole-rock analyses from the two stratigraphically oldest samples (holocrystalline, aphyric olivine basalts) that were analyzed (units 82 and 84; Samples 152-917A-83R-2, 113-118 cm, and 88R-8, 46-50 cm) show evidence of excess radiogenic ^{40}Ar (Fig. II.2). Both give coherent step age plateaus

Table II.2. ^{40}Ar-^{39}Ar plateau and isochron age calculations from the southeast Greenland Margin, ODP Leg 152.

Core and sample interval (cm)	Material	Plateau age by $1/\sigma^2$(m.y.)	Plateau age by $\%^{39}Ar$ (m.y.)	^{39}Ar % of Total	Isochron age (m.y.)	N	$^{40}Ar/^{36}Ar$ intercept ± 1σ	SUMS/ (N-2)
152-917A-23R-1A, 31-36	basalt	60.1 ± 0.8	60.6 ± 2.3	99	59.4 ± 2.4	8	319.4 ± 3.4	275.3
152-917A-23R-1B, 31-36	basalt	60.8 ± 1.0	60.9 ± 24	81	60.6 ± 1.8	4	297.2 ± 7.2	0.2
152-917A-24R-1, 8-10	feldspar from tuff	62.2 ± 0.4	62.3 ± 1.4	100	62.3 ± 1.4	16	299.7 ± 2.1	375.5
152-917A-40R-4, 15-20	basalt	60.7 ± 1.2	61.3 ± 2.0	51	60.3 ± 4.2	6	291.9 ± 16.8	452.0
152-917A-52R-1, 46-49	dacite	61.7 ± 0.5	61.6 ± 1.4	96	61.0 ± 1.2	8	300.0 ± 0.8	7.4
152-917A-69R-2, 48-53	groundmass plagioclase	60.4 ± 0.7	60.6 ± 1.8	97	60.3 ± 1.6	7	301.3 ± 3.3	42.6
152-917A-83R-2, 113-118	basalt	68.2 ± 1.6	68.2 ± 2.2	72	63.3 ± 1.2	4	413.2 ± 32.2	0.6
152-917A-88R-8, 46-50	basalt	64.1 ± 2.2	64.4 ± 3.8	82	63.3 ± 1.0	5	319.1 ± 7.6	1.0
152-918D-94R-2, 42-47	basalt	51.9 ± 0.8	51.9 ± 1.9	97	51.9 ± 1.2	7	294.8 ± 0.8	5.1

Samples 152-917A-23R-1A, 31-36 cm, and 152-917A-23R-1B, 31-36 cm, are replicate analyses, the latter measured on the AEI MS-10S and the former on the MAP 215-50. Errors for both step age plateaus and isochrons are reported to 2σ. Ages are corrected for ^{37}Ar decay, half-life = 35.1 days. $\lambda_\varepsilon = 0.581 \times 10^{-10}\ yr^{-1}$; $\lambda_\beta = 4.962 \times 10^{-10}\ yr^{-1}$. N refers to the number of steps used in the isochron calcuation.

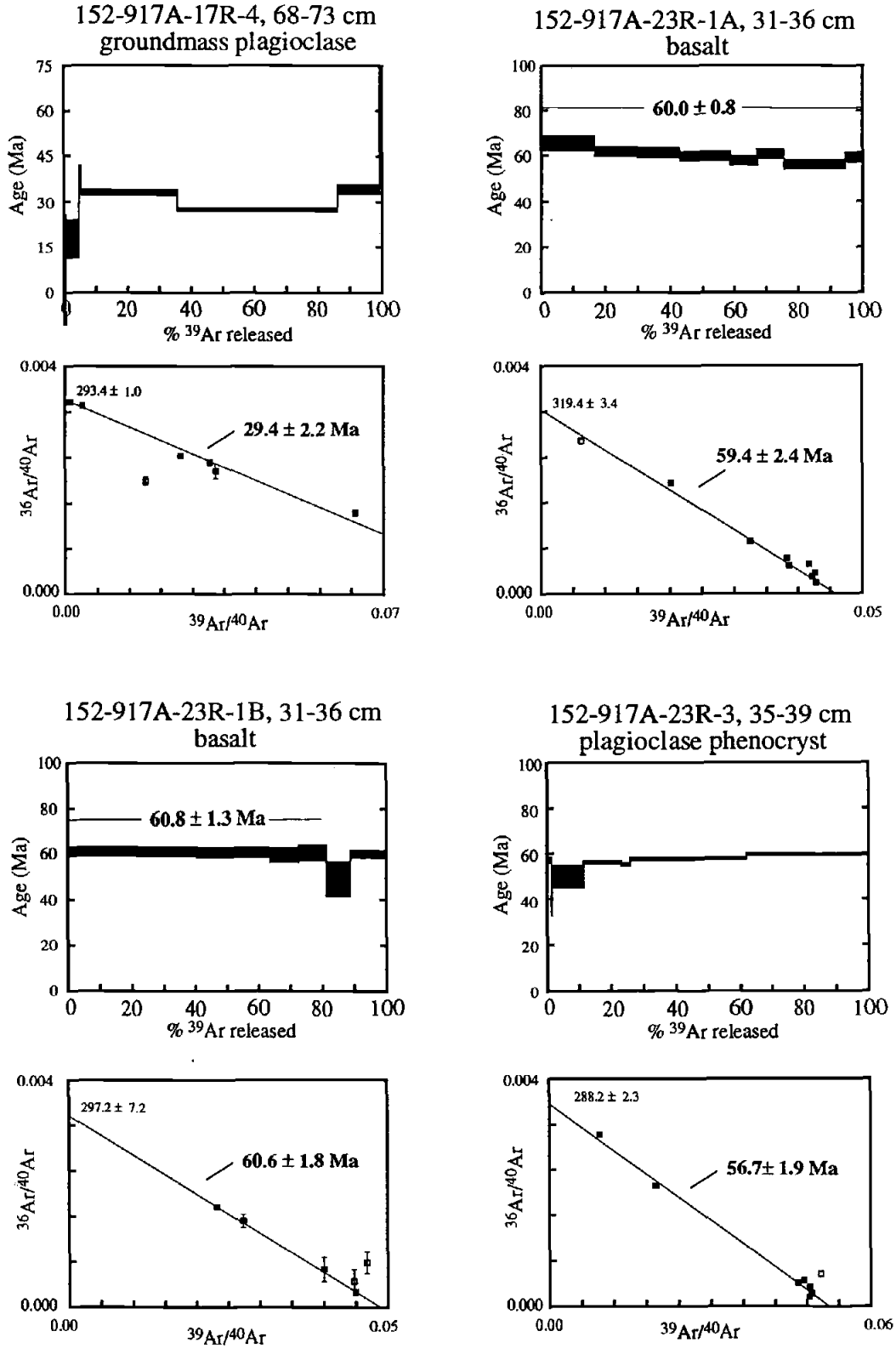

Figure II.2: Step age spectra and isotope correlation diagrams from ^{40}Ar-^{39}Ar incremental heating experiments for Site 917 samples. The thickness of the bar for each step age in the age spectrum indicates the 2σ analytical uncertainty in age.

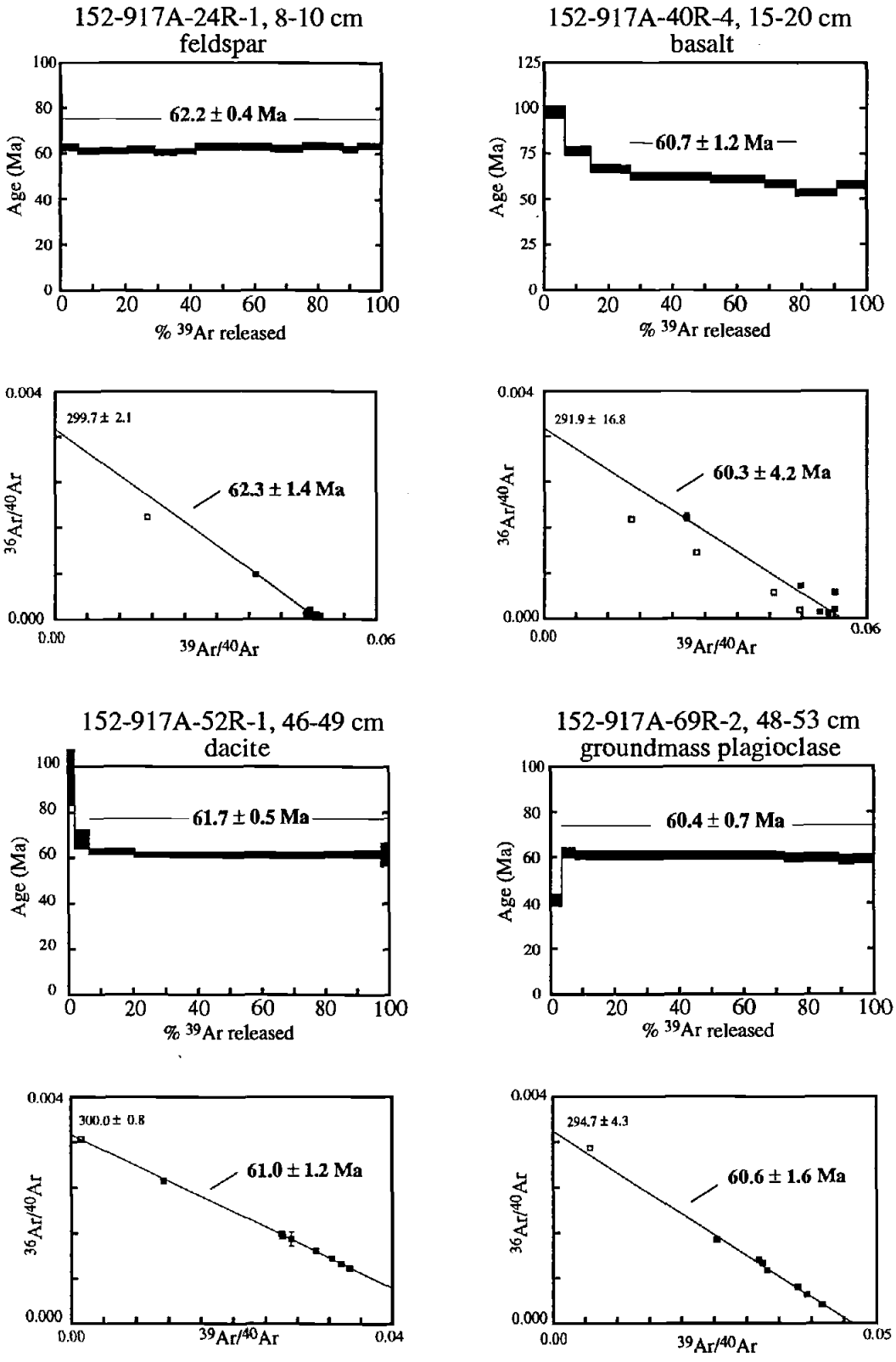

Figure II.2 (cont'd)

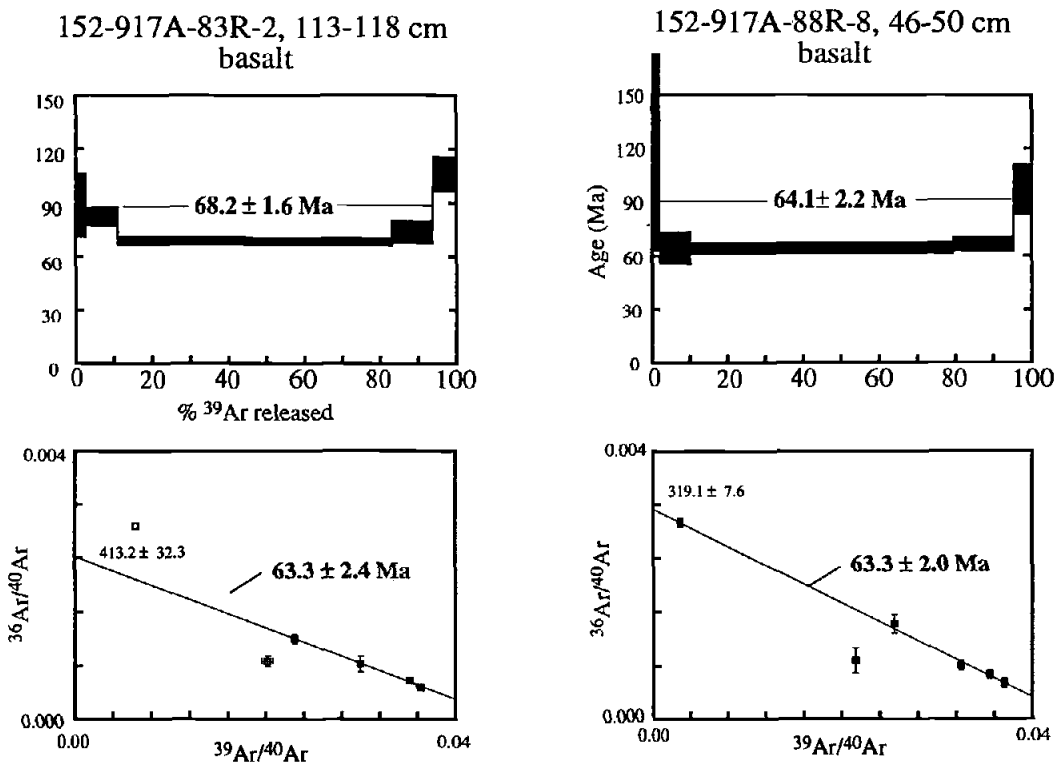

Figure II.2 (cont'd)

of 68.2 ± 1.6 Ma and 64.1 ± 2.2 Ma, respectively (Table II.1). However, the saddle-shaped age spectra in which there are higher ages for the first and last few heating steps is a pattern often seen in rocks that contain excess ^{40}Ar (Lanphere and Dalrymple, 1976). This conclusion is supported by the high initial $^{40}Ar/^{36}Ar$ derived from the isotope correlation diagrams. The isochrons give identical ages (63.3 ± 2.0 and 63.3 ± 2.4 Ma, respectively) which are concordant with the more precise ages from the middle series tuff and lavas.

Another mechanism for producing a disturbed age spectrum is a loss of radiogenic ^{40}Ar or an addition of K due to alteration. This is demonstrated by the plagioclase crystals from the unit 35B (Sample 152-917A-23R-3, 35-39 cm) ash tuff (Fig. II.2) which show step ages that gradually increase with increasing temperature steps, approaching, but not reaching the age derived from the vitric tuff (unit 35D; Sample 152-917A-24R-1, 1-10 cm).

Sample 152-917A-40R-4, 15-20 cm, shows a general decrease in step ages with increasing temperature. Such a pattern can be ascribed to recoil of ^{39}Ar during irradiation. We picked the middle three steps to calculate a plateau age. These three points are so tightly grouped on the correlation diagram that they do not form a linear trend, so a regression was fitted to these and two other near-colinear points. The resulting isochron is concordant with the plateau age.

The reliable radiometric ages (i.e., those that have concordant plateau and isochron ages and near-atmospheric initial Ar compositions) are not entirely consistent with stratigraphic position, i.e., the oldest measured ages are not from the lowermost samples (Fig. II.3). The lower and middle series lavas appear to have erupted without a significant break either shortly prior to magnetic chron C27n or shortly after C27n (Larsen, Saunders, Clift et al., 1995) which suggests that the measured age range (62-60 Ma) is greater than the actual period of eruption. The slightly younger age of feldspar separates from sample 917A-69R-2 (Fig. II.2) could be due to a small amount of radiogenic ^{40}Ar loss from alteration in some of the basaltic samples (evident in the lowest temperature step from the age spectrum). Of all the age results from the middle and lower lava series at Hole 917A, the most reliable come from the vitric ash flow tuff feldspar (unit 35D, Sample 152-917A-24R-1, 8-10 cm; plateau age of 62.2 ± 0.4 Ma) and the dacite (unit 55, Sample 152-917A-52R-1, 46-49 cm; plateau age of 61.7 ± 0.5 Ma) from the middle series. These two are the freshest, have the highest in K_2O content (and

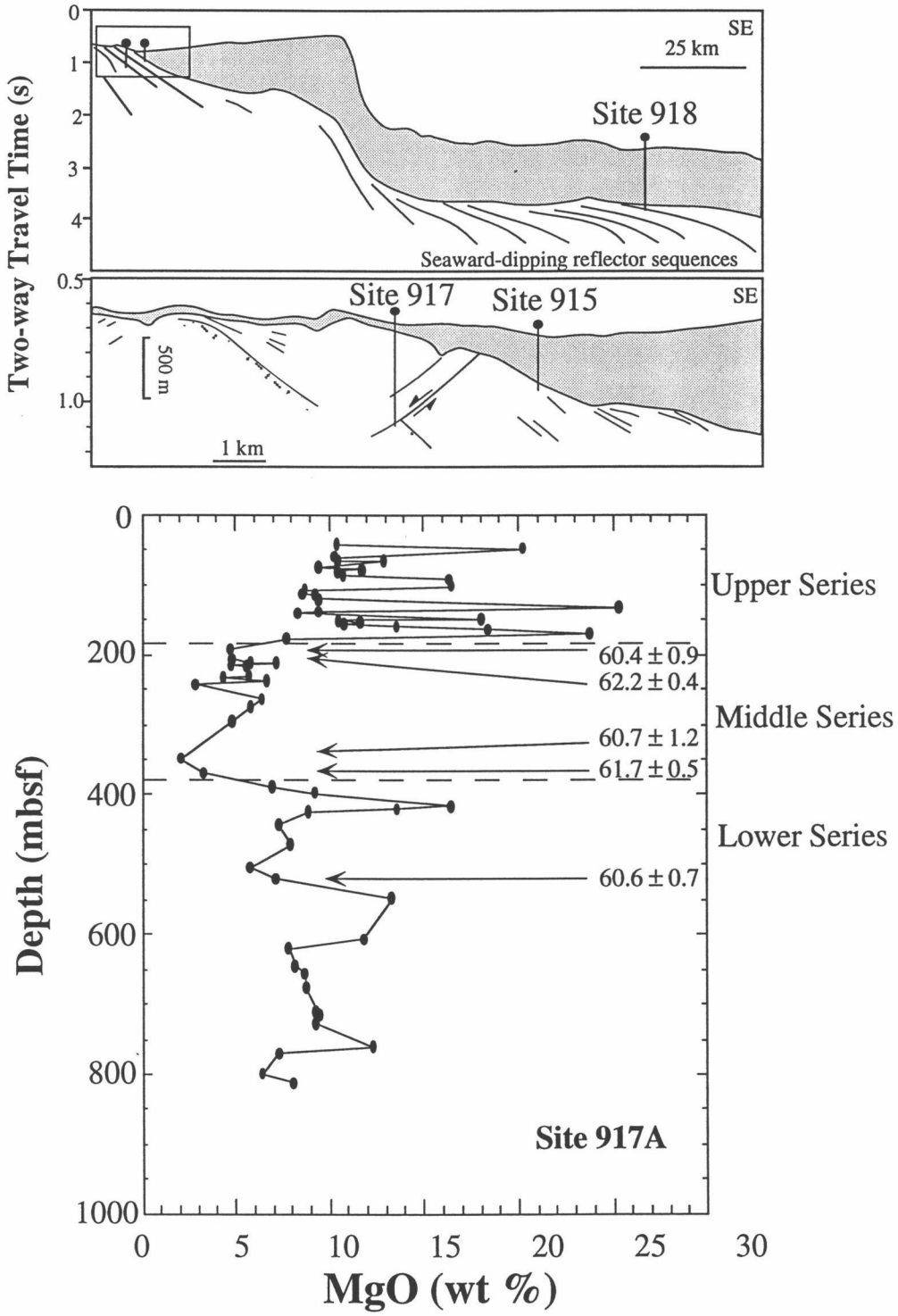

Fig. II.3: Interpreted seismic cross-section of the SE Greenland margin (from Larsen, Saunders, Clift, et al., 1995) and depth vs. MgO from site 917A.

are therefore less susceptible to the effects of minor ^{40}Ar loss), give excellent, detailed age spectra, and a mean age of 62.0 ± 0.3 Ma. Thus, our best estimate for the formation of the Site 917 middle and lower series is 61-62 Ma. A reliable radiometric age for the upper series was not obtained.

Hole 915A

Two samples from the one unweathered lava flow unit (unit 3) of Hole 915A were analyzed. Plagioclase phenocrysts from Sample 152-915A-24R-2, 78-84 cm, yielded a disturbed step-age spectra with anomalously old ages (Fig. II.4). The old step ages could be due to magmatic ^{40}Ar released from the melt inclusions in the plagioclase, coupled with the low K_2O content (and therefore low radiogenic ^{40}Ar) of the crystals. Because of the low radiogenic ^{40}Ar, even small amounts of excess ^{40}Ar can affect the calculated age. This interpretation assumes that the melt inclusions did not re-equilibrate with atmospheric Ar and retained a magmatic Ar composition.

Similar patterns are seen in the analyses of inclusion-bearing plagioclases from Hole 917A (units 60 and 68; Samples 152-917A-55R-4, 4-9 cm, and 64R-2, 29-35 cm). The age spectra from all these samples do not show the saddle-shape that the whole-rock samples from the base of the Hole 917A lower series display. Rather, the spectra show discontinuous step ages that do not form a coherent age plateau. This difference could be due to the variable release of Ar from the melt inclusions throughout the step heating. An isochron calculated from the Sample 152-915A-24R-2 isotope correlation diagram gives a poorly constrained age that is within the range expected from the lavas (55.4 ± 14.0). However, the scatter in the data points used in the linear regression resulted in a high uncertainty for the calculated age. The phenocryst-free groundmass from Sample 152-915A-24R-2 did not show any evidence of excess ^{40}Ar, but a coherent age plateau was not generated. The linear array of the data on a correlation diagram is dispersed and does not give an isochron. Similarly discordant results were obtained from a whole-rock analysis of Sample 152-915A-25R1 (Fig. II.3).

Hole 918D

A whole rock analysis of the Hole 918D sill (unit 1; Sample 152-918D-94R-2, 42-47 cm) gave excellent results (Table II.2) with identical plateau and isochron ages (51.9 ±

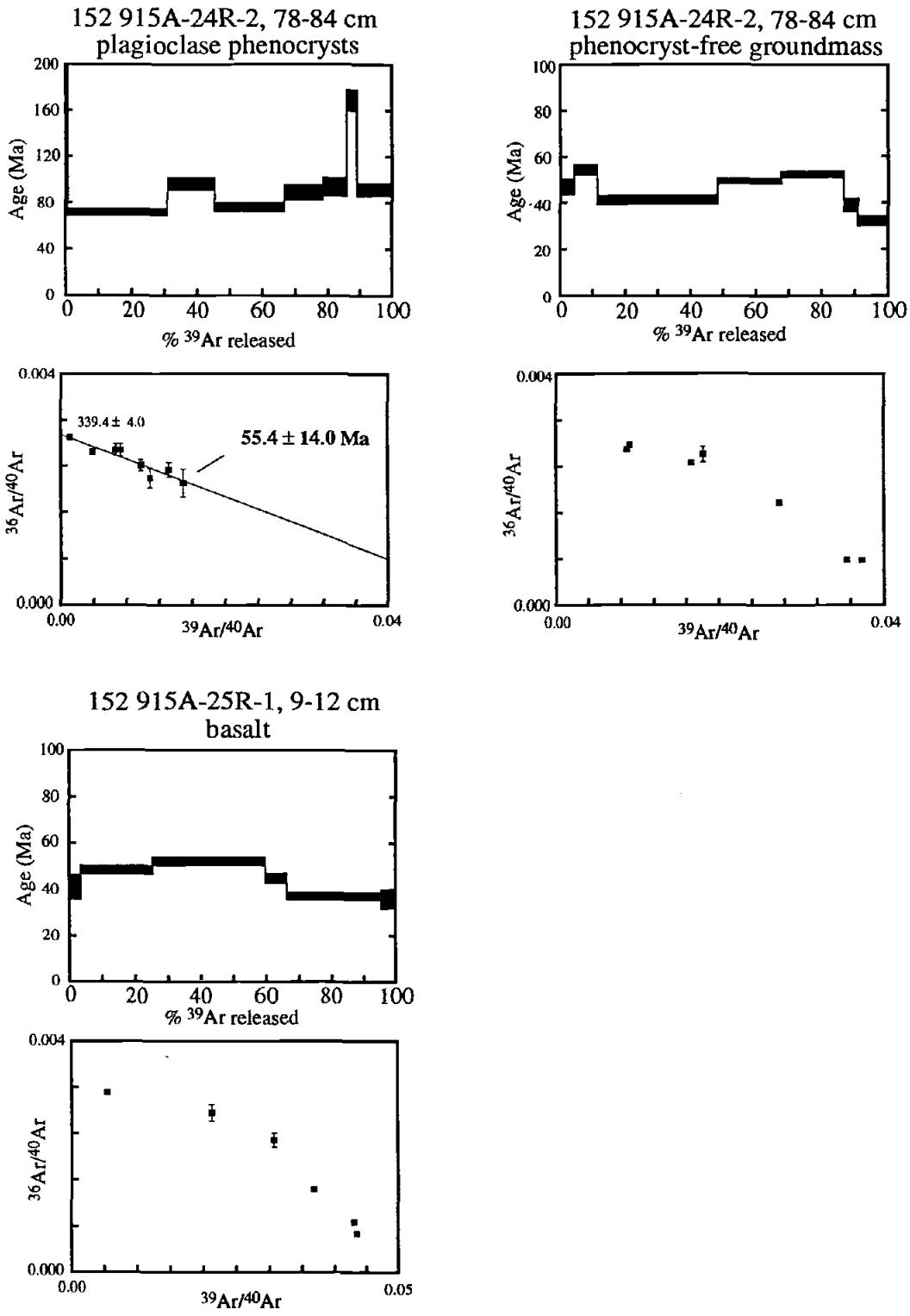

Figure II.4: Step age spectra and isotope correlation diagrams from ^{40}Ar-^{39}Ar incremental heating experiments for Site 915 samples. The thickness of the bar for each step age in the age spectrum indicates the 2σ analytical uncertainty in age.

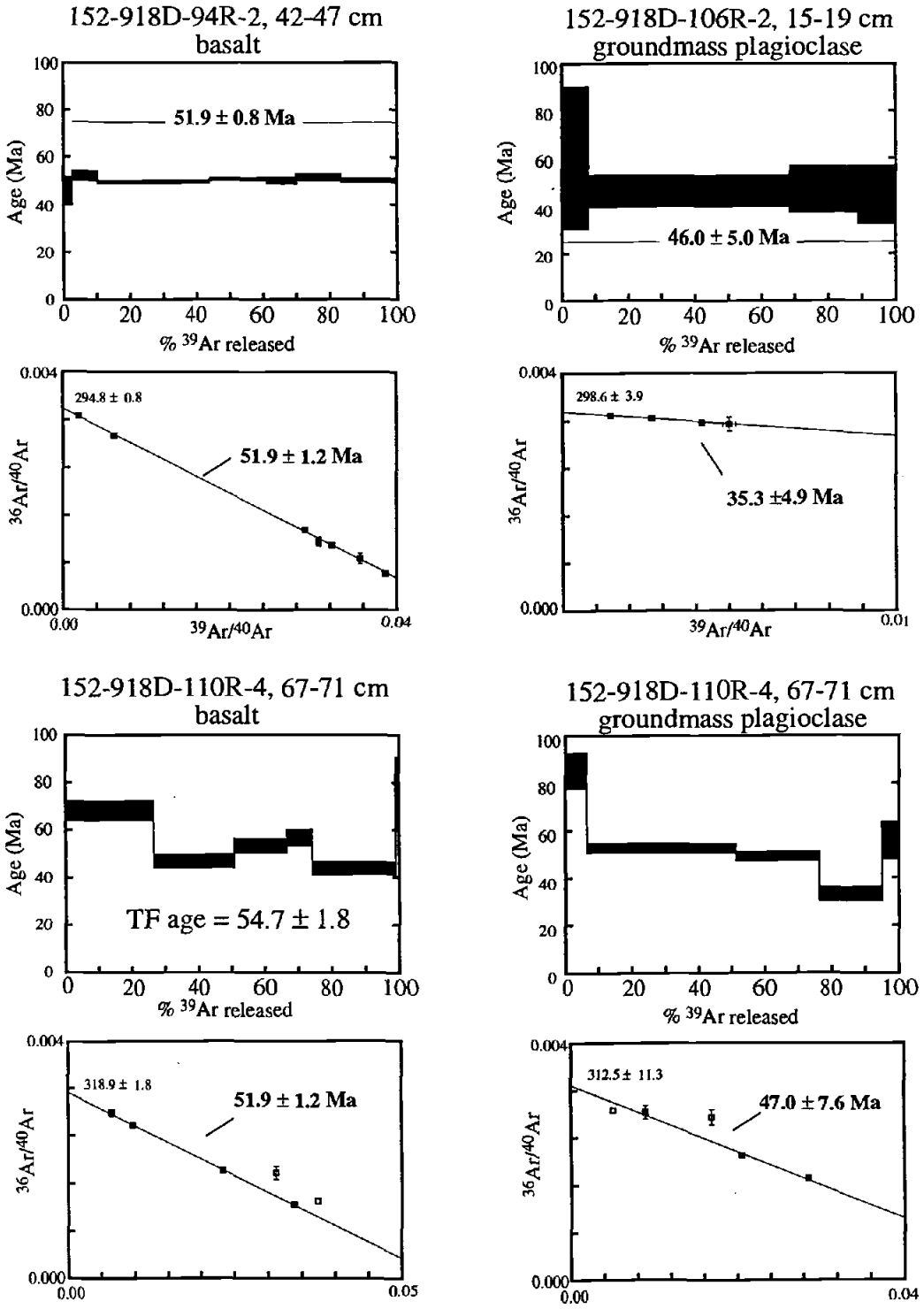

Figure II.5: Step age spectra and isotope correlation diagrams from ^{40}Ar-^{39}Ar incremental heating experiments for Site 918 samples. The thickness of the bar for each step age in the age spectrum indicates the 2σ analytical uncertainty in age.

0.8 and 51.9 ± 1.2 Ma). However, no meaningful results were derived from the whole-rock and groundmass plagioclase analyses of the two deeper basement lavas that were analyzed. The whole-rock analysis of unit 11B (Sample 152-918D-106R-2, 15-19 cm) displayed scattered step ages that reflect an excess ^{40}Ar component (Fig. II.5). The groundmass plagioclase from this sample contained large proportions of atmospheric ^{40}Ar, leading to imprecise ages (plateau age of 46.0 ± 5.0 Ma and an apparent isochron age of 35.3 ± 4.9 Ma). However, these ages are too young given the constraint placed by the age of the overlying sill and the young ages could be due to the effects of alteration.

Analyses of whole-rock and groundmass plagioclase from unit 14 (Sample 152-918D-110R-4, 67-71 cm) yield scattered age spectra (Fig. II.5). The whole rock analysis does not yield a coherent age plateau, though a combined total fusion (TF) age (54.7 ± 1.8 Ma) gives an age that is plausible given the age of the overlying sill. The groundmass plagioclase did not yield a coherent plateau either, though the second step, which had ~45% of the total ^{39}Ar released, has an age of 52.6 ± 2.0 Ma. Isochrons from both the whole rock and groundmass plagioclase can be made from steps that fall in a linear array. However, the resulting ages are too young. In summary, no reliable age information has been obtained from the basement lavas at Site 918.

Rockall Plateau/Hatton Bank

Hole 555

Two of the whole-rock analyses from Hole 555 gave reliable but imprecise ages (Table II.3). Sample 81-555-69-3, 121-129 cm, revealed a good four-step plateau age of 57.6 ± 1.3 Ma and a concordant but imprecise isochron age of 51.6 ± 9.0 Ma. Sample 81-555-90-2, 102-109 cm, gave similar results (plateau 57.1 ± 5.6 Ma; isochron 56.0 ± 5.4 Ma) but less a precise plateau age due to much higher concentrations of atmospheric ^{40}Ar (Fig. II.6).

Hole 553A

The whole-rock analyses from Hole 553A show disturbed age spectra (Fig. II.6). Sample 81-553A-46-3, 116-123 cm, had one large step containing about 70% of the total

Table II.3. ^{40}Ar-^{39}Ar plateau and isochron age calculations from the Hatton Bank, DSDP Leg 81

Core and sample interval (cm)	Material	Plateau Age by $1/\sigma^2$(m.y.)	Plateau Age by $\%^{39}Ar$ (m.y.)	^{39}Ar % of Total	Isochron Age (m.y.)	N	$^{40}Ar/^{36}Ar$ Intercept $\pm 1\sigma$	SUMS/ (N-2)
81-555-69-3, 121-129	basalt	57.6 ± 1.3	58.1 ± 2.4	82	51.6 ± 9.0	4	365.2± 10.8	2.8
81-555-90-2, 102-109	basalt	57.1 ± 5.6	56.7 ± 11.3	88	56.0 ± 5.4	3	300.2± 9.7	0.5

Errors for both step age plateaus and isochrons are reported to 2σ. Ages are corrected for ^{37}Ar decay, half-life = 35.1 days. $\lambda_\varepsilon = 0.581 \times 10^{-10}\ yr^{-1}$; $\lambda_\beta = 4.962 \times 10^{-10}\ yr^{-1}$. N refers to the number of steps used in the isochron calcuation.

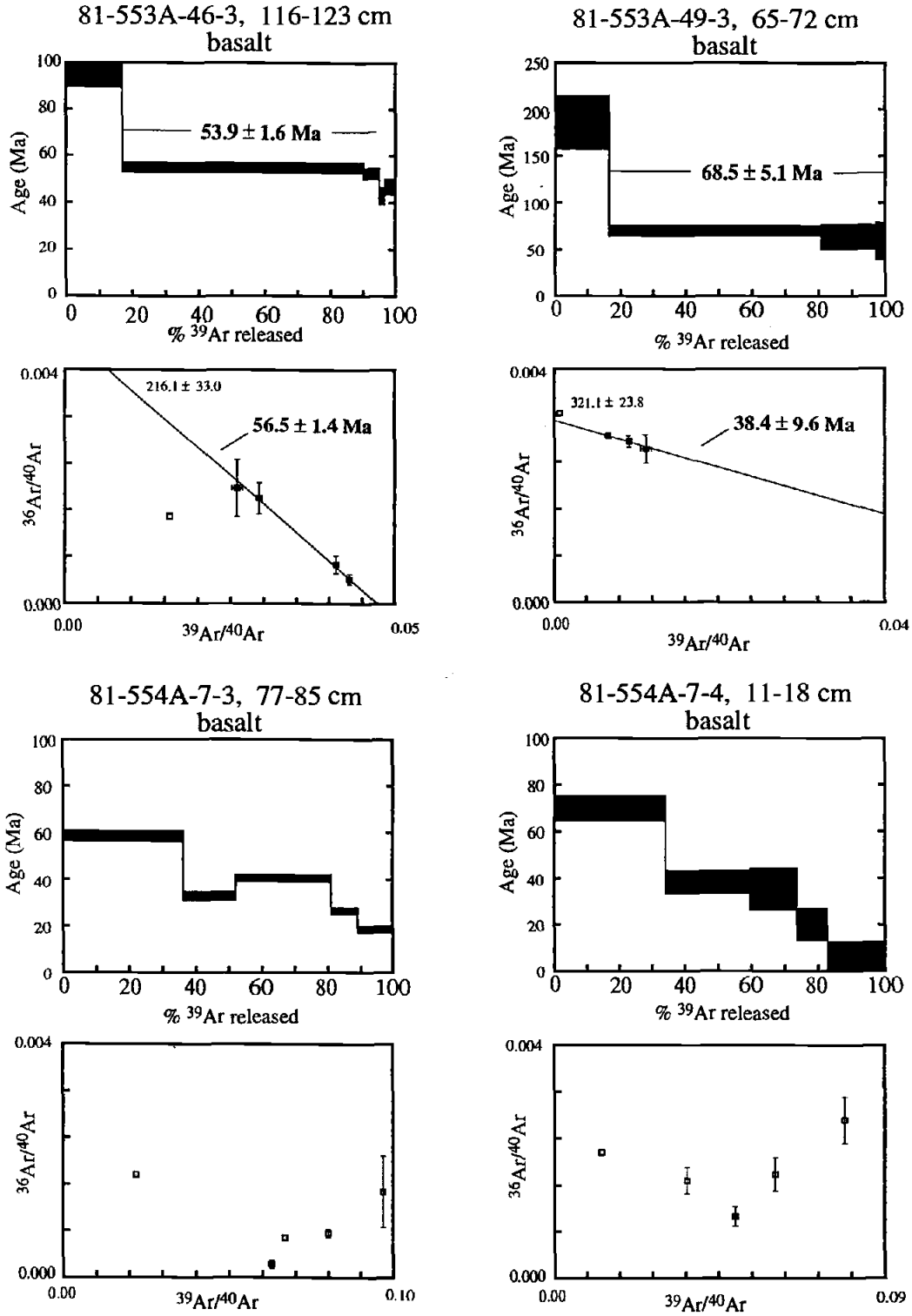

Figure II.6: Step age spectra and isotope correlation diagrams from ^{40}Ar-^{39}Ar incremental heating experiments for DSDP Leg 81. The thickness of the bar for each step age in the age spectrum indicates the 2σ analytical uncertainty in age.

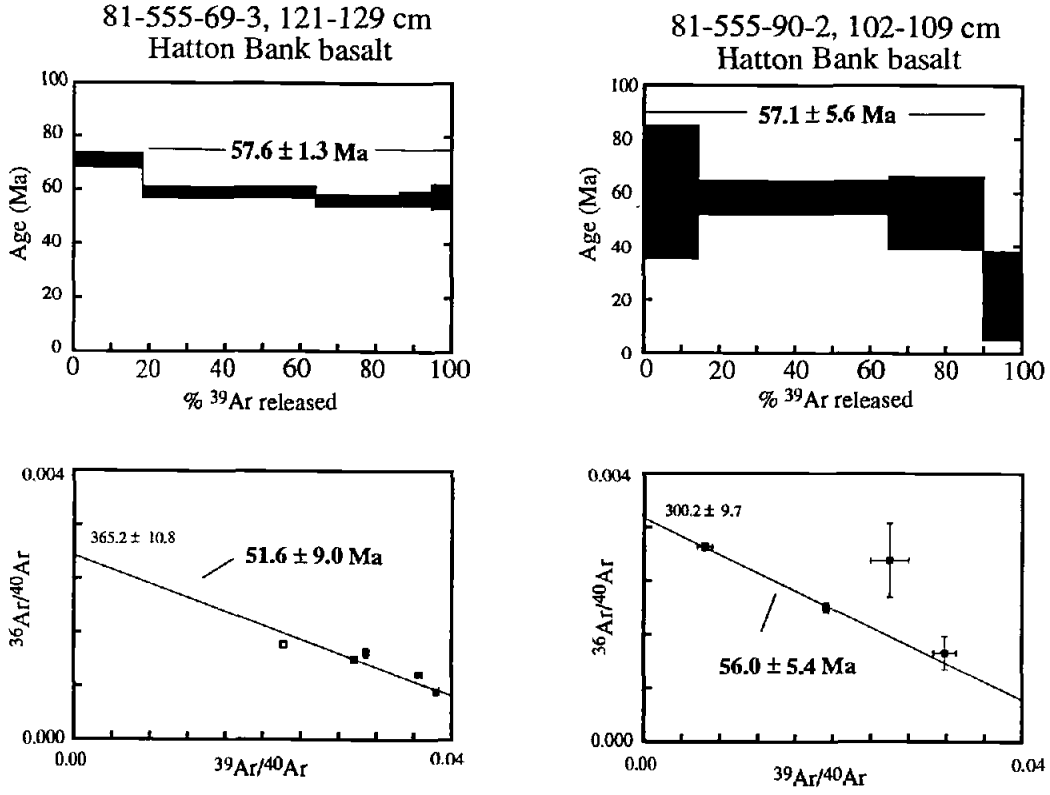

Figure II.6 (cont'd)

^{39}Ar released that has an age of 55.0 ± 2.2 Ma. An isochron made from a regression of four of the roughly linearly aligned data points gave an age of 56.5 ± 1.4 Ma, although the initial $^{40}Ar/^{36}Ar$ intercept (216.1 ± 33.0) is well below the atmospheric ratio, due to the analytical artifact of decreasing age with increasing temperature. These ages may be approximately correct given the age of the intercalated sediments at Site 555 but cannot be considered reliable without further corroboration. Sample 81-553A-49-3, 65-72 cm, gave discordant plateau and isochron ages of 68.5 ± 5.1 Ma and 38.4 ± 9.6 Ma, respectively.

Hole 554A

The whole-rock analyses from Hole 554A demonstrated very disturbed age spectra and no isochron information. The steady decrease in the step ages with increasing temperature is probably due to the effect of ^{39}Ar and ^{37}Ar recoil and redistribution during irradiation. In a fine grained, multi-mineralic matrix, ^{39}Ar can be expelled from higher K_2O, lower temperature sites into adjacent lower K_2O, higher temperature sites (and ^{37}Ar from higher to lower CaO sites). This will result in an age spectrum that displays progressively younger ages with increasing temperature, such as that seen in the sample from Sample 81-554A-7-4, 11-18 cm (Fig. II.6).

Discussion

Southeast Greenland Margin

The results from the ^{40}Ar-^{39}Ar incremental heating experiments show that initial volcanism at the studied portion of the southeast Greenland margin began by 61-62 Ma with the eruption of continentally contaminated lavas and tuffs. However, because no reliable ages were obtained from the Site 917 upper series lavas, the Site 915 lavas, or the Site 918 basement lavas, the complete magmatic history of the area must be constrained indirectly. The 61-62 Ma age of initial volcanism places a maximum age on these intermediate lavas while the 52 Ma age sill at Site 918 is a minimum. What is unknown is whether or not magmatism was continuous between 62 and 52 Ma or if there were significant breaks in volcanism. The sediment horizon that separates the Site 917 middle series and upper series represents a hiatus, but of unknown duration. The change from evolved, continentally-contaminated basalts and dacites to slightly contaminated, more

"oceanic" olivine basalts and picrites (Fitton et al., this volume) also suggests a significant discontinuity. Such a change in volcanism may have required a dramatic change in the configuration of the mantle melting environment and magmatic plumbing system. However, without precise ages for the Site 917 upper series lavas, the duration of the hiatus remains unknown.

The Sites 915 and 918 basement lavas have MORB-like compositions with no evidence of crustal contamination (Fitton et al., this volume). If these reversely magnetized lavas represent the main part of the SDRS, they may have erupted within chron 24R (Larsen, Saunders, Clift, et al., 1995; 53-56 Ma, Berggren et al., in press), as long as 5 m.y. after the eruption of the Site 917 lower and middle series lavas. The last magmatic event in this part of the southeast Greenland margin was the formation of the Site 918 sill at 52 Ma. This age is consistent with the early Eocene age (55-51 Ma) of the surrounding sediments (Larsen, Saunders, Clift et al., 1995). The sill, therefore, places a minimum on the age of submergence.

Rockall Plateau/Hatton Bank

The Leg 81 samples all show disturbed spectra and imprecise ages. Taken together, the results from the two Site 555 lavas and the large age step from one of the Site 553 samples indicate a general eruption age of 55-58 Ma for the southwest Rockall Plateau lavas. These ages are slightly older than the K-Ar ages (52.3 ± 1.7 and 54.5 ± 2.0 Ma) reported by Macintyre and Hamilton (1984). As previously mentioned, the Rockall Plateau lavas have MORB-like compositions (Harrison and Merriman, 1984; Macintyre and Hamilton, 1984), similar to the sites 915 and 918 lavas, and can be grouped as an oceanic series. Because we have been unable to obtain reliable radiometric ages from the Leg 152 oceanic series, we tentatively assign these lavas to the period 58-57 Ma based on the compositional similarities to the Rockall lavas.

North Atlantic Volcanism

The new radiometric ages can be used to better assess the timing of volcanic events associated with the opening of the North Atlantic. In the following section, the

new ages are compared to published ages for other NAVP localities. However, one should bear in mind some potential problems with such a comparison. First, there is a notable lack of reliable radiometric ages for many of the localities. Many of the K-Ar ages show a wide range as a result of alteration and excess ^{40}Ar (e.g., Noble et al., 1988). Comparison of the radiometric ages to age estimates derived from fossil assemblages can be problematic. The numerical age assigned to a specific fossil zone depends on the time-scale that is used. In addition, some of the fossil ages are based on dinoflagellate assemblages correlated to calcareous nannoplankton (NP) zones, which are then in turn correlated to an absolute age scale. This chain of correlations can add significant uncertainty to the accuracy of the age estimate. In this section, the Berggren et al. (in press) timescale is used. However, this timescale does not report NP zones, so to assign a numerical age range to NP zones, the position of the NP zones to the plankton (P) zones of Berggren et al. (1985) are matched to the P zones of the Berggren et al. (in press) timescale.

The 61-62 Ma initial age of volcanism for the southeast Greenland margin is equivalent to the fossil ages derived from sediments between the stratigraphically oldest lavas in West Greenland (Larsen et al., 1992) (Fig. II.7). Initial volcanism in West Greenland was characterized by the eruption of picritic lavas (the Vaigat Formation; Larsen et al., 1992). A nannoplankton assemblage in sediments near the base of the Vaigat Formation corresponds to zone NP3 (Fig. II.7; Perch-Nielsen, 1973; Jürgensen and Mikkelsen, 1974, as cited in Larsen et al., 1992). Dinoflagellate assemblages in sediments associated with the lowest lithostratigraphic member of the Vaigat Formation are interpreted to range in age from latest Early Paleocene to early Late Paleocene (60-61 Ma; Larsen et al., 1992). Radiometric ages of some of the earliest lavas from the British Tertiary Province (Isles of Mull, Muck, and Eigg) are summarized by Musset et al. (1988) and Musset (1986). Four of the early lavas from the Isle of Mull were reliably dated by ^{40}Ar-^{39}Ar, yielding ages that range from 61.1 ± 1.4 Ma to 59.34 ± 0.9 Ma (1σ error) (Mussett, 1986). Early lavas on Muck and Eigg, two small islands north of Mull, are dated by ^{40}Ar-^{39}Ar at 63.0 ± 3.4 and 63.3 ± 1.8 Ma, respectively (1σ error) (Dagley and Mussett, 1986). Thus, initial NAVP volcanism occurred in at least three widespread regions (and maybe more) prior to 60 Ma.

Continental breakup and active plate separation in the North Atlantic occurred well after the initial pulse of magmatism. Sea floor spreading is recorded to have begun by anomaly 24R (53-56 Ma, Berggren et al., in press) and thus postdates the initial

volcanic episode by about 4-5 m.y. Continental breakup occurred simultaneously with magmatism that was centralized along the present margins of the North Atlantic. SDRS lavas associated with this event include the oceanic series from Leg 152, the Leg 81 (Rockall Plateau) lavas, and the Hole 642E (Vøring Plateau) lavas. Subaerially exposed lavas on East Greenland also erupted during the second magmatic episode. The Scoresby Sund area have been radiometrically dated by ^{40}Ar-^{39}Ar incremental heating methods at 56.7 ± 4.3 Ma (2σ error) (Hansen et al., 1993). The most reliable K-Ar ages from the lavas near Kangerdlugssuaq indicate an eruption age of 56-54 Ma (Noble et al., 1988). To the north of Kangerdlugssuaq between 73° and 74°N, lavas from the lower part of the volcanic stratigraphy have ^{40}Ar-^{39}Ar ages of 58-57 Ma (Upton et al., 1995).

A compilation of the new radiometric ages presented here, published NAVP lava ages, and fossil ages of ash layers in sediments in the North Sea (Knox and Morton, 1988; Morton et al., 1988) indicate that the bulk of the province is the product of two distinct pulses of magmatism, one occurring prior to 60 Ma and the other beginning around 57 Ma (Fig. II.7). Although there are reported radiometric ages for intrusions formed during the interval between the two pulses (Mussett et al., 1988), their total volume is relatively minor.

In a pre-drift reconstruction of the North Atlantic (e.g., White, 1992), the initial eruptions occurred up to 2000 km apart. The synchronous formation of the lavas requires a mechanism that induces simultaneous volcanism over a wide area and can produce the high temperature, picritic melts that are observed in West Greenland and in the Site 917 lower series. In addition to being broadly distributed, these early volcanic rocks were erupted in different tectonic settings: West Greenland was adjacent to the opening Northern Labrador Sea (Chalmers, 1991), Southeast Greenland was situated in a previously stable cratonic region (Bridgewater et al., 1976), and the British lavas were erupted into Mesozoic rift basins (Thompson and Gibson, 1991). The widespread initial volcanism from at least these three localities may have been the result of the arrival of the Iceland mantle plume.

A plume impact model (Richards et al., 1989) is one of several geodynamic models for the NAVP that features a central role for the Iceland mantle plume. In this model, the arrival of the Iceland plume head at the base of the lithosphere resulted in widespread volcanism. Another model (White and McKenzie, 1989) proposes that volcanism was promoted by lithospheric thinning, which allowed upwelling and

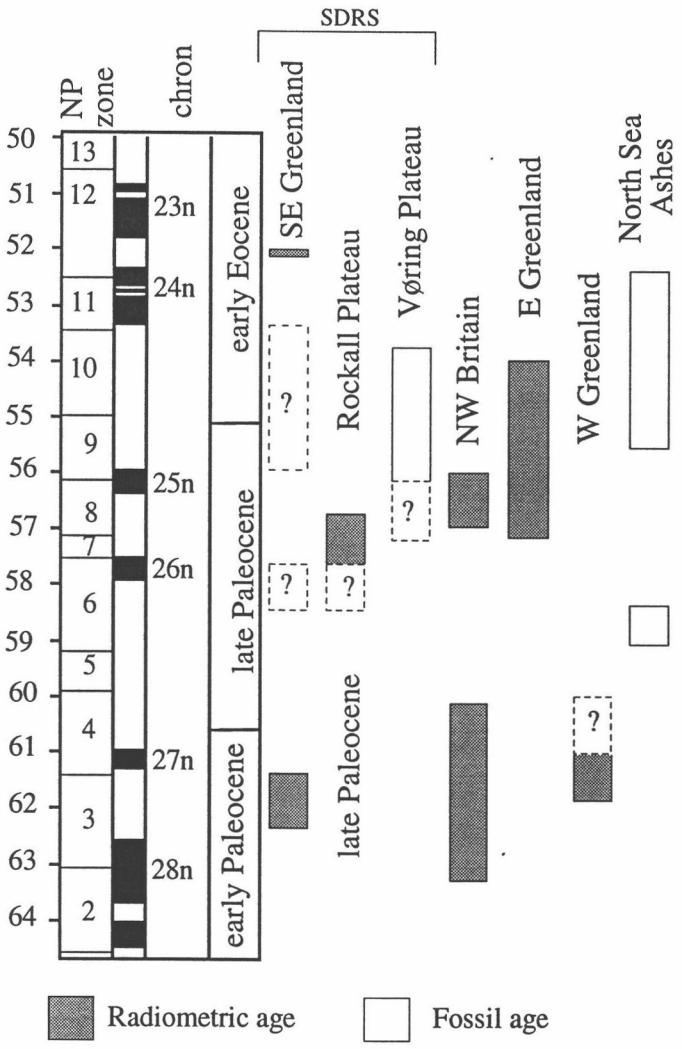

Figure II.7: Compilation of ages for the NAVP. SE Greenland and Rockall Plateau radiometric ages are presented in this paper. Published radiometric ages from West Greenland (Larsen et al., 1992) , East Greenland (Noble et al., 1988; Hansen et al., 1993; Upton et al., 1995) , northwest Britain (Dagley and Mussett, 1986; Mussett, 1986) , the Vøring Plateau (Boulter and Mancum, 1989) , and North Sea sediments (Knox and Morton, 1988; Morton et al., 1988) . We cannot discount older ages in the eastern Atlantic SDRS because the lower lavas were not sampled. The dashed range near 57 Ma for the southeast Greenland SDRS represents our inferred age for the oceanic lava series. The magnetic and numerical timescale is from Berggren et al. (in press) and the NP zones are from Berggren et al. (1985).

decompression melting of asthenosphere previously heated by the "incubated" mantle plume. According to the latter model, the earliest widespread volcanism in West Greenland and the British Isles is attributed to localized rifting when the mantle plume arrived. However, if volcanism at 62-61 Ma were driven by localized lithospheric extension, it is improbable that an area in a previously-formed extensional environment (West Greenland) would experience volcanism at the same time as an area of thick, Archean crust (SE Greenland). We would anticipate that the thick crust would require a substantial period to thin sufficiently to allow asthenospheric upwelling and melting. Therefore, the plume incubation model is not consistent with widespread, pre-rift initial volcanism. A third model asserts that a steady state Iceland mantle plume existed prior to 62 Ma and that the differences in the timing of volcanism (i.e., earlier volcanism in West Greenland relative to East Greenland) are caused by plate motion over the hotspot (Lawver and Müller, 1994). This is inconsistent with widespread (at least 2000 km broad) volcanic centers at 62-61 Ma if the Iceland plume was similar to its present size.

The initial magmatic pulse was limited by the thick continental lithosphere which could have acted as a cap at 62 Ma and prevented initially larger extents of partial melting and volcanism (e.g. Fram and Lesher, 1993). It was not until continental separation allowed upwelling of the mantle (much of it part of the hot plume head) that the second phase of magmatism occurred (White and McKenzie, 1989). This second phase of magmatism was more extensive than the initial pulse and was centralized along the present margins of the North Atlantic.

White (1992) suggested that the northwest-southeast line between West Greenland and northern Britain indicated that the initial plume had the form of a rising sheet. The new data support a general northwest-southeast trend of initial volcanism, but if the plume were a sheet of rising mantle, it was thick and irregularly shaped. Without information about the timing of the initial volcanism in other parts of the NAVP, an analysis of the shape and extent of the initial plume cannot be determined.

Conclusions

Volcanism at the southeast Greenland margin began by 61-62 Ma with the eruption of continentally contaminated lavas. After an apparent hiatus, volcanism resumed with the eruption of lavas with negligible crustal contamination and a more

MORB-like composition. Similar oceanic lavas from the southwest Rockall Plateau, which are just south of the conjugate margin to southeast Greenland, gave imprecise ages of 57-58 Ma. The apparent hiatus in volcanism appears to be widespread in the NAVP, and it is probable that the bulk of the province was formed during two distinct magmatic episodes. The 61-62 Ma initial age of volcanism for the southeast Greenland margin is similar to the age of the older lavas on West Greenland and northwest Britain. We associate this early stage of widespread volcanism with the arrival of the Iceland mantle plume. The later lavas of the SDRS and East Greenland began to erupt at about 57 Ma during plate separation and are the result of lithospheric thinning and creation of oceanic lithosphere from upwelling of anomalously hot asthenospheric mantle.

Chapter III: The Nicoya Peninsula, Costa Rica: A Single Suite of Caribbean Oceanic Plateau Magmas

Abstract

The pre-Tertiary oceanic crust exposed on the west coast of Costa Rica has been broadly referred to as the Nicoya Complex. This project was designed to determine the age of the Nicoya Complex in the Nicoya Peninsula, Playa Jacó, and the Quepos Peninsula using ^{40}Ar-^{39}Ar dating and to determine petrologic relationships between the different localities using major, trace, and Sr-Nd-Pb isotopic data. Radiometric ages of basalts and diabases from the Nicoya Peninsula are 88-90 Ma and two intrusive rocks (a gabbro and plagiogranite) are 84 Ma. The combined geochemical data indicate that the sampled Nicoya Peninsula rocks belong to a single suite related by fractional crystallization of similar parental magmas. Trace element ratios and Nd and Pb isotopic ratios indicate a common mantle source distinct from that for mid-ocean ridge basalts. The Jacó lavas are geochemically similar to the Nicoya Peninsula suite and a single age of 84 Ma is identical to the age of the Nicoya Peninsula intrusives. The one analyzed Quepos basalt has a radiometric age of 60 to 64 Ma and is more enriched in incompatible elements relative to the Nicoya rocks, although similarities in trace element ratios and Nd and Pb isotopic ratios indicate that the Quepos and Nicoya/Jacó lavas were derived from a similar mantle source, possibly the Galapagos hotspot mantle source.

Introduction

Obducted oceanic crust exposed on the west coast of Costa Rica is broadly referred to as the Nicoya Complex (Dengo, 1962) (Fig. III.1). These rocks are composed of intermingled basalts (massive and pillowed flows, dikes, and breccias), gabbros and plagiogranites (e.g., Kuijpers 1980; Alvarado et al. 1993; Denyer and Arias 1993) and are generally limited to coastal peninsulas, such as the Nicoya Peninsula. The full extent of the obducted crust is not precisely known, but it is possible that the Nicoya Complex is part of a belt of accreted Mesozoic oceanic crust that extends through Panama into western Colombia (e.g., Escalante, 1990).

Sediments associated with the mafic rock are restricted to pockets of radiolarite (chert). Based on the fossil ages of the radiolarite, previous workers have divided the rocks into an upper and a lower unit (Schmidt-Effing, 1979; Kuijpers, 1980; Bourgois et al., 1984; Gursky et al., 1984; Wildberg, 1984; Frisch et al., 1992). The lower unit is considered to be normal oceanic crust of Jurassic to early Cretaceous age and the upper unit is a suite of Late Cretaceous basalts subdivided (based on composition) into a suite of Late Cretaceous oceanic rocks associated with the Caribbean oceanic plateau and a primitive arc series (Wildberg, 1984).

The Caribbean oceanic plateau (also called the Caribbean Cretaceous Basalt Province by Donnelly et al., 1990) is composed of the thick oceanic crust that makes up the core of the Caribbean Plate and numerous pieces of obducted oceanic crust along the plate margin (Donnelly et al., 1990). Debatable aspects of the Caribbean plateau include its eruption location (Pacific or in situ) and its tectonic setting (i.e., intraplate or ridge-centered). The pre-existing oceanic lithosphere that purportedly lies beneath the plateau has not yet been definitively identified in any of the on-land exposures nor has it been sampled by deep sea drilling. The exposed oceanic crust in western Costa Rica may play a very important role in understanding the nature of the plateau if indeed the lower series of the Nicoya Complex represents this pre-existing oceanic crust. By evaluating the age and composition of the lavas we may constrain the origin of the plateau. In addition, comparison of the Nicoya Complex to the rest of the Caribbean plateau (including other on-land sections and a limited DSDP Leg 15 samples) will help determine any temporal and spatial variations within the province. This project was designed to 1) determine the radiometric age of rocks from the lower Nicoya series, 2) test the idea of an upper and lower series using ^{40}Ar-^{39}Ar dating and geochemistry, 3) better constrain the nature of the Nicoya rocks with an improved geochemical dataset, and 4) compare the geochemistry and geochronology of the Nicoya rocks to other Caribbean plateau localities. In addition, some samples were collected from Playa Jacó and the Quepos Peninsula for comparison to the Nicoya rocks. I report ^{40}Ar-^{39}Ar ages as well as major, trace, and Sr, Nd, and Pb isotopic data from these three localities. My data show that rocks from the Nicoya Peninsula erupted at 88-90 Ma, which is the age of other on-land Caribbean plateau sites (Chapter VI). The geochemical data, in conjunction with previously published data, show that all of the collected rocks from the Nicoya Peninsula come from a similar mantle source and can be related by fractional crystallization of similar parental melts. Nd and Pb isotopic ratios from a subset of the collected samples are similar and are distinct from normal mid-ocean ridge basalts erupted on the East Pacific Rise. Altogether, my data, combined with

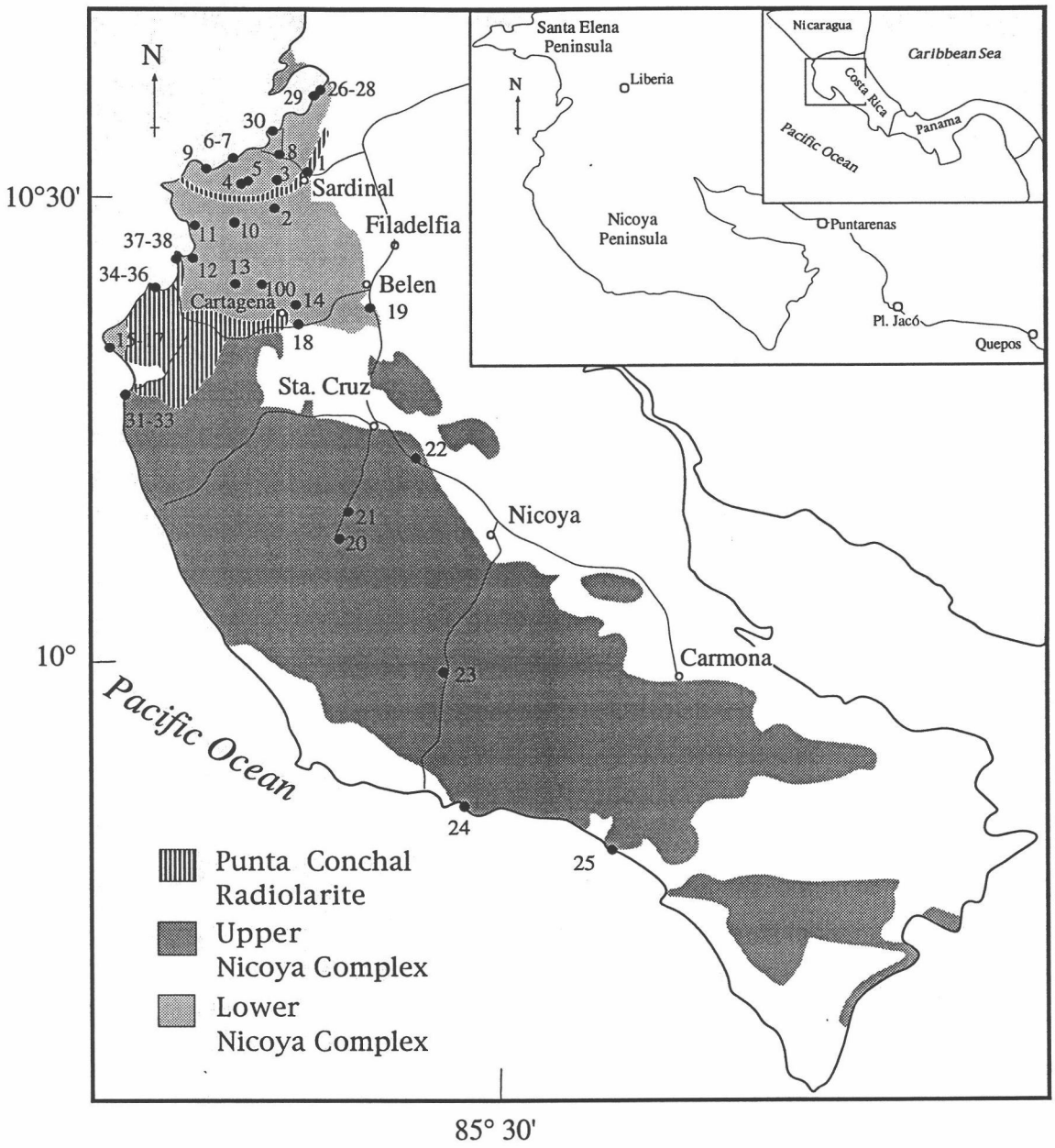

Fig. III.1: Map of western Costa Rica and the Nicoya Peninsula. Sample sites are numberedand are used with the prefix NC93 in the text. The geological units are taken from Gursky et al. (1984).

previously published data, do not support the division of the Nicoya Peninsula igneous rocks into two or more divisions; rather, they appear to be genetically related and are part of the Caribbean oceanic plateau.

Previous Work

The term Nicoya Complex has been used broadly by many authors and generally refers to all oceanic rocks in western Costa Rica Jurassic to Cretaceous age . For clarity, the rocks will be referred to by their locality, so the term Nicoya in this paper will refer to the Nicoya Peninsula (samples designated NC in Table III.1). In addition to the rocks of the Nicoya Peninsula, Nicoya Complex rocks also crop out on the Santa Elena Peninsula (Fig. III.1). The Santa Elena Peninsula is the northernmost section and is composed of serpentinized harzburgite and gabbros cut by dikes (e.g. de Boer 1979). The ultramafic rocks from the Santa Elena Peninsula are regarded as basal to the Nicoya Complex basalts (de Boer, 1979; Azéma and Tournon, 1980), apparently due to the proximity of the two peninsulas. However, the Santa Elena rocks will not be considered in this paper because they were not sampled. Basalts are exposed along the coast to the south of the Nicoya Peninsula at Playa Jacó, Playa Herradura, the Quepos Peninsula, and the Osa Peninsula (Schmidt-Effing, 1979; Berrange and Thorpe, 1988; Frisch et al., 1992).

Donnelly (1994) summarized the previous studies of the Nicoya Complex and noted that there is considerable irregularity in the interpretation of the stratigraphy and origin of the rocks. This likely reflects the deformation and variable alteration experienced by the rocks, uncertainties in their ages, and the inclusion of all mafic and oceanic material in western Costa Rica into a single assemblage. Because this area lies along the margin of the subducting Cocos Plate, several authors have considered the Nicoya Complex an accretionary prism of several slices of oceanic material (Galli-Olivier, 1979; Schmidt-Effing, 1979; Kuijpers, 1980). Most authors agree that the Nicoya Complex of the Nicoya Peninsula can be subdivided into two general units, termed the Matapalo and Esperanza units by Kuijpers (1980) and Bourgois et al. (1984). This division was originally based on fossil age and field observations (Schmidt-Effing, 1979; Baumgartner et al., 1984), though no contact between the two units is observed (Kuijpers, 1980). Kuijpers (1980) considered these two units to be oceanic crust that differed in age and not necessarily in composition. Later studies by Wildberg (1984) and Gursky et al. (1984) referred to these two units as the Lower and Upper Nicoya and separated the units by a radiolarite layer

(Punta Conchal Formation). Although the sketch maps of Kuijpers (1980), Bourgois et al. (1984), and Gursky et al. (1984) generally show the Lower Nicoya/Matapalo unit in the northern part of the Nicoya Peninsula, the coverage for the unit is different in all these maps, reflecting the ambiguity in their division.

Geochemical studies of the Nicoya Complex rocks (Wildberg 1984; Frisch et al. 1992) used these previously described stratigraphic designations as a basis for interpreting their data. Wildberg (1984) interpreted major element and limited rare earth element (REE) and Sr isotopic data as showing at least three rock series: the Lower Nicoya Complex that he correlated to Jurassic-Early Cretaceous MORB and an Upper Nicoya Complex subdivided into MORB-like lavas associated with the Caribbean Plateau and a primitive arc series. Frisch et al. (1992) reported major element and some trace element data as well as paleomagnetic measurements for rocks along most of western Costa Rica. They interpreted their geochemical data as showing MORB, within-plate basalts, and primitive island-arc tholeiites, though these rock types are dispersed throughout the Nicoya Peninsula and do not follow any pre-existing delineations. The assignment of a primitive arc series was based on lower TiO_2 and high $^{87}Sr/^{86}Sr$ in some of the basalts.

Previous radiometric ages (K-Ar) of the Nicoya Peninsula rocks compiled by Alvarado et al. (1993) range from 30-73 Ma, reflecting the effects of alteration and Ar loss and not the actual span of volcanism. There have been several reports of fossil ages from the radiolarite assemblages that occur throughout the peninsula. These assemblages have been assigned ages of Early Jurassic to Late Cretaceous (early Santonian) (Galli-Olivier, 1979; Bourgois et al., 1984; Baumgartner et al., 1984) and are distributed throughout the complex with no apparent correlation to the different stratigraphic units. There are no reported depositional contacts between the radiolarite and the igneous rocks. During my field work, I observed only faulted or igneous (where lavas intrude the radiolarite) contacts. The Nicoya Peninsula igneous rocks are conformably overlain by the Late Campanian to Maastrichtian age Sabana Grande sediments (Bourgois et al., 1984; ~75-70 Ma, Gradstein et al. 1994). This formation appears to have been deposited in deep water and is composed of a sedimentary basalt/radiolarite breccia base overlain by thin siliceous mudstones grading into limestone (Bourgois et al., 1984).

There are no reported radiometric or fossil ages for the Playa Jacó/Herradura rocks. The basalts at Quepos contain Paleocene foraminifera and are overlain by Early Eocene sediments (Schmidt-Effing, 1979; Baumgartner et al., 1984), slightly older than the K-Ar

age of 46.2 ± 4.4 Ma (Appel, 1990 as cited in Alvarado et al., 1992). Berrangé et al. (1989) reported K-Ar ages and summarized the range of fossil ages for sediments associated with the Osa Peninsula rocks. The fossils indicate ages from Jurassic to Eocene, although the K-Ar ages show a range from 78 to 44 Ma.

Sample Descriptions and Mineralogy

Rock samples were collected from the Nicoya Peninsula, Playa Jacó, and Quepos in March of 1993. Sample locations are shown in Fig. III.1 and brief descriptions are given in Table III.1. Sampling was concentrated in the northern Nicoya Peninsula, given the goal of characterizing the Lower Nicoya (Matapalo) unit. The best exposures are along the coast and at roadcuts. However, even at large exposures, stratigraphic information such as bedding or paleohorizontal direction is impossible to determine due to the heavy faulting, surficial weathering, and the often limited outcrop visibility. Some outcrops show spheroidally weathered rocks in which rounded clasts of diabase are found in a matrix of heavily weathered and friable material. This weathering pattern is similar to that seen in massive lava flows of the Columbia River flood basalts. Gabbroic intrusions in the Nicoya Peninsula have variable textures even over a scale of centimeters. Gabbroic samples NC93-14A and -14B were taken only few meters apart yet NC93-14B has twice the crystal size (~1 cm) and 1.5% less MgO compared to NC93-14A . Heavily weathered surfaces obscure the relationship of the two samples. No pillow basalts were observed in the northwestern peninsula during this sampling excursion. Basalts NC93-20 and NC93-21 were taken from Vista al Mar, a ~1000 m high feature apparently composed completely of basalt flows. In the southern part of the peninsula, sample NC93-24 (Playa Carillo) was taken near a volcaniclastic breccia similar to sample NC93-25 (Playa Coyote). At Playa Tamarindo and Punta Sabana, heavily altered dikes penetrate the primary bedding of the radiolarite.

Fractured, massive basalt flows exposed at the northern and southern ends of Playa Jacó were also sampled as well as at a roadcut on the coast road just south of Playa Jacó (Table III.1). All the basalts in Quepos are heavily altered and only three samples were taken from the beach just north of the entrance to Manuel Antonio National Park (Table III.1).

Table III.1: Costa Rica Sample Descriptions

Sample	Location description	Rock Type	Condition
NC93-1	Exposed hillside, Rta. 151 just N of Sardinal, spheroidal blocks in weathered matrix	diabase	plag 50% replaced by clays
NC93-2	Massive basalt in Río Brasil, Pilas	med. grain basalt	slight alteration, moderate alteration near qtz veins
NC93-3	Exposed hill near roadside, 2 km W of Sardinal	med-fine grain basalt	slight alteration, plag 0-10% replaced by clays
NC93-4	Massive basalt in small creek bed, N side of Cerro Volcán, many qtz veins	diabase	heavily altered, plag 100% replaced, some relict cpx
NC93-5	Exposure on hillside near trail to Cerro Volcán, spheroidal blocks in fractured matrix.	diabase	heavily altered, similar to NC93-4
NC93-6	Coastal exposure, S end of Punta Cirial	plagiogranite	heavily altered, plag completely replaced by albite + clays
NC93-7	Coastal exposure, S end of Punta Cirial	diabase	heavily altered, some relict cpx
NC93-8	Quarry at Pl. Hermosa/Pl. del Coco road fork, spheroidal blocks	diabase	mod. alteration, 50% plag replaced by clays, qtz veins
NC93-9	W end of Pl. Matapalo, cliff of massive basalt, highly fractured and veined	diabase	holocrystalline, light alteration
NC93-10	Roadcut, Cuesta Nuevo Colón, gabbro in faulted contact with basalt	plagiogranite	heavily altered, plag completely replaced by albite + clays
NC93-11	Small roadcut across from entrance to Hotel Pl. Azucar, spheroidal blocks	med. grain basalt	slight alteration, plag 10% replaced by clays
NC93-12	Flat-lying outcrop in field N of Cerro Brasilar near Pl. Potrero, massive, gabbroic	plagiogranite	heavily altered
NC93-13	Roadcut 3 km north of Tempate	diabase	slight alteration, some plag cores beginning to alter to clays
NC93-14	N of El Edén, follow Quebrada Salto to hill where rock exposed, great variation in grain size over short distance, with contact unknown	(a) diabase (b) coarse gabbro	(a) slightly altered, similar to NC93-13 (b) heavily altered, plagioclase almost completely replaced though some primary twinning seen, graphic qtz-plag
NC93-15	Coastal exposure, N of Pta. Carbón, S base of Cabo Velas	Fe-rich gabbro	heavily altered, plag replaced by albite + clay, px with fractured texture altering to secondary oxides
NC93-16	Coastal exposure, N of Pta. Carbón, S base of Cabo Velas	gabbro	plag 75-100% replaced by clays, cpx relatively fresh, some qtz + clay veins
NC93-17	Pta. Carbón	gabbro	variably altered, plag 25-100% replaced, some qtz veins
NC93-18	Quarry 2 km west of Coyolito, overlain by radiolarite, contact inaccessible	med. grain basalt	light alteration, some qtz veins
NC93-19	Quarry off Rta. 21, S end of Palestina	basalt	no thin section, but heavily altered in hand sample
NC93-20	Roadcut at top of Vista al Mar	fine grain basalt	light to mod. alteration
NC93-21	Roadcut between Vista al Mar and Santa Cruz	med.-fine grain basalt	light alteration
NC93-22	Roadcut between Sta. Cruz and Nicoya	basalt	seriate texture, variably altered, plag 0-50% replaced by clays, some calcite veins
NC93-23	Roadcut between Belen and Cuesta Grande, 15-20 m high	fine grain basalt	plag 100% replaced, some calcite veins

Table III.1 (cont'd)

Sample	Location description	Rock Type	Condition
NC93-24	S end of Pl. Carillo, outcrop of basalt, basaltic breccia and siltstone, basalt in faulted contact with basaltic breccia containing fragments of basalt and radiolarite, overlain by siltstone	med. grain basalt	variably altered, 25-100% plag replacement, some qtz veinlets
NC93-25	Cliff at N end of Pl. Coyote (Pta. Bejuca)	breccia	diabasic textured clasts in fine matrix, heavily altered, plag replaced by clays, cpx replaced by oxides and amphibole
NC93-26	Coastal exposure, S of Pl. Monte del Barco (N of Pl. Panama)	plagiogranite	heavily altered, plag replaced by albite + clay, px with fractured texture altering to secondary oxides
NC93-27	Coastal exposure, S of Pl. Monte del Barco	plagiogranite	same as NC93-26
NC93-29	Pta. Arenilla, N of Pl. Panama	diabase	variably altered, plag 25-90% replaced, higher degree of alteration near fractures and veins
NC93-30	S end of Pl. Hermosa	basalt	heavily fractured and cut by veins, no primary plag, some relict cpx
NC93-31	S end of Pl. Tamarindo, overlain by coarse carbonate ss (qtz, basalt pebbles, shells, and radiolarite clasts; Sabana Grande formation), radiolarite intruded by dike	dike basalt	heavily altered
NC93-32	S end of Pl. Tamarindo	gabbro,	variably altered, plag 25-100% replaced
NC93-33	S end of Pl. Tamarindo	gabbro	variably altered, heavily cut by qtz veinlets
NC93-34	N. side of Punta Sabana, flat-lying and cliff-exposed basalt/diabase and radiolarite, basalt in igneous and fault contact w/ radiolarite, radiolarite (red and gray/white) cut by dikes	diabase	light alteration, plag 0-25% replaced by clays
NC93-35	N. side of Punta Sabana	diabase	light alteration
NC93-36	N. side of Punta Sabana	diabase	light alteration, plag generally prisitine
NC93-37	S base of Pta. Salinas, high cliffs of diabas/gabbro, radiolarite at top of cliff	gabbro	variably altered, plag 25-5% replaced
NC93-38	S base of Pta. Salinas	diabase	light alteration
NC93-100		cumulate gabbro	10-20 mm plag, 5-10 mm cpx, fresh, 1-2 mm pseudomorphs of olivine in diabasic matrix
JC93-1	Roadcut 1.2 km S of last entrance to Pl. Jacó, massive, fractured basalt, no seds, 20 m high	med. grain basalt	variably altered
JC93-2	S end of Pl. Jacó, massive, sample from inside fractured block	basalt	heavily altered
JC93-3	N end of Pl. Jacó Basalt crops out on cliffs and flat lying on beach, similar to S end	basalt	variahly altered, plag 25-100% replaced, heavy veinlet penetration
QP93-1	S end of beach #1, basalt in cliff and large "islands" on beach, massive with columnar joints, some alteration and veins	fine grain basalt	mod. alteration, rare partially resorbed plag phenocrysts
QP93-2	Cliff near S end of beach	fine grain basalt	heavily altered

Thin sections were made for all of the samples in order to determine their mineralogy and suitability for geochemical and geochronological analyses. The rocks were classified into five categories based on petrographic observations: basalt, basaltic breccia, diabase, gabbro, and plagiogranite. Basaltic samples are fine grained and aphyric and consist of plagioclase, pyroxene, Fe-Ti oxides, and altered mesostasis. Only one basaltic breccia was collected (NC93-25), and it is composed of a heavily altered matrix surrounding heavily altered basalt clasts. Diabasic samples have the same mineralogy as the basalts except that they are holocrystalline, are coarser grained, and have trace amounts of tabular apatite. Spheroidally weathered samples are usually diabasic in texture. Gabbroic samples have the same mineralogy as the basalts and diabases, but have grain sizes up to 5 mm. The plagiogranites all have coarse textures and are composed of plagioclase, quartz, greenish clinopyroxene (hedenbergite), and Fe-Ti oxides. The plagioclase and quartz often occur together in a myrmekitic texture. The cumulate gabbro (NC93-100) contains large (~4 cm diameter) unzoned plagioclase (An_{85-86}; Table III.2), clinopyroxene (En_{51}; Table III.3), and trace olivine (completely replaced by iddingsite) set in a diabasic matrix of plagioclase, clinopyroxene, and Fe-Ti oxides.

The rocks show varying degrees of alteration with most samples having relatively pristine pyroxene and relatively pristine to partially altered plagioclase (to colorless clays). In the basalts, the mesostasis has altered to chlorite and small secondary oxides. Small veins of prehnite and rare calcite are found in most of the samples and the density of veins correlates with the general degree of alteration. The most altered sample is the basaltic breccia (NC93-25) in which only small pieces of primary clinopyroxene remain. The plagiogranites are all moderately to heavily altered such that the plagioclase has been completely replaced by albite and clays and primary twinning is rarely visible.

Table III.2: Nicoya Peninsula Plagioclase Analyses

	Na_2O	MgO	Al_2O_3	SiO_2	K_2O	CaO	FeO	Total	% An
Plagiogranite									
NC93-15	8.90	0.00	22.38	65.16	0.07	2.86	0.19	99.55	15.0
NC93-15	7.78	0.00	24.77	61.39	0.10	5.70	0.28	100.02	28.7
NC93-15	9.90	0.01	21.11	66.54	0.05	1.61	0.10	99.31	8.2
NC93-15	11.29	0.00	20.37	68.16	0.06	0.24	0.06	100.18	1.2
NC93-15	11.18	0.00	19.81	66.76	0.05	0.31	0.01	98.12	1.5
NC93-15	9.96	0.00	22.30	63.59	0.12	3.53	0.13	99.63	16.3
NC93-27	6.12	0.00	26.62	58.36	0.08	8.64	0.39	100.21	43.6
NC93-27	6.45	0.01	26.06	58.62	0.07	8.05	0.39	99.64	40.6
NC93-27	8.90	0.01	22.94	62.50	0.08	4.30	0.15	98.89	21.0
NC93-27	5.98	0.02	26.49	59.38	0.06	8.12	0.35	100.39	42.7
NC93-27	6.77	0.00	26.01	58.89	0.10	7.21	0.31	99.29	36.8
NC93-27	8.00	0.02	23.74	60.19	0.11	5.37	0.22	97.64	26.9
NC93-26	10.60	0.02	20.64	66.10	0.06	1.27	0.11	98.80	6.2
NC93-26	10.70	0.00	20.60	66.42	0.04	1.11	0.09	98.95	5.4
NC93-26	9.96	0.02	21.52	64.45	0.11	2.47	0.08	98.61	12.0
NC93-26	11.72	0.00	19.82	67.04	0.05	0.17	0.01	98.80	0.8
NC93-26	11.44	0.01	19.84	66.41	0.07	0.35	0.09	98.21	1.7
NC93-10	9.83	0.01	20.68	65.83	0.29	1.29	0.08	98.01	6.6
NC93-10	10.78	0.01	20.81	66.25	0.13	1.23	0.06	99.27	5.9
NC93-10	10.48	0.01	20.25	67.46	0.40	0.72	0.11	99.44	3.6
NC93-10	10.08	0.00	21.02	67.36	0.65	1.25	0.07	100.43	6.2
NC93-10	10.08	0.01	20.45	67.56	0.12	0.67	0.16	99.05	3.5
NC93-10	10.00	0.04	20.52	67.90	0.25	0.80	0.13	99.63	4.1
Gabbro									
NC93-14B	3.98	0.16	29.01	54.13	0.03	12.12	0.69	100.11	62.6
NC93-14B	4.52	0.18	29.00	52.26	0.04	12.46	0.59	99.05	60.2
NC93-14B	10.51	0.00	20.25	66.23	0.28	1.10	0.19	98.56	5.4
NC93-14B	9.79	0.00	21.19	65.19	0.44	2.10	0.25	98.96	10.3
NC93-14B	9.76	0.00	21.34	64.77	0.38	2.42	0.21	98.89	11.8
NC93-14B	8.46	0.06	23.64	61.70	0.06	5.08	0.28	99.28	24.8
NC93-14B	7.97	0.11	24.10	60.22	0.07	5.27	0.37	98.10	26.7
Cumulate Gabbro									
NC93-100	1.65	0.20	33.17	46.62	0.00	17.47	0.48	99.58	85.4
NC93-100	1.55	0.23	33.38	46.31	0.02	17.55	0.48	99.52	86.1
NC93-100	1.52	0.18	33.61	45.99	0.01	17.78	0.51	99.60	86.6
NC93-100	1.71	0.23	33.35	46.46	0.03	17.58	0.46	99.81	84.9
NC93-100	1.69	0.22	33.48	46.66	0.01	17.42	0.49	99.95	85.0
NC93-100	1.73	0.22	33.32	46.44	0.02	17.43	0.48	99.64	84.7
NC93-100	1.66	0.22	33.40	46.58	0.01	17.33	0.48	99.68	85.1

Beam current 30 nA and accelerating voltage 15 kV. 10 s counting times for all elements. See Appendix 4 for standard analyses.

Table III.2 (cont'd)

	Na_2O	MgO	Al_2O_3	SiO_2	K_2O	CaO	FeO	Total	% An
Diabase									
	core								
NC93-36	1.66	0.07	33.71	46.76	0.01	17.63	0.88	100.71	85.41
	2.33	0.06	33.01	48.35	0.02	16.27	0.87	100.91	79.29
	5.73	0.06	27.72	56.14	0.07	10.03	0.58	100.33	48.95
	3.92	0.14	30.25	52.02	0.05	13.36	0.85	100.60	65.16
	rim								
NC93-36	3.32	0.13	30.76	50.65	0.02	14.36	1.02	100.26	70.43
	6.00	0.03	27.16	57.13	0.11	9.37	0.86	100.66	46.04

Table III.3: Nicoya Peninsula Pyroxene Analyses

	MgO	Al_2O_3	SiO_2	CaO	MnO	FeO	TiO_2	Cr_2O_3	Total	% En	% Fs	% Wo
Plagiogranite Clinopyroxene												
NC93-6	1.07	0.21	48.11	19.32	0.78	27.74	0.05	–	100.28	3.5	51.0	45.5
NC93-6	0.65	0.18	47.30	20.32	0.86	28.45	0.01	–	100.14	2.1	51.1	46.8
NC93-6	0.60	0.12	48.11	20.20	0.76	28.34	0.02	–	100.62	1.9	51.3	46.8
NC93-15	1.48	0.27	48.53	20.19	0.82	26.77	0.06	–	100.80	4.8	48.4	46.8
NC93-15	1.17	0.36	48.20	19.82	0.67	26.67	0.10	–	99.79	3.8	49.3	46.9
NC93-15	1.41	0.29	47.68	20.02	0.84	26.52	0.10	–	99.55	4.6	48.5	46.9
NC93-15	2.26	0.27	48.03	20.54	1.46	24.82	0.07	–	100.19	7.3	45.0	47.7
NC93-15	2.03	0.22	47.60	20.10	1.14	26.21	0.02	–	100.16	6.5	47.2	46.3
NC93-15	2.32	0.21	47.47	20.75	1.45	24.52	0.03	–	99.44	7.5	44.4	48.1
NC93-15	1.81	0.40	48.39	19.28	1.04	25.54	0.10	–	100.35	6.0	47.8	46.2
NC93-15	2.02	0.31	48.81	19.85	0.91	25.50	0.07	–	100.60	6.6	46.8	46.6
NC93-27	6.13	0.13	50.06	21.39	0.53	20.46	0.04	–	100.96	18.6	34.8	46.6
NC93-27	5.99	0.19	49.87	20.45	0.64	20.51	0.04	–	100.27	18.6	35.7	45.6
NC93-27	5.62	0.11	49.98	20.95	0.62	21.40	0.03	–	100.96	17.2	36.7	46.1
NC93-27	8.88	1.07	50.16	14.67	0.56	23.71	0.63	–	101.87	27.1	40.6	32.2
NC93-27	9.06	1.08	49.92	14.72	0.53	23.64	0.63	–	101.76	27.5	40.3	32.2
NC93-27	9.45	1.03	49.39	13.18	0.69	24.94	0.64	–	101.51	28.7	42.5	28.8
Cumulate Gabbro Clinopyroxene												
NC93-100	16.63	2.85	52.24	20.11	0.14	6.40	0.49	–	101.18	48.0	10.4	41.7
NC93-100	16.93	2.82	52.46	20.11	0.19	6.39	0.47	–	101.72	48.4	10.3	41.3
NC93-100	16.87	2.90	52.05	19.88	0.18	6.33	0.50	–	101.09	48.6	10.2	41.2

Table III.3 (cont'd)

	MgO	Al_2O_3	SiO_2	CaO	MnO	FeO	TiO_2	Cr_2O_3	Total	% En	% Fs	% Wo
Diabase Clinopyroxene												
	Cr-rich augite core											
NC93-36	17.86	3.17	52.07	19.80	0.14	5.77	0.21	0.65	99.83	50.6	9.2	40.3
NC93-36	17.54	2.14	52.68	18.16	0.27	8.73	0.32	0.37	100.41	49.4	13.8	36.8
NC93-36	17.72	2.16	53.08	20.25	0.15	6.37	0.29	0.27	100.45	49.4	10.0	40.6
NC93-36	17.89	3.02	52.76	20.64	0.13	4.86	0.21	0.74	100.41	50.5	7.7	41.8
	Cr-poor rim											
NC93-36	13.16	1.18	51.14	16.68	0.42	17.40	0.60	0.00	100.78	37.7	28.0	34.3
NC93-36	13.57	1.55	50.96	15.90	0.33	16.49	0.65	0.01	99.65	39.6	27.0	33.4
	Cr-poor core											
NC93-36	17.83	2.06	53.05	19.87	0.20	7.49	0.32	0.05	101.04	49.1	11.6	39.3
NC93-36	17.38	1.80	52.70	18.26	0.27	9.01	0.36	0.03	99.99	48.9	14.2	36.9
NC93-36	17.77	1.75	53.08	19.04	0.19	7.82	0.32	0.02	100.15	49.6	12.2	38.2
Diabase Pigeonite												
	Core											
NC93-36	25.70	1.22	54.37	4.66	0.37	14.27	0.20	0.04	100.88	69.4	21.6	9.0
NC93-36	25.08	1.22	54.54	5.49	0.35	14.02	0.21	0.00	100.96	68.0	21.3	10.7
NC93-36	26.14	0.74	55.13	3.64	0.29	14.56	0.13	0.01	100.70	70.8	22.1	7.1
	Fe-rich rim											
NC93-36	13.04	0.50	50.21	3.98	0.86	31.14	0.25	0.00	100.02	39.1	52.4	8.6
NC93-36	12.84	0.49	50.18	4.12	0.77	31.57	0.25	0.01	100.28	38.3	52.9	8.8
NC93-36	10.96	0.28	49.49	3.41	0.86	34.84	0.16	0.00	100.04	33.3	59.3	7.4

Beam current set at 50 nA and accelerating voltage of 15 kV. Analyses are single points with 10 s counting time for all elements except 20 s for Fe.

Results

Geochronology

Age determinations for whole-rock and plagioclase separates from the least altered samples were performed at Oregon State University using standard ^{40}Ar-^{39}Ar incremental heating techniques (Duncan and Hargraves, 1990; Duncan and Hogan, 1994). Whole-rock samples were either crushed in bulk in a ceramic jaw crusher and sieved to a uniform 0.5-1mm grain size or made into mini-cores. Plagioclase crystals were magnetically separated from diabase, gabbro, and plagiogranite samples, checked for purity under a binocular microscope, and washed for 30 sec in 5% HF. All samples were ultrasonically cleaned in distilled water. Samples were sealed in evacuated quartz glass vials and irradiated for 6 hours at the OSU TRIGA nuclear reactor facility. Neutron flux during irradiation was monitored by FCT-3 biotite (27.7 Ma, Hurfurd and Hammerschmidt 1985). Ar isotopes of the crushed whole rock samples and some of the plagioclase separates (~500 mg) were determined using an AEI MS-10S mass spectrometer. The mini-cores and the other plagioclase separates (~100 mg) were analyzed using an MAP 215-50 mass spectrometer.

Individual ages for each ^{40}Ar-^{39}Ar temperature step were calculated after corrections for background, mass fractionation, and isotopic interferences and atmospheric argon contamination ($^{40}Ar/^{36}Ar = 295.5$). Step heating results are detailed in Appendix 2. From the heating steps, age spectrum diagrams (age vs. % ^{39}Ar released) were generated (Fig. III.2). Plateau ages were calculated from consecutive steps that are concordant within 1σ error using the procedure described in Dalrymple et al. (1988), in which step ages were weighted by the inverse of their variance (Table III.4). Isotope correlation diagrams ($^{36}Ar/^{40}Ar$ vs. $^{39}Ar/^{40}Ar$) were also made for each analysis, in which the slope is proportional to the age (isochron) and the inverse of the y-intercept gives the initial $^{40}Ar/^{36}Ar$ composition. The isochron ages are calculated using the same steps used in the plateau ages.

I define a reliable age, i.e., one that is representative of the crystallization age, based on the criteria of Pringle (1993):

1) A well-defined age spectrum plateau of at least three concordant consecutive steps that represents at least of 50% of the total ^{39}Ar released.

2) An isochron age concordant with the plateau age and with an F-distribution (for the parameter SUMS/N-2) below the cutoff value at the 95% confidence level.

3) The $^{40}Ar/^{36}Ar$ intercept is statistically indistinguishable from the atmospheric value 295.5.

The SUMS/N-2 cutoff values are taken from Table 2 of Pringle (1993). For three, four, and five point isochrons, the cutoff values are 3.84, 3.00, and 2.60, respectively.

Nicoya Peninsula

Many of the samples displayed erratic step ages such that no age plateaus or isochrons could be discerned. This can be attributed to a combination of alteration and the low K_2O contents of the rocks. Some of the plagioclase separates (NC93-36 and NC93-9) gave step ages that increased with increasing temperature, up to 180 Ma. Evidently they contained some component of excess radiogenic ^{40}Ar of which even small amounts can produce erroneous ages, given the low K_2O content of these rocks. The altered plagioclase separates from the plagiogranite samples gave non-concordant step ages that were usually less than 80 Ma. In this section, I report only the results from the samples that yielded reliable crystallization ages (Table III.4).

Of thirteen analyzed samples from the Nicoya Peninsula, seven gave reliable crystallization ages (Fig. III.2). Five (four basalts and one diabase) gave plateau ages from 88.0 to 92.5 Ma (a weighted mean of the ages is 88.5 Ma). Plagioclase separates from a gabbro (NC93-14B) and a plagiogranite (NC93-26) gave statistically indistinguishable plateau ages of 83.8 ± 1.1 Ma and 83.2 ± 1.3, respectively. The significantly lower ages of the intrusive rocks relative to the analyzed basalts and diabase suggest that an intrusive event occurred after initial basalt eruptions.

Jacó

One of two analyzed basalts from Jacó (JC93-1) yielded a reliable crystallization age with a three-step (of four) plateau of 84.2 ± 1.8 Ma, an isochron of 83.4 ± 2.5 Ma, and an initial $^{40}Ar/^{36}Ar$ ratio of 295.6 ± 6.9 (Fig. III.2). The lower initial step indicates some radiogenic ^{40}Ar loss from less retentive sites. The consistent plateau and isochron age of this sample indicate a volcanic event younger than the eruption of the Nicoya Peninsula basalts but perhaps related to the intrusions.

Table III.4: ^{40}Ar-^{39}Ar Plateau and Isochron Age Calculations for Basaltic Rocks from the Nicoya Complex, Costa Rica

Sample	Material	Plateau Age by $1/\sigma^2$(m.y.)	^{39}Ar % of Total	Isochron Age (m.y.)	N	$^{40}Ar/^{36}Ar$ Intercept ± 1σ	SUMS/ N-2
Nicoya Peninsula basalt and diabase							
NC93-2	whole rock	90.3 ± 3.2	100	87.8 ± 0.3	4	296.3 ± 2.6	1.00
NC93-3	whole rock	92.5 ± 5.4	100	86.8 ± 7.4	5	302.0 ± 6.6	0.52
NC93-18	whole rock	89.7 ± 1.7	100	92.3 ± 3.0	5	294.0 ± 4.4	0.47
NC93-20	whole rock	89.9 ± 2.8	100	85.9 ± 3.3	5	299.7 ± 6.7	0.16
NC93-34	whole rock	88.0 ± 0.7	97	86.4 ± 1.3	5	308.1 ± 5.5	0.29
Nicoya Peninsula Intrusives							
NC93-14B	plagioclase	83.8 ± 1.1	100	80.9 ± 1.1	7	301.5 ± 1.1	2.00
NC93-26	plagioclase	83.2 ± 1.3	100	83.2 ± 2.0	7	295.2 ± 2.3	2.2
Playa Jacó							
JC93-1	whole rock	84.2 ± 1.8	92	83.4 ± 2.5	3	295.6 ± 6.9	0.08
Quepos							
QP93-1	whole rock	63.9 ± 0.5	51	60.1 ± 0.7	3	376.7 ± 20.7	0.08

Ages calculated using the following decay constants: $\lambda_\varepsilon = 0.581 \times 10^{-10}\ yr^{-1}$, $\lambda_\beta = 4.963 \times 10^{-10}\ yr^{-1}$. Isotopic interferences for the OSU TRIGA reactor are: $(^{36}Ar/^{37}Ar)_{Ca} = 2.64 \times 10^{-4}$, $(^{39}Ar/^{37}Ar)_{Ca} = 6.73 \times 10^{-4}$, and $(^{40}Ar/^{39}Ar)_K = 1.00 \times 10^{-3}$

Fig. III.2: Plotted step age spectra and isotope correlation diagrams for each ^{40}Ar-^{39}Ar analysis from Costa Rica. The length of each step age refers to the fraction of the total ^{39}Ar released and the thickness of the step is the $\pm 1\sigma$ error. The horizontal lines adjacent to the plateau age indicate the steps used in the age calculation. The filled squares in the correlation diagrams were used in a weighted linear regression to obtain an isochron age. The inverse of the y-intercept of the regression gives the initial $^{40}Ar/^{36}Ar$ ratio.

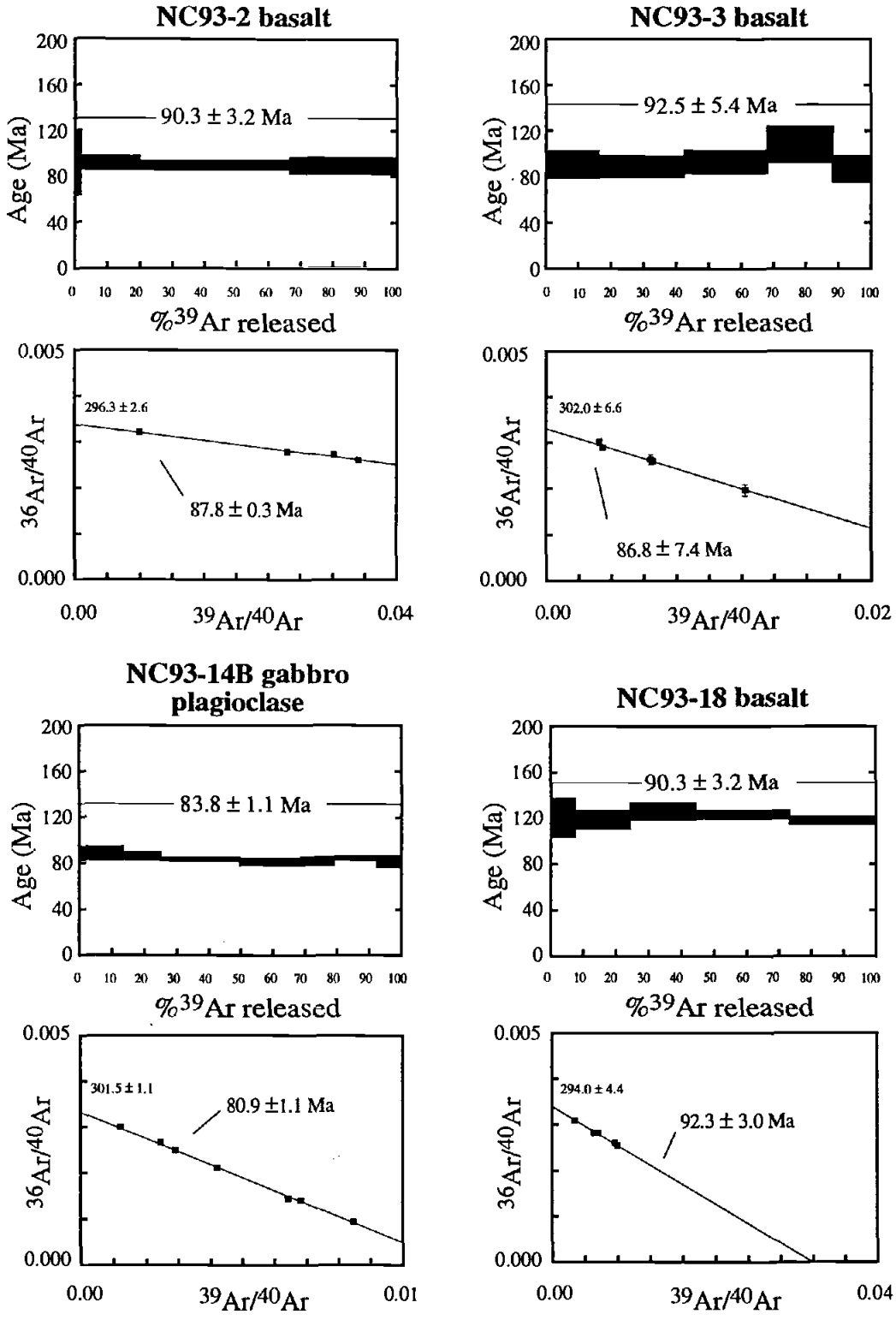
NC93-2 basalt
90.3 ± 3.2 Ma
Age (Ma)
%39Ar released
296.3 ± 2.6
87.8 ± 0.3 Ma
36Ar/40Ar
39Ar/40Ar
NC93-3 basalt
92.5 ± 5.4 Ma
302.0 ± 6.6
86.8 ± 7.4 Ma
NC93-14B gabbro plagioclase
83.8 ± 1.1 Ma
301.5 ± 1.1
80.9 ± 1.1 Ma
NC93-18 basalt
90.3 ± 3.2 Ma
294.0 ± 4.4
92.3 ± 3.0 Ma

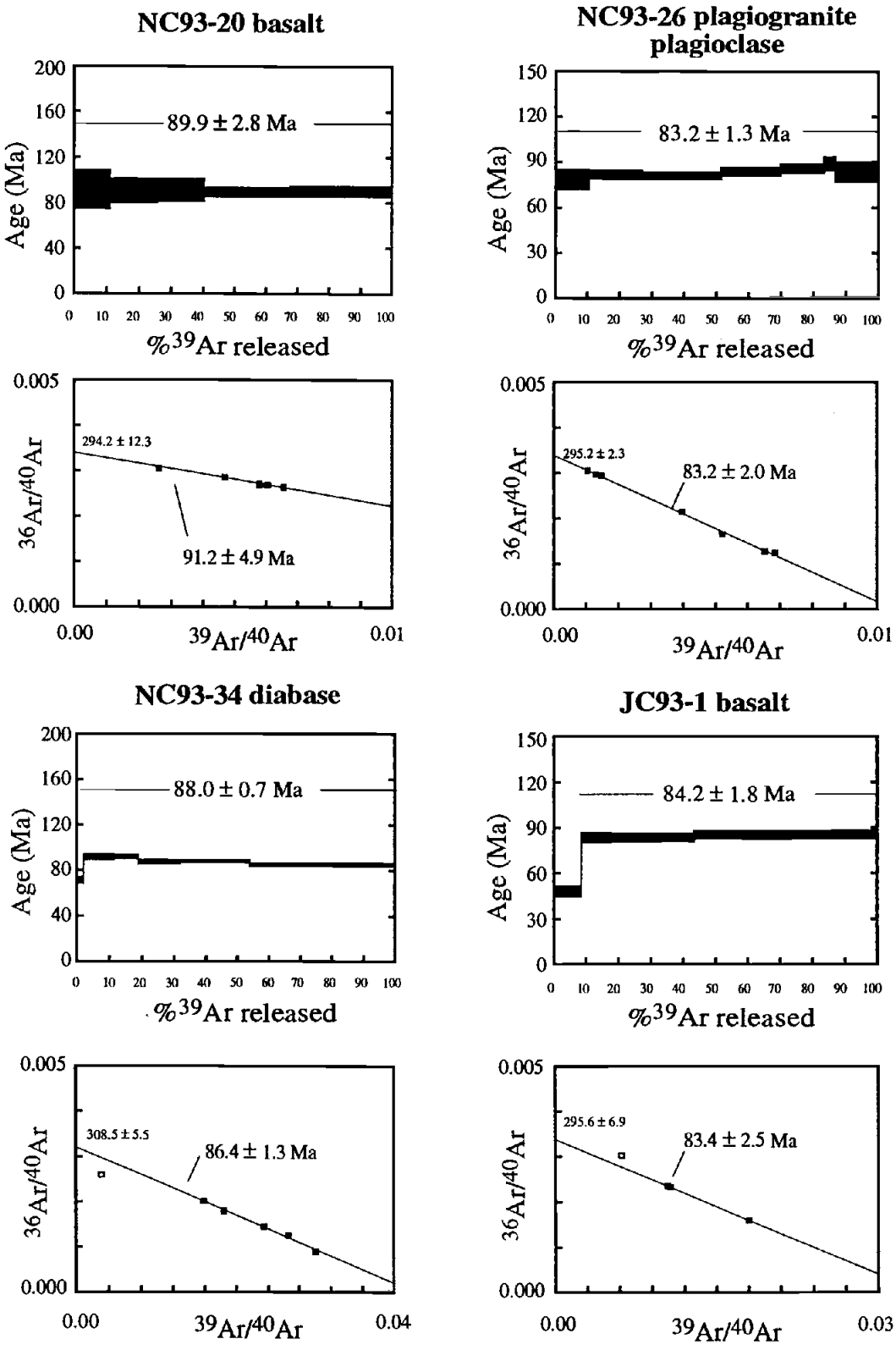
NC93-20 basalt
89.9 ± 2.8 Ma
Age (Ma)
%39Ar released
294.2 ± 12.3
91.2 ± 4.9 Ma
36Ar/40Ar
39Ar/40Ar
NC93-26 plagiogranite
plagioclase
83.2 ± 1.3 Ma
295.2 ± 2.3
83.2 ± 2.0 Ma
NC93-34 diabase
88.0 ± 0.7 Ma
308.5 ± 5.5
86.4 ± 1.3 Ma
JC93-1 basalt
84.2 ± 1.8 Ma
295.6 ± 6.9
83.4 ± 2.5 Ma

QP93-1 basalt

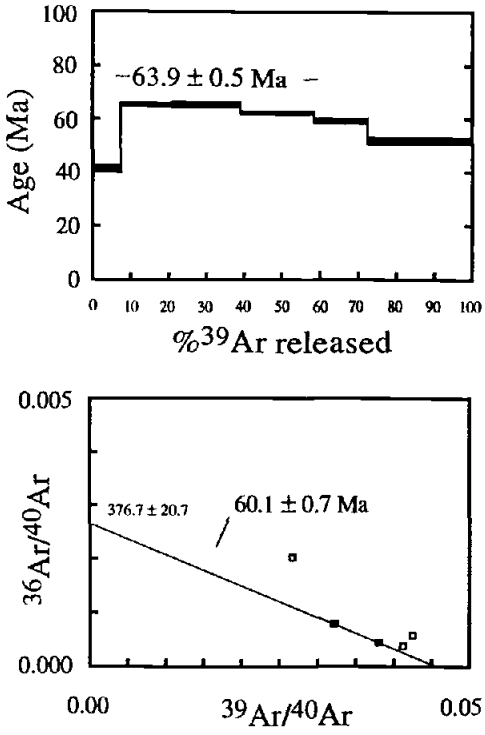

Quepos

Only one Quepos sample (QP93-1) was considered suitable for analysis, although it is altered and very fine grained. A three-step (of six) plateau gave an age of 63.9 ± 0.5 Ma, although the isochron age derived from the same steps is slightly younger (60.1 ± 0.7 Ma) and the initial Ar isotopic composition is considerably higher than atmospheric (376.7) (Fig. III.2). The younger ages of the higher temperature steps can be attributed to recoil of ^{39}Ar during irradiation, a problem often encountered with very fine samples. The range given by the isochron and plateau ages is consistent with the Paleocene age of sediments intercalated with the basalts (Schmidt-Effing, 1979; Baumgartner et al., 1984) and so the actual crystallization age is likely to be between 60 and 64 Ma.

Mineral Chemistry

Analyses of plagioclase and pyroxene were performed using a Cameca SX50 microprobe on polished thins sections of the cumulate gabbro (NC93-100), the most MgO rich diabase (NC93-36), and epoxy plug-mounted pyroxene and feldspar separates from a non-cumulate gabbro (NC93-14B) and several of the plagiogranite samples (NC93-6, -15, -26, -27). Results are reported in Tables III.2 and III.3.

Plagioclase

The cumulate gabbro has An-rich plagioclase megacrysts that are relatively homogenous ($An_{84.6-86.6}$). The diabase (NC93-36) contains a range of plagioclase compositions, from $An_{85.4}$ to $An_{46.0}$. The plagiogranite feldspars show highly variable An content with the more altered examples having very low An content, probably due to albitization of the plagioclase (Table III.2). The closest to primary igneous compositions for each plagiogranite sample are most likely those with the highest An contents.

Pyroxenes

The cumulate gabbro has relatively homogeneous augite megacrysts ($En_{48.0-48.6}$). These compositions are almost identical to the most primitive clinopyroxenes in the NC93-36 diabase. NC93-36 has two types of coexisting pyroxene: a CaO-rich augite and a Ca-poor pigeonite (Table III.3; Fig. III.3). Based on the petrographic textures, it appears that clinopyroxene crystallized before the pigeonite. The rim of one of the pigeonites is very rich in Fe and appears to be the product of a late crystallizing liquid. The lack of exsolution lamellae in the augite and pigeonite indicate relatively rapid cooling of the diabase. Cr in the

pyroxenes appears to be controlled by the proximity of the crystal to magnetite. Pyroxenes adjacent to magnetite have no Cr while pyroxenes isolated from magnetite are very Cr-rich, one having 7400 ppm. This can either indicate post-crystallization re-equilibration or diffusion of Cr during co-precipitation of pyroxene and magnetite. The pyroxenes in the plagiogranites are Fe-rich hedenbergites. NC93-27 is an Fe-rich gabbro which has at least two distinct groups of clinopyroxenes that differ in Wo content (Fig. III.3).

Taken together, the pyroxene data show a trend that is generally consistent with fractional crystallization of a tholeiitic magma series where the increase in Fe coincides with a decrease in temperature. In the Ca-rich pyroxenes, this is coupled with an initial decease in Wo content with a later increase in Wo. The pattern in Fig. III.3 is roughly similar to the trends seen in the Skaergaard intrusion (e.g., Deer et al., 1992). The most primitive augites are also similar to the most primitive augites in the Palisades sill (Deer et al., 1992). The augite and low-Ca pyroxene pairs can be used as a geothermometer (Lindsley, 1983) and these indicate a maximum magma temperature of ~1100°C.

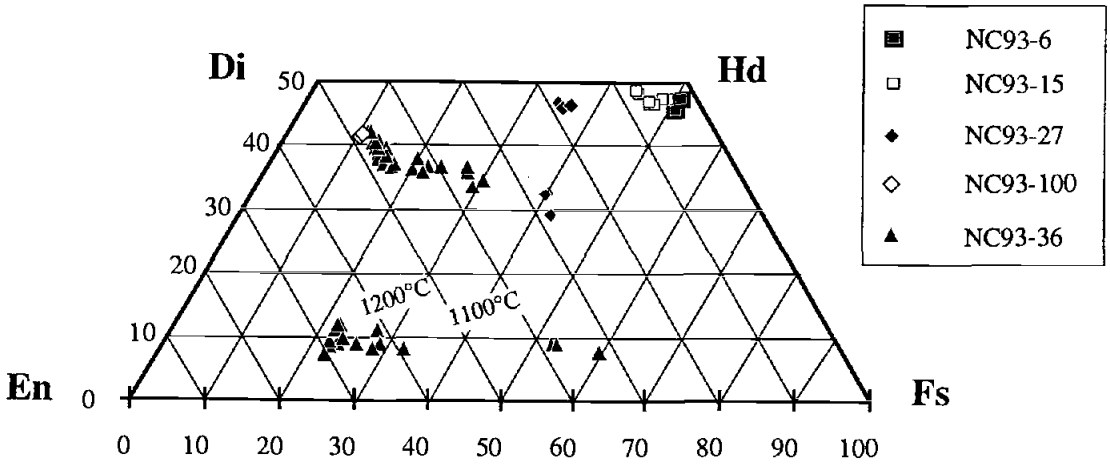

Fig. III.3. Nicoya Peninsula pyroxene compositions plotted on quadrilateral. Isotherms are from Lindsley (1983).

Geochemistry

All the samples (except NC93-19, which was heavily altered, and NC93-100) were analyzed for major elements and Ni, Cr, Sc, V, Sr, and Y by X-ray fluorescence (XRF) at Washington State University using a Rigaku 3370 spectrometer. A subset of the samples was analyzed for Rb, Y, Zr, Nb, Ba, Hf, Ta, Pb, Th, U, and the rare earth elements (REE) using a V.G. Plasmaquad inductively-coupled plasma mass spectrometer (ICP-MS) at Oregon State University. Sample powders for the XRF and some of the ICP-MS analyses were made in a tungsten carbide mill. For some of the ICP-MS analyses, cleaned rock chips were powdered in a ceramic mortar. There were no apparent differences between the ICP-MS results from sample duplicates using the two preparation methods except the tungsten carbide-powdered samples gave higher Ta values. Accordingly, Ta concentrations for these samples are not reported. Pb concentrations were reliably measured in only some of the samples, although the measured standard unknown (W-1) values were slightly low (Appendix 4). In an attempt to correct for this, sample values were normalized to the accepted W-1 standard values.

Sr, Nd, and Pb isotopic ratios were acquired at the Department of Geological Sciences at Cornell University using a V.G. Sector 54 mass spectrometer. Approximately 500 mg aliquots of rock were leached for two hours in 6 N HCl prior to dissolution. A separate aliquot of NC93-20 was not leached. Sr samples were loaded on single tungsten filaments. Nd and Pb samples were loaded on single rhenium filaments

Major and Trace Elements

Major and trace element data are listed in Table III.5. The basalts, diabases, and gabbros from the Nicoya Peninsula and Jacó have tholeiitic compositions with MgO contents ranging from 10.7-4.0%. The plagiogranites have andesitic to dioritic compositions (52 - 69% SiO_2). The two analyzed Quepos rocks are transitional to alkalic basalts. All of the rocks are geochemically similar to those presented in previous studies (Wildberg, 1984; Frisch et al., 1992) except that the Quepos analyses reported by Frisch et al. (1992) have systematically low SiO_2 contents and high loss on ignition (LOI), indicating they may have been highly altered. In an attempt to obviate this problem, the

Quepos major element analyses from Frisch et al. (1993) were recalculated assuming 1% LOI.

Major element data from the Nicoya Peninsula, Jacó, and Quepos reported in this study and previous studies (Wildberg, 1984; Frisch et al., 1992) are plotted on variation diagrams (Fig. III.4). The previous Nicoya data are all from locations within the Nicoya Peninsula and exclude the Santa Elena Peninsula rocks. Jacó rocks are all those described as Jacó, Herradura Jacó, and Herradura in Frisch et al. (1992). Previously reported Quepos rock compositions are also from Frisch et al. (1992). Some of the scatter in the data can be attributed to analytical error (which can be amplified by the low concentrations of some elements) and alteration. It is possible that some of the differences between the data presented in this paper and those from previously published sources are due to interlaboratory biases. Nevertheless, in addition to illustrating the wide range in MgO content for the Nicoya rocks, all of the data show coherent trends for all of the elements (except those obviously affected by alteration, such as K and Rb). The major element compositions are broadly similar to mid-ocean ridge basalt (MORB) and FeO shows an enrichment trend characteristic of a tholeiitic magma series. Trace element variation diagrams (Fig. III.4) also show a single trend for the relatively immobile compatible (Cr and Ni) and incompatible (Zr, Nb, and Y) elements. A first-order interpretation of the trends suggests that the rocks are derived from similar parent magmas by fractional crystallization. The Jacó rocks fall along the Nicoya trend and the Quepos basalts show distinctly different trends for some of the elements (such as Al_2O_3 and FeO) and are notably enriched in some of the incompatible elements (P_2O_5 and TiO_2) at a given MgO content.

All of the basalts are aphyric, so they probably represent liquid compositions. The same can be said for the diabases, except the most MgO-rich diabase, NC93-36. Its high CaO/Al_2O_3, CaO, and Cr suggest an accumulation of clinopyroxene in the bulk sample and, therefore, should not be regarded as a liquid composition. This is an important consideration when trying to define a parental composition to the rock suite. The best candidate for a parental composition is NC93-11 as it is the most MgO-rich basalt and is only slightly altered. It is possible that the diabase NC93-36 is from a heterogeneously zoned sill with a bulk composition similar to the least evolved basalt, NC93-11. The very high FeO content (24.6%) of the NC93-15 plagiogranite can be attributed to an accumulation of magnetite and therefore should not be regarded as a liquid composition.

Table III.5: Major and Trace Element Analyses for the Costa Rica Rocks

	NC93-1	NC93-2	NC93-3	NC93-4	NC93-5	NC93-6	NC93-7	NC93-8
SiO_2	48.19	50.18	50.5	51.46	51.06	69.13	46.81	49.08
Al_2O_3	13.76	13.58	14.44	13.54	12.96	11.76	11.16	14.14
TiO_2	2.459	1.682	1.042	1.716	1.63	0.575	4.349	1.588
FeO (total)	15.93	13.31	10.55	12.36	12.56	9.52	19.53	12.56
MnO	0.227	0.227	0.209	0.209	0.212	0.096	0.319	0.244
CaO	10.39	10.57	12.66	10.13	9.82	2.65	8.67	10.97
MgO	5.53	6.59	8.82	6.71	6.77	0.31	4.54	7.29
K_2O	0.12	0.11	0.07	0.09	0.04	0.25	0.32	0.2
Na_2O	2.69	2.73	1.59	2.6	2.64	6.03	3.05	2.65
P_2O_5	0.087	0.133	0.072	0.138	0.131	0.138	0.098	0.126
Total	99.38	99.11	99.95	98.95	97.82	100.46	98.85	98.85
Mg#	0.41	0.50	0.62	0.52	0.52	0.06	0.32	0.53
Ni	0	48	91	49	47	5	0	59
Cr	21	70	288	51	65	2	3	114
Sc	54	46	52	49	50	12	63	53
V	936	406	319	414	398	1	223	412
Sr	132	140	171	146	610	99	97	134
Rb	1.44	1.09	0.54					2.26
Y	29	34	22					33
Zr	60	107	58					104
Nb	4.7	5.8	3.4					5.7
Ba	29	20	10					40
La	3.43	3.99	2.31					3.98
Ce	9.69	11.43	6.89					11.59
Pr	1.59	1.93	1.13					1.90
Nd	8.22	9.99	5.83					9.60
Sm	2.73	3.39	1.92					3.25
Eu	1.01	1.20	0.72					1.21
Gd	3.59	4.19	2.65					4.03
Tb	0.78	0.89	0.51					0.89
Dy	4.72	5.35	3.27					5.35
Ho	1.06	1.22	0.75					1.20
Er	2.94	3.38	2.17					3.39
Tm	0.45	0.52	0.33					0.51
Yb	2.79	3.34	2.03					3.28
Lu	0.42	0.51	0.31					0.50
Hf	2.05	2.98	1.57					2.96
Ta			0.23					
Pb			0.32					
Th	0.21	0.38	0.27					0.43
U	0.06	0.11	0.04					0.11

Major elements and Sc, Cr, Ni, V, and Sr determined by XRF; all other trace elements determined by ICP-MS. See Appendix 4 for standard analyses.

Table III.5 (cont'd)

	NC93-9	NC93-10	NC93-11	NC93-12	NC93-13	NC93-14A	NC93-14B	NC93-15
SiO_2	50.05	59.2	50.05	56.12	50.47	49.55	51.43	51.85
Al_2O_3	14.15	13.74	14.27	14.68	14.26	13.99	13.38	8.5
TiO_2	1.331	1.331	0.998	1.466	1.256	1.556	1.874	1.771
FeO (total)	11.46	12.18	10.38	10.46	10.77	12.55	13.46	24.6
MnO	0.216	0.18	0.175	0.147	0.194	0.213	0.21	0.358
CaO	11.98	4.06	12.11	7.17	12.35	11.43	9.11	6.37
MgO	7.32	1.17	8.93	2.22	8.26	7.04	5.51	0.68
K_2O	0.15	0.16	0.07	0.05	0.1	0.12	0.14	0.1
Na_2O	1.73	6.32	1.86	5.94	2.33	2.54	3.11	3.85
P_2O_5	0.11	0.357	0.067	0.362	0.093	0.079	0.142	0.651
Total	98.5	98.7	98.91	98.62	100.08	99.07	98.37	98.73
Mg#	0.56	0.16	0.63	0.30	0.60	0.53	0.45	0.05
Ni	68	0	84	0	87	31	18	0
Cr	115	3	200	2	242	16	8	0
Sc	44	23	55	26	49	52	47	44
V	338	0	323	26	330	601	415	0
Sr	211	77	100	39	146	133	298	84
Rb	1.16		0.42		1.31	2.32	2.17	
Y	21		15		21	23	34	
Zr	66		31		43	52	69	
Nb	4.5		3.0		4.3	4.0	7.2	
Ba	33		11		66	25	41	
La	2.71		1.98		3.20	2.83	5.16	
Ce	7.39		5.40		8.50	7.99	13.73	
Pr	1.22		0.91		1.43	1.32	2.24	
Nd	5.95		4.52		7.13	6.84	11.42	
Sm	2.04		1.55		2.33	2.24	3.68	
Eu	0.86		0.59		0.87	0.93	1.34	
Gd	2.77		2.16		3.19	2.84	4.59	
Tb	0.54		0.41		0.60	0.64	0.95	
Dy	3.48		2.65		3.71	3.79	5.64	
Ho	0.73		0.59		0.82	0.86	1.19	
Er	1.92		1.51		1.92	2.27	3.30	
Tm	0.32		0.25		0.32	0.36	0.47	
Yb	1.96		1.44		1.81	2.30	3.19	
Lu	0.31		0.23		0.31	0.35	0.51	
Hf	1.74		0.94		1.36	1.66	2.22	
Ta	0.31		0.18		0.29			
Pb								
Th	0.25		0.11		0.18	0.24	0.31	
U	0.06		0.03		0.04	0.08	0.09	

Table III.5 (cont'd)

	NC93-16	NC93-17	NC93-18	NC93-20	NC93-21	NC93-22	NC93-23	NC93-24
SiO_2	48.12	48.21	50.83	50.6	49.63	51.32	50.15	51.95
Al_2O_3	13.11	12.42	13.99	14.34	13.78	12.92	13.04	11.7
TiO_2	2.599	2.111	1.026	0.976	2.147	2.533	2.516	2.117
FeO (total)	16.83	16.13	10.25	9.65	14.22	13.96	14.22	17.13
MnO	0.286	0.237	0.194	0.198	0.214	0.208	0.266	0.241
CaO	8.4	9.8	11.66	12.54	9.92	9.53	10.03	7.49
MgO	5.24	6.46	8.82	8.73	6.4	5.03	5.71	5.18
K_2O	0.08	0.31	0.1	0.06	0.07	0.14	0.09	0.16
Na_2O	3.2	2.76	2.13	1.82	2.8	2.45	2.82	3.21
P_2O_5	0.065	0.089	0.071	0.067	0.174	0.295	0.241	0.164
Total	97.93	98.53	99.07	98.98	99.36	98.39	99.08	99.34
Mg#	0.38	0.44	0.63	0.64	0.47	0.42	0.44	0.37
Ni	0	17	93	106	54	40	43	11
Cr	12	17	284	209	84	67	61	11
Sc	53	60	50	50	50	48	56	53
V	473	741	324	319	525	409	501	541
Sr	158	127	218	178	90	103	97	85
Rb		2.09	0.47	0.80	0.41		0.97	
Y		31	16	15	46		48	
Zr		63	49	44	146		165	
Nb		3.6	3.3	3.0	9.1		10.5	
Ba		15	31	7	29		28	
La		4.31	2.16	2.15	5.96		7.09	
Ce		10.33	5.87	5.59	16.08		19.64	
Pr		1.41	0.96	0.91	2.67		3.07	
Nd		7.68	4.95	4.76	13.25		15.65	
Sm		2.53	1.69	1.60	4.39		5.11	
Eu		1.01	0.65	0.61	1.52		1.64	
Gd		3.54	2.26	2.15	5.71		6.31	
Tb		0.72	0.46	0.43	1.20		1.23	
Dy		4.46	2.79	2.62	7.12		7.77	
Ho		0.99	0.62	0.56	1.65		1.77	
Er		2.82	1.64	1.51	4.60		5.19	
Tm		0.47	0.27	0.24	0.70		0.81	
Yb		2.70	1.60	1.55	4.52		5.12	
Lu		0.42	0.23	0.24	0.71		0.78	
Hf		1.83	1.29	1.18	4.05		4.38	
Ta		0.25	0.20	0.18			0.72	
Pb		0.26						
Th		0.26	0.14	0.16	0.67		0.95	
U		0.05	0.05	0.06	0.21		0.53	

Fig. III.5 (cont'd)

	NC93-25	NC93-26	NC93-27	NC93-29	NC93-30	NC93-31	NC93-32	NC93-33
SiO_2	50.25	63.62	57.58	50.96	50.58	49.7	51.31	50.09
Al_2O_3	12.68	11.18	11.31	13.93	13.44	13.9	14.47	13.45
TiO_2	2.501	1.022	2.003	2.017	1.694	1.015	1.025	1.294
FeO (total)	15.68	13.51	16.45	14.32	13.5	8.95	11.18	11.86
MnO	0.256	0.16	0.236	0.258	0.268	0.155	0.221	0.215
CaO	7.73	4.06	5.73	7.37	10.02	9.62	10.48	10.03
MgO	4.93	0.39	1.44	3.99	7.13	9.42	6.36	6.28
K_2O	0.27	0.14	0.54	0.24	0.23	0.45	0.17	0.18
Na_2O	4.81	5.74	4.4	4.02	3.24	3.54	2.75	2.72
P_2O_5	0.246	0.288	0.449	0.192	0.138	0.067	0.103	0.094
Total	99.35	100.11	100.14	97.3	100.24	96.82	98.07	96.21
Mg#	0.38	0.05	0.15	0.36	0.51	0.68	0.53	0.51
Ni	23	0	0	0	48	127	34	36
Cr	31	1	0	10	65	318	12	18
Sc	46	23	34	39	47	49	49	48
V	536	2	13	364	413	305	276	357
Sr	75	83	109	384	117	107	763	337
Rb	2.70			1.61	2.32		1.89	
Y	61			45	36		28	
Zr	80			150	117		59	
Nb	12.0			8.7	6.3		3.9	
Ba	33			30	30		93	
La	8.89			6.50	4.53		2.93	
Ce	22.93			17.23	12.80		8.43	
Pr	3.75			2.81	2.12		1.42	
Nd	18.86			14.45	11.07		7.40	
Sm	6.16			4.49	3.75		2.57	
Eu	1.95			1.56	1.31		1.00	
Gd	7.87			5.72	4.48		3.62	
Tb	1.70			1.24	0.99		0.68	
Dy	9.77			7.31	5.91		4.27	
Ho	2.18			1.66	1.33		0.95	
Er	6.08			4.57	3.79		2.72	
Tm	0.92			0.72	0.56		0.42	
Yb	5.75			4.43	3.62		2.49	
Lu	0.87			0.70	0.54		0.40	
Hf	3.05			4.11	3.16		1.63	
Ta							0.26	
Pb							0.41	
Th	0.55			0.67	0.46		0.24	
U	0.35			0.17	0.15		0.05	

Table III.5 (cont'd)

	NC93-34	NC93-35	NC93-36	NC93-37	NC93-38	NC93-100	QP93-1	QP93-2
SiO_2	51.19	51.5	50.55	51.99	51.62		49.44	51.03
Al_2O_3	14.72	14.44	14.43	13.7	15.07		13.29	14.39
TiO_2	1.006	1.086	0.69	1.586	1.011		2.943	2.099
FeO (total)	9.44	10.14	7.91	12.55	9.48		11.77	9.83
MnO	0.202	0.187	0.16	0.213	0.18		0.191	0.195
CaO	12.01	11.17	14.25	10.25	12.25		7.68	8.56
MgO	8.55	8.2	10.69	6.4	8.63		7.33	7.21
K_2O	0.38	0.07	0.07	0.11	0.07		0.87	0.46
Na_2O	2.54	3.14	1.53	2.93	2.4		5.38	5.85
P_2O_5	0.07	0.076	0.05	0.118	0.064		0.271	0.17
Total	100.11	100.01	100.33	99.85	100.78		99.17	99.79
Mg#	0.64	0.62	0.73	0.50	0.64		0.55	0.59
Ni	100	100	155	55	117		120	64
Cr	296	319	1028	49	438		269	185
Sc	53	52	47	53	50		34	40
V	333	330	268	425	313		383	324
Sr	139	98	103	119	107		275	111
Rb	3.23	1.22	0.96	1.38	0.47	1.0	11.78	
Y	17	21	11	30	16	16	36	
Zr	39	42	27	55	35	34	194	
Nb	3.5	4.1	2.2	6.0	2.6	2.5	19.0	
Ba	66	13	34	48	9	12	159	
La	2.43	3.16	1.46	3.60	2.02	1.80	13.54	
Ce	6.44	8.15	3.68	10.01	5.36	5.37	34.14	
Pr	1.07	1.26	0.66	1.69	0.92	0.90	4.92	
Nd	5.30	6.26	3.19	8.56	4.53	4.52	22.58	
Sm	1.77	1.99	1.08	2.93	1.57	1.51	6.00	
Eu	0.68	0.75	0.44	1.05	0.66	0.69	1.99	
Gd	2.30	2.67	1.45	3.85	2.09	2.08	6.77	
Tb	0.46	0.50	0.30	0.74	0.44	0.39	1.21	
Dy	2.82	3.16	1.82	4.55	2.77	2.51	6.53	
Ho	0.62	0.71	0.41	1.02	0.59	0.53	1.28	
Er	1.56	1.97	1.14	2.85	1.63	1.50	2.96	
Tm	0.26	0.29	0.19	0.44	0.26	0.23	0.48	
Yb	1.54	1.77	1.13	2.62	1.64	1.37	2.62	
Lu	0.26	0.28	0.19	0.41	0.24	0.22	0.41	
Hf	1.14	1.18	0.75	1.53	1.00	0.98	4.62	
Ta	0.23	0.27	0.14	0.39	0.19	0.18	1.24	
Pb		0.32						
Th	0.20	0.20	0.10	0.31	0.22	0.24	1.38	
U	0.05	0.05	0.03	0.07	0.05	0.14	0.34	

Table III.5 (cont'd)

	JC93-1	JC93-2	JC93-3	Primary Melt
SiO_2	51.38	50.41	49.57	49.07
Al_2O_3	14.63	14.28	14.43	12.27
TiO_2	1.127	1.276	1.23	0.86
FeO (total)	9.86	9.55	11.56	10.69
MnO	0.175	0.174	0.216	0.18
CaO	12.19	11.63	10.89	10.44
MgO	8.79	8.87	8.68	14.78
K_2O	0.05	0.07	0.13	0.06
Na_2O	2.08	3.42	2.77	1.60
P_2O_5	0.079	0.091	0.091	0.06
Total	100.36	99.77	99.57	
Mg#	0.64	0.65	0.60	0.73
Ni	88	123	97	900
Cr	311	366	202	
Sc	54	49	52	
V	335	311	343	
Sr	87	145	76	
Rb	0.41		0.87	
Y	18		21	
Zr	50		55	
Nb	4.5		3.4	
Ba	12		22	
La	2.73		2.73	
Ce	7.46		7.26	
Pr	1.21		1.20	
Nd	5.95		6.24	
Sm	1.89		2.00	
Eu	0.71		0.75	
Gd	2.56		2.64	
Tb	0.47		0.52	
Dy	3.11		3.34	
Ho	0.68		0.76	
Er	1.77		2.01	
Tm	0.30		0.34	
Yb	1.72		2.06	
Lu	0.29		0.32	
Hf	1.29		1.52	
Ta	0.30		0.23	
Pb				
Th	0.28		0.26	
U	0.07		0.07	

Fractional Crystallization

The role of fractional crystallization in the evolution of the Nicoya Peninsula rocks can be assessed using the variation diagrams in Fig. III.4. The decreasing concentrations of certain elements or ratios with decreasing MgO content gives an indication of the crystallization and removal of certain minerals. All of the major element variation diagrams, with the exception of FeO and TiO_2, show continuous, roughly linear trends. FeO and TiO_2 both increase with decreasing MgO until ~4% MgO, at which point they decrease. This inflection is likely due to the appearance of Fe-Ti oxides on the liquidus. At greater MgO content, there are no obvious inflections in the trend and, therefore, the fractionating assemblage remained relatively constant. The fractionation of clinopyroxene is evident from the continuous decrease in CaO/Al_2O_3, Sc, and Cr with decreasing MgO. The decrease in Al_2O_3 and Ni can be attributed to the removal of plagioclase and olivine, respectively. Overall, the variation diagrams are consistent with the removal of clinopyroxene, plagioclase, and olivine from ~9% MgO to ~4% MgO, at which point Fe-Ti oxides join the fractionating assemblage.

Petrographic observations are generally consistent with this interpretation. As previously stated, all samples (except NC93-100) are aphyric and so petrographic observations are of limited help in determining the fractionating mineral assemblage. However, the gabbro NC93-100 contains cumulate clinopyroxene (En_{51}), plagioclase (An_{85}), and what appear to be olivine pseudomorphs set in a basaltic matrix. Based on the similarity in the plagioclase and clinopyroxene compositions of the gabbro and the diabase NC93-36, the gabbro is probably a cumulate of the early crystallizing phases of the Nicoya suite and is consistent with the three-phase saturation with olivine, clinopyroxene, and plagioclase of the magmas during early crystallization.

An estimate of the degree of fractional crystallization represented by the basaltic portion of the Nicoya Peninsula rock suite can be calculated using an incompatible trace element, such as Zr and the equation for Rayleigh fractional crystallization, $C_L/C_O = F^{[D-1]}$, where C_L is the Zr concentration in the most differentiated basalt (NC93-29; 4.0% MgO), C_O is the Zr concentration in the most primitive basalt that represents a liquid composition (NC93-11; 8.9% MgO), F is the fraction of melt remaining, and D is the bulk partition coefficient for Zr. Since Zr is an incompatible element in olivine, clinopyroxene, and plagioclase, the D value is about 0. Using these values, F is 0.20 or 80% fractional

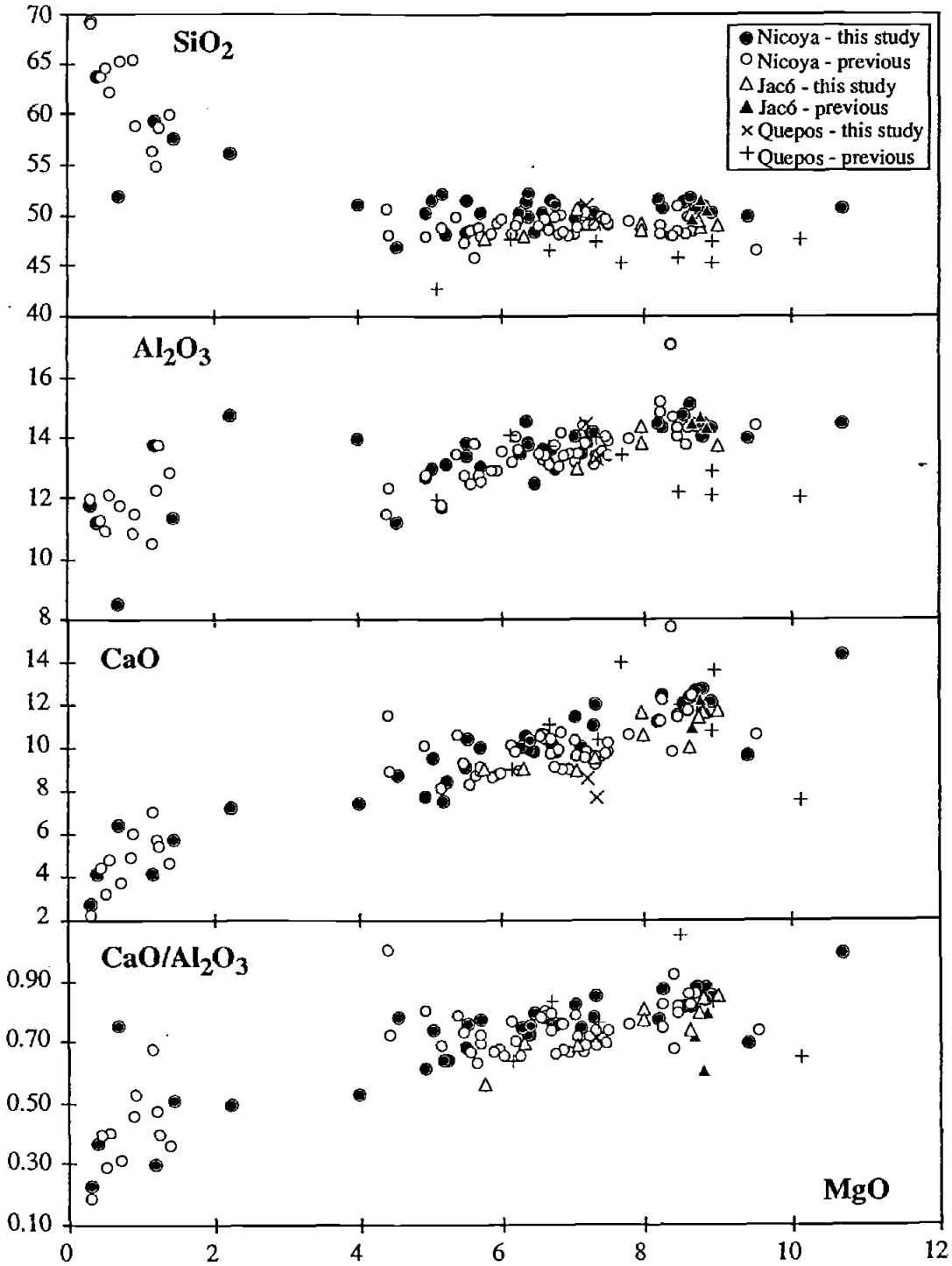

Fig. III.4. Variation diagrams for mafic rocks from the Nicoya Peninsula, Jacó/Herradura,and Quepos. Previously published data are from Wildberg (1984) and Frisch et al. (1994).

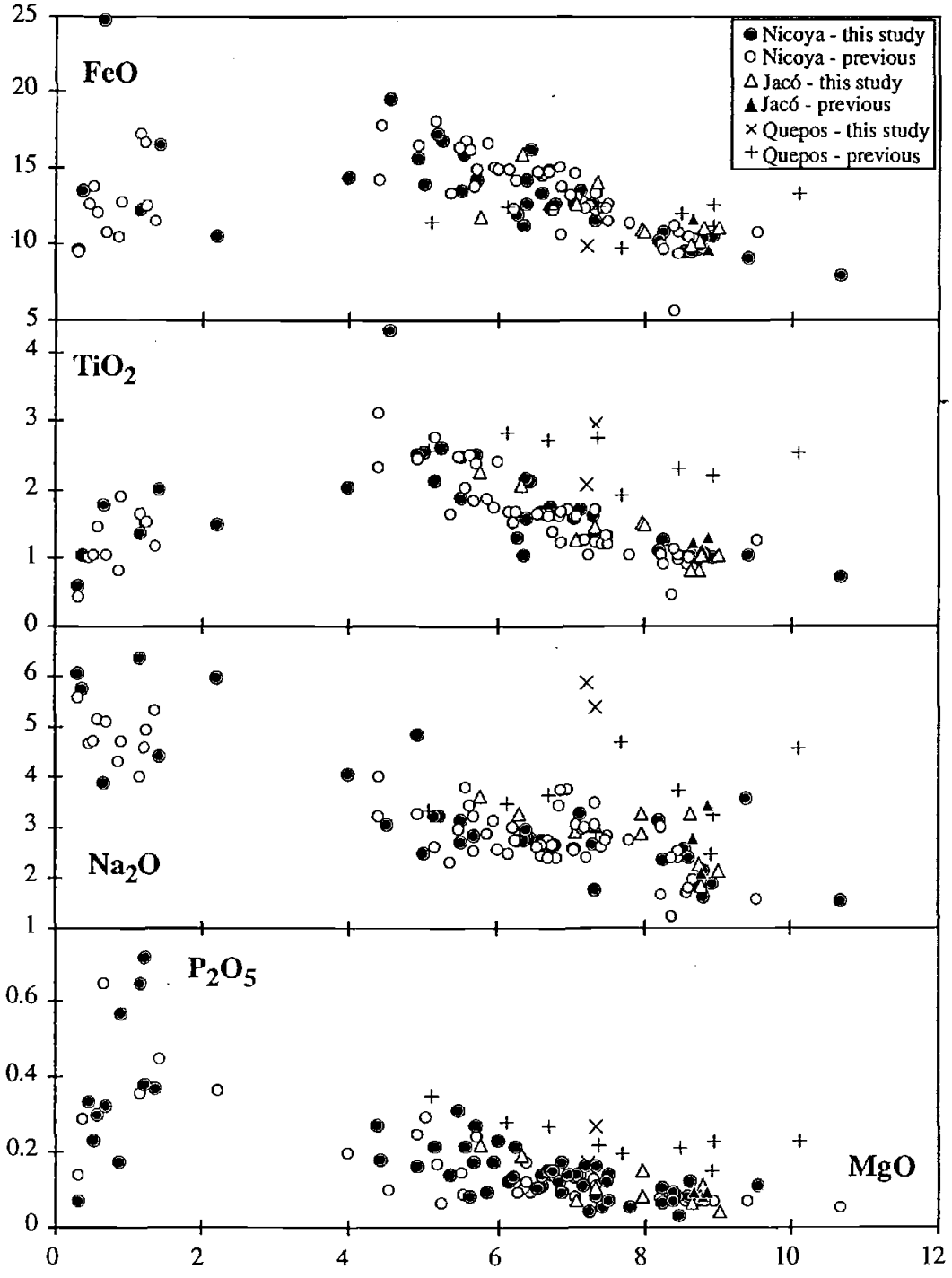

Fig. III.4 (cont'd).

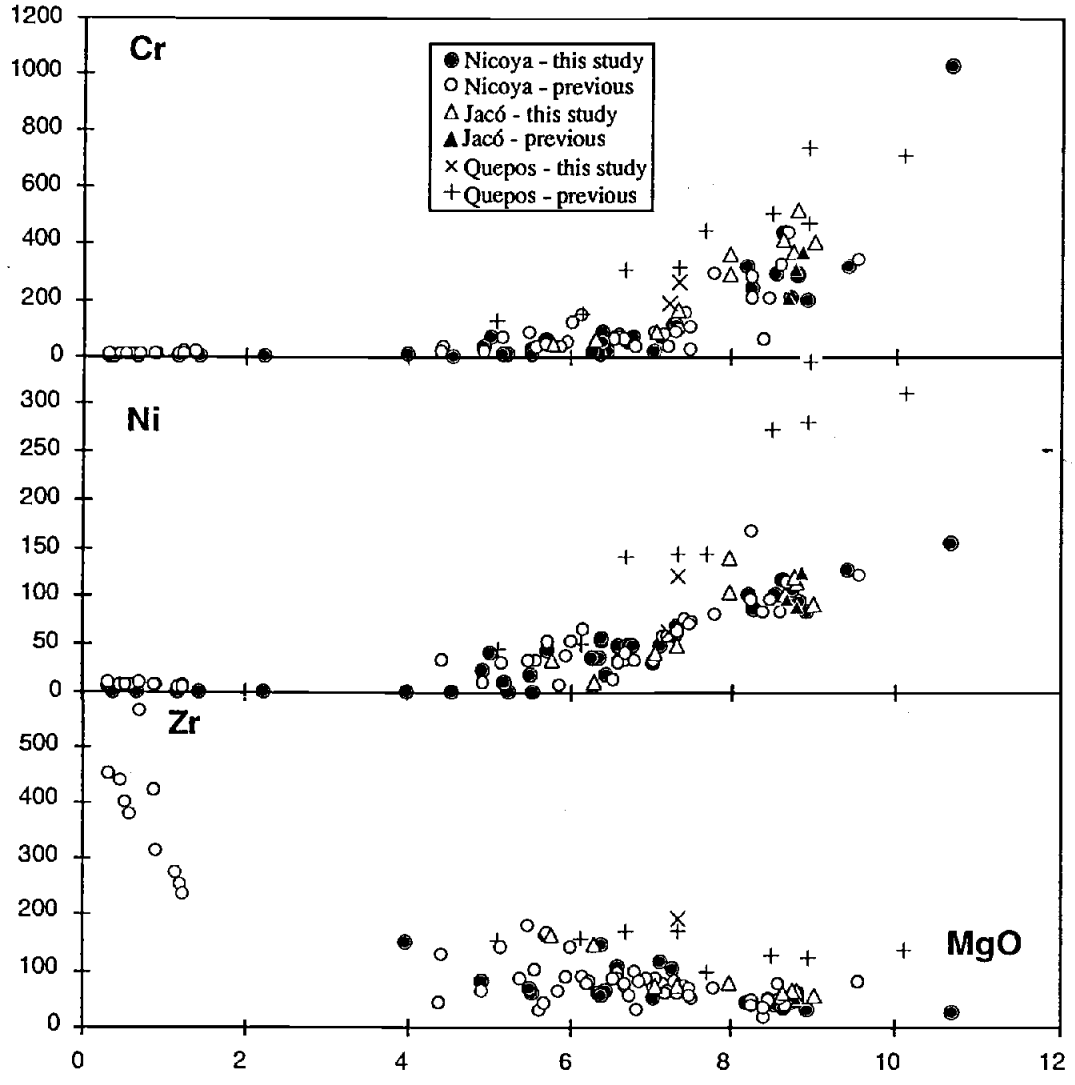

Fig. III.4 (cont'd).

crystallization. Such a degree of crystallization may leave a residual liquid that is no longer basaltic, so Zr may have been slightly compatible in the fractionating clinopyroxene.

The major and trace element data indicate that the plagiogranites are derived from the more primitive tholeiitic basalts. This is consistent with a model described by Wildberg (1987), in which the plagiogranites are derived by a two-stage process of fractional crystallization and later filter-pressing of a tholeiitic magma. The latter process leaves a residual Fe-rich diabase/gabbro, such as samples NC93-7 and NC93-15.

Comparison to MORB

I compare the Nicoya Peninsula rocks to MORB glasses from the East Pacific Rise from 13°S to 5°N and from the westernmost part of the triple junction of the East Pacific Rise and the Galapagos Spreading Center (from the JOI compilation) in Fig. III.5. The East Pacific Rise data show relatively coherent trends for all elements; these trends are distinct from the Nicoya suite for some elements. Unlike the Nicoya rocks, the MORB data show an inflection in CaO and Sc between 7% and 8% MgO, indicating the appearance of clinopyroxene on the liquidus at that time and, thus, low pressure fractionation. As discussed previously, clinopyroxene in the Nicoya suite appears to have been part of the fractionating mineral assemblage from at least ~9% MgO and lower. Because the primary effect of high pressure fractional crystallization is to increase the temperature at which clinopyroxene appears on the liquidus (e.g., Bender et al. 1978; Grove et al. 1992; Langmuir et al. 1992), fractional crystallization of the Nicoya magmas may have occurred at pressures significantly greater than 1 atm.

This possibility was tested using the COMAGMAT model (Ariskin et al., 1993), which can be used to simulate fractional crystallization of a basaltic magma at various pressures. The model uses empirically derived data to calculate mineral-melt equilibria solutions at given temperatures and liquid compositions. The most primitive liquid composition of the Nicoya series, NC93-11, was used as a starting composition for model runs at 1 atm and 3 kbar. The model was run until 80% of the liquid had crystallized (~3% MgO) and phase proportions, mineral compositions, and liquid compositions were calculated at 1% crystallization intervals. The results of the liquid compositions are plotted in Fig. III.5. For the 1 atm simulation, olivine first appeared on the liquidus, followed by plagioclase, then clinopyroxene at 7.5% MgO. For the 3 kbar run, olivine appeared

briefly, disappeared as clinopyroxene appeared (at 8.2% MgO), and reappeared at 7.9% MgO. Plagioclase appeared almost simultaneously with clinopyroxene in the 3 kbar run. The calculated En content of the initial clinopyroxene is slightly lower ($En_{48.9}$) than the most primitive Nicoya clinopyroxenes (En_{51}). Overall, the 3 kbar liquid line of descent shows a better (though not exact) fit to the Nicoya data than the 1 atm model run, consistent with fractional crystallization of the parental magmas at depths ~ 3 kbar. Alternatively, the different liquid lines of descent may be due to differences in the compositions of the parental magmas.

To examine whether the differences between the MORB and Nicoya magmas are a result of differences in the depth of fractional crystallization (from parental melts of similar major element composition) or of differences in parental melt composition, I compared the two datasets at 9% MgO. The two datasets have comparable CaO and FeO, but Al_2O_3, which behaves incompatibly and is depleted from the mantle during partial melting (e.g., Forsyth, 1992), appears to be significantly higher in the MORB magmas. Other incompatible elements in the Nicoya suite, such as TiO_2, P_2O_5, Zr, and Y, are also slightly to significantly lower than the MORB suite at 9% MgO (Fig. III.5). These differences cannot be attributed to differences in the fractionated mineral assemblage. Rather, they must reflect a relative depletion in these elements in the magmas that are parental to the Nicoya suite. So the Nicoya rocks appear to have been derived from melts that are compositionally distinct from MORB melts and therefore it is not certain that the Nicoya magmas fractionated at relatively high pressures.

In summary, the major and trace element compositions of the Nicoya Peninsula rocks indicate that all of the igneous rocks collected and analyzed to date can be related by fractional crystallization from similar parental melts. The Jacó basalts are compositionally similar to the Nicoya rocks while the Quepos basalts are distinct. The Nicoya rocks, though grossly similar to MORB lavas, are different in terms of some major and trace elements. These differences may partly be attributed to what appears to be a difference in the appearance of clinopyroxene on the liquidus, possibly due to a difference in the pressure at which crystallization occurred. This is plausible if one assumes that the Nicoya lavas erupted through pre-existing oceanic lithosphere (evident from the included radiolarite), which could have served as a mechanical boundary that allowed pooling of melts. However, some of the differences between the Nicoya and MORB suites must also be due to differences in the parental magmas. The Nicoya suite is relatively depleted in Al_2O_3, TiO_2, P_2O_5, Zr, and Y and enriched in Sc. These depletions suggest that the

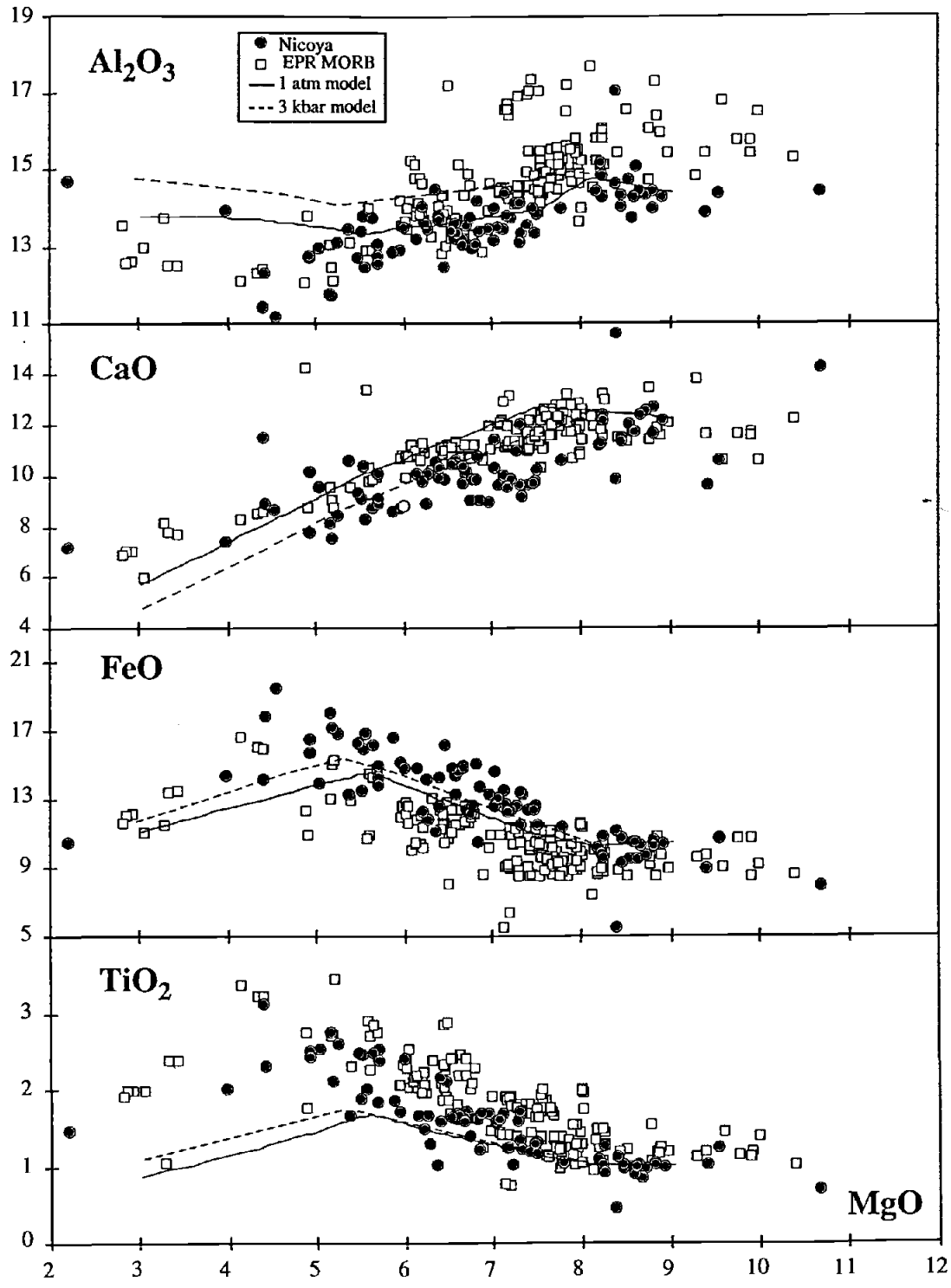

Fig. III.5. Variation diagrams comparing the Nicoya Penisula data to EPR MORB (from the JOI compilation). Lines are the calculated liquid lines of descent using the COMAGMAT model (Ariskin et al., 1993) run at 1 atm and 3 kbar using NC93-11 as a starting composition.

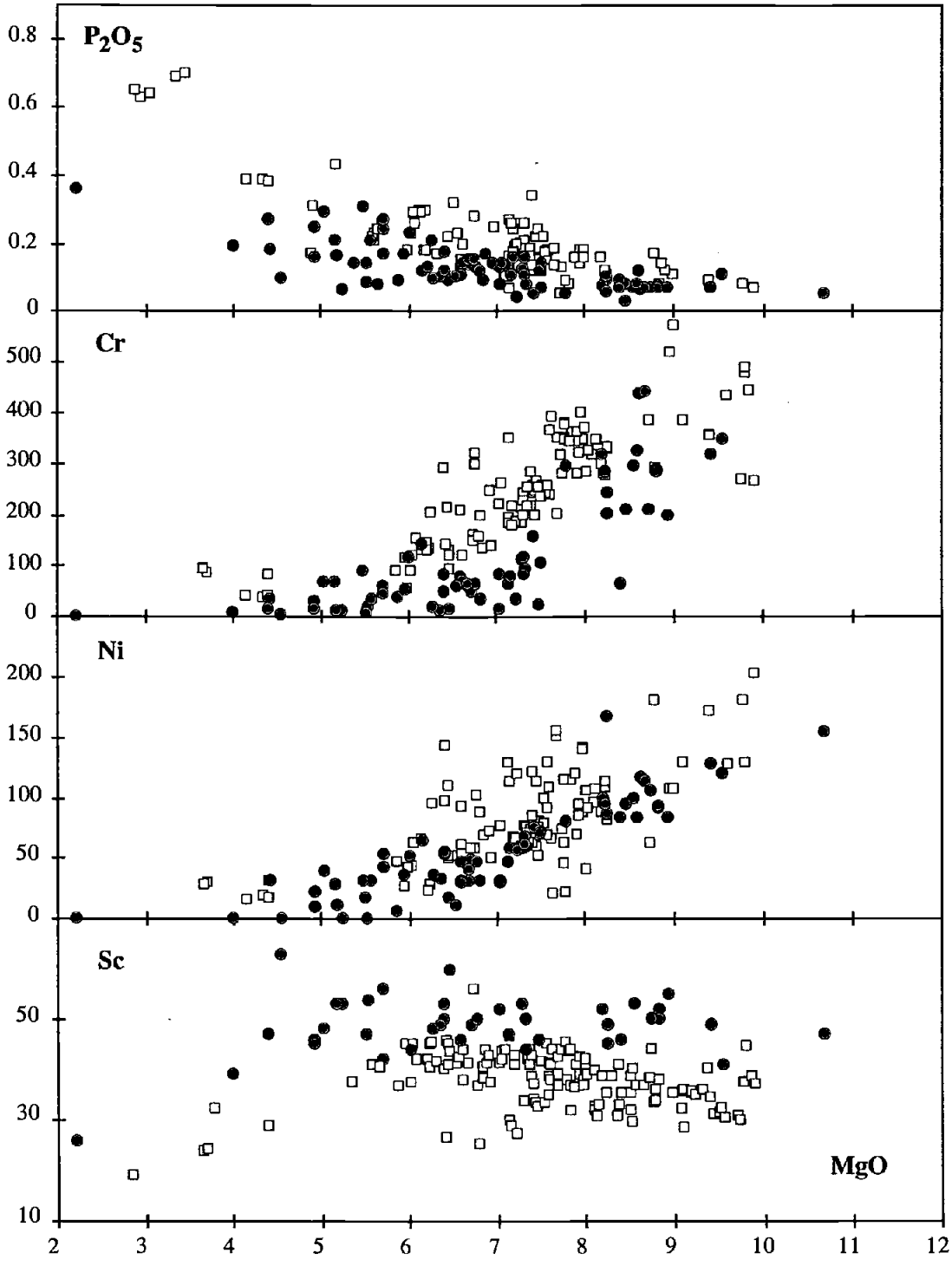

Fig. III.5 (cont'd).

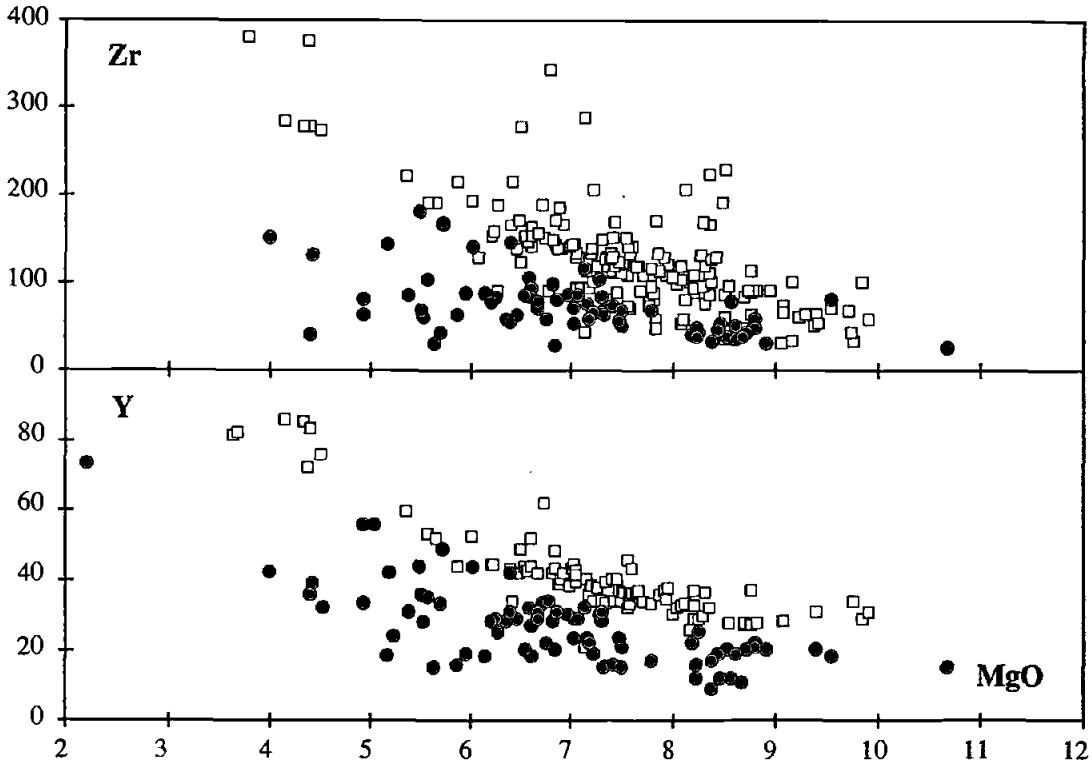

Fig. III.5 (cont'd).

Nicoya rocks were either derived from a mantle source more depleted than a MORB source or that they were derived from greater extents of partial melting from a mantle similar to or possibly more enriched than a MORB source. The REE and the isotopes suggest the latter case.

Rare-Earth Elements

Figure III.6 shows the chondrite-normalized rare earth element analyses from previous studies and their unit designation. All show relatively flat patterns and the new data confirm this. The uniform patterns of the REE are consistent with the Nicoya Peninsula rocks belonging to a single, cogenetic suite. All of the Nicoya rocks (including the matrix of the NC93-100 cumulate gabbro) have slightly LREE-depleted to slightly LREE-enriched chondrite-normalized REE patterns ($La/Yb_n = 0.77\text{-}1.21$; $Ce/Yb_n = 0.85\text{-}1.23$) with the absolute abundances of the REE increasing with decreasing MgO (although the La/Yb ratios do not change systematically with MgO content). The two analyzed Jacó rocks also have relatively flat REE patterns (La/Yb_n 0.90 and 1.08) which, along with the variation diagrams, suggests that they and the Nicoya Peninsula rocks were derived from similar parental magmas. The Quepos basalt has a LREE-enriched pattern (La/Yb_n 3.51). This observation and the differences in the variation diagrams and the younger age demonstrates that the Quepos rocks were derived from different parental magmas than the Nicoya and Jacó rocks.

Normal MORB have LREE-depleted patterns, though some enriched MORB, typically in areas near hotspots, do have flat to LREE-enriched patterns. These observations and the differences in some of the major and trace elements discussed in the previous section indicate that the Costa Rica rocks were derived from parental magmas distinct from magmas parental to normal MORB.

Isotopes

Sr, Nd, and Pb isotopic ratios are excellent tracers of mantle source composition because they remain unchanged during partial melting and fractional crystallization and differences in these ratios among magmas can be ascribed to mixing of magmas or mantle sources. However, several problems arise when trying to obtain isotopic data from old,

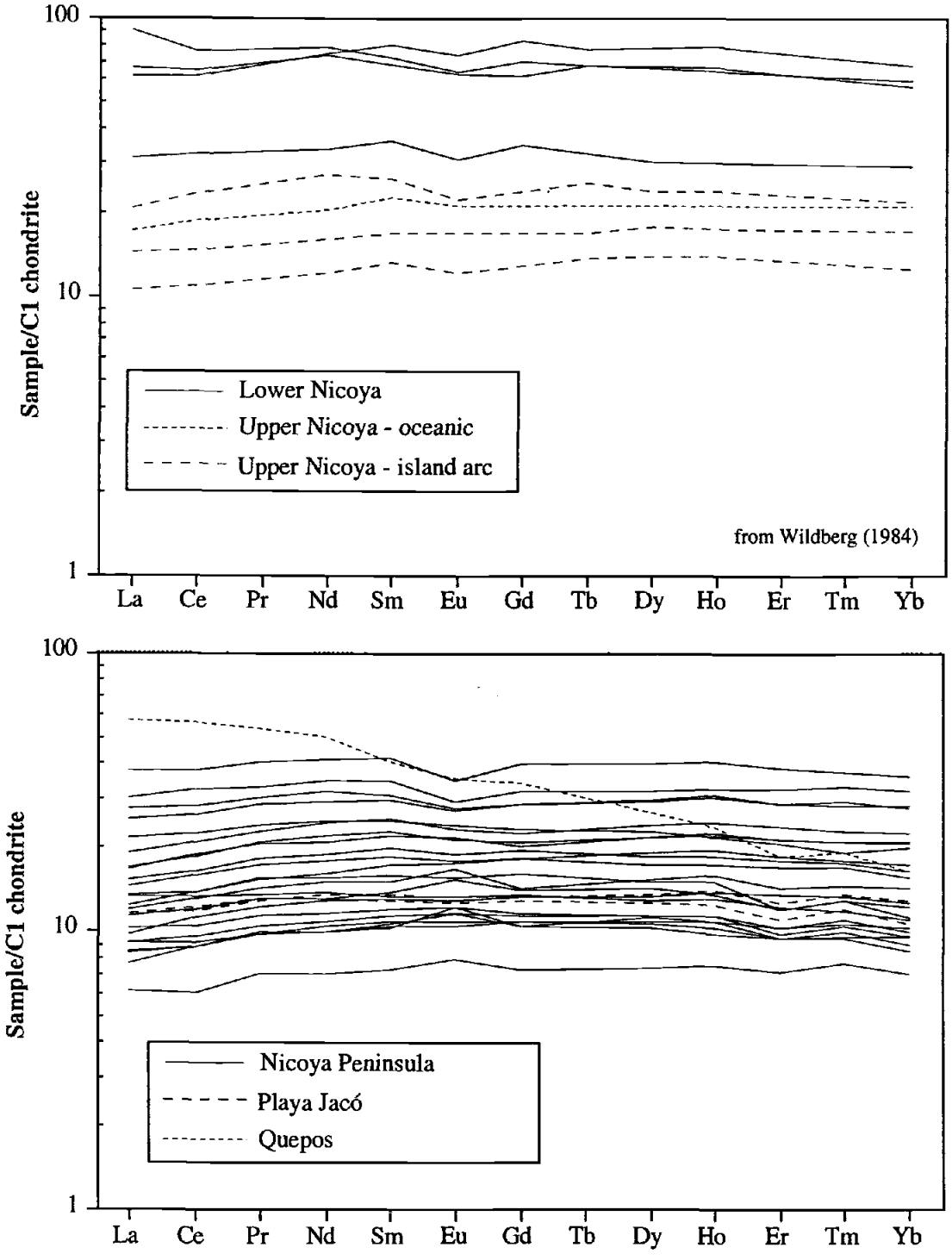

Fig. III.6. C1 chondrite-normalized rare earth element diagrams. Chondrite values from McDonough and Sun (1995). The upper figure are data from Wildberg (1984) and his designated divisions. The lower figure showsdata reported in Table III.5.

altered rocks. First, alteration can modify the original Rb and Sr rock concentrations and increase the $^{87}Sr/^{86}Sr$ ratios (in the case of seawater alteration). Acid leaching of altered rocks prior to dissolution and analysis has been shown to reduce the $^{87}Sr/^{86}Sr$ values to reliable magmatic values in certain cases (Taras and Hart, 1987). Sm and Nd are relatively immobile during alteration (Staudigal and Hart, 1983) and leaching of samples seems to make no difference in the $^{143}Nd/^{144}Nd$ and very minor differences for Pb isotopic ratios (Taras and Hart, 1987). In addition to alteration effects, the isotopic ratios (radiogenic daughter/non-radiogenic isotope) will increase after magma crystallization due to radioactive decay of the parent isotope. Initial ratios can be determined if the reliable parent/daughter ratios and the age of the rock are known.

Six of the freshest Nicoya Peninsula samples, two Jacó basalts, and one Quepos basalt were analyzed for Sr, Nd, and Pb isotopes and the data are presented in Table III.6. Both measured and calculated initial ratios are reported, with age corrections calculated using the ICP-MS measurements for parent/daughter ratios and the radiometric ages reported earlier. Because reliable Pb concentrations were not obtained for some of the samples, probable Pb concentrations were calculated by assuming a linear relationship between Pb and another incompatible element, La. One potential problem with using the ICP-MS data is that the sample aliquots used in isotopic analyses were acid-leached and the ICP-MS samples were not. However, this does not appear to have been a significant problem. The leached and unleached aliquots of sample NC93-20 yielded little difference in any of the ratios (Table III.6). Replicate isotopic analyses of some of the samples were performed on separate sample dissolutions and show excellent reproducibility (Table III.6).

Sr isotopic ratios from unleached Nicoya rocks have been previously presented by Wildberg and Baumann (1988). Their Upper and Lower Nicoya ocean floor basalts and plagiogranites are indistinguishable in their range of $^{87}Sr/^{86}Sr$ values (0.7027-0.7040), and their designated primitive arc rocks, although having generally higher values, overlap with their "oceanic" series. All of the samples presented here fall within this range (0.70313-0.70460). However, given the mobility of Sr and the degree of alteration of some of the Costa Rica rocks, variations in Sr isotopic ratios may not be diagnostic of source mantle characteristics. This is certainly evident from a plot of $^{87}Sr/^{86}Sr$ vs. $^{143}Nd/^{144}Nd$ (Fig. III.7). $^{87}Sr/^{86}Sr$ ratios show considerable scatter while the $^{143}Nd/^{144}Nd$ ratios are relatively constant for all of the Costa Rica samples. It is possible that the original Sr isotopic signature of the rocks has been altered by Sr addition from seawater and this would be a valid conclusion considering that the most altered of the analyzed samples

(QP93-1) has the highest $^{87}Sr/^{86}Sr$ though similar $^{143}Nd/^{144}Nd$ ratio. However, sample NC93-34 is virtually unaltered and therefore its high $^{87}Sr/^{86}Sr$ ratio cannot be readily explained by alteration. This sample was taken near an included pod of radiolarite, so it is possible that the Sr isotopic signature has been increased by the assimilation of pelagic sediments (which may have seawater $^{87}Sr/^{86}Sr$ ratios ~0.7075 during the Cretaceous (Faure, 1986). Kerr et al. (in press) showed that the high $^{87}Sr/^{86}Sr$ ratios in some Curaçao lavas can be attributed to contamination from a carbonate source. Although the lowest $^{87}Sr/^{86}Sr$ ratios from the Costa Rica rocks may closely reflect the actual magmatic ratios, Sr isotopes cannot be reliably used as indicators of mantle sources in these lavas.

The contamination from pelagic sediments that is evident from the Sr isotopes is not apparent in the Nd and Pb isotopes (nor, for that matter, in the trace element data). This is not unexpected for Nd, as Nd concentrations in pelagic sediments are very low. The range of initial $^{143}Nd/^{144}Nd$ ratios for the samples is small (0.51285-0.51289) and considerably lower than the range of present day East Pacific Rise basalts (Fig. III.7). The Pb isotopic ratios also show a restricted range and show no evidence of a mixing trend toward pelagic sediment Pb isotopic compositions (Doe, 1970) (Fig. III.7). Sample NC93-34, which shows evidence of pelagic sediment contamination from the Sr isotopes, does not fall towards the seawater values. On $^{206}Pb/^{204}Pb$ vs. $^{207}Pb/^{204}Pb$ and $^{206}Pb/^{204}Pb$ vs. $^{208}Pb/^{204}Pb$ diagrams, the Costa Rica rocks plot in a group that is more radiogenic than present day East Pacific Rise basalts. Considering the analytical error and unknown (but relatively small) error associated with age correction using the ICP-MS parent/daughter elemental ratios, the Pb and Nd isotopic ratios of all of the analyzed samples are not appreciably different, though NC93-11 and NC93-34 have $^{206}Pb/^{204}Pb$ and $^{208}Pb/^{204}Pb$ ratios considerably more radiogenic than the others. Together, the Nd and Pb isotopic data show that the mantle source for the Nicoya Peninsula, Jacó, and Quepos magmas were rather similar and distinct from the upper mantle source for MORB.

Table III.6: Sr, Nd, and Pb Isotopic Analayses for Costa Rica Rocks

Sample	$\frac{^{87}Sr}{^{86}Sr_m}$	$\frac{^{87}Sr}{^{86}Sr_i}$	$\frac{^{143}Nd}{^{144}Nd_m}$	$\frac{^{143}Nd}{^{144}Nd_i}$	εNd_i	$\frac{^{206}Pb}{^{204}Pb_m}$	$\frac{^{206}Pb}{^{204}Pb_i}$	$\frac{^{207}Pb}{^{204}Pb_m}$	$\frac{^{207}Pb}{^{204}Pb_i}$	$\frac{^{208}Pb}{^{204}Pb_m}$	$\frac{^{208}Pb}{^{204}Pb_i}$
NC93-20u	0.70346	0.70345	----	----	----	19.23	19.16	15.56	15.56	38.87	38.81
NC93-20	0.70341	0.70340	0.512967	0.512843	6.26	19.28	19.21	15.59	15.58	38.97	38.90
NC93-18	0.70393	0.70392	0.512990	0.512863	6.65	19.28	19.02	15.58	15.57	38.93	38.71
NC93-34	0.70450	0.70442	0.512977	0.512853	6.45	19.62	19.12	15.63	15.61	39.39	38.75
NC93-13	0.70329	0.70326	0.512981	0.512860	6.59	19.34	19.15	15.63	15.62	39.14	38.84
NC93-11	0.70316	0.70314	0.513014	0.512886	7.10	19.68	19.22	15.60	15.58	39.47	38.89
NC93-3	0.70361	0.70360	0.512985	0.512863	6.65	19.33	19.20	15.60	15.60	39.08	38.81
NC93-3R	0.70346	0.70344	----	----	----	19.26	19.13	15.57	15.56	38.91	38.64
JC93-1	0.70347	0.70345	0.512955	0.512848	6.36	19.37	19.21	15.58	15.57	39.04	38.84
JC93-1R	0.70344	0.70342	----	----	----	19.34	19.19	15.56	15.55	38.98	38.78
JC93-3	0.70313	0.70310	0.512987	0.512878	6.94	19.38	19.06	15.60	15.58	39.06	38.69
JC93-3R	----	----	----	----	----	19.40	19.09	15.60	15.59	39.12	38.75
QP93-1	0.70460	0.70450	0.512916	0.512850	6.40	19.43	19.21	15.61	15.60	39.06	38.77
QP93-1R	----	----	----	----	----	19.40	19.18	15.58	15.57	38.94	38.66

All samples were acid leached prior to dissolution except NC93-20u. The "m" subscript denotes measured values; the "i" subscript denotes values age corrected using concentrations from ICP-MS analyses and 90 Ma for the Nicoya rocks, 84 M for the Jaco rocks, and 63 Ma for the Quepos sample. Replicates are denoted with "R" and are complete replicates, i.e., they are analyses of separate rock sample aliquots.

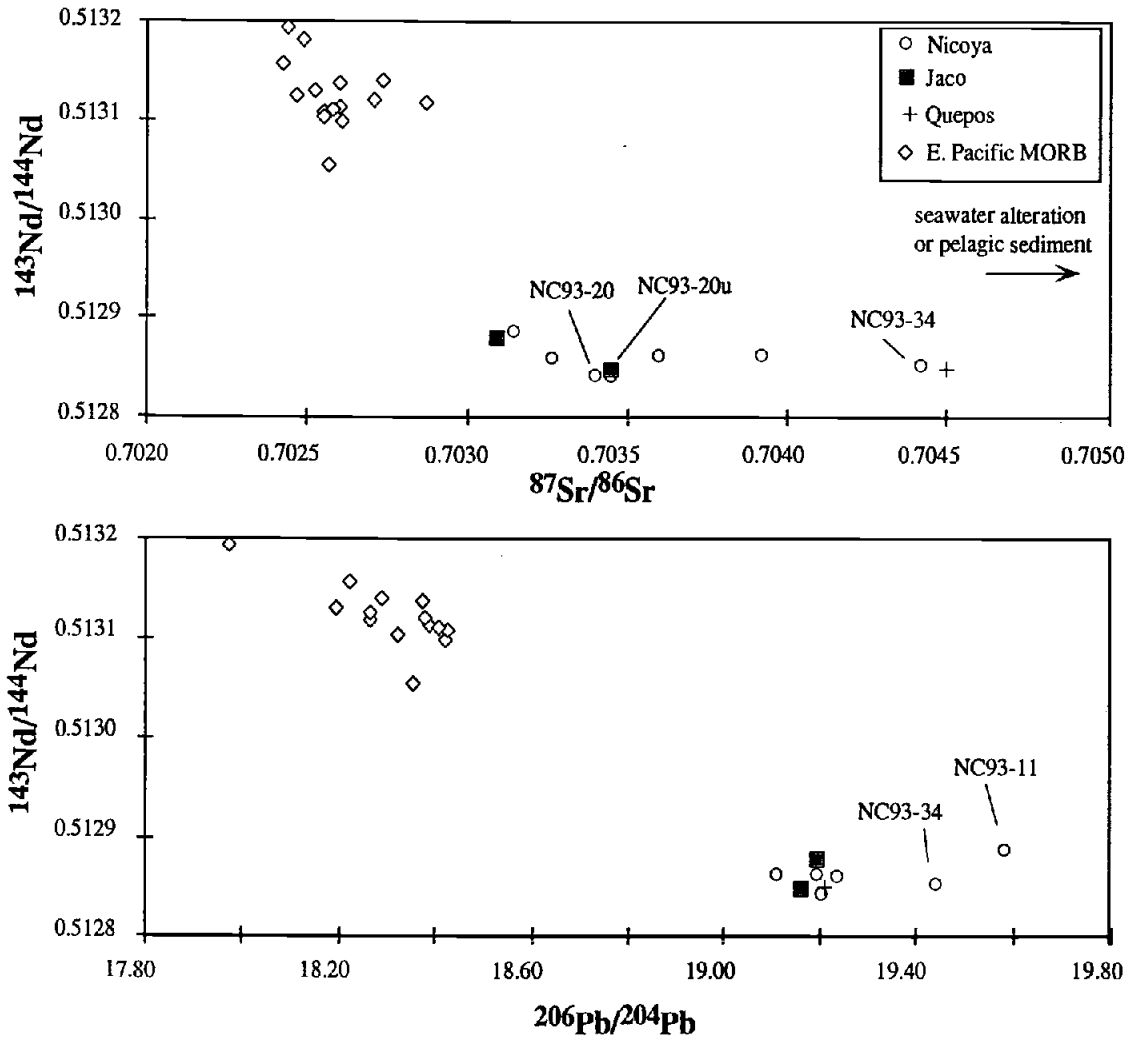

Fig. III.7. Sr, Nd, and Pb isotopic ratio plots. East Pacific MORB data are from White et al. (1987) and Prinzhofer et al. (1989). Pelagic sediment field from Doe (1970).

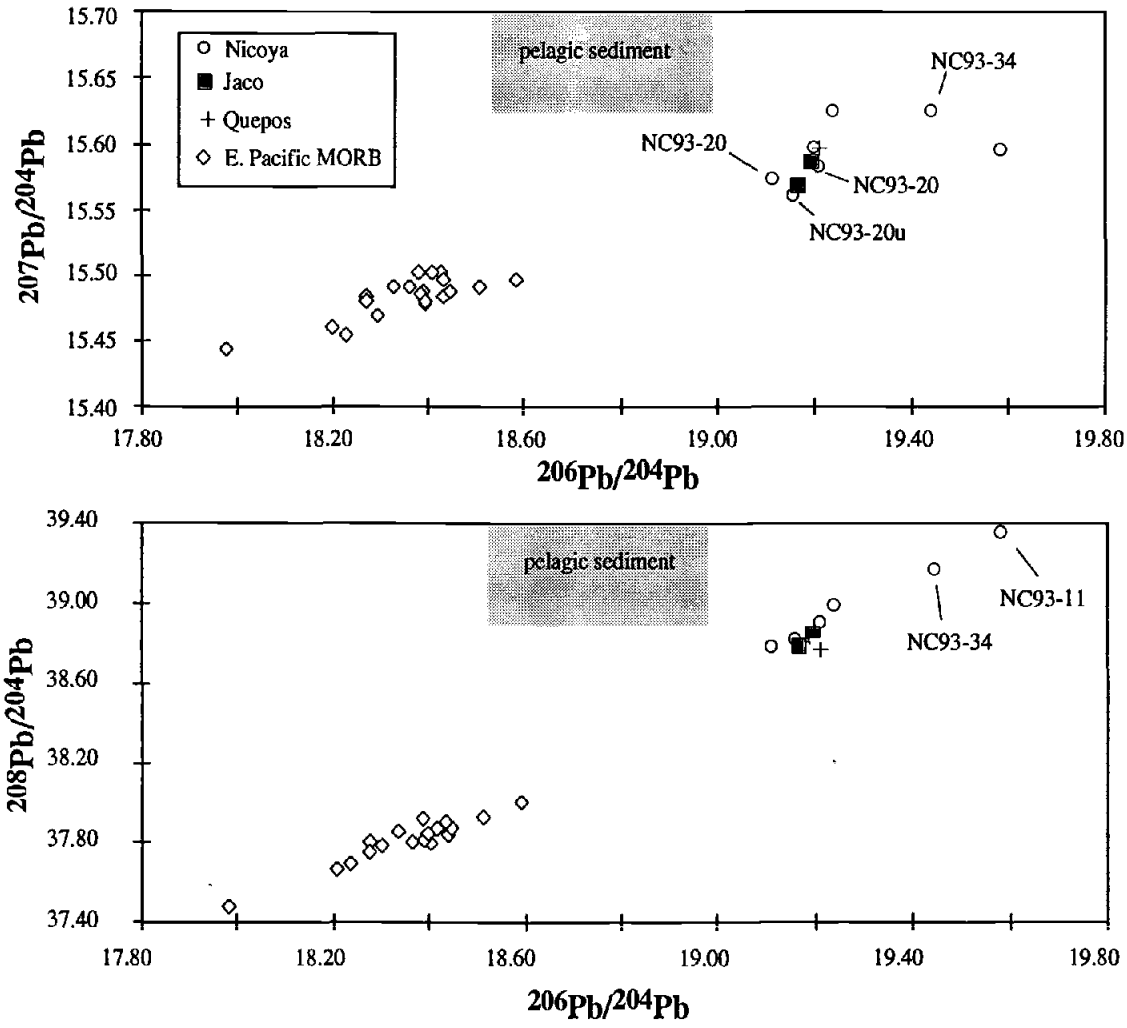

Fig. III.7. (cont'd)

Discussion

My combined geochronological and geochemical data do not support the previously proposed divisions for the Nicoya Peninsula mafic rocks. Rather, most or all of the exposed rocks appear to have been derived from similar parental magmas by fractional crystallization. In this section, I treat the Nicoya Peninsula rocks as a single suite and use the geochemical data to investigate the characteristics of the mantle from which the rocks were derived and to make comparisons with the Jacó and Quepos rocks. I will attempt to constrain the conditions of melting that produced the magmas and then later integrate all of the observations into a synthesis for the magmatic history of the Nicoya Complex.

Mantle Source

The Nd and Pb isotopic ratios show that the Nicoya rocks and probably the Jacó and Quepos basalts were derived from similar mantle sources which are distinct from the one that is parental to normal MORB. In terms of mantle end members described by isotopic composition (e.g., Zindler and Hart, 1986), the Costa Rica rocks could be interpreted as a mixture between DMM (depleted upper mantle) and a HIMU (enriched) source. Like isotopic ratios, some ratios of highly incompatible elements in basalts are not affected by melting and fractional crystallization processes and are therefore thought to reflect the ratios of the mantle source. In addition, some trace element ratios can differentiate between different proposed mantle sources for ocean island basalts (Weaver, 1991).

Weaver (1991) showed that ratios of LREE and high field strength elements (HFSE), such as La/Nb, can differentiate between different mantle endmembers (e.g., HIMU, EMI, EMII). For the Nicoya rocks, La/Nb ratios exhibit a narrow range (0.60-0.79) and do not change with increasing La concentration (i.e., increasing fractional crystallization). The Jacó (La/Nb = 0.61 and 0.81) and Quepos (La/Nb = 0.71) rocks fall within this range. This range is within that of HIMU ocean island basalts such as St. Helena (average La/Nb 0.69) and Tubuaii (average La/Nb 0.72) and distinct from MORB (La/Nb ~1.00) and EMI and EMII ocean island basalts, which have higher La/Nb values between 0.90 and 1.20. This strengthens the argument that the Nicoya rocks are genetically related and also suggests that all the collected Costa Rica rocks were derived

from a mantle source with HIMU affinities. However, given the small sample set from Jacó and Quepos, further analyses would be needed to corroborate this assertion.

Parental /Primary Magma

Before quantitatively assessing the mantle melting conditions from which the Costa Rica magmas were derived, a primary magma (i.e., the unmodified liquid derived from mantle melting)needs to be determined. It is unlikely that the source mantle underwent isobaric, batch melting, yielding a single primary magma. Rather, polybaric melting of a column of mantle probably occurred with discrete melt packets pooling at different depths. Aggregation of incremental melts is envisioned for the melting process beneath mid-ocean ridges (e.g., Klein and Langmuir, 1987; Johnson et al., 1990; Grove et al., 1992). Constraints on this process can be determined using the petrological and geochemical observations, although it must be kept in mind that the processes that produced the Nicoya lavas may have differed significantly from those that produce MORB .

A primary melt composition can be estimated from the most primitive lava. As I mentioned in the results section, NC93-11 represents the most primitive liquid composition, but it does not appear to be a primary melt. Hess (1992) stated several criteria for defining a primary melt for MORB: 1) olivine is the sole silicate liquidus phase at 1 atm, 2) the melt should be in equilibrium with a mantle assemblage at the depth of segregation, 3) the Mg# should reflect Fe-Mg equilibrium with mantle olivine (Fo_{91-92}), i.e., an Mg# of 0.68-0.75, 4) the Ni content should be in the range of 300-500 ppm. With the Nicoya data, I can check the last two criteria. NC93-11 has an Mg# of 63 (assuming that 90% of FeO_{total} is FeO; and, using an olivine-liquid K_d [Fe/Mg] of 0.3 (Roeder and Emslie, 1970), it is in equilibrium with Fo_{85}, low for lherzolite olivine (Fo_{88-91}; Hess, 1992). A Ni content of 84 ppm is also too low to be considered a primary melt.

A hypothetical primary melt can be constructed by adding olivine to the melt until it is in equilibrium with mantle olivine (~Fo_{90}). I added Fo_{88} olivine in 1% increments to NC93-11 until the model liquid was in equilibrium with Fo_{90} after 15% addition. The calculated liquid composition has an Mg# of 0.73 and a Ni content of 900 ppm (Table III.5). An assumption in this exercise is that only olivine crystallized from magmas more primitive than NC93-11. Therefore, the separation of NC93-11 to a potential primary magma by 15% fractional crystallization must be regarded as a minimum.

Melting Conditions

The mineralogy and composition of the source mantle as well as the degree of mantle melting that produced the Nicoya suite can be constrained using the geochemistry of the natural magma and calculated primary melt compositions. Major element compositions of MORB have been used to make relative comparisons of the degree and depth of melting beneath spreading ridge systems (e.g., Klein and Langmuir, 1987). In this type of evaluation, Na_2O and FeO concentrations of MORB glasses are backtracked to 8 wt. % MgO (Na_8 and Fe_8). Klein and Langmuir (1987) showed that regionally averaged Na_8 and Fe_8 vary throughout the global ridge network and that these variations reflect the integrated degree of melting and depth of melting which they argued is ultimately determined by mantle temperature. However, this type of analysis directly applied to the Costa Rica rocks may be misleading because of the demonstrated differences in either depth of crystal fractionation or primary magma composition. In addition, since Na_2O can be mobilized during alteration, the use of Na_8 as a indicator of the degree of melting may give erroneous results.

A better approach to constraining the conditions of melt generation would be to use the REE data because the chondrite-normalized patterns give an indication of the source composition and mineralogy and help to place constraints on the depth and degree of melting. Because the heavy REE are compatible in garnet, a light REE-enriched melt will be produced from a mantle that retains residual garnet after melting. Thus, the normalized REE pattern displayed by the Quepos basalt could mean that the primary magma was derived from melting the mantle at depths in which garnet is a stable phase (20 kbar/60 km; Ringwood, 1975) and remained in the residue after melting. Alternatively, the mantle source could have been enriched in the light REE. The relatively flat REE pattern displayed by the Nicoya and Jacó rocks could be produced by melting a primitive mantle composition (1.5 times chondritic) either at relatively shallow depths where garnet is not stable (< 60 km) or to the point where garnet is melted completely. Alternatively, the flat pattern could be derived from the mixing and melting of light REE-depleted and light REE-enriched mantle sources. This alternative seems unlikely based on the consistent REE patterns of all of the rocks.

A quantitative approach to constraining the degree of mantle melting that produced the Costa Rica magmas can be made using simple forward modeling which incorporates batch melting equations. Although it is more likely that fractional or near-fractional melting

occurred, the pooling of fractional melts could have produced melt compositions identical to batch melting (Shaw, 1970; Johnson et al., 1990; Langmuir et al., 1992). The goal of this exercise is to produce a general match to the REE pattern of potential primary magmas. In this model, a set of partition coefficients and modal percentages are chosen for the mantle mineral phases olivine, garnet, clinopyroxene, and orthopyroxene. By modulating the starting composition, the modal melting proportions, and the degree of batch melting, resulting melt compositions are plotted and compared to the natural compositions. Several problems are introduced that should be noted. One is that reported mineral/melt partition coefficients are variable. In particular, olivine Kd values derived experimentally differ from those inferred from olivine analyses in natural rocks (F. Frey, pers. comm.). However, the range of values does not dramatically affect the model. Another problem is the again lack of a primary magma composition. The hypothetical primary magma for the Nicoya rocks should have a pattern similar to NC93-11, but at lower abundances. Assuming that La is completely incompatible and 15% fractional crystallization from the primary melt produced NC93-11, the primary melt should have a La concentration of 1.70 ppm.

Model melt compositions are derived using non-modal batch melting such that the concentration of an element in the liquid (C_l), relative to an initial concentration in the solid source (C_o) is calculated using the equation:

$$C_l / C_o = \frac{1}{(D + F(1-P))}$$

where D is the bulk mineral-melt partition coefficient, F is the fraction of melt produced, and P is the summation of products of the mineral proportions (p) and the partition coefficients (k) ($P = \sum p_\alpha k_\alpha$). The proportions of the mantle assemblage and the melting proportions are taken from Frey (1983) and the partition coefficients are taken from Frey et al. (1978). The initial mantle composition is the bulk silicate earth of McDonough and Sun (1995). Assuming a modal composition of a garnet-bearing mantle as ol:opx:cpx:gt in proportions of 0.55:0.25:0.10:0.10 and 15:15:30:40 proportions of melting, derivative liquids will have a light REE-enriched pattern until 25% melting, at which point garnet is melted out. At 35% melting, clinopyroxene has melted out and the resulting liquid has a flat REE pattern and a La concentration of 1.85 ppm. The NC93-11 pattern is actually slightly light REE-depleted (Fig. III.8) which suggests that the mantle source is slightly depleted. I can match this pattern by constructing a depleted mantle that is the residual of the primitive mantle after 1% melt is removed. A mixture of primitive mantle and this hypothetical depleted mantle in 3:1 proportions melted to 30% gives a slightly light REE-

depleted composition with La at 1.70 ppm (Fig. III.8). This is not a perfect match as the HREE Yb and Lu concentrations from the model melt are slightly high, but it is close. Thus, the potential primary magma for the Nicoya suite can be derived from 30-35% batch melting of a mix of primitive mantle and depleted mantle in either the garnet or spinel stability fields.

I can attempt to match the REE pattern of the Quepos basalt, although without a knowledge of the primary magma composition the degree of mantle melting will not be well constrained. The pattern of QP93-1 indicates that either the mantle source was enriched in LREE or that garnet was residual in the source mantle, or both. Assuming a primitive mantle composition, I used a garnet-bearing (as above) and spinel-bearing (ol:opx:cpx 0.55:0.25:0.20 melting in proportions of 0.20:0.20:0.60) source. As expected, melting of

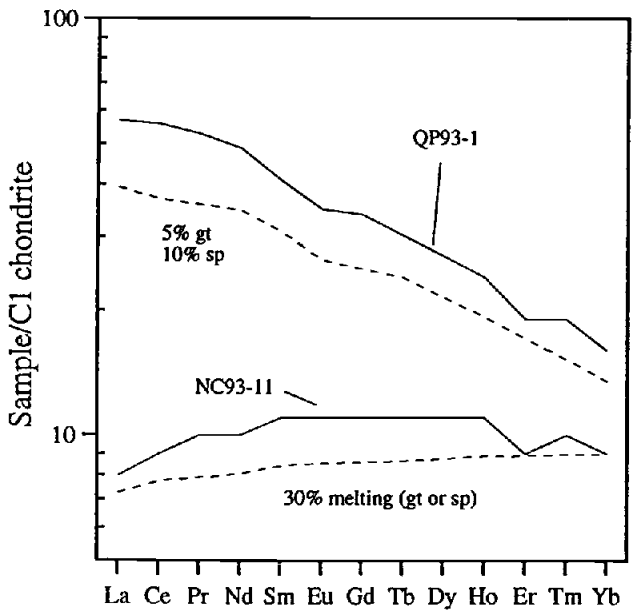

Fig. III.8. Non-modal batch melting model results for the rare earth elements. The LREE-enriched model line is a mix of a 5% melt from a garnet peridotite and 10% melt of a spinel peridotite. The starting composition was a primitive mantle (McDonough andSun, 1995). The slightly LREE-depleted line is a 30% melt of a mantle consisting of 75% primitive composition and 25% depleted (primitive mantle with 1% melt removed) composition.

the spinel-bearing assemblage results in an almost flat pattern. Melting of the garnet-bearing mantle to 5% and 10% results in patterns that are too depleted in the heavy REE, so the QP93-1 basalt could have been derived from pooled polybaric melts, i.e., a mix of melts from the garnet and spinel stability fields. A 1:1 mixture of a 5% melt of the garnet-bearing mantle and a 10% melt of the spinel-bearing mantle produces a good match to the QP93-1 pattern at lower concentrations (Fig. III.8). Approximately 30% fractional crystallization would be needed to arrive at the QP93-1 composition from this hypothetical primary melt.

Synthesis of Observations

Ideally, the interpretation of the petrogenetic history of a suite of igneous rocks should be based on the integrated observations from fieldwork, petrography, geochronology, and chemistry. Unfortunately, in western Costa Rica, individual flow units are virtually impossible to identify and stratigraphic relationships between the different outcrops are unconstrained. Therefore, we must rely more on the geochemical and age data in interpreting the magmatic history of the Nicoya Complex. I have made a case that the rocks of the Nicoya Peninsula are part of a single suite of variably differentiated rocks derived from similar parental magmas. Based on the ^{40}Ar-^{39}Ar studies, the magmas crystallized at 88 to 90 Ma while some intrusive rocks are slightly younger at 84 Ma. The previous designations of a lower unit of normal mid-ocean ridge generated crust and an upper unit partially made of oceanic plateau lavas (Schmidt-Effing, 1979; Kuijpers, 1980; Bourgois et al., 1984; Gursky et al., 1984; Wildberg, 1984; Frisch et al., 1992), originally based on the fossil ages of the radiolarite outcrops, are incorrect. The addition of a later primitive arc series by Wildberg (1984) and Frisch et al. (1992) was based on the observation that some rocks have relatively low concentrations of certain HFSE (Zr, Ti), which can be a characteristic of arc lavas. However, these studies did not note that the same lavas also have relatively high MgO contents and the depletion of HFSE (as well as other incompatible elements) is readily explained if most of the rocks belong to a suite dominated by fractional crystallization.

The ages of the two dated intrusions suggests that some magmatic activity post-dated initial extrusive activity by at least 4 m.y. Since the extrusive sections require rapid cooling (probably seafloor eruptions based on the reported pillow basalts and the overlying

pelagic sediments), it is reasonable that the slow cooling required for the intrusions occurred later in a thickened crustal section.

This study does not definitively state that all of the pre-Tertiary rocks of the Nicoya Peninsula are from the same suite. The radiolarite must have been deposited on oceanic crust that is at least of Jurassic age (H-J. Gursky, pers. comm.). I have shown that the rocks that have thus far been analyzed do not fit into this description in terms of their age or geochemistry. The radiolarite and the igneous rocks at all of the outcrops visited during this study had either faulted or igneous contacts, never an obviously sedimentary contact. Taken together, I conclude that the radiolarite was either picked up by massive volcanic flows or heavily penetrated by sills and dikes. Implicit in this conclusion is that the Late Cretaceous magmas erupted in an intraplate setting through pre-existing oceanic crust. Some of the older oceanic igneous crust over which the radiolarite was deposited may be found by continued sampling and analysis.

Eruption through pre-existing lithosphere provides a mechanism to explain the apparent crystal fractionation at depths greater than those at which normal MORB magmas are pooled. Because the lithospheric thicknesses at mid-ocean ridges are relatively negligible, melts would conceivably pool at shallow depths. In contrast, the parental melts of the Nicoya suite may have pooled beneath the pre-existing oceanic lithosphere, resulting in fractional crystallization at depths deeper than MORB magmas. It is also possible that the relatively early onset of clinopyroxene crystallization was due to a greater diopside component in the Nicoya parental magmas relative to those of normal MORB. However, this is not evident given the similarity in CaO between the Nicoya magmas and MORB at 9% MgO.

In the field, the Jacó rocks are identical to the Nicoya Peninsula suite: massive, faulted and fractured basalt flows; but the one radiometric age indicates that magmatism occurred at 84 Ma. It is not clear at this point whether volcanism in this region was continuous from 88 to 84 Ma, but it is possible that the Jacó basalt and the 84 Ma Nicoya gabbro (NC93-14B) are related based on their similarity in age and composition. The compositional similarity between all of the Nicoya and Jacó rocks indicates that there was no change in mantle source or conditions between 90 and 84 Ma. Though heavily altered and sparsely analyzed, the Quepos basalts are considerably younger than the Nicoya and Jacó suite and have compositions that differ in major and trace element abundances. It is possible that the Quepos lavas represent an accreted seamount (M. Meschede, pers.

comm.) that originated on the subducting Cocos Plate. As indicated by the trace element and isotopic ratios, the Quepos lavas appear to have been derived from a mantle source similar to that of the Nicoya and Jacó rocks. If this is the case, then there must have been a long-term, active magmatic anomaly in the area. The best candidate is the Galapagos hotspot. It is very likely that the Quepos lavas were part of an older, now subducted extension of the aseismic Cocos Ridge, which was produced by the northeast motion of the Cocos Plate over the Galapagos hotspot (Hey et al., 1977). The possible relationship between Costa Rica rocks and the Galapagos hotspot is explored further in Chapter IV.

It has been previously suggested that a portion of the Nicoya Complex is related to the thick Caribbean crust (e.g., Wildberg, 1984), which is considered to be the remnant of an oceanic plateau produced by initial volcanism of the Galapagos hotspot (Duncan and Hargraves, 1984). The ages presented here fall within the narrow range of radiometric ages from rocks in Haiti, Curaçao, Colombia, and Gorgona Island (Chapter IV) and the relatively flat REE patterns and Nd and Pb isotopic ratios of the Nicoya and Jacó rocks are identical to some of the Caribbean plateau lavas. However, none of the other outcrops of the Caribbean plateau display the highly differentiated magma compositions seen in the Nicoya Complex nor the abundance of included, older radiolarite. This may indicate some difference in the pre-oceanic plateau setting of the Nicoya locality relative to the other studied localities (see Chapter IV).

Conclusions

My combined data indicate that most of the mafic oceanic rocks of the Nicoya Peninsula belong to a single magmatic suite that began erupting at ~ 90 Ma. The data are not consistent with the division of the Nicoya Peninsula rocks into separate suites. The dating results show that four basalts and diabases from the Lower Nicoya unit (as defined by Gursky et al. 1984) were erupted in the Late Cretaceous (90-88 Ma), not in Jurassic to Early Cretaceous. The one reliable age from a basalt in the Upper Nicoya unit (NC93-20) is within the age range of the Lower Nicoya. A gabbro and a plagiogranite in the Lower Nicoya unit is slightly younger at 84 Ma, suggesting intrusive activity occurred after basalt extrusion. I cannot discount the possibility that Jurassic to Early Cretaceous oceanic crust does exist in the Nicoya Peninsula and that these have not been sampled. The coherent trends in the variation diagrams, the similarity in the REE diagrams, and the similarity in Nd and Pb isotopes provide strong evidence that the rocks collected thus far from the

Nicoya Peninsula are related to the same event. This event is most likely the formation of the Caribbean oceanic plateau based on similarities in age and compositions to exposed sections of the plateau around the Caribbean plate margins (Chapter IV). The Playa Jacó/Herradura basalts are slightly younger than the Nicoya Peninsula basalts and diabases based on a single reliable age (84 Ma), but are compositionally identical. The Quepos basalts, based on a single age of a basalt, are significantly younger and formed by lesser degrees of partial melting of a mantle source similar to the one from which the Nicoya magmas were derived. All or most of the obducted mafic material in western Costa Rica rocks is possibly a product of the Galapagos hotspot.

Chapter IV: An Oceanic Flood Basalt Province Forms the Caribbean Plate

Abstract

The thick oceanic crust of the Caribbean plate is the remnant of an oceanic plateau that has been inserted between North and South America. During its emplacement, the margins of the plateau have been uplifted above sealevel and and exposed by erosion, displaying the intrinsic features of the plateau. I present the results of ^{40}Ar-^{39}Ar radiometric dating of basalts from some of these on-land sections and drill sites from Leg 15 of the Deep Sea Drilling Project. At least five widely spaced on-land sections yielded ages ranging from 91 to 88 Ma. The poorly constrained radiometric ages from the drill cores combined with the Coniacian ages of associated sediments indicate a maximum crystallization age of ~90 Ma in the Venezuelan Basin. The combined ages indicate that the bulk of the Caribbean plateau erupted as flood basalts (i.e., catastrophic, short-lived volcanism). Plate reconstructions place the Caribbean plateau in the vicinity of the Galapagos hotspot at 90 Ma. Magmatism at 76 Ma is evident in Curaçao, Western Colombia, Haiti, and at DSDP drill site 152 (ODP site 1001) near the Hess Escarpment. This apparent second magmatic phase may have been caused by lithospheric extension during the tectonic emplacement of the plateau between North and South America or later volcanic activity caused by movement of the plateau away from the hotspot (plume stem).

The compositions of the 90 Ma magmas vary throughout the plateau and also within individual sites. Limited isotopic data are consistent with derivation from a mix between a depleted upper mantle and an enriched plume source with HIMU affinities (Galapagos hotspot?). The La/Nb ratios of the majority of the lavas are <0.80, similar to HIMU ocean island basalts and distinct from other mantle sources as well as the Ontong-Java plateau (which has isotopic affinities to the EMI/EMII mantle components). Zr/Nb ratios of 10-20 for the Caribbean plateau lavas are higher than HIMU ocean island basalts (~5). It is possible that the higher Zr/Nb ratios of the plateau basalts reflect higher degrees of partial melting compared to present day ocean island basalts.

Introduction

Oceanic plateaus are thick (20+ km) accumulations of oceanic crust rising 3-4 km above the surrounding seafloor. They are poorly understood features within the general plate-tectonic scheme of ocean basins because of their enormous size and relative inaccessibility, i.e., they are submerged in intraplate locations at considerable depth and are usually covered with thick sedimentary sequences. Our current fragmentary understanding is a result of geophysical surveys (seismic, gravity, magnetic) and Deep Sea Drilling Project (DSDP) and Ocean Drilling Program (ODP) sampling of plateaus such as the Ontong Java plateau (Leg 130) and the Kerguelen plateau (Legs 119, 120), which have been effective in documenting their volcanic origin and thus confirming their oceanic nature. The contemporaneity of widely distributed basement ages indicates that the plateaus (about 10 million km^3 or more) were built during very brief periods (a few million years?) and thus represent volcanic events greatly exceeding steady state crustal accretion rates. Such plateaus appear to be oceanic equivalents of continental flood basalt provinces which may be caused by the massive, initial eruptive phase of plumes rising from deep in the mantle (Richards et al., 1989; Campbell and Griffiths, 1990; Larson, 1991).

There are a number of difficulties in studying submarine features of this size (0.5 to 1.0×10^6 km^2). It is generally possible to sample a small fraction of the total area and limited drillstring penetration means that only the uppermost volcanic units are sampled. As a result, the early eruptive products and much of the internal structure of an undeformed plateau cannot be reached. Fortunately, the margins of an oceanic plateau which makes up much of the core of the Caribbean Plate (hereafter referred to as the Caribbean plateau) have been tectonically uplifted and are subaerially exposed (Fig. IV.1).

An inherent problem with studying these sections is they are highly faulted and their stratigraphic position and original location on the intact plateau are uncertain. Nevertheless, these sections give the most realistic opportunity for studying the internal structure and composition of an oceanic plateau short of very deep ocean drilling. I present the results of ^{40}Ar-^{39}Ar dating of rocks from some of the exposed margins of the Caribbean plateau and from drill cores from DSDP Leg 15. Reliable radiometric ages were obtained from the Dumisseau Formation of Haiti, the Curaçao Lava Formation of Curaçao, and the Central Cordillera and Gorgona Island of Colombia (Fig. IV.1). These

ages, combined with those from the Nicoya Complex of Costa Rica (Chapter III), indicate that the bulk of the plateau formed at 91-88 Ma, consistent with a flood basalt origin. Plate reconstruction models (Duncan and Hargraves, 1984) place the plateau within the vicinity of the Galapagos hotspot at 90 Ma, suggesting a genetic relationship. Radiometric ages of 76 Ma for basalts from Colombia and for a sill in the upper part of the Curaçaolavas, together with Campanian sediments in Haiti and at DSDP site 152 document a second pulse of magmatism. This second pulse may have resulted from either extension during tectonism or from volcanism associated with the stem of the mantle plume.

Previous Work

The core of the Caribbean plate is divided into the Colombian and Venezuelan basins, separated by a north-south topographic high named the Beata Ridge (Fig. IV.1). The basins are covered by flat lying sediments and irregularities in the topography of the basement are attributed to primary volcanic features (e.g., Bowland and Rosencrantz, 1988). The Venezuelan Basin is bounded to the east by the Aves Ridge and to the north and south by two deformed belts, the Muertos Trough and the southern Caribbean deformed belt. The Colombian Basin is bounded by the southern Caribbean deformed belt, the North Panama deformed belt to the west, and the 1000 km long Hess Escarpment to the north. To the northwest of the Hess Escarpment lies the southern Nicaragua Rise and the Cayman Trough.

Early seismic surveys of the region (Officer et al., 1957; Ewing et al., 1960; Ewing et al., 1967) demonstrated that the crust beneath the Caribbean Sea is much thicker than normal oceanic crust and more closely resembles oceanic plateaus in the western Pacific. The igneous basement of the thickened crust is represented seismically by the B" reflector (Fig. IV.1), which was characterized by a smooth horizon (relative to normal ocean floor) (Ewing et al., 1967). However, later studies discovered areas within the Venezuelan and Colombian basin where the B" is rougher (similar to normal oceanic crust) and occurs at relatively greater depths than the smooth B" basement (Ludwig et al., 1975; Diebold et al., 1981; Bowland and Rosencrantz, 1988). The relationship between the smooth and rough B" reflectors has been interpreted to be that of extended normal, older oceanic crust (rough B") overlain by Upper Cretaceous sills and flows (smooth B") (Bowland and Rosencrantz, 1988; Diebold et al., 1995). The nature of the southern

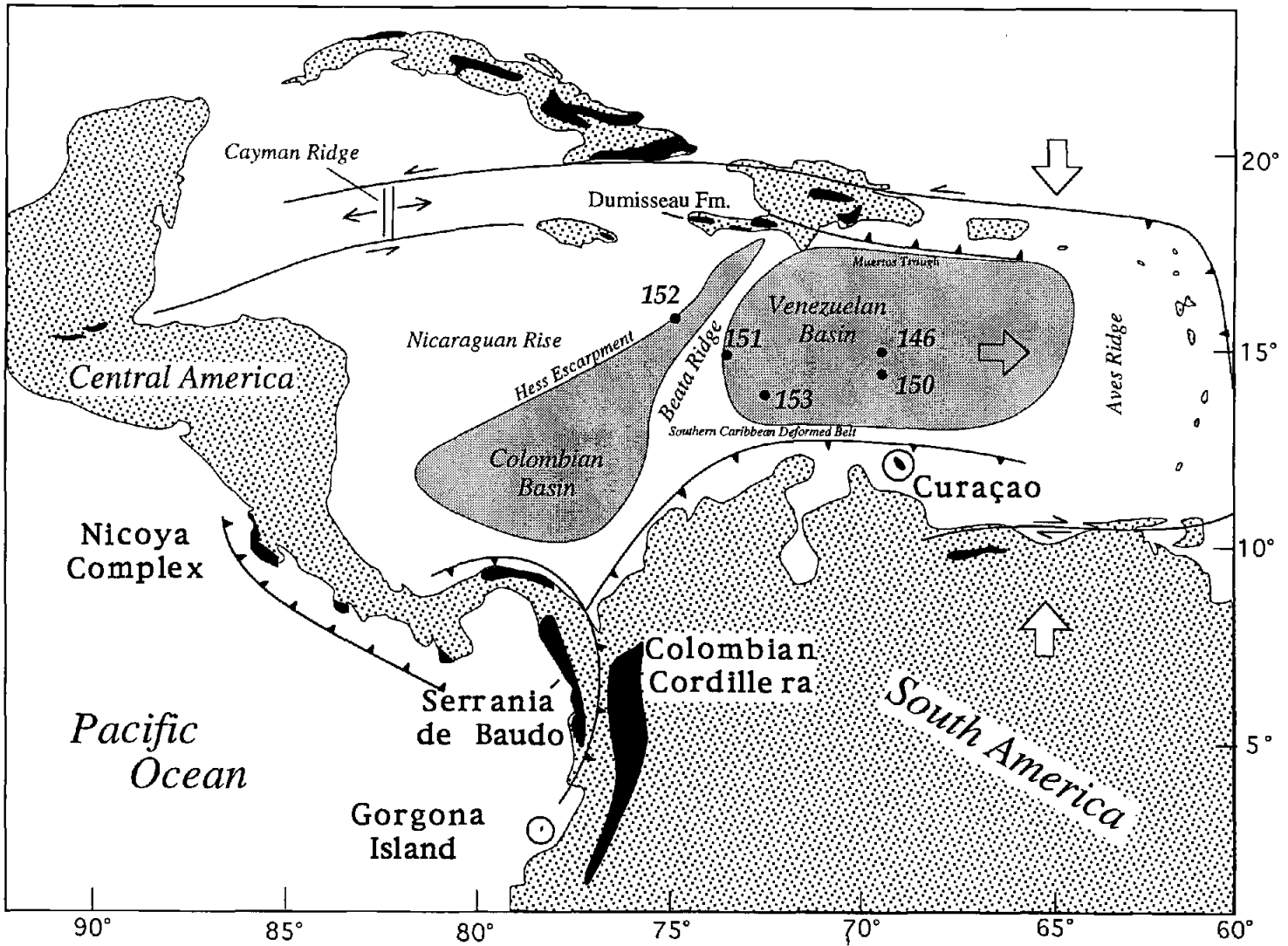

Fig. IV.1: Schematic map of the Caribbean region. Shown are the extent of the B" basement reflector (gray), the obducted plateau margins (black; Donnelly et al., 1990) and DSDP 15 drill sites (filled circles).

Nicaragua Rise is unknown, although sparse seismic data (Ewing et al., 1960; Edgar et al., 1971) show crustal velocities similar to the Colombian Basin but up to twice as thick. Pindell and Barrett (1990) suggested that the southern Nicaragua Rise is constructed of tectonically stacked B" crust. The Beata Ridge appears to be an extensional feature that post-dates formation of the plateau (Diebold et al., 1995).

DSDP Leg 15 drilled into the uppermost few meters of the igneous crust (Edgar and Saunders, 1973) at five sites (four within the smooth B"): three in the Venezuelan Basin (sites 146, 150, 153), one from the Beata Ridge (site 151), and one from the Nicaraguan Rise/Hess Escarpment (site 152) (Fig. IV.1). Site 152 differs from the other DSDP sites in that it is located on thinned crust (rough B") between the Hess Escarpment and the Beata Ridge (Diebold et al., 1995). The Colombian Basin has not been sampled by drilling. In contrast to normal ridge-formed oceanic crust, the DSDP Leg 15 rocks are characterized by thick, coarse-grained, basaltic sills (with a notable lack of pillowed material) overlain by, or intruding, foraminiferal limestone (Donnelly et al., 1973). Fossils within the overlying or intruded sediments are as old as Coniacian (89.0-85.8 Ma; Gradstein et al., 1994) in the Venezuelan Basin to early Campanian at site 152. The lack of metalliferous hydrothermal sediments and pillowed lava flows suggests that the crust was not derived from a mid-ocean ridge setting. Rather, the extraordinary thickness of the crust and the similar sediment ages over the basement in the Venezuelan Basin led Donnelly (1973) to conclude that the region had experienced a flood basalt event.

Plate reconstructions are consistent with Caribbean plateau formation in the Pacific on top of the now subducted Farallon plate and subsequent emplacement between North and South America (Burke et al., 1978; Duncan and Hargraves, 1984; Pindell and Barrett, 1990). Duncan and Hargraves (1984) proposed that the plateau was the product of initial volcanism from the Galapagos hotspot between 100 and 80 Ma. The age of the crust over which the Caribbean plateau was erupted is unknown, although interpreted magnetic anomalies from the Venezuelan Basin indicate formation at the Phoenix-Pacific-Farallon triple junction around 134 Ma (Hall, 1995) . However, Burke et al. (1978) and Donnelly (1985) have argued that magnetic anomaly interpretations are suspect because of overprinting from Late Cretaceous magmatism.

Subduction and faulting at the margins of the Caribbean Plate during emplacement into its present position have exposed numerous fragments of oceanic crust, some of which are distinctively arc related, i.e., they display arc-related chemical

signatures (e.g., Ta and Nb depletions) and a range of igneous lithologies (basalt, andesite, dacite) (Donnelly et al., 1990). Other formations, however, have geochemical signatures, lithologic structure, and fossil ages similar to the DSDP Leg 15 samples, which led Donnelly et al. (1990) to group them within a single Caribbean province (referred to as the Caribbean Cretaceous Basalt Province). The most prominent and best preserved of these exposed sections occur in Haiti, Curaçao, Western Colombia, Gorgona Island, and Costa Rica (Fig. IV.1).

Dumisseau Formation

The Dumisseau Formation of southwestern Haiti is made up of pillowed and massive basalts and picrites interlayered with thin pelagic sediments. The sediments range in age from possibly Early Cretaceous-Cenomanian to Late Santonian for the lower basalts and Late Campanian (~75 Ma) in the upper basalts (Maurasse et al., 1979). The formation is overlain by Maastrichtian limestones. Sayeed et al. (1978) reported a K-Ar age of 75 ± 1.5 Ma for a dolerite intruding the upper part of the sequence.

Curaçao

The Curaçao Lava Formation makes up most of the island of Curaçao (Beets et al., 1982) and is described in detail by Klaver (1987), who divided the volcanic stratigraphy into three sections. The lower part is composed of pillowed basalts and picrites, hyaloclastites, and some dikes, the middle part is composed of olivine and olivine-plagioclase tholeiitic pillow basalts, and the upper part is composed of olivine-plagioclase and plagioclase-clinopyroxene tholeiitic pillow basalts, hyaloclastites, and sills. The lavas appear to become progressively more differentiated higher in the lava pile, having an estimated total thickness of 5 km (Klaver, 1987). The time span of accumulation appears to be short given the lack of intercalated sediments. The only reported pelagic sediments are a sequence of siliceous shales and limestones containing ammonites that have been identified as mid-Albian (~105 Ma; Gradstein et al., 1994) by Wiedmann (1978). Klaver (1987) noted that the hyaloclastites associated with these sediments are, unlike the rest of the formation, encrusted with Fe-Mn coatings. Kerr et al. (1996a) pointed out that the ammonites are rather poorly preserved, incomplete, and

distorted and that there is a possibility that they were misidentified. There are two reported K-Ar ages from the Curaçao Lava Formation: 118 ± 10 Ma and 126 ± 12 Ma (Santamaria and Schubert, 1974)

Western Colombia

Fault-bounded, pillowed and massive basalts, picrites, and diabase sills are found in the Serrania de Baudo, Western Cordillera, and western edge of the Central Cordillera of Colombia (Goosens et al., 1977; McCourt et al., 1984; Millward et al., 1984; Spadea et al., 1989), separated from Paleozoic continental rocks to the east by the Romeral fracture zone (Fig. IV.2). The lava sequences are reportedly up to 5000 m thick (De Souza et al., 1984). The Serrania de Baudo (Basic Igneous Complex of Goosens et al., 1977) is exposed along the coast and is separated from the Western Cordillera (Diabase Group; e.g., McCourt et al., 1984) by sedimentary basins. The Western Cordillera is separated from Cenezoic sediments to the east by the Patia-Cauca fault zone. Picrites, basalts, and diabases on the western edge of the Central Cordillera have been broadly referred to as the Amaime Terrane (Aspden and McCourt, 1986), which is subdivided (from north to south) into the Cauca Complex, the Amaime Formation, and the Los Azules Complex (McCourt et al., 1984; Aspden and McCourt, 1986) .

There are no age data for the Serrania de Baudo. Lavas of the Western Cordillera are intercalated with sediments belonging to the Espinal Formation, in which fossils from the upper part of the formation suggest a post-Coniacian age (Barrero, 1979), although a K-Ar age of 136 ± 20 Ma is reported by Barrero (1979). In southwestern Colombia, tholeiitic rocks associated with the Diabase Group (El Tambo-El Peñol massif) gave a range of K-Ar ages (83-40 Ma), which can be attributed to alteration and the low K_2O contents of the samples (De Souza et al., 1984). The El Tambor stock, which intrudes the Diabase Group, gives a whole-rock Rb-Sr isochron age of 94 ± 16 Ma and hornblende mineral separate K-Ar ages of 83 ± 2 Ma and 84 ± 2 Ma (McCourt et al., 1984). The Amaime Formation is intruded by the Buga batholith. Reported radiometric ages for the batholith are variable: K-Ar dating of hornblende gave 113 ± 10 Ma (Toussant et al., 1978), 69 ± 2 Ma, 71 ± 2 Ma, and 76 ± 2 Ma (McCourt et al., 1984). K-Ar dating of biotite gave 89 ± 2 Ma and a two-point Rb-Sr isochron made from a biotite and a hornblende gave 99 ± 4 Ma (McCourt et al., 1984). Overall, the age of the western Colombia oceanic terranes is not well constrained by the existing radiometric ages.

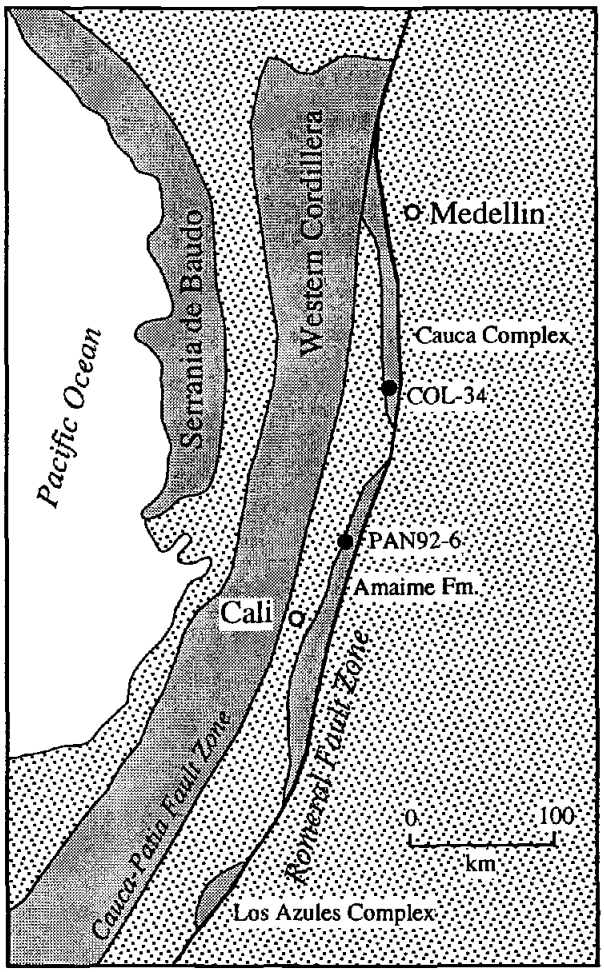

Fig. IV.2: Schematic map of western Colombia (based on Aspden and McCourt, 1986). The three basic divisions of the Mesozoic oceanic material are shown: the Serrania de Baudo, the Western Cordillera, and the Central Cordillera/Amaime Terrane. The latter section is further subdivided into the Cauca Complex, Amaime Formation, and Los Azules Complex. The sample localities are shown (filled circles).

Gorgona Island

Gorgona is a small island off the coast of Colombia that is known for the only Phanerozoic occurrence of komatiites (Fig. IV.3) (Gansser et al., 1979). The island is constructed of uplifted and faulted blocks of volcanic and intrusive mafic and ultramafic rocks overlain by undeformed Tertiary sediments (Echeverria, 1980). Walker et al., (1991) determined a 155 ± 43 Ma Re-Os isochron for the komatiites and a 88.1 ± 3.8 Ma Re-Os isochron for transitional tholeiitic basalts. Given the imprecision of the komatiite isochron, the possibility that it could represent a mixing line between two mantle source compositions (Walker et al., 1991), and the field observations that indicate that the komatiites and the basalts are interlayered (M. Storey, pers. comm.), it is reasonable to conclude that all of the lavas are coeval.

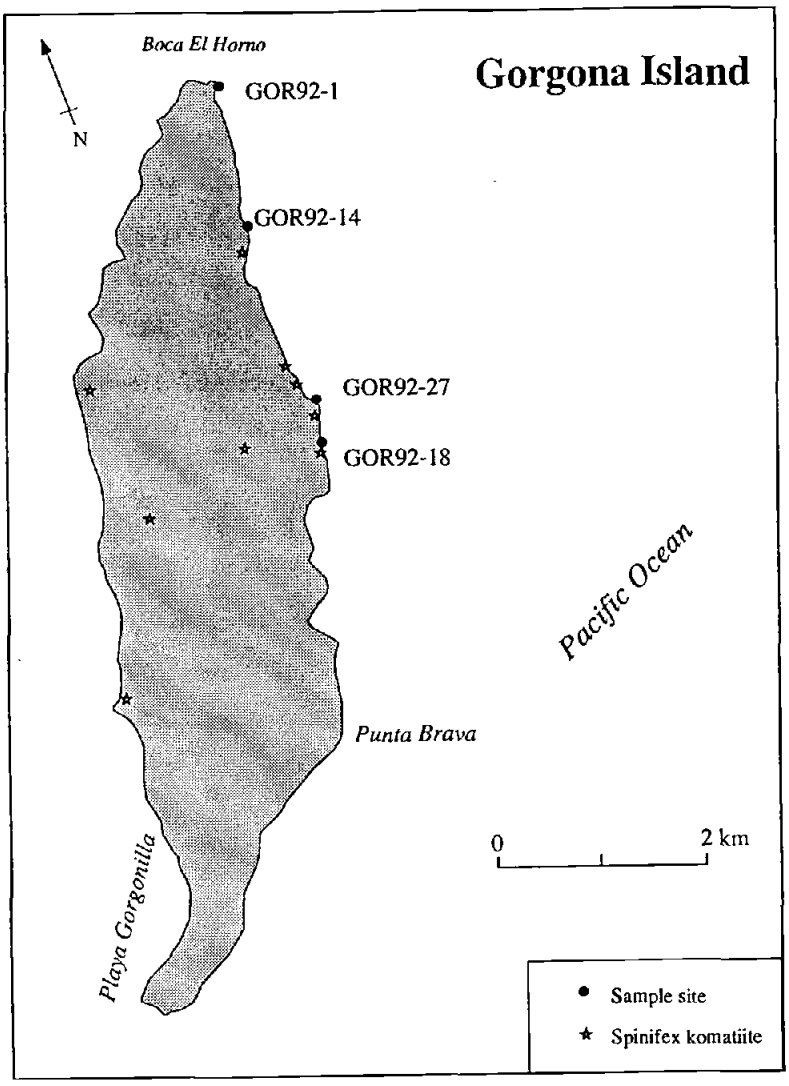

Fig. IV.3: Schematic map of Gorgona Island. Sample sites (filled circles) and komatiite exposures (stars) are shown.

Costa Rica

The Nicoya Complex is the general term used for Mesozoic-age ocean crust that makes up the basement of western Costa Rica and parts of Panama (e.g., Dengo, 1962). The basalts, diabases, and gabbros from the Nicoya Peninsula and Playa Jaco are related to the Caribbean plateau (Chapter III) with ages of 91-88 Ma for the Nicoya Peninsula basalts and an 84 Ma age for an intrusive gabbro. A basalt from Playa Jaco also gives an age of 84 Ma.

Samples and Analytical Methods

For all localities, the freshest and the most differentiated samples (highest primary K_2O) were selected and, where possible, the samples spanned the volcanic stratigraphy. The relative stratigraphic positions of some of the Dumisseau Formation lavas are reported by Sen et al. (1988), although there are samples analyzed for this work that were not reported in that paper. Relative stratigraphic control is also available for the Curaçao rocks (Klaver, 1987). There is no stratigraphic information for the Colombian and Gorgona Island samples. The DSDP Leg 15 samples were selected at the core repository at Lamont-Doherty Earth Observatory; no more than a few meters of core were recovered from any of the sites.

Age determinations on whole-rock and plagioclase separates were performed at Oregon State University using standard ^{40}Ar-^{39}Ar incremental heating techniques (Duncan and Hargraves, 1990; Duncan and Hogan, 1994). Whole-rock samples were either crushed in bulk in a ceramic jaw crusher and sieved to a uniform 0.5-1mm grain size or made into mini-cores (~2 mm long and 4 mm diameter). Groundmass plagioclase crystals were magnetically separated from DSDP Leg 15 diabases, hand picked under a binocular microscope, and were quickly rinsed in weak HF. All samples were ultrasonically cleaned in distilled water. All samples were sealed in evacuated quartz glass vials and irradiated for 6 hours at the OSU TRIGA nuclear reactor facility. Neutron flux during irradiation was monitored by FCT-3 biotite (27.7 Ma, Hurfurd and Hammerschmidt, 1985). Ar isotopes of the crushed whole rock samples (500-700 mg) were determined using an AEI MS-10S mass spectrometer. Samples were heated inductively with a radio frequency (RF) coil. The mini-cores and the plagioclase

separates (~100 mg) were analyzed using an MAP 215-50 mass spectrometer attached to a low-blank extraction line. These samples were heated with a double-vacuum resistance furnace.

Individual ages for each ^{40}Ar-^{39}Ar step were calculated after corrections for background, mass fractionation, and isotopic interferences and an assumed initial atmospheric argon content ($^{40}Ar/^{36}Ar = 295.5$). Individual step ages and Ar isotopic measurements for each sample are reported in Appendix 3. From the heating steps, age spectrum diagrams (age vs. % ^{39}Ar released) were generated. Ar plateau ages were calculated from consecutive steps that are concordant within 1σ error using the procedure described in Dalrymple et al. (1988), in which step ages were weighted by the inverse of their variance (Table IV.1). Isotope correlation diagrams ($^{36}Ar/^{40}Ar$ vs. $^{39}Ar/^{40}Ar$) were also made for each analysis, in which the slope is proportional to the age (isochron) and the inverse of the y-intercept gives the initial $^{40}Ar/^{36}Ar$ composition. The isochrons are calculated using the same steps used in the Ar plateau ages except where noted (Table IV.1).

I define a reliable age, i.e., one that is representative of the crystallization age, based on the criteria of Pringle (1993):

1) A well-defined age spectrum plateau of at least three concordant consecutive steps that represents at least of 50% of the total ^{39}Ar released.

2) A concordant isochron age in which the F-distribution (SUMS/N-2) is below the cutoff value at the 95% confidence level.

3) The $^{40}Ar/^{36}Ar$ intercept is statistically indistinguishable (within 1σ) from the atmospheric value 295.5

The SUMS/N-2 cutoff values are taken from Table IV.2 of Pringle (1993). For three, four, and five point isochrons, the cutoff values are 3.84, 3.00, and 2.60, respectively.

Major and trace element compositions for some of the rocks were determined by X-ray fluorescence (XRF) at Washington State University and inductively-coupled plasma mass spectrometry (ICP-MS) at Oregon State University. The existing DSDP Leg 15 trace element data (Bence et al., 1975) are limited, so the samples from each basement site were analyzed by ICP-MS to obtain a more complete dataset (Table IV.2).

Table IV.3 reports major and trace element data for Curaçao (Koraal Tabak sill), Colombia, and Haiti.

Results

DSDP Leg 15

The DSDP Leg 15 ^{40}Ar-^{39}Ar analyses gave generally poor results, brought about by low K_2O contents and contamination from atmospheric and excess ^{40}Ar components. Four samples from site 146 gave discordant results (Table IV.1, Fig. IV.4). Two of the samples, 15-146-42-3 and 15-146-43-3 gave apparent two-step Ar plateaus (of ~40% of the total ^{39}Ar released) of 90.6 ± 3.2 and 92.1 ± 4.7 Ma, respectively. Isochrons constructed from the linearly aligned steps are concordant within error with the Ar plateau ages and $^{40}Ar/^{36}Ar$ intercepts are near atmospheric, although the 15-146-43-4 sample had a SUMS/(N-2) value above the cutoff for statistical significance. Stratigraphically positioned between these two samples is 15-146-43-1, which gave a seemingly reliable Ar plateau age of 116.5 ± 3.2 Ma, a concordant isochron age, and an atmospheric $^{40}Ar/^{36}Ar$ intercept. Considering the Coniacian (89.0-85.8 Ma; Gradstein et al., 1994) age of the sediments that the site 146 sills intrude (Edgar and Saunders, 1973), this age cannot be accurate and must reflect excess ^{40}Ar contamination.

One sample from site 150 gave a two-step Ar plateau of 94.3 ± 2.8 Ma (65% of the total ^{39}Ar released), a concordant isochron of 95.7 ± 6.2 Ma (constructed from all of the steps), and a near atmospheric $^{40}Ar/^{36}Ar$ intercept. A whole rock analysis of a site 153 basalt gave an apparently reliable 100.1 ± 1.9 Ma Ar plateau and 98.0 ± 1.5 Ma isochron age, but an analysis of groundmass plagioclase using the MAP-215 mass spectrometer shows heterogeneously distributed excess ^{40}Ar. An isochron plot of data from the plagioclase gives an age of 87.3 ± 2.4 Ma and a $^{40}Ar/^{36}Ar$ intercept of 353.4. Two whole rock samples from site 152 displayed step ages that decreased with increasing temperature, an indication of ^{39}Ar recoil losses. Calculated total fusion ages for these two samples yielded 43.2 ± 1.0 and 71.8 ± 0.8 Ma. Together, none of the analyses from the DSDP Leg 15 samples provided entirely reliable radiometric ages. Nevertheless, the sills at sites 146 and 150 intrude Coniacian sediments, placing a maximum age on their crystallization. The age of the Beata Ridge (site 151), Hess Escarpment (site 152), and the entire Colombian Basin remain undated by radiometric methods, although site 152

Table IV.1: ^{40}Ar-^{39}Ar Plateau and Isochron Age Calculations from the Caribbean Plateau

Sample	Material	Plateau Age by $1/\sigma^2$(m.y.)	^{39}Ar % of Total	Isochron Age (m.y.)	N	$^{40}Ar/^{36}Ar$ Intercept $\pm 1\sigma$	SUMS/ (N-2)
DSDP Leg 15							
146-42-3, 103-106	whole rock	90.6 ± 3.2*	40	85.9 ± 4.5	4	298.1 ± 0.7	1.6
146-43-4, 94-96	whole rock	92.1 ± 4.7*	44	93.7 ± 9.1	3	293.0 ± 1.4	4.3†
150-11-2, 11-13	whole rock	94.3 ± 2.8*	56	95.7 ± 6.2	6	296.1 ± 1.2	2.0
Dumisseau Formation, Haiti							
HA76-120	whole rock	89.2 ± 1.5	68	90.0 ± 4.9	3	280.0 ± 14.6	10.2†
HA77-28	whole rock	88.7 ± 1.5	58	96.2 ± 5.6	3	285.2 ± 24.2	0.11
HA76-165	whole rock	90.6 ± 1.1	100	92.2 ± 1.1	5	292.5 ± 4.6	4.8†
HA74-24	whole rock	91.2 ± 0.6	87	91.1 ± 1.3	5	295.8 ± 5.9	0.81
HA74-25	whole rock	92.0 ± 4.8	54	89.8 ± 1.1	5	305.2 ± 1.7	1.41
Curaçao							
79BE-73	whole rock	89.5 ± 1.0	98	93.2 ± 1.3	5	288.8 ± 2.9	1.17
BK79-262	whole rock	88.0 ± 1.2	94	92.0 ± 5.7	6	291.1 ± 3.6	1.75
BE79-249	whole rock	75.9 ± 0.5*	72	77.5 ± 3.2	3	253.9 ± 15.3	13.9†
79KV-9	whole rock	75.8 ± 2.0	94	77.3 ± 2.9	3	293.7 ± 1.5	7.86†
Gorgona Island							
GOR92-1	whole rock	86.7 ± 4.6§	88	---	-	---	---
GOR92-14	whole rock	88.3 ± 1.9§	56	---	-	---	---
GOR92-18	whole rock	87.1 ± 3.2§	48	---	-	---	---
GOR92-27	whole rock	87.9 ± 2.1	100	86.1 ± 6.1	3	283.3 ± 1.5	11.8†
Western Colombia							
PAN92-6	whole rock	91.7 ± 2.7	89	94.7 ± 6.4	3	292.4 ± 15.6	0.25
COL34-2	whole rock	76.3 ± 1.7	100	77.0 ± 1.7	6	294.6 ± 7.9	0.45
COL34-3	whole rock	76.3 ± 1.6	74	72.6 ± 4.7	3	298.7 ± 6.4	0.66

Ages calculated using the following decay constants: $\lambda_\varepsilon = 0.581 \times 10^{-10}$ yr^{-1}, $\lambda_\beta = 4.963 \times 10^{-10}$ yr^{-1}. Isotopic interferences for the OSU TRIGA reactor are: $(^{36}Ar/^{37}Ar)_{Ca} = 2.64 \times 10^{-4}$, $(^{39}Ar/^{37}Ar)_{Ca} = 6.73 \times 10^{-4}$, and $(^{40}Ar/^{39}Ar)_K = 1.00 \times 10^{-3}$

* Two-step plateau ages

† Values exceed the 95% confidence level cutoff

§ Middle step age of three

Table IV.2: ICP-MS Trace Element Data for DSDP Leg 15 Samples

	146-42-2, 62-65	146-43-1, 132-135	146-43-4, 94-96	150-11-1, 87-89	150-11-2, 11-13	150-12-1, 91-93	151-14-1, 139-141	151-15-1, 122-124	152-24-1, 125-127	152-24-2, 38-40	153-20-1, 39-41	153-20-2, 81-83
Cr	307	338	318	325	309	309	324	293	228	222	149	150
Ni	116	120	116	113	112	111	112	113	66	73	82	75
Ba	11.9	10.8	9.4	13.3	12.6	12.6	47.5	47.5	5.5	5.6	15.1	11.0
Sc	43.35	45.32	44.40	46.44	44.98	46.16	39.98	38.33	54.94	56.31	50.76	49.53
Sr	122.7	125.6	124.6	127.9	106.7	108.2	318.6	296.0	100.2	99.1	122.8	123.0
Rb	0.70	0.66	0.38	0.88	0.85	0.84	23.87	21.99	10.32	4.69	0.55	0.28
Y	23.1	21.6	21.7	23.0	21.5	22.8	33.8	33.4	45.6	42.7	31.7	30.5
Nb	3.30	3.04	3.15	3.56	3.57	3.64	23.85	22.32	2.06	2.02	4.54	4.51
Zr	61.2	56.7	58.4	65.3	63.3	65.6	185.7	173.8	84.1	81.2	79.4	79.9
Cs	0.03	0.02	0.03	0.01	0.01	0.02	0.37	0.72	0.14	0.04	0.01	0.01
La	2.93	2.32	2.40	2.69	2.63	2.75	16.63	15.65	2.21	1.82	3.40	3.24
Ce	8.15	6.81	6.98	7.81	7.64	7.83	39.40	36.95	7.59	6.80	9.51	9.52
Pr	1.23	1.17	1.17	1.30	1.28	1.31	5.81	5.30	1.42	1.36	1.60	1.59
Nd	6.4	5.8	6.0	6.7	6.5	6.7	26.1	24.4	8.3	8.1	8.3	8.1
Sm	2.1	2.0	2.0	2.2	2.2	2.2	6.5	6.0	3.3	3.3	2.8	2.8
Eu	0.81	0.77	0.78	0.87	0.85	0.87	2.19	2.05	1.28	1.25	1.08	1.09
Gd	2.87	2.66	2.73	2.95	2.88	2.88	7.07	6.91	4.87	4.93	3.86	3.81
Tb	0.56	0.53	0.54	0.57	0.55	0.58	1.11	1.09	1.02	1.01	0.77	0.75
Dy	3.51	3.29	3.42	3.55	3.44	3.51	6.05	5.93	6.74	6.37	4.85	4.66
Ho	0.78	0.74	0.78	0.78	0.74	0.78	1.22	1.21	1.52	1.49	1.09	1.08
Er	2.17	2.13	2.14	2.25	2.07	2.18	3.04	3.07	4.46	4.34	3.17	2.99
Tm	0.32	0.33	0.33	0.37	0.33	0.34	0.43	0.45	0.68	0.71	0.51	0.47
Yb	2.00	1.94	2.01	2.11	2.04	2.01	2.38	2.42	4.06	4.15	3.02	2.86
Lu	0.32	0.31	0.31	0.32	0.30	0.31	0.36	0.35	0.61	0.63	0.47	0.45
Hf	1.62	1.52	1.53	1.76	1.70	1.76	4.73	4.45	2.46	2.50	2.17	2.16
Ta	0.22	0.20	0.22	0.25	0.23	0.25	1.45	1.34	0.14	0.14	0.30	0.33
Pb	0.33	0.36	0.26	0.70	0.22	0.25	1.07	1.21	0.30	0.26	0.63	0.34
Th	0.24	0.23	0.24	0.27	0.27	0.28	1.90	1.83	0.13	0.13	0.31	0.33
U	0.06	0.05	0.06	0.06	0.06	0.06	1.20	0.67	0.81	0.94	0.08	0.10

Table VI.3: Major and Trace Element Data from On-Land Caribbean Plateau Sites

	Western Colombia			Koraal Tabak Sill		Dumisseau Formation		
	COL34-2	COL34-3	PAN92-6	79KV-9	79KV-10	HA74-24	HA74-25	HA76-105
SiO2	51.67	51.28	50.25	50.18		49.81	50.02	47.75
TiO2	1.11	0.91	1.06	0.98		1.11	1.24	2.68
Al2O3	14.07	14.30	14.33	14.35		14.32	15.96	18.18
Fe_2O_3			11.8					
FeO	9.38	8.39		9.89		10.24	10.28	10.99
MnO	0.18	0.17	0.198	0.17		0.19	0.19	0.15
MgO	8.71	9.33	8.17	8.43		9.07	7.06	5.47
CaO	12.86	12.65	11.66	11.80		12.81	13.33	4.40
Na2O	1.43	1.79	2.16	2.76		1.81	1.92	5.71
K2O	0.05	0.05	0.07	0.13		0.08	0.04	1.36
P2O5	0.09	0.07	0.09	0.06		0.09	0.10	0.53
Total	99.55	98.94	99.79	98.75		99.53	100.14	97.22
Cr	331	403		246	287	341	225	2
Ni	131	137		97	172	118	78	5
V	301	280		263	255	301	317	90
Ba	23.66	13.731		5.91	11.31	20.9	11.3	238.8
Sc	41.6	35.9		37.7	50.3	36.7	45.4	10.1
Sr	106.0	92.8	90.6	76.9	65.0	88.7	111.9	
Rb	0.71	0.35	0.7	0.71	0.32	0.93	0.43	12.21
Y	19.81	15.93	23.2	14.0	11.9	19.8	23.9	17.4
Nb	5.7	4.5	4.1	3.0	1.4	4.1	4.6	47.1
Zr	61.95	50.14	55.2	37.0	22.6	59.4	65.4	212.5
Cs	0.00	0.01		0.01	0.01	0.01	0.01	0.27
La	4.25	3.16		1.80	1.10	3.15	3.68	24.61
Ce	10.27	8.05		4.89	2.90	8.09	9.14	51.86
Pr	1.58	1.29		0.85	0.55	1.29	1.48	6.02
Nd	7.34	6.10		4.19	2.75	6.28	7.25	24.50
Sm	2.28	1.88		1.42	1.02	2.09	2.42	4.93
Eu	0.82	0.71		0.55	0.39	0.76	0.90	1.68
Gd	2.90	2.33		2.04	1.42	2.74	3.07	5.19
Tb	0.54	0.44		0.38	0.31	0.55	0.60	0.76
Dy	3.32	2.67		2.43	1.89	3.36	3.77	3.75
Ho	0.71	0.59		0.51	0.43	0.75	0.87	0.67
Er	1.82	1.54		1.38	1.15	1.98	2.18	1.54
Tm	0.32	0.25		0.22	0.20	0.31	0.36	0.24
Yb	1.83	1.51		1.37	1.15	1.88	2.27	1.44
Lu	0.30	0.25		0.22	0.19	0.30	0.35	0.23
Hf	1.68	1.35		1.06	0.71	1.58	1.76	4.30
Ta	0.38	0.29		0.21	0.09	0.27	0.28	2.50
Pb	0.46	1.02		0.00	0.00	0.16	0.27	2.62
Th	0.43	0.30		0.13	0.08	0.31	0.39	2.92
U	0.12	0.08		0.03	0.02	0.09	0.10	0.76

Fig. IV.4: Plotted step age spectra and isotope correlation diagrams for each ^{40}Ar-^{39}Ar analysis from DSDP Leg 15 sites. The length of each step age refers to the fraction of the total ^{39}Ar released and the thickness of the step is the $\pm 1\sigma$ error. The horizontal lines adjacent to the plateau age indicate the steps used in the age calculation. The filled squares in the correlation diagrams were used in a weighted linear regression to obtain an isochron age. The inverse of the y-intercept of the regression gives the initial $^{40}Ar/^{36}Ar$ ratio.

DSDP 15-146-42-2, 62-65 cm
basalt

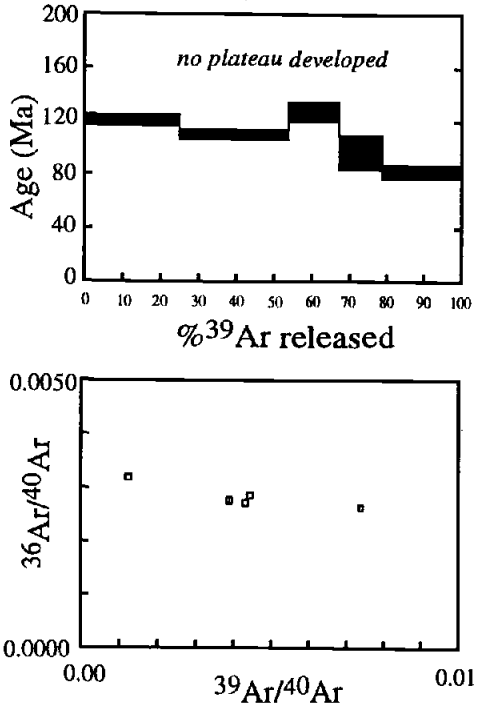

DSDP 15-146-42-3, 103-106 cm
basalt

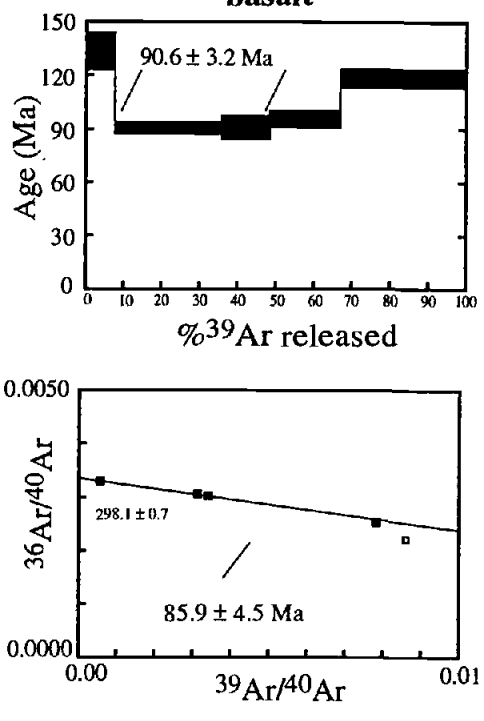

DSDP 15-146-43-1, 131-125 cm
basalt

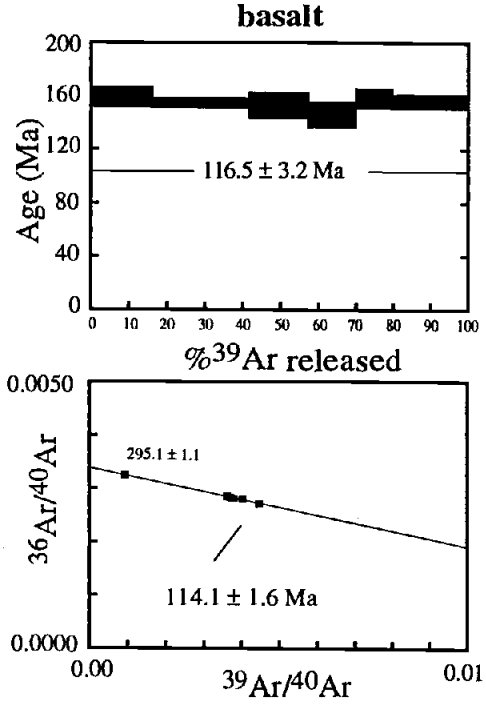

DSDP 15-146-43-4, 94-96 cm
basalt

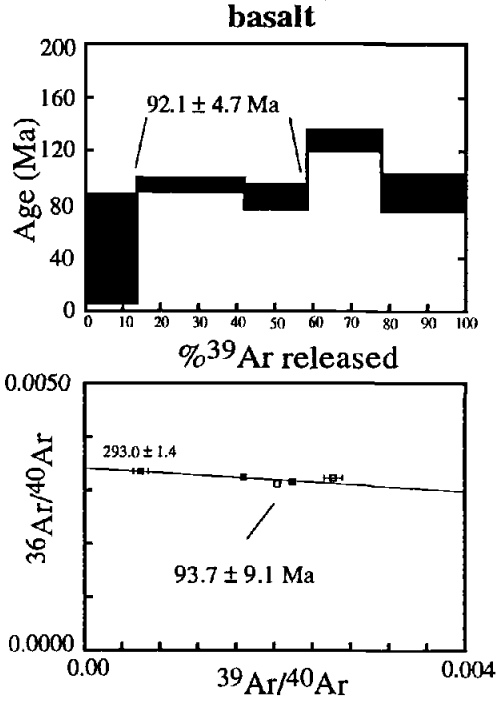

DSDP 15-150-11-2, 11-13 cm, basalt

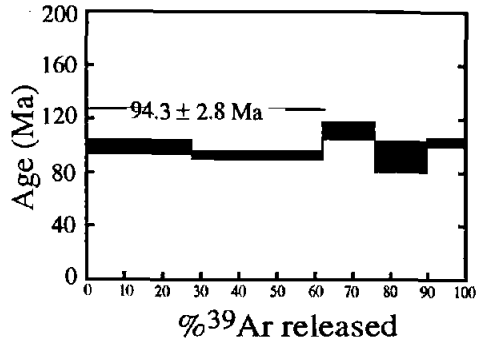

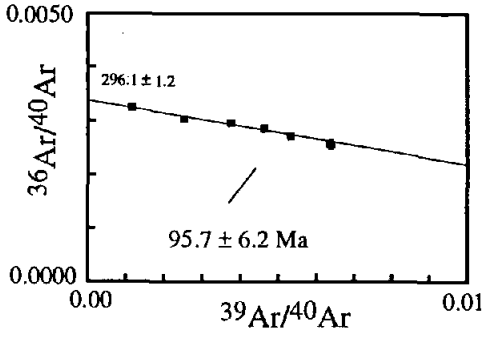

DSDP 15-153-20-1, 39-41 cm, basalt

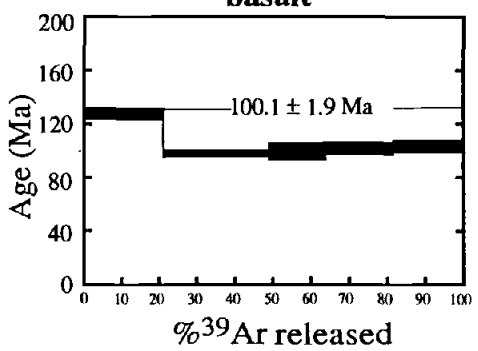

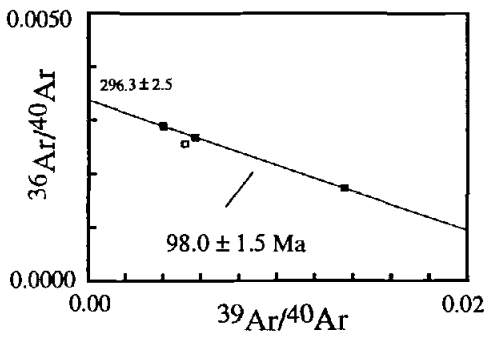

DSDP 15-153-20-1, 39-41 cm, plagioclase

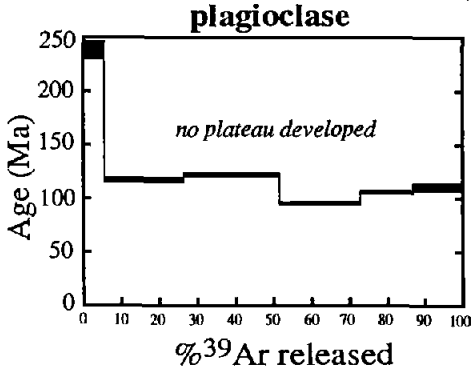

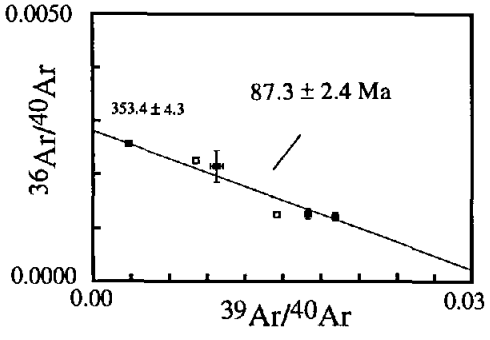

must be younger than the Venezuelan Basin lavas given the Campanian age of the sediments included in the basaltic sills (Edgar and Saunders, 1973). Radiometric dating of the Hess Escarpment samples recovered during ODP Leg 165 is in progress.

Bence et al. (1975) divided the DSDP Leg 15 rocks into a high K_2O-TiO_2, light rare earth element (LREE) enriched group (site 151; Beata Ridge) and a more depleted, LREE-depleted group similar to mid-ocean ridge basalt (MORB; all other sites). My trace element data (Table IV.2) generally confirm this, but the LREE-depleted group consists of the slightly LREE-depleted lavas from Venezuelan basin sites (146, 150, and 153) and the very LREE-depleted rocks from site 152 (Fig. IV.5a). The REE patterns of the Venezuelan basin rocks are parallel and, given the apparent similarities in age, are probably related to the same magmatic event and differ by the degree of fractional crystallization from similar parental magmas. Later magmatism at site 152 appears to have been derived from a more depleted mantle that is similar to an upper mantle MORB source.

The Dumisseau Formation

Five of the six analyzed samples from the Dumisseau Formation (supplied by F. Maurasse, Florida International University) yielded reliable ages (Table IV.1, Fig. IV.6). The initial heating steps of four of these samples are considerably older than the higher-temperature steps used in the Ar plateau age calculations, suggesting either a common source of excess ^{40}Ar, due to interaction with a low temperature fluid that was enriched in ^{40}Ar, or recoil loss of ^{39}Ar from a low-temperature alteration phase. All Ar plateau and isochron ages are concordant and y-intercepts are near atmospheric composition, although two (HA76-120 and HA76-165) have SUMS/(N-2) values above the cutoff. Ar plateau ages are between 88.7 ± 1.5 to 92.0 ± 4.8, all within analytical uncertainty, with a weighted mean of 90.7 ± 0.5 Ma. The weighted mean of the isochron ages is 91.7 ± 0.8 Ma. Magmatism may also have occurred later given the late Campanian sediments interbedded in the upper basalts (Maurasse et al., 1979) and the 75 ± 1.5 Ma age of a late-stage sill in the upper part of the sequence (Sayeed et al., 1978).

Most of the Dumisseau Formation basalts reported in Sen et al. (1988) are LREE-enriched, similar to the basalts recovered at DSDP site 151 (Beata Ridge). The exception is a basalt in the lower section of the formation that is LREE-depleted, similar to rocks

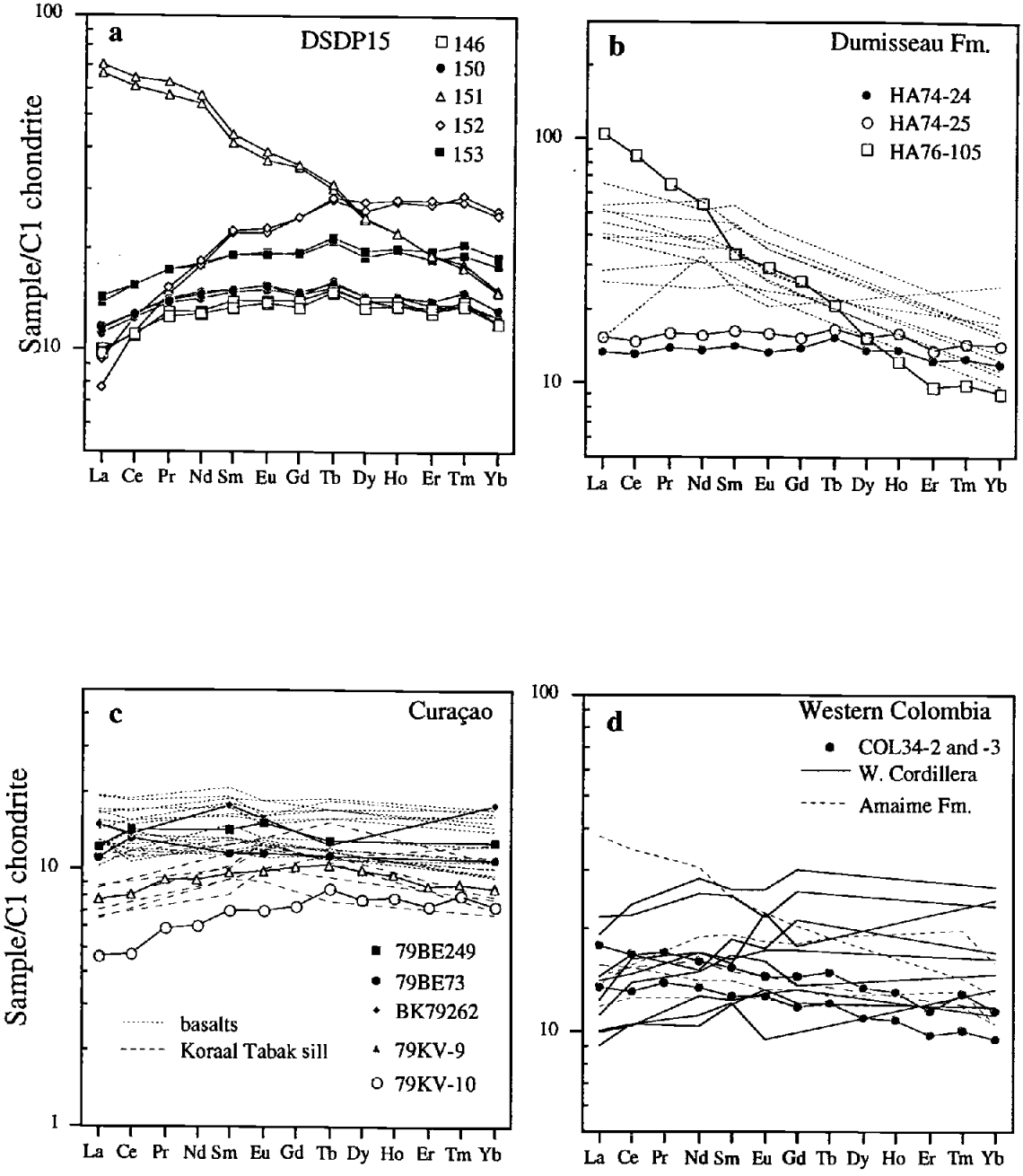

Fig. IV.5: Compiled chondrite-normalized rare earth element (REE) diagrams. The values were all normalized using C1 chondrite from McDonough and Sun (1995). **a)** DSDP Leg 15 sites (Table VI.2). **b)** Dumisseau Formation; dashed lines are from Sen et al. (1988) and the other values are from Table VI.3. **c)** Curaçao; fine dashed lines are basalts from Klaver (1987). The samples highlighted with filled symbols are also basalts from Klaver (1987) and were analyzed for this project. The coarse dashed line (Klaver, 1987) and the samples highlighted with open symbols (Table VI.3) are from the Koraal Tabak sill. **d)** Western Colombia; solid lines from Millward et al. (1984), dashed lines from Aspden and McCourt, 1986.

Fig. IV.6: Plotted step age spectra and isotope correlation diagrams for each ^{40}Ar-^{39}Ar analysis from the Dumisseau Formation, Haiti. The length of each step age refers to the fraction of the total ^{39}Ar released and the thickness of the step is the $\pm$ 1σ error. The horizontal lines adjacent to the plateau age indicate the steps used in the age calculation. The filled squares in the correlation diagrams were used in a weighted linear regression to obtain an isochron age. The inverse of the y-intercept of the regression gives the initial $^{40}Ar/^{36}Ar$ ratio.

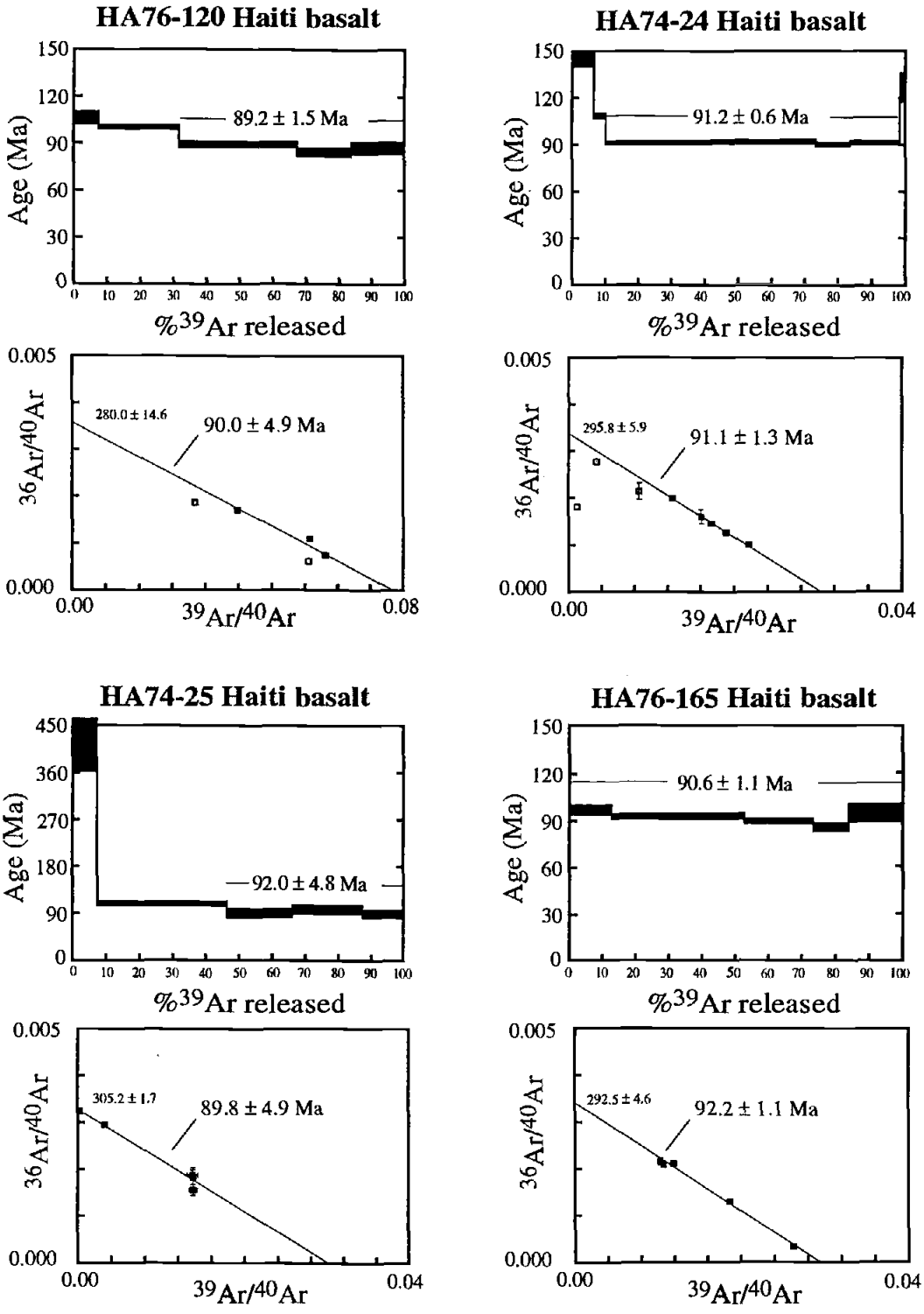
HA76-120 Haiti basalt
Age (Ma)
89.2 ± 1.5 Ma
%39Ar released
36Ar/40Ar
280.0 ± 14.6
90.0 ± 4.9 Ma
39Ar/40Ar
HA74-24 Haiti basalt
91.2 ± 0.6 Ma
295.8 ± 5.9
91.1 ± 1.3 Ma
HA74-25 Haiti basalt
92.0 ± 4.8 Ma
305.2 ± 1.7
89.8 ± 4.9 Ma
HA76-165 Haiti basalt
90.6 ± 1.1 Ma
292.5 ± 4.6
92.2 ± 1.1 Ma

HA77-28 Haiti basalt

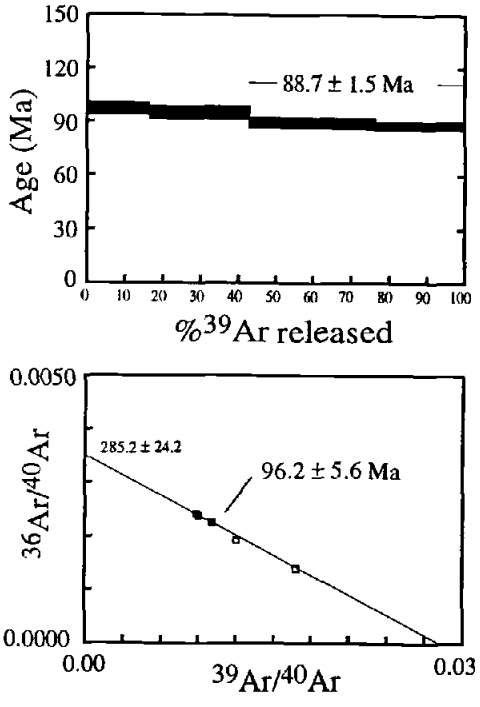

HA76-173A Haiti basalt

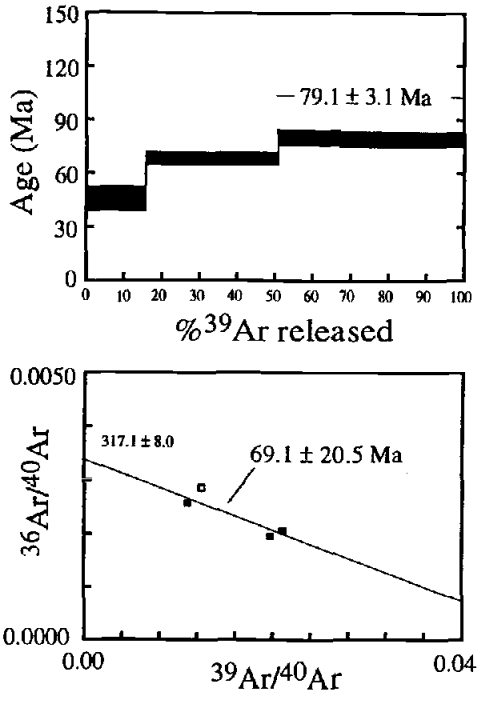

HA76-173B Haiti basalt

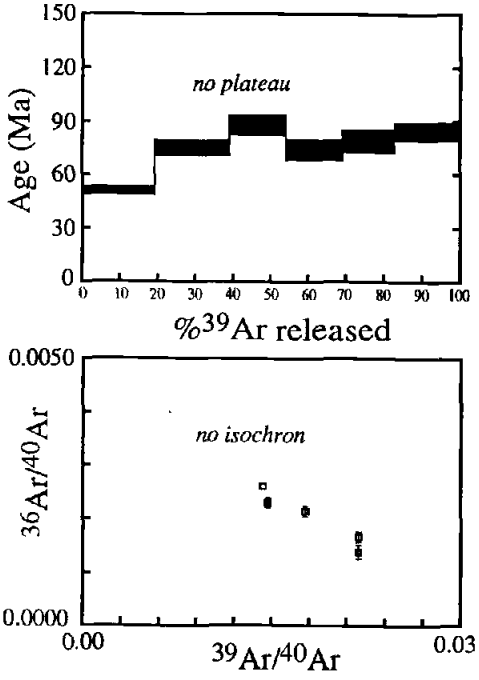

from DSDP site 152. The LREE-depleted basalt was not analyzed in this study. Relative stratigraphic positions for the samples reported here are, from stratigraphically oldest to youngest, HA77-28, HA76-120, and HA76-165 (Sen et al., 1988) . HA74-24 and HA74-25 are not reported in any previous publications and are compositionally distinct from the other Dumisseau lavas in having flat REE patterns at 15x chondrites(Fig. IV.5b). Both of these samples are fresh, well-crystallized, olivine-plagioclase-clinopyroxene phyric basalts with most olivine altered to iddingsite and some interstitial mesostasis altered to chlorite. The ages from these samples are statistically indistinguishable from those of the LREE-enriched samples at ~90 Ma, indicating simultaneous eruption of compositionally distinct lavas.

HA76-105 is a very fine-grained, alkalic basalt that was not dated because it is slightly altered and highly vesicular. It is LREE-enriched (Fig. IV.5b), but more so than the lavas reported by Sen et al. (1988) and is also more enriched in incompatible elements (e.g., P_2O_5) at similar MgO concentration (~5%). Without any age or stratigraphic information, its relationship to the Caribbean plateau is unknown. Nevertheless, this sample is useful in noting the compositional diversity of lavas in Haiti.

The Curaçao Lava Formation

Three of the five analyzed basalts from Curaçao (supplied by G. Klaver, Ryjks Museum, The Netherlands) yielded reliable ages (Table IV.1, Fig. IV.7). An olivine tholeiite pillow from the lower part of the volcanic stratigraphy (79BE-73) and a plagioclase-clinopyroxene dolerite from the upper part (BK79-262) gave Ar plateau ages between 88 and 90 Ma (88.9 ± 0.8 Ma weighted mean) with slightly higher isochron ages (93.1 ± 1.3 Ma weighted mean). The higher isochron ages reflect the slightly lower $^{40}Ar/^{36}Ar$ intercepts for these samples. There is no known natural process that can reduce this ratio below atmospheric (295.5), so the initial ratios were probably atmospheric and therefore the age spectra better reflect the crystallization age. 79BE-249 is a plagioclase-clinopyroxene pillow basalt from the upper part of the lava pile and gave a two-step Ar plateau of 75.9 ± 1.0 Ma; an isochron constructed from these two steps and the previous step yielded an age of 77.5 ± 3.2 Ma, but with an initial $^{40}Ar/^{36}Ar$ ratio

Fig. IV.7: Plotted step age spectra and isotope correlation diagrams for each ^{40}Ar-^{39}Ar analysis from Curaçao. The length of each step age refers to the fraction of the total ^{39}Ar released and the thickness of the step is the $\pm 1\sigma$ error. The horizontal lines adjacent to the plateau age indicate the steps used in the age calculation. The filled squares in the correlation diagrams were used in a weighted linear regression to obtain an isochron age. The inverse of the y-intercept of the regression gives the initial $^{40}Ar/^{36}Ar$ ratio.

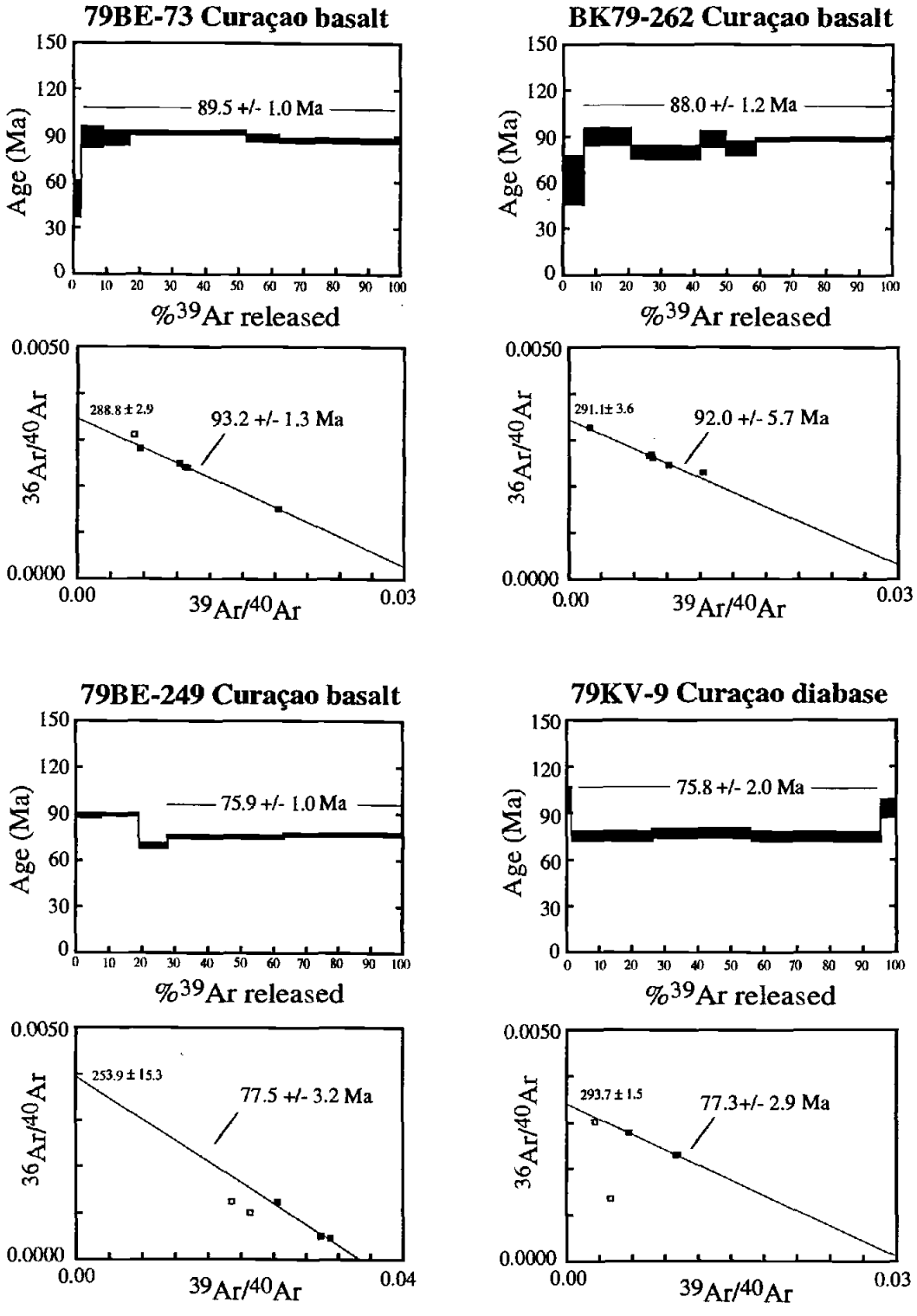
79BE-73 Curaçao basalt
89.5 +/- 1.0 Ma
Age (Ma)
%39Ar released
288.8 ± 2.9
93.2 +/- 1.3 Ma
36Ar/40Ar
39Ar/40Ar
BK79-262 Curaçao basalt
88.0 +/- 1.2 Ma
Age (Ma)
%39Ar released
291.1± 3.6
92.0 +/- 5.7 Ma
36Ar/40Ar
39Ar/40Ar
79BE-249 Curaçao basalt
75.9 +/- 1.0 Ma
Age (Ma)
%39Ar released
253.9 ± 15.3
77.5 +/- 3.2 Ma
36Ar/40Ar
39Ar/40Ar
79KV-9 Curaçao diabase
75.8 +/- 2.0 Ma
Age (Ma)
%39Ar released
293.7 ± 1.5
77.3+/- 2.9 Ma
36Ar/40Ar
39Ar/40Ar

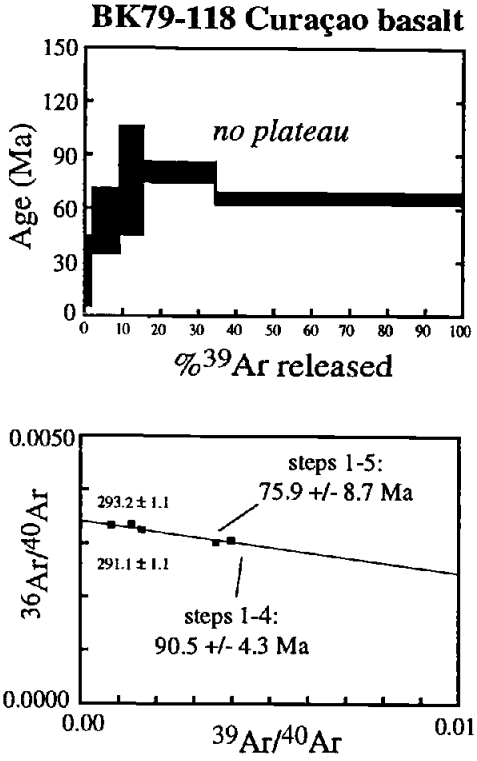
BK79-118 Curaçao basalt
150
120
90
60
30
0
Age (Ma)
no plateau
0 10 20 30 40 50 60 70 80 90 100
%39Ar released
0.0050
0.0000
36Ar/40Ar
293.2 ± 1.1
291.1 ± 1.1
steps 1-5:
75.9 +/- 8.7 Ma
steps 1-4:
90.5 +/- 4.3 Ma
0.00
0.01
39Ar/40Ar

significantly below atmospheric and a SUMS/(N-2) value well above the cutoff. The ages of this sample cannot be considered reliable. 79KV-9 is from the >200 m thick Koraal Tabak sill (Klaver, 1987) and is considerably younger than the basalts with a 75.8 ± 2.0 Ar plateau age and a 77.3 ± 2.9 Ma isochron. Although the isochron regression appears to be a good fit, the SUMS/N-2 value is slightly above the cutoff.

The two ~90 Ma Curaçao basalts bracket the upper and lower limits of the volcanic stratigraphy, indicating that the bulk of the lava pile was built over a short duration which is equal to or less than the precision of the dates (1-2 m.y.). The Koraal Tabak sill was emplaced up to 14 m.y. after initial volcanism. Most of the lavas and the picrites have flat to slightly LREE-enriched patterns while the Koraal Tabak sill samples show slightly LREE-depleted patterns (Fig. IV.5c). Overall, the data show at least two compositionally distinct magmatic events, initial production of the lava pile at ~90 Ma of flat to slightly LREE-enriched compositions and later sill intrusion of slightly LREE-depleted magmas at ~76 Ma.

Western Colombia

Three samples from the western edge of the Central Cordillera of Colombia (supplied by M. Storey, Danish Lithosphere Centre, Copenhagen) were analyzed. Results are given in Table IV.1 and Fig. IV.8, but only one (PAN92-6; dolerite) yielded a coherent age spectrum and isochron (91.7 ± 2.7 Ma and 94.7 ± 6.4 Ma, respectively). PAN92-6 was taken from a roadcut ~50 km north of Cali in what would be the Amaime Formation of Aspden and McCourt (1986). Basalts COL34-2 and -3 (supplied by J. Estrada) are also from the Central Cordillera, but to the north of PAN92-6 in the Cauca Complex of Aspden and McCourt (1986) (in the Rio Cauca valley just west of Manizales). Both samples gave identical Ar plateau ages (76.3 ± 1.6 and ± 1.7 Ma) and concordant isochron ages with a weighted mean of 76.5 ± 1.6 Ma. These latter two samples are relatively fresh and there is no evidence in the age spectra for radiogenic ^{40}Ar loss due to alteration.

COL34-2 and COL-34-3 show slightly LREE-enriched patterns, similar to some of the Central Cordillera Amaime Formation rocks (Millward et al., 1984; Aspden and McCourt, 1986) (Fig. IV.5d) There are no compositional data for PAN92-26. The Western Cordillera basalts, although undated, have generally flat REE patterns (Millward

Fig. IV.8: Plotted step age spectra and isotope correlation diagrams for the ^{40}Ar-^{39}Ar analysis from Western Colombia that yielded reliable ages. The length of each step age refers to the fraction of the total ^{39}Ar released and the thickness of the step is the $\pm 1\sigma$ error. The horizontal lines adjacent to the plateau age indicate the steps used in the age calculation. The filled squares in the correlation diagrams were used in a weighted linear regression to obtain an isochron age. The inverse of the y-intercept of the regression gives the initial $^{40}Ar/^{36}Ar$ ratio.

PAN92-6 Colombia diabase

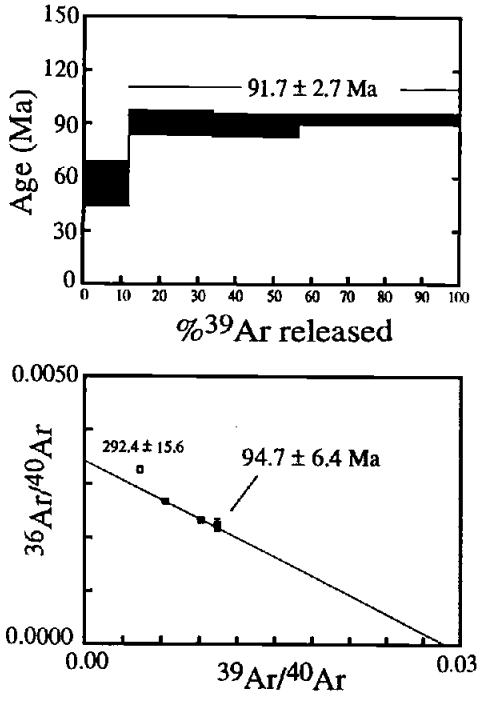

COL34-2 Colombia basalt

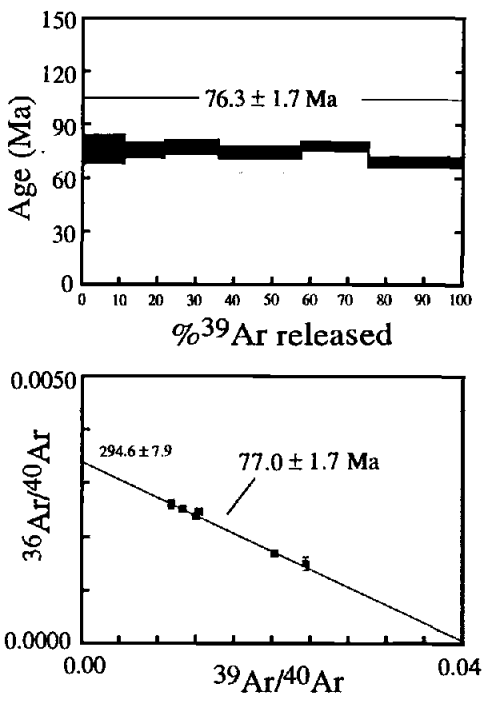

COL34-3 Colombia basalt

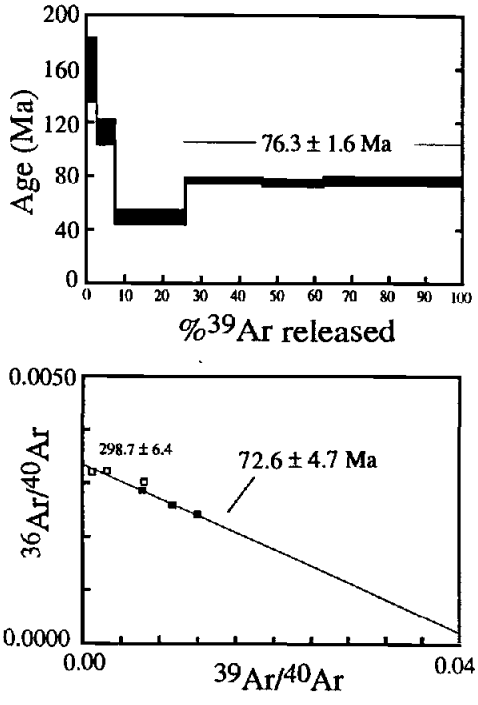

et al., 1984). Although somewhat sparse, the combined radiometric ages and compositional data suggest that the Amaime Formation and the Cauca Complex appear to be similar in composition, separated by ~14 m.y.

Gorgona Island

Five samples from Gorgona Island (Fig. IV.9) were analyzed by ^{40}Ar-^{39}Ar dating methods. Because of the low K_2O contents of the Gorgona basalts (and necessarily low amounts of radiogenic ^{40}Ar) they were analyzed using three heating steps to minimize analytical error. Although none of the individual analyses yielded a reliable age as I have defined previously, together they indicate crystallization ages of ~88 Ma. One sample (GOR92-27) gave a three-step Ar plateau age of 87.9 ± 2.1 Ma and a poorly constrained isochron of 86.1 ± 6.1 Ma. GOR92-1 gave a two-step Ar plateau age of 87.6 ± 4.6 Ma and the middle step ages of two other samples (GOR92-18 and GOR92-14) are 88-87 Ma (Table IV.1). These ages are consistent with the 88.1 ± 3.8 Ma Re-Os isochron of Walker et al. (1991) for Gorgona basalts. Because field relations indicate that the komatiites and the basalts are coeval (M. Storey, pers. comm.), komatiite extrusion probably occurred at ~88 Ma.

There are no REE data for the samples reported here, although the Gorgona Island basalts show a wide compositional range from LREE-depleted to LREE-enriched (Echeverria, 1980; Aitken and Echeverria, 1984; Kerr et al., 1996b). The komatiites are consistently LREE-depleted. We conclude that all of the Gorgona lavas erupted at ~88 Ma, so, like the Dumisseau Formation, coeval volcanism was compositionally heterogeneous.

Discussion

Timing of Caribbean Plateau Volcanism

The Coniacian age (89.0-85.8 Ma; Gradstein et al., 1994) of sediments overlying the igneous basement of the Venezuelan Basin, coupled with the 91-88 Ma ^{40}Ar-^{39}Ar

Fig. IV.9: Plotted step age spectra for each ^{40}Ar-^{39}Ar analysis from Gorgona Island. The length of each step age refers to the fraction of the total ^{39}Ar released and the thickness of the step is the $\pm 1\sigma$ error. The horizontal lines adjacent to the plateau age indicate the steps used in the age calculation. The isotope correlation diagram for the one sample that yielded three linear steps is shown. The inverse of the y-intercept of the regression gives the initial $^{40}Ar/^{36}Ar$ ratio.

GOR92-27 Gorgona basalt

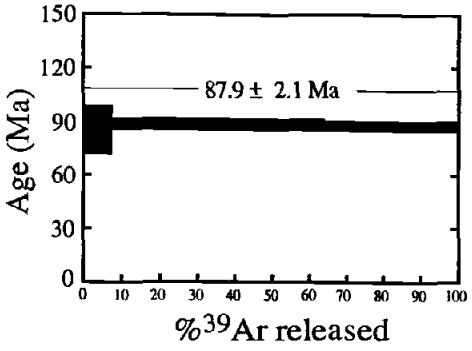

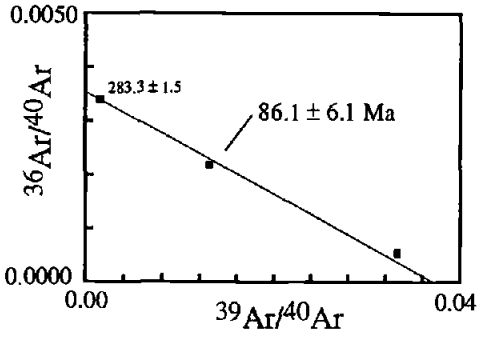

GOR92-1 Gorgona basalt

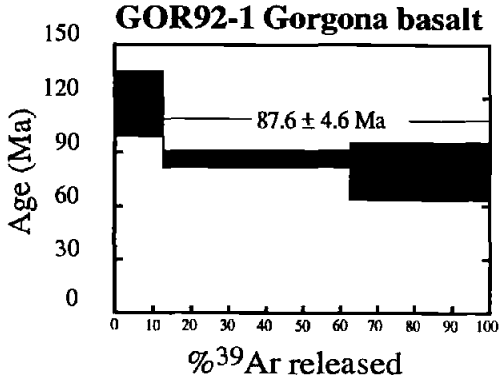

GOR92-14 Gorgona basalt

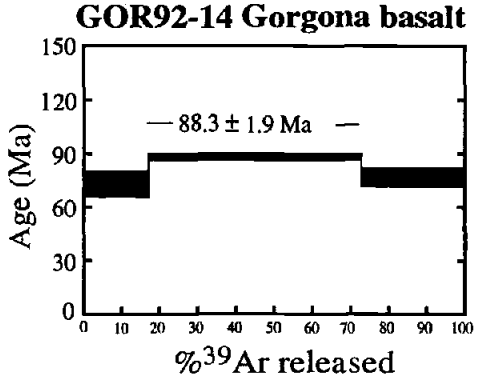

GOR92-18 Gorgona basalt

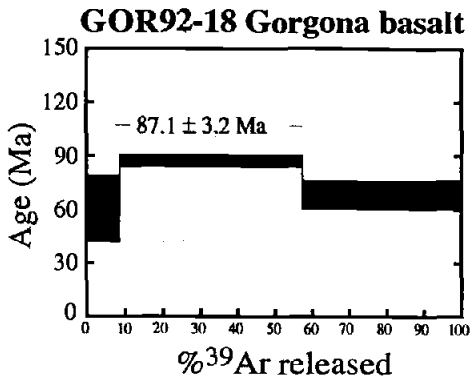

GOR92-37 Gorgona basalt

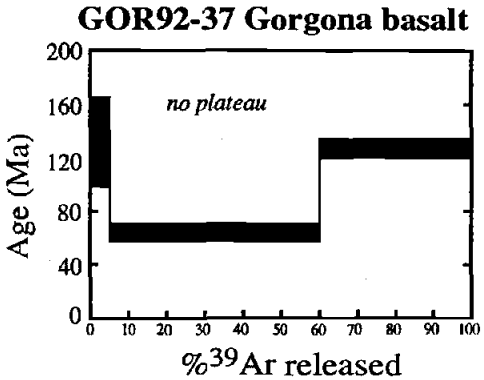

Discussion

Timing of Caribbean Plateau Volcanism

The Coniacian age (89.0-85.8 Ma; Gradstein et al., 1994) of sediments overlying the igneous basement of the Venezuelan Basin, coupled with the 91-88 Ma ^{40}Ar-^{39}Ar ages (weighted mean of 89.5 Ma ± 0.3 Ma including the Nicoya Complex ages in Chapter III) of five widely distributed on-land mafic sections of the Caribbean Plate margins indicate a flood basalt origin for much of the Caribbean plateau. It is possible given the 1 to 2 m.y. error of the analyses that the actual duration of volcanism could have been shorter, i.e., the spread in the ages could reflect analytical uncertainty rather than the actual span of crystallization ages. Plate reconstructions (Duncan and Hargraves, 1984; Pindell and Barrett, 1990) place the plateau within the vicinity of the Galapagos hotspot at ~90 Ma, consistent with a mantle plume origin.

The ~76 Ma magmatism at Curaçao, Western Colombia, and possibly site 152 and Haiti may represent a second magmatic phase in the region. We cannot preclude that magmatism occurred between 88 Ma and 76 Ma, as a later phase of intrusion and basalt eruption is apparent at 84 Ma in the Nicoya Complex (Chapter III). Nevertheless, magmatism at 76 Ma was widespread, perhaps as extensive as initial magmatism at ~90 Ma. The relative volumes of Caribbean plateau magma production for the ~90 Ma and ~76 Ma are not precisely known, but if the Curaçao lavas are taken as a representative cross-section of the plateau, initial magmatism was likely to have been much more voluminous.

Two or more phases of widespread magmatism are evident in other LIPs (Bercovici and Mahoney, 1995). ^{40}Ar-^{39}Ar dating of the Ontong-Java oceanic plateau lavas from ODP drill sites and obducted parts of the plateau on the Solomon Islands (~1500 km from the drill sites) indicate that initial magmatism occurred at ~121 Ma followed by a second, widespread but compositionally similar phase at ~90 Ma (Mahoney et al., 1993; Tejada et al., in press). There is evidence for younger volcanism from tectonic exposures in the Solomon Islands and this has been attributed to the passing of the plateau over the Samoa or Rarotonga hotspots (Tejada et al., in press). The North Atlantic Volcanic Province (NAVP) is a volcanic rifted margin associated with the Tertiary opening of the North Atlantic (e.g., Dickin, 1988) . In Chapter II, I suggested

that the NAVP was built during at least two distinct volcanic phases; initial, widespread volcanism at ~62 Ma (West Greenland, southeast Greenland, and northwest Britain) followed by more voluminous magmatism at 56-55 Ma centralized along the rifted margins .

For the NAVP, it is possible that the initial volcanism marked the arrival of the Iceland mantle plume at the base of the continental lithosphere. The thick lithosphere may have restricted initial mantle upwelling and melting and it was not until plate separation that large-scale upwelling of hot mantle occurred (White and McKenzie, 1989). Initial production of the Ontong-Java plateau may similarly have been due to the arrival of the Louisville hotspot (Richards et al., 1989; Mahoney and Spencer, 1991; Tarduno et al., 1991); but why a second phase of compositionally similar magmatism occurred 30 m.y. later is not clear. Bercovici and Mahoney (1995) suggested that two magmatic phases are a result of the dynamics of interactions between mantle plumes and compositional/phase transitions in the mantle. Using tank experiments, they demonstrated that the intial plumehead can detach from the plume conduit at a viscosity boundary (the 670 km discontinuity in the mantle) and that a smaller second plume head will form and rise ~ 10 m.y. after the initial plume head. However, this model is not consistent with volcanism occurring 30 m.y. later on the original edifice as it predicts later volcanism at the site of the hotspot.

A more reasonable model for the later magmatism on the Caribbean plateau involves lithospheric extension. At 76 Ma, the plateau was being emplaced between North and South America (Pindell and Barrett, 1990) and it is possible that associated compression and/or extension allowed upwelling and melting of remaining hot mantle. Recent tomographic imaging of the mantle below Brazil shows that a residual thermal (and possibly chemical) anomaly from the Parana flood basalt event appears to have remained relatively fixed to the overlying lithosphere for 130 Ma (VanDecar et al., 1995). If the mantle beneath the Caribbean plateau remained anomalously hot, any extension of the plateau crust could have allowed mantle upwelling and melting. An alternative explanation is continued eruption of magmas from the plume stem as the plateau moved NE after volcanism from the plumehead subsided, magmas continued to erupt . However, we would not expect such widespread volcanism at 76 Ma if volcanism was restricted to the stem of the plume. Thus, volcanism due to widespread extension is the most consistent model to explain the later phase of volcanism

Magma Emplacement Rates

With the new radiometric ages, approximate emplacement rates for Caribbean Plateau magmatism can be calculated using volume estimates. Larson (1991) suggested that the combined volume of the Venezuelan and Colombian Basins is about 10 x 10^6 km^3 and I come to similar conclusions after subtracting 9 km of underlying (pre-existing) crust. This estimate does not include the on-land sections, any subducted plateau material, or the southern Nicaragua Rise. Kerr et al. (1996a) suggested that the volume of the plateau may actually double if the obducted crust in Western Colombian is included. If 90% of the volume (using 10 x 10^6 km^3) were emplaced between 91 and 88 Ma, the average emplacement rate would be 3 km^3-yr^{-1}, or about the total present oceanic crustal accretion rate at mid-ocean ridges (Chase, 1972). This estimate could conceivably double or triple if the tectonized and subducted parts of the plateau were included.

Eruption Environment

Most reconstructions of the tectonic evolution of the Caribbean plate show a Pacific origin for the Caribbean plateau (Burke et al., 1978; Duncan and Hargraves, 1984; Pindell and Barrett, 1990), having erupted over pre-existing oceanic crust in an intra-plate setting. Frisch et al. (1992) used paleomagnetic data to show that the Costa Rica lavas erupted near the equator and, consistent with formation over the Galapagos hotspot at 90 Ma. Chert beds exposed on the northern Caribbean margin (Puerto Rico, Hispaniola, and La Desirade) contain Jurassic and early Cretaceous age radiolarian chert that were derived from the subducting Farallon Plate (Mattson and Pessagno, 1979; Montgomery et al., 1994). Boreal radiolarian species in these sequences indicate a Pacific origin.

Lower Jurassic to early Cretaceous radiolarian chert in the Nicoya Peninsula of Costa Rica (Schmidt-Effing, 1979; Kuijpers, 1980; Baumgartner et al., 1984; Bourgois et al., 1984) is intruded by 90-88 Ma Caribbean Plateau lavas (Chapter III). This observation suggests that part of the plateau was erupted in an intraplate setting rather than on a mid-ocean ridge.

A Jurassic age for the pre-existing oceanic crust beneath the western edge of the plateau is considerably older than the 134 Ma age suggested by Hall (1995). However, his conclusions are based on interpreted magnetic anomalies from the Venezuelan basin and it is possible that the pre-existing crust in this region of the plateau is younger. Unlike the other on-land exposures of the Caribbean plateau, the Nicoya Complex has highly differentiated tholeiitic magmas that could have formed beneath a thick mechanical boundary such as old, relatively cool crust. The Curaçao lavas are situated to the south of the Venezuelan Basin and there are no exposures of highly differentiated magmas. Rather, there is an abundance of picrites and high MgO basalts (Klaver, 1987). One possibility for this difference between the Curaçao and Nicoya lavas could be the age and thickness of the pre-existing oceanic crust. Young and therefore thin oceanic lithosphere could have allowed more vigorous mantle upwelling and higher degrees of partial melting. Older, thicker crust could have acted as a mechanical barrier to reduce the relative amount of mantle upwelling and melting and to allow pooling and differentiation of melts.

A Compositionally Heterogeneous Plateau

The exposed margins of the Caribbean Plateau allow a widely distributed sampling of the province. The new radiometric ages and existing isotopic and trace element data can be used to examine possible spatial and temporal variability of mantle source and/or melting conditions (depth and degree of melting) that were involved during plateau formation. Fig. IV.5 shows that, in terms of the REE, contemporaneous lavas are compositionally heterogeneous throughout the plateau and within the same locality. The diversity of magma types within the entire Caribbean Plateau has been highlighted in previous works. Donnelly (1995) and Kerr et al. (1996a) divided the Caribbean rocks into three general groups based on REE patterns: LREE-depleted, LREE-enriched, and flat-REE . However, it is evident from Fig. IV.5 that while this is generally true, these designations can describe virtually any igneous rock and, in reality, the Caribbean rocks display a continuous spectrum of REE patterns with different degrees of LREE enrichment or depletion.

The LREE-enriched basalts (La/Yb_n of 3.0-4.8) and flat-REE basalts (La/Yb_n of 1.1) of the Dumisseau Formation erupted at ~90 Ma, although stratigraphic relations of the two rock types are unknown as is the age of the LREE-depleted samples at the base of

the exposed section (Sen et al., 1988). The flat-REE patterns of the Dumisseau Formation are virtually identical to those of the Nicoya Peninsula (La/Yb_n 0.9-1.1), although, in terms of REE abundance at a given % MgO, the Dumisseau lavas are more enriched. Flat-REE patterns are also seen in some of the Gorgona Island lavas, although a wide array of compositions can be found there as well (Echeverria, 1980; Aitken and Echeverria, 1984; Kerr et al., 1996b). The ~90 Ma Curaçao lavas are all flat to slightly LREE-enriched (La/Yb_n 1.0-1.1) (Klaver, 1987; Kerr et al., in press). The flat REE patterns could have been generated by melting a mantle source of primitive composition (either an actually primitive mantle source or a, perhaps coincidental, mix of a depleted and enriched mantle) in the absence of garnet or to such a degree that garnet is not a residual phase.

Magmatism at ~76 Ma was also compositionally diverse. The 76 Ma Koraal Tabak sill in Curaçao is slightly LREE-depleted, distinct from the flat to slightly LREE-enriched ~90 Ma Curaçao lavas. The ~76 Ma lavas from Western Colombia are slightly LREE-enriched, more so than the ~90 Ma Curaçao lavas. The Campanian (76 Ma?) site 152 lavas are LREE-depleted. The Venezuelan DSDP sites (146, 150, and 153 intruding Coniacian/Santonian sediments) have identical, slightly LREE-depleted patterns that are similar to the Koraal Tabak sill. Whether or not they were contemporaneous is unknown.

The diverse REE patterns cannot be attributed to a common mantle source melted to variable degrees at different depths and, therefore, the plateau was derived from a heterogeneous mantle source. The character of the source(s) can be best constrained using isotopic ratios, although published Sr, Nd, and Pb isotopic data for the Caribbean Plateau are limited. Fig. IV.10 shows Sr, Nd and Pb isotopic data and a field for modern MORB from the East Pacific Rise. The plateau data are not corrected for age, but a representative correction of a Costa Rica sample (Chapter III) is shown. There is a great deal of scatter in the Sr isotopic data and this can be attributed to Sr addition from seawater alteration or possibly from the assimilation of pre-existing altered oceanic crust and/or carbonate (Kerr et al., in press; Chapter III). The lowest $^{87}Sr/^{86}Sr$ ratios at a given $^{143}Nd/^{144}Nd$ ratio (which are not affected by alteration or small amounts of assimilation) are more likely to be representative of the primary magmatic $^{87}Sr/^{86}Sr$. These and the $^{143}Nd/^{144}Nd$ ratios show two general groups: a depleted MORB-like group and a more radiogenic (HIMU) group. The Gorgona Island komatiites and LREE-depleted basalts (K-tholeiites) and the Venezuelan Basin DSDP Leg 15 sites have the higher $^{143}Nd/^{144}Nd$ ratios that are within the MORB field, although the Venezuelan Basin samples have

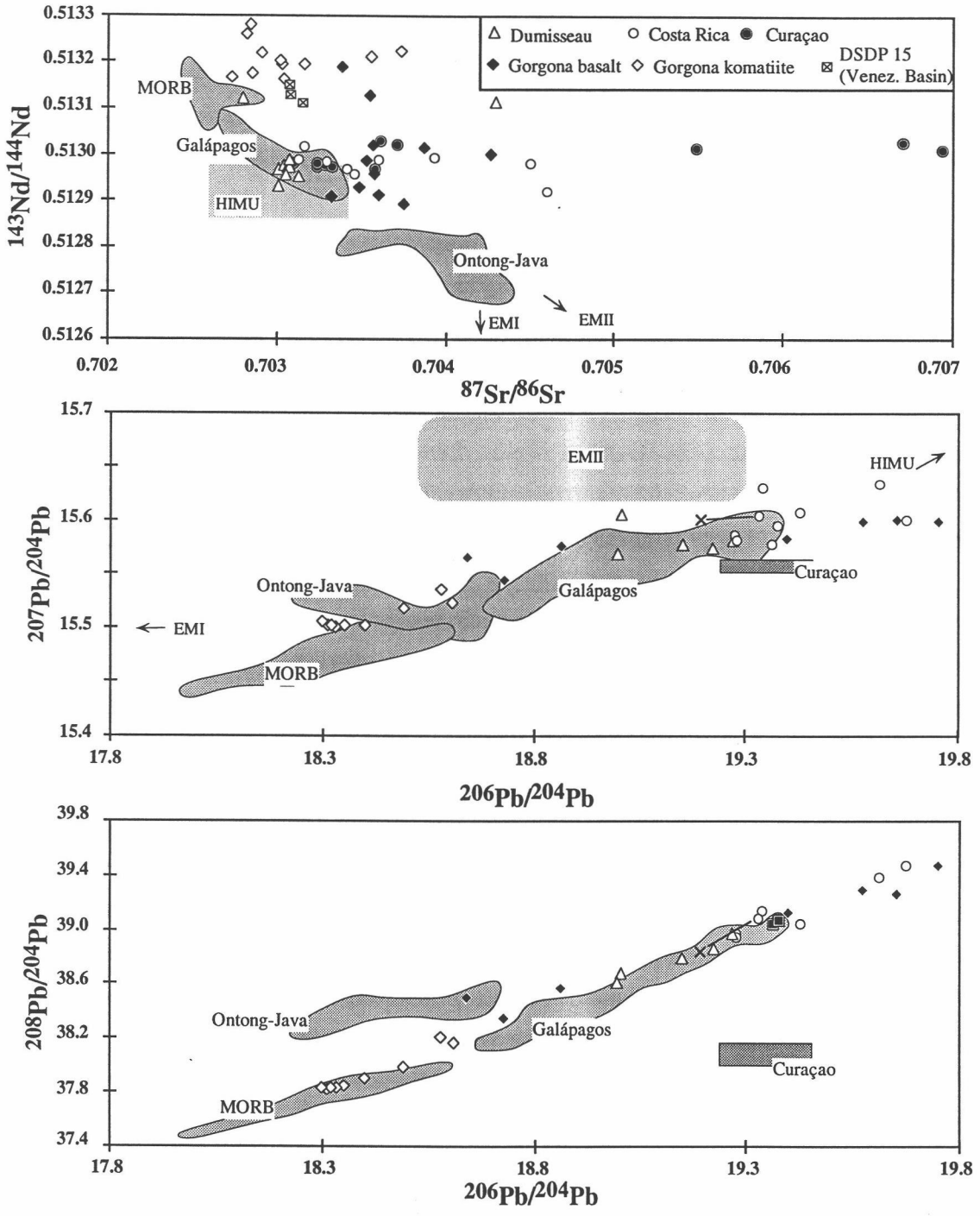

Fig. IV.10: Isotopic ratio plots for the Caribbean plateau lavas. The Dumisseau Formation data are from Sen et al. (1988), the Curaçao Sr and Nd data from Kerr et al. (in press) and the Pb isotopic fields from Hergt et al. (1995), the Gorgona Island data from (Aitken and Echeverria, 1984; Dupré and Echeverría, 1984) . East Pacific MORB glass data from (White et al., 1987; Prinzhofer et al., 1989) . Galapagos field is composed of data from Isabela and Fernandina islands (White et al., 1993) .

slightly lower ratios than the Gorgona lavas. The Haiti, Curaçao, Gorgona transitional (T) tholeiites (flat to enriched REE patterns), and Costa Rica $^{143}Nd/^{144}Nd$ ratios overlap and plot close to the HIMU field. This distribution follows the REE patterns where the LREE-depleted lavas have $^{143}Nd/^{144}Nd$ ratios similar to MORB and the flat to LREE-enriched rocks are derived from a more enriched mantle source.

The Pb isotopic data are generally consistent with the Sr and Nd isotopic data in that the lavas lie between a MORB-like source and an enriched, HIMU-like source (Fig. IV.10). Unfortunately, there are no data for the DSDP Leg 15 samples and only a range reported by Hergt et al. (1995) for the Curaçao lavas (although the low $^{208}Pb/^{204}Pb$ ratios are probably an analytical or typographical error). In $^{206}Pb/^{204}Pb$ vs. $^{207}Pb/^{204}Pb$ and $^{206}Pb/^{204}Pb$ vs. $^{208}Pb/^{204}Pb$ space, the data show a coherent linear trend rather than the two groups evident from the $^{87}Sr/^{86}Sr$ vs. $^{143}Nd/^{144}Nd$ plot. This trend could represent a mixing between a depleted mantle source and an enriched (HIMU) plume source.

As a comparison, I have overlain isotopic data from the Ontong-Java plateau (Mahoney and Spencer, 1991; Mahoney et al., 1993), which are distinct from the array of the Caribbean rocks. This indicates that the two plateaus were derived from different mantle sources (which may be a mix of several mantle source components). The Ontong-Java magmas have a distinctive "DUPAL" signature (Mahoney et al., 1993) or, in terms of plume source end-members (Zindler and Hart, 1986), EMI/EMII.

The ratios of some incompatible elements, such as La/Nb, are thought to be unaffected by melting and fractionation processes and can therefore be used, much like isotopic ratios, as tracers of mantle sources (e.g., McKenzie and O'Nions, 1995). In addition, La/Nb can be used to discriminate between mantle plume end-members (Weaver, 1991). The Gorgona komatiites, depleted tholeiites and the site 152 samples have La/Nb ratios within the range of MORB (Fig. IV.11), consistent with derivation from an upper mantle source. The other on-land samples, including the 76 Ma samples, have lower La/Nb ratios within or near the range of HIMU ocean island basalts. This is consistent with the isotopic ratios, with the exception of the Venezuela Basin (sites 146, 150, and 153). The La/Nb ratios are within the range of the enriched samples, though near the upper boundary. The Ontong-Java lavas have La/Nb values within the EMI/EMII and primitive mantle fields.

Relationship to the Galapagos Plume

Previous workers noticed a rough similarity between the isotopic composition of some of the Caribbean rocks to recent Galapagos lavas (Sen et al., 1988; Storey et al., 1991; Kerr et al., 1996a). Unfortunately, recent Galapagos lavas display a wide range of isotopic compositions and are derived from a heterogeneous mantle source (White et al., 1993) that encompasses at least four distinct end members (Harpp, 1995). Harpp (1995) suggested that the most probable plume endmember is represented by lavas from the area near Fernandina and Isabela Islands, which are the most active and have the highest $^{3}He/^{4}He$ ratios (Graham et al., 1993; Kurz et al., 1993). The Galapagos field in Fig. IV.10 also encompasses most of the Caribbean rocks except for the Gorgona komatiites at the more depleted end and the Gorgona T-tholeiites and two of the Costa Rica rocks at the more enriched end. The more enriched samples from Gorgona Island and Costa RIca would lie closer to the Galapagos field if the intitial values at the time of eruption could be precisely determined. The similarity between the Galapagos and the Caribbean Plateau lavas is consistent with the plateau being produced by the Galapagos plume, although it does not unequivocally prove it. Such a conclusion assumes that the plume composition has remained constant over the past 90 m.y., but given the relationship of other LIPs to hotspots and the plate reconstructions showing the plateau over the Galapagos hotspot at 90 Ma, a genetic Galapagos-Caribbean Plateau relationship is currently the most viable model.

Mantle Dynamics

I have thus far demonstrated that the Caribbean Plateau is essentially an oceanic flood basalt province that began erupting by at least ~90 Ma. Plateau magmas were derived from at least two mantle sources, a depleted and an enriched source with HIMU affinities (Galapagos). High degrees of melting were required to produce the basalts (~30%; Klaver, 1987; Kerr et al., in press; Chapter III) and possibly more for the Gorgona komatiites (Echeverria, 1980). The excessive thermal conditions (relative to mid-ocean ridge systems) and the mixing of an enriched plume and depleted upper mantle source is consistent with derivation of the plateau from a decompressing plume head composed of lower mantle material mixed with depleted upper mantle during ascent (Richards et al., 1989).

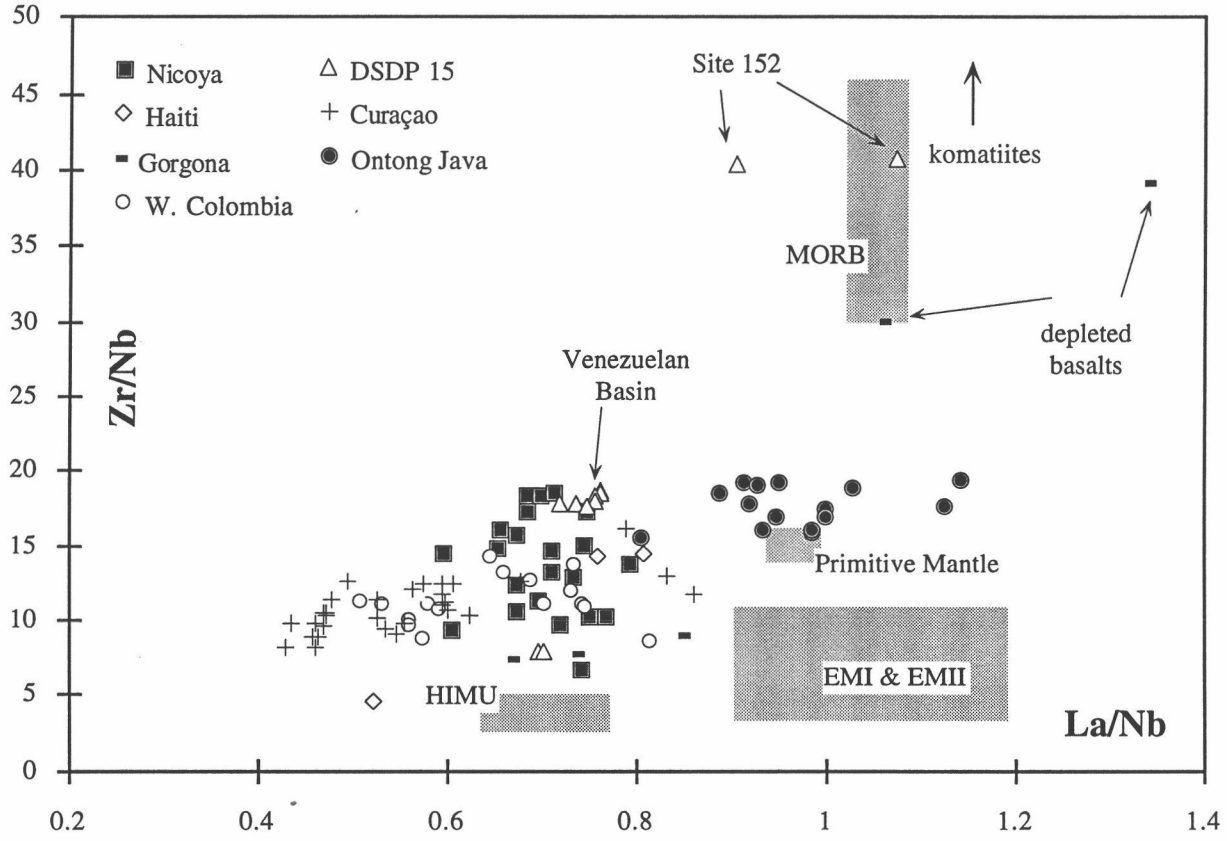

Fig. IV.11: Zr/Nb vs. La/Nb plot for the Caribbean plateau. Sources for data are: Nicoya Peninsula (Costa Rica), Chapter III; Dumisseau Formation (Haiti) (Sen et al., 1988) and Table 3; Gorgona Island, (Kerr et al., 1996b) ; Western Colombia, (Millward et al., 1984; Aspden and McCourt, 1986) , and Table III; DSDP Leg 15, Table 2; Curaçao (Klaver, 1987) and Table 3; Ontong Java plateau (Mahoney et al., 1993). Fields for HIMU, EMI/EMII and MORB from Weaver (1991). Field for primitive mantle from McDonough and Sun (1995).

The Caribbean and Ontong-Java plateaus are both wholly oceanic plateaus (i.e., they erupted within an oceanic basin) and therefore can give some insights into mantle dynamics and composition without potential contamination from continental lithosphere. In the context of mantle end-members (Zindler and Hart, 1986), the Caribbean Plateau may be related to a HIMU source and the Ontong-Java to EMI or EMII. The evolution of plume source end-members is a debatable topic and several authors have suggested that subducted oceanic crust is involved (e.g., White, 1985; Weaver, 1991). Weaver (1991) suggested, on the basis of isotopic and trace element data, that the ocean island basalt end-members (HIMU, EMI, and EMII) are derived predominantly from ancient subducted oceanic crust with (EMI and EMII) or without (HIMU) sediments . He showed that HIMU and the EM end-members can be distinguished from one another using ratios of LREE (e.g., La) and high-field strength elements (HFSE; e.g., Nb) or large-ion lithophile elements (LILE; e.g., Rb) and explained that a fractionation between HFSE and LREE and LILE can occur during subduction processes. This is consistent with recent lab experiments of brine/melt partitioning (e.g., Keppler, 1996) which show that the subduction/dehydration process does not remove the HFSE (Nb, Ta, Zr, and Ti) but does mobilize the LREE and LILE. In addition, Pb is removed preferentially to U and Th by hydrothermal fluids, increasing the U/Pb and Th/Pb ratios of the residual plate. So, subducted oceanic crust without sediments will have low La/Nb ratios and, over billions of years, radiogenic Pb isotopic ratios (i.e., the HIMU endmember). The EM end members have higher La/Nb ratios and this can be attributed to higher LREE/HFSE and LILE/HFSE ratios in the subducted material from the addition of sediments.(e.g., shales have La/Nb ratios ~8; Mason, 1966). The correlation of the isotopic and La/Nb ratios of the oceanic plateaus to ocean island basalt end members generally supports this hypothesis.

Although the La/Nb ratios from both the Caribbean and Ontong-Java plateaus overlap with ocean island basalts, they have considerably higher Zr/Nb ratios (Fig. IV.11). Zr/Nb ratios can be fractionated by partial melting (if high-Ca pyroxene is a residual phase) as Zr is more compatible than Nb (Green et al., 1989; Forsythe et al., 1994). Therefore, the Zr/Nb ratio should increase with increasing degrees of partial melting. Zr/Nb correlates roughly with the degree of LREE enrichment as the DSDP site 151 (Beata Ridge), LREE-enriched Gorgona Island lavas (Kerr et al, 1996), and the highly LREE-enriched HA76-105 from the Dumisseau Formation (although of unknown age) have the lowest Zr/Nb ratios (Fig. IV.11).

Zr/Nb is a HFSE/HFSE ratio and should not be fractionated during mantle domain formation if this process is dominated by ancient subduction events. The similarity in Zr/Nb of ocean island basalts (~5) with affinities to different source end-members is consistent with this interpretation. The higher Zr/Nb ratios of the Caribbean and Ontong-Java plateau lavas relative to HIMU and EMI/EMII ocean island basalts can be attributed to higher degrees of partial melting required for the plateau magmas relative to recent ocean island basalts. Since the fractionation between Zr and Nb is determined by residual clinopyroxene (Green et al., 1989; Forsythe et al., 1994), the Zr/Nb ratios of the plateau lavas probably approach the Zr/Nb ratios of the mantle sources if they indeed are products of close to 30% partial melting (Mahoney et al., 1993; Chapter III). The implication is that the Zr/Nb ratios for the HIMU and EMI/EMII end-members range between 10-20, close to primitive mantle.

If indeed the Zr/Nb ratios of the plateau lavas (10-20) reflect the Zr/Nb ratio of the mantle source, then this is not consistent with the idea that the HIMU sources is derived solely from ancient subducted crust as we would expect Zr/Nb ratios of oceanic crust (>30) (the high Zr/Nb relative to primitive for MORB is probably due to the ancient melting and depletion of the upper mantle). So, there must have been some Nb additional mantle sources, possibly primitive mantle.

Conclusions

^{40}Ar-^{39}Ar ages of 91-88 Ma for obducted oceanic crust on the margins of the Caribbean Plate indicate a flood basalt origin for the Caribbean plateau. Widespread but apparently smaller volume magmatism occurred at ~76 Ma and may have been caused by extension during the tectonic emplacement of the plateau between North and South America or by continuing volcanism from the plume stem as the plateau moved to the northeast. Average magma emplacement rates at ~90 Ma are approximately 3 km^3/yr, but this would be larger if the unknown amount of obducted and subducted material were taken into account. Actual magma emplacement could have been in discrete, large-scale events rather than continuous effusion over 91-88 Ma.

Contemporaneous magmatism at both ~90 Ma and ~76 Ma was compositionally heterogeneous. The majority of the on-land lavas were derived from an enriched source having HIMU characteristics seen at some ocean islands, but probably at higher degrees of partial melting. The Gorgona komatiites and depleted basalts are the only ~90 Ma

lavas that are derived from a depleted upper mantle source similar to that for MORB. Magmatism at ~76 Ma was also compositionally heterogeneous and apparently as widespread as initial volcanism.

The DSDP Leg 15 samples were not successfully dated. The intruded sediments of the Venezuelan Basin indicate that the sills are no older than ~90 Ma and perhaps younger. The slight LREE-depletions, the Sr and Nd isotopic data, and the low La/Nb ratios of these samples indicate that they are slightly more enriched than MORB, but slightly less than most of the on-land lavas.

At ~90 Ma the Caribbean plateau was located over the Galapagos hotspot, suggesting a hotspot origin for the province. The similarity of isotopic compositions of the plateau lavas and recent Galapagos lavas is consistent with this hypothesis.

Chapter V. Ocean Plateau Volcanism and Global Ocean Anoxia: Hydrothermal Links at the Cenomanian-Turonian Boundary

C.W. Sinton and R.A. Duncan

submitted to Economic Geology

Abstract

The Cenomanian-Turonian boundary is marked globally by the extinction of marine invertebrates and an increase in the accumulation and preservation of organic carbon-rich sediments. This boundary also coincides with the timing of large-scale volcanism from at least three large igneous provinces: the Ontong-Java and Caribbean oceanic plateaus and the Madagascar flood basalts. In this paper, we assess the possibility that hydrothermalism associated with large-scale submarine magmatism directly contributed to the reduction of dissolved O_2 in the oceans. We find that an average eruption rate could not have resulted in widespread O_2 depletion assuming a present day ocean chemistry. However, it is possible that short-lived magmatic pulses (<1000 yr?) could have overwhelmed the O_2 budget in a poorly-oxygenated Cretaceous ocean and led to brief episodes of anoxia and dysoxia throughout the deep ocean.

Introduction

Large igneous provinces (LIPs) are massive emplacements of predominantly mafic intrusive and extrusive rock (Coffin and Eldholm, 1994) that formed during short-lived magmatic pulses throughout Earth history (e.g., Duncan and Pyle, 1988; Renne et al., 1995). LIPs, which include continental flood basalt provinces, volcanic rifted margins, and oceanic plateaus, have recently become an important topic in global geology because their size and proposed catastrophic formation have important implications for mantle dynamics and global environmental impact (e.g., extinction events). For brief periods, the formation of LIPs involves crustal accretion rates which are in excess of mid-ocean ridge rates of crustal production (Duncan and Richards, 1991; Larson, 1991). Such rapid, voluminous submarine eruptions must have had a considerable impact on the global marine environment and ocean chemistry. However, because there is no modern (active) analog for LIPs, the consequences of plateau

formation remain obscure and evidence can be found only in the sedimentary record and hydrothermally altered rocks of the buried plateaus.

Volcanism from the Caribbean oceanic plateau, the Ontong-Java oceanic plateau, and the Madagascar flood basalt province is roughly coeval with the Cenomanian-Turonian (C-T) boundary (Chapter IV; Mahoney et al., 1993; Storey et al., 1995). This time interval is characterized by widely distributed organic-rich, deep-sea sediments (black shales), which are thought to indicate global anoxia in deep ocean water (Schlanger and Jenkyns, 1976), which in turn caused the extinction of marine invertebrates (e.g., Raup and Sepkoski, 1984; Hart and Ball, 1986; Raup and Sepkoski, 1986). Recent papers have suggested that there was a sharp increase in hydrothermal input to the global ocean at the C-T boundary (Orth et al., 1993; Ingram et al., 1994). However, the causal relationship between ocean plateau volcanism, seawater anoxia, and species extinction is not clear. In this paper, we explore the relationship between global ocean anoxia, extinction, and hydrothermalism produced by ocean plateau volcanic eruptions. In particular, we examine the possible consumption of dissolved O_2 in seawater by oxidation of magmatic sulfide and reduced metals during hydrothermal processes. We find that an average eruption rate could not have resulted in widespread O_2 depletion. However, given the discrete nature of the black shale deposits and the probable lower concentrations of dissolved O_2 in ocean bottom water during the Cretaceous, it is possible that large, short-lived magmatic pulses could have overwhelmed the O_2 budget and led to brief episodes of anoxia and dysoxia throughout the water column.

The Cenomanian-Turonian Boundary

The C-T boundary is a clearly defined Cretaceous extinction event (Raup and Sepkoski, 1984; Raup and Sepkoski, 1986). It is marked by the sudden disappearance of many species and severe drop in the diversity of molluscs, bivalves, dinoflagellates, and planktic and benthic foraminifera (Hart and Ball, 1986; Kuhnt et al., 1986; Brasier, 1988; Jarvis et al., 1988; Hart and Leary, 1989), although extinction of macrofossils in the epicontinental Western Interior Basin was drawn out and occurred in discrete steps (Elder, 1989; Harries, 1995). Extinction can be attributed to anoxia and appears to have occurred in mid-water and shelf species e.g. (Kuhnt et al., 1986). Radiolarian and marine vertebrates (such as fish) apparently did not suffer large-scale extinction as there is

abundant radiolarian tests and fish debris in the black shales (Kuhnt et al., 1986). What is remarkable about the C-T boundary is that it is globally represented in oceanic, shelf, and epicontinental settings by an accumulation of marine organic carbon-rich sediments (black shales) that have been interpreted as evidence for global bottom water anoxic or dysoxic conditions (Fig. V.1) (e.g., Schlanger and Jenkyns, 1976; Hart and Ball, 1986; Brasier, 1988; Hart and Leary, 1989). The black shales occur as discrete layers surrounded by sediments deposited under oxic conditions, indicating anoxic conditions were transient (Sarmiento et al. 1988). The global extent of these low oxygen conditions is evident from an increase in the $\delta^{13}C$ in coeval limestones, consistent with increased burial of organic material in seafloor sediments (Scholle and Arthur, 1980; Schlanger et al., 1987).

The formation of Cretaceous black shales is a vigorously debated topic and it is not the purpose of this paper to give a complete review of the literature (for a recent review, see Wignall, 1994). In the present ocean, anoxic zones are found in restricted areas (e.g., semi-enclosed basins) and regions of intense nutrient supply (i.e., upwelling zones), and the widespread conditions required for anoxia at the C-T boundary implies fundamental changes in ocean circulation and/or the production and deposition of organic matter (Sarmiento et al., 1988). Two general schemes that have been proposed for ancient black shale formation are high productivity and enhanced preservation of organic material. Schlanger and Jenkyns (1976) first suggested that the high sea level and transgression onto continental areas during the Cretaceous spurred primary productivity due to an increase of warm shallow water and terrestrial nutrients, increasing the depth range and possibly the intensity of the oxygen minimum zone. This process can be referred to as "organic overloading" by Wignall (1994). The high abundance of radiolaria, which indicate increased productivity, in some of the black shales supports this idea (e.g., Hart and Ball, 1986; Kuhnt et al., 1986).

The enhanced preservation model relies on a reduction in the oxygen dissolved in seawater, thus reducing the oxidation of organic detritus. This can be accomplished by 1) inhibiting the formation of cold bottom water by reduced latitudinal thermal gradients at the ocean surface (e.g., Schlanger and Jenkyns, 1976), 2) reducing the O_2 content of bottom water at the source (Brass et al., 1982), or 3) inhibiting bottom water ventilation by morphological barriers or density stratification. The first two mechanisms are inter-related because the warmer surface water temperatures during the Cretaceous would have decreased the formation of cold bottom water at the poles and increased the amount of

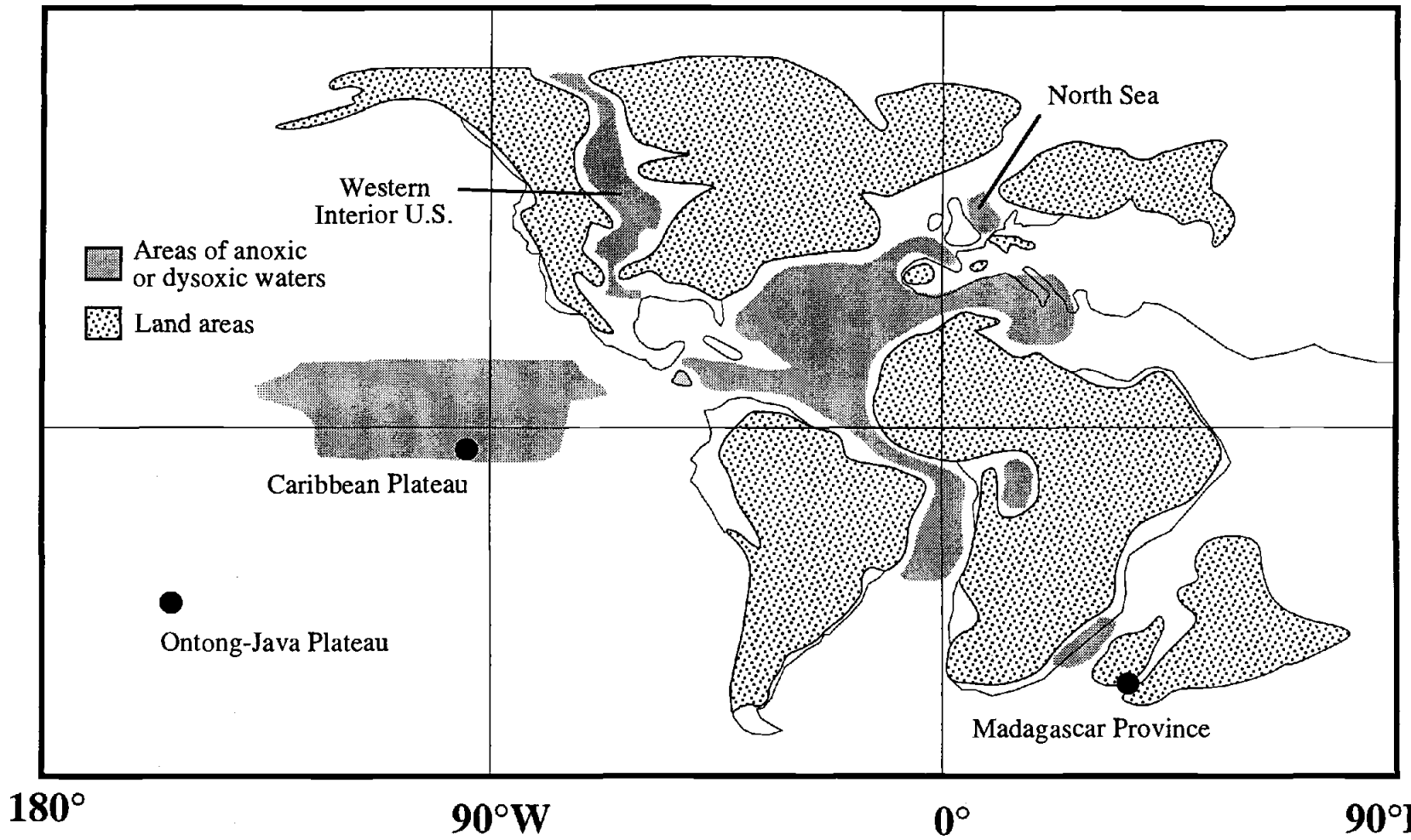

Figure V.1. Map of reconstructed plate positions at ~90 Ma based on Wignall (1994) and Scotese (1989). Land areas are shown in stipple and present continental margins are shown in fine line. The approximate area of anoxic or dysoxic conditions (shaded regions; Wignall, 1994) and the paleopositions of the Ontong-Java and Caribbean plateaus and the Madagascar flood basalts are shown.

high-salinity, warm bottom waters that form at tropical latitudes (Brass et al., 1982). Although the vigor of Cretaceous bottom water circulation cannot be determined, a higher bottom water temperature would cause a decrease in the solubility and concentration of O_2 in bottom water (Brass et al., 1982).

Previous papers have utilizing a combination of enhanced preservation and increased productivity to explain black shale formation did not satisfactorily explain all aspects of the C-T boundary event (e.g., Wignall, 1994). For instance, it is difficult to explain the abrupt and discrete nature of the extinctions and black shale deposition (and low O_2 conditions) in various paleoceanographic settings (a big ocean and several small seas). If anoxia were due to the combined effects of a warmer climate and of higher sea level (due to shallow oceanic basins and smaller ice caps) thought to be characteristic of the entire the middle Cretaceous, it is unclear why there was a sharp, global increase in organic carbon preservation at the C-T boundary (Herbin et al., 1986). It also seems counterintuitive that high species mortality occurred during what appear to have been excellent conditions for species expansion (Kaufmann, 1986; Arthur, 1991; Larson, 1991).

One factor not examined by most studies is the impact of catastrophic submarine volcanism. While some studies have attributed potential increased atmospheric CO_2 and global warming (and sea level rise) to the general high level of volcanism during the Cretaceous (e.g., Arthur et al., 1991; Larson, 1991), they do not address the possible effects of large-scale but short-duration magmatic events on seawater chemistry. Recently, abrupt increases in geochemical signals possibly associated with submarine volcanism have been observed at the C-T boundary. Ingram et al. (1994) demonstrated that the $^{87}Sr/^{86}Sr$ ratios in fish teeth in the C-T (Bonarelli) black shale of Italy decreased sharply, suggesting a sudden 10-15% increase in volcanic Sr in ocean water. Orth et al. (1988) showed that concentrations of some trace metals (Sc, Ti, V, Cr, Mn, Co, Ni, Ir, Pt, and Au) increased in both black shales and carbonates at the C-T boundary. Based on trace element ratios, they suggest a tholeiitic magma source from the Caribbean/East Pacific region. We examine the possibility that the volcanism from the Caribbean and the Ontong-Java oceanic plateaus were the sources for the observed increases in magmatic material in seawater.

LIP Volcanism at the C-T boundary

The Caribbean oceanic plateau forms the core of the Caribbean Plate and numerous tectonically uplifted sections along the plate margins. Seventeen ^{40}Ar-^{39}Ar incremental heating ages from the obducted margins of the Caribbean Plateau range from 93 to 87 Ma, with a weighted mean of 89.5 Ma ± 0.3 Ma (Chapter IV), indicating that the bulk of the plateau was formed over a relatively short time, possibly as the initial phase of activity of the Galapagos hotspot (Duncan and Hargraves, 1984). The Ontong-Java Plateau, the world's largest volcanic feature, is located in the Western Pacific and appears to have been built during at least two magmatic pulses, the first possibly associated with the Louisville hotspot (e.g., Mahoney et al., 1993) and the second of unknown origin (Tejada et al., in press). ^{40}Ar-^{39}Ar radiometric dating of Ontong-Java lavas recovered from ocean drilling and those from the uplifted and exposed sections of the plateau on the adjacent Solomon Islands indicate plateau volcanism occurred at ~121 and ~90 Ma (Mahoney et al., 1993; Tejada et al., in press), although there are some volumetrically minor volcanics of late Eocene age on the Solomon Islands. Nine ^{40}Ar-^{39}Ar incremental heating ages for the second magmatic phase range from 96 to 84 Ma (Mahoney et al., 1993; Tejada et al., in press) with a weighted mean of 90.5 ± 0.8 Ma for the drill cores and 91.8 ± 0.3 Ma for the Solomon Islands localities. It is not possible at this point to resolve what proportions of the plateau were erupted during the 121 and 90 Ma phases, but given that lavas of both ages are found at the drill sites and the Solomon Islands (~1500 km from the drill sites), these events were apparently widespread. Both the Caribbean and Ontong-Java plateaus appear to be predominantly made of lavas that erupted in a submarine environment and exhibit varying degrees of low grade alteration associated with hydrothermal processes. Some of the Caribbean Plateau localities also contain hyaloclastite interbeds (e.g., Klaver, 1987).

A third magmatic event (and possible source of increased hydrothermal activity) near the C-T boundary is the Madagascar flood basalt province that erupted during the separation of Madagascar from India. A mean age of ^{40}Ar-^{39}Ar analyses of these lavas is 87.6 ± 0.6 Ma (Storey et al., 1995), though earlier volcanism is evident from basalt flows within sediments of Cenomanian to Turonian age (Besairie and Collignon, 1972). It is possible that a portion of the volcanics erupted in a submarine environment, but this has not been documented.

The absolute age of the C-T boundary has been estimated in several recent Mesozoic timescales. In a comparison of timescales by Gradstein et al. (1994), the C-T boundary ranges from about 90 to 93 Ma. The Gradstein et al. (1994) timescale places the C-T boundary at 93.5 ± 0.2 Ma, based on ^{40}Ar-^{39}Ar total fusion ages for sanidines in bentonite layers that are found in the Western Interior U.S. (Obradovich, 1993). These ages were calibrated against an age of 520.4 Ma for the monitor mineral MMhb-1 hornblende. If the ages are referenced to 513.9 Ma (Lanphere et al., 1990), which has been used for the radiometric ages of the LIPs reviewed here, this results in a boundary age of 92.1 ± 0.2 Ma. Although the ages for the Ontong-Java and the Caribbean plateaus are slightly younger than the Obradovich (1993) C-T boundary age, we note that given the analytical uncertainty of the plateau lava ages (generally 1-2 m.y. at 1σ) the C-T boundary and the plateau lava eruption ages overlap. In addition, the dated lavas are predominantly from the top of the plateau, missing the earliest lavas.

Oxygen Depletion During Hydrothermal Cycling

The large-scale eruptions from the Caribbean and Ontong-Java plateaus, and possibly the Madagascar flood basalts are the best candidates as sources for increased hydrothermal input to the oceans at the C-T boundary. Arthur et al. (1991) suggested that black shale formation at the Aptian-Albian boundary was a result of increased CO_2 released during volcanism which may have inhibited O_2 dissolution in seawater. We are suggesting there is a connection between increased magmatism, ocean anoxia, and marine extinction. A similar mechanism was proposed by Walker (1986) who speculated that the oxidation of magmatic sulfides and metals during hydrothermal processes depleted the dissolved O_2 in past oceans.

Describing the hydrothermal system associated with ocean plateau volcanism is difficult as there are no presently active analogs. In addition, we do not know the volume of material erupted during the ~90 Ma volcanic phase of the Ontong-Java Plateau nor if there was significant submarine volcanism associated with the Madagascar flood basalts. What we can do is estimate the volume of the Caribbean Plateau and, therefore, the possible O_2 consumption from hydrothermal processes. We envision that the consumption of dissolved O_2 occurs within two general settings: 1) within the crust during hydrothermal circulation and 2) in the water column where reduced metals and sulfides from the hydrothermal plumes react with dissolved O_2. In the crust, high

temperature reactions between seawater and cooling lava use the O_2 in the seawater to oxidize metals (such as Fe) and sulfides. This is evident from studies of hydrothermal alteration of seafloor basalts and by the lack of oxygen in vented hydrothermal solutions at mid-ocean ridges (e.g., Von Damm, 1990). Therefore, we can assume that all seawater that circulates through a high temperature hydrothermal system is anoxic. Metal sulfides injected into the water column would be subject to oxidation, but determining the proportion of the total sulfides that are actually oxidized in this manner is difficult as there are no studies that have addressed this problem.

We have tried to quantitatively assess the consumption of O_2 in seawater by sulfide oxidation by estimating the amount of sulfide released from Caribbean Plateau eruptions. The S in submarine tholeiitic MORB magmas is predominantly sulfide (Wallace and Carmichael, 1992) as is the S in high-temperature hydrothermal fluids vented at mid-ocean ridges (Von Damm, 1990). Given that the Caribbean lavas are MORB-like in major element composition, we can assume that most of the S in them is reduced. Sulfur is released from magmas either as a volatile (H_2S) during eruption and degassing (depth dependent) or from mobilization during seawater alteration. The amount of S released during degassing was probably small because there are no reported vesicular rocks from the Caribbean province and all appear to have been erupted significantly below sea level. It is likely that much of the S was retained in the lava as sulfide globules. Sulfide would then have been mobilized by hydrothermal processes and become available for reaction with O_2 in seawater. Andrews (1979) demonstrated that up to 50-60% of primary S in tholeiitic MORB lavas can be released by seawater alteration.

In modeling we start with several assumptions (Table V.1). We use an estimated volume of 1×10^7 km^3 for the Caribbean Plateau, based on the combined area of the two major basins of the Caribbean Sea (Venezuelan and Colombian) and an average crustal thickness determined from seismic studies (e.g., Bowland and Rosencrantz, 1988). This value of 1×10^7 km^3 agrees with that estimated by Larson (1991). The calculated volume does not take into account the obducted plateau margins or any material that has been subducted, although Kerr et al. (1996) estimated that obducted sections in western Colombia may double the plateau volume. The S content of oceanic basaltic magmas ranges from 800 to 2500 ppm (Wallace and Carmichael, 1992) and we choose a conservative 1000 ppm as the average S concentration in the Caribbean lavas. Using an average density of 2.7×10^{15} g-km^{-3} for the lavas, the total mass of S is 5.4×10^{17} g (1.7×10^{16} mol). A proportion of the plateau volume consists of plutonic and underplated

material that never had contact with seawater, but if we assume that the estimated 5 km thickness of the lava pile on the island of Curaçao (Klaver, 1987) is representative of the rest of the plateau, up to ~50% of the calculated volume consists of lava flows. In the model, we set the proportion of the plateau exposed to hydrothermal alteration at 50% and 25% and, of this amount, 50% and 25% of the available S is oxidized. Assuming the reaction:

$$H_2S + 2O_2 = 2H^+ + SO_4^{2-}$$

in which two moles of O_2 are consumed for every mole of S.

Table V.1: Assumptions in calculating sulfide oxidation

Volume of Caribbean plateau	1×10^7 km^3
Duration of plateau formation	3 m.y.
Average S content of lavas	1000 ppm
Average density of lavas	2.7×10^{15} g-km^{-3}
Average O_2 content of seawater	1-2 ml-l^{-1}
Volume of seawater	1.35×10^9 km^3
Seawater residence time	1000 yr
Reaction	$H_2S + 2O_2 = 2H^+ + SO_4^{2-}$

We first examine an extreme case by assuming that the plateau erupts instantaneously and there is no O_2 recharge from the atmosphere. We calculate 4.2×10^{17} - 1.1×10^{17} mol O_2 consumed using the range of the amount of the plateau exposed and oxidized. The total amount of O_2 in seawater (assuming an average concentration of 1 - 2 ml-l^{-1} below the mixed layer) is 1.2×10^{17} - 6.0×10^{16} mol. So instantaneous plateau formation could have rendered a large proportion of the oceans anoxic (beneath the mixed layer). In another case, we can use an average eruption rate assuming that the bulk of the plateau was built over 3 m.y. (Chapter IV). This leads to an average O_2 consumption rate of 1.4×10^{11} - 3.5×10^{10} mol-yr^{-1}. Assuming no O_2 recharge and 1 to 2 ml-l^{-1} O_2 in seawater, it would take on the order of tens of millions of years for the ocean below 1000m to be rendered anoxic by hydrothermal sulfide oxidation. Even if we were to take into account oxidation of metals and additional hydrothermal input from a large but unknown volume of Ontong-Java eruptions and the fact that only a portion of the total oceans was anoxic (or dysoxic), it would be impossible to use up all of the O_2 in seawater once recharge is taken into account. The flux of O_2 from recharge (assuming a 1000 yr residence time) is five orders of magnitude larger than the average O_2 consumption rate calculated in our model.

Table V.2: Model results

Average oxygen consumption rate	1.4×10^{11} -3.5×10^{10}	mol/yr
Total seawater oxygen	4.2×10^{17} - 1.1×10^{17}	mol
Oxygen recharge rate	1.2×10^{14} - 6.0×10^{13}	mol/yr

The oxygen consumption rates are calculated assuming 25-50% of the plateau experienced hydrothermal alteration and 25-50% of the available sulfide oxidized. The oxygen content of seawater and the recharge rate are based on 1-2 ml-l^{-1}.

These results are consistent with comparisons to present fluxes from mid-ocean ridge settings. The average crustal production rate for the Caribbean Plateau was about 3.3 km^3-yr^{-1}, slightly higher than estimates for the present average oceanic crustal production rate of 3 km^3-yr^{-1} (Chase, 1972) to 1.5 km^3-yr^{-1} ("background level"; Larson and Olson, 1991). It is obvious that present crustal production rates do not incur ocean anoxia and, in light of our calculations, neither will doubling or tripling crustal accretion. Estimates for the cycling of seawater through mid-ocean ridge hot hydrothermal systems are on the order of 10 m.y. (from a compilation in Peucker-Ehrenbrink et al., 1994), much slower than the rate of oxygen recharge, so simple O_2 reduction by present rates of hydrothermal circulation is not a viable mechanism for ocean anoxia.

We think that given the probable low O_2 content of Cretaceous seawater and the existence of enclosed ocean basins at the time, brief periods (10^3-10^4 yr) of anoxia could have been produced by large, short-lived pulses of magmatism. Radiometric dating of the Caribbean Plateau rocks cannot further resolve the magmatic history within this age range, but we think that it is probable that massive, single eruptions of thousands of km^3 were produced during discrete pulses. This conclusion is based on comparison with continental flood basalts, such as the Columbia River basalts, where single flows with volumes up to 1,500 km^3 were erupted in as short a period as a few days (Swanson and al, 1975). In this case, an averaged flux rate is not applicable and much greater fluxes of sulfide and hydrothermal cycling would have occurred over short periods. Such events may have forced anoxic or dysoxic conditions on a susceptible ocean, i.e., low O_2 content.

In Fig. V.2, we show a conceptual diagram of a Cretaceous oceanic basin. Salient points are the possible control of middle to bottom water circulation by warm, saline, and

poorly-oxygenated waters from the continental shelf and the construction of an oceanic plateau well into the O_2-minimum zone. We show representative O_2-depth profiles for the present ocean and a hypothetical Cretaceous ocean, which was relatively depleted in dissolved O_2 below the mixed layer. We envision that short-lived but large volume flood basalt flows from the plateau will dramatically increase hydrothermal circulation through the lava pile and expel thermally buoyant "megaplumes" carrying metal sulfide particles into the water column. These plumes would have been similar in composition to those observed recently at the Gorda and Juan de Fuca ridges (Baker, 1994), but orders of magnitude greater volume. O_2 consumption resulted from the oxidation of sulfides and metals in the lava pile and in the water column and possibly from an increase in primary productivity (and oxidation of organic matter) due to an increased supply of nutrients from the megaplumes (Vogt, 1989). The catastrophic nature of the eruptions could have overwhelmed the poorly oxygenated Cretaceous seawater below the mixed layer, leading to brief periods (thousands of years?) of seawater anoxia and the extinction of some marine organisms. This hypothesis is generally consistent with the apparent survival of fish and radiolaria at the C-T event as they resided in the upper, well-mixed and oxygenated part of the water column.

Conclusions

The Cenomanian-Turonian boundary is marked globally by the extinction of marine invertebrates, an increase in the accumulation and preservation of organic carbon-rich sediments, and massive submarine lava eruptions from the Caribbean and Ontong-Java oceanic plateaus. Although at this point we cannot give concrete support for a direct relationship between oceanic plateau volcanism and ocean anoxia, we can demonstrate that average eruption rates could not have significantly reduced deep ocean O_2 levels in the present ocean. However, Cretaceous oceans were probably less oxygenated (below the mixed layer) than the present oceans and it is probable that hydrothermal activity associated with short-lived but massive magmatic pulses may have been responsible for brief periods of anoxia and, consequently, marine species extinction. We suggest that seawater O_2 was consumed during hydrothermal circulation through the lava pile and by the oxidation of reduced metals and sulfides ejected into the water column in thermally buoyant megaplumes.

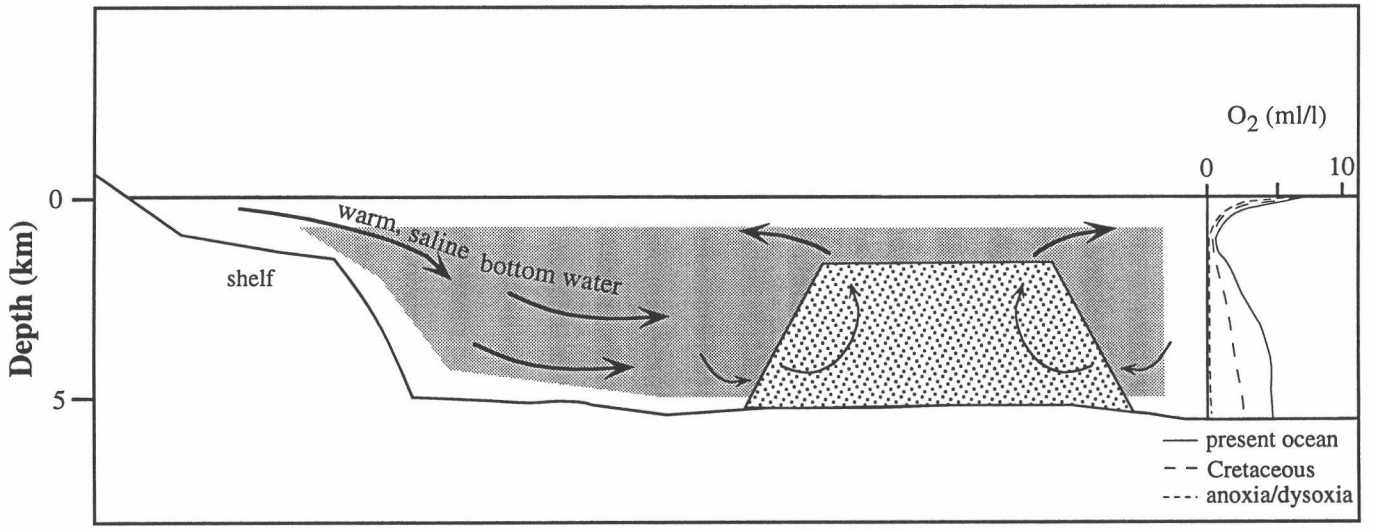

Figure V.2. Schematic of a Cretaceous ocean basin during construction of an oceanic plateau. Deep waters are formed from warm, saline epicontinental basins. The low O_2 of the warm waters coupled with the possible high surface productivity enlarge the oxygen minimum zone in the water column (inset, at right). Short-lived but widespread anoxia and dysoxia (gray area) could have been brought about by massive plateau eruptions and associated "megaplumes" of hydrothermal effluents.

Chapter VI: Conclusions

Perhaps the most important finding of this work is that precise age measurements are the cornerstone for constructing accurate magmatic histories for large igneous provinces. Not only can the age of a given magmatic unit be determined, but radiometric ages for widely spaced magmatic units within a province can be used to describe the duration of volcanism and any spatial progression of volcanism. Furthermore, when coupled with geochemical data, the sequence and timescales for melting and tectonic processes or input from different mantle sources can be examined. Even so, as is true for geology in general, there is never too much data that can be collected. So although I have described possible magmatic histories for the North Atlantic Volcanic Province (NAVP) and the Caribbean plateau that are consistent with the existing ages, the actual evolution of each province is certain to have been more complex. As we gather more data, I think we will find that each LIP has had a particular history that was governed primarily by the interplay of mantle dynamics (plume size and shape, vigor of upwelling) and the local structure of the lithosphere through which the magmas are erupted.

It is apparent that both the NAVP and the Caribbean plateau were built by at least two discrete magmatic events. Bercovici and Mahoney (1995) noted that several other LIPs have had such histories and attributed this to a "double plume head" model of an initially large eruption event followed by a smaller event (see Chapter IV). However, this model is not consistent with the two-phase (or more) magmatism evident on the Ontong-Java and Caribbean oceanic plateaus because the later phases of magmatism occurred in the same region as initial volcanism. The double plume head model predicts a second, smaller flodd basalt episode at the site of the hotspot, from which the initial plateau will have moved. The model is also not consistent with the observations of the NAVP because in this case it is the second phase of magmatism that is more voluminous and is probably related to tectonic control (lithospheric thinning) rather than plume flux (White and McKenzie, 1989). In all of three of these examples, there is evidence that initial volcanism can be attributed to the arrival of a mantle plume. However, I think that later magmatism may be controlled predominantly by lithospheric structure rather than mantle plume dynamics, particularly in light of the work by VanDecar et al. (1995) who demonstrated that a velocity anomaly beneath Brazil may be hot lower lithosphere associated with flood basalt volcanism that occurred tens of millions of years ago.

Although the data I have presented indicate that the magmatic histories of two LIPs are more complex than previously envisioned, it is still evident that LIP events are transient. These transient yet catastrophic magmatic pulses are one of two modes of Earth dynamics, the other being the relatively steady-state motions of plate tectonics. It is relatively easier to examine plate tectonic processes compared to LIP processes because there are currently active examples of tectonic, such as mid-ocean ridges and subduction zones. Because of this, plate tectonic processes are better understood, but they are not neccessarily more important than LIP processes in terms of the evolution and development of the Earth. Future studies of LIP processes are therefore essential in creating a more balanced paradigm for the evolution of the Earth.

Specific areas of study that would be affected by transient, catastrophic volcanism are mantle convection and biological evolution. The basic question of how and where in the mantle LIPs are intitiated is not known. However, they must require large scale and relatively rapid convection of the mantle, perhaps even affecting or related to convection in the mantle (e.g., Larson, 1991). In terms of biological evolution, I highlighted in Chapter V the possible relationship between LIP volcanism and species extinction. In fact, LIP eruption may be the most important endogenic process that has affected species evolution. Altogether, to better understand the history of the Earth, we need to better understand LIPs.

Bibliography

Aitken, B. G. and Echeverria, L. M., 1984. Petrology and geochemistry of komatiites and tholeiites from Gorgona Island, Colombia. *Contrib. Min. Pet.*, 86: 94-105.

Allegre, C. J., 1982. Chemical geodynamics. *Tectonophys.*, 81: 109-132.

Alvarado, G. E., Kussmaul, S., Chiesa, S., Gillot, P.-Y., Appel, H., Wörner, G. and Rundle, C., 1993. Resumen cronoestratigráfico de las rocas ígneas de Costa Rica basado en dataciones radiométricas. *J. South Am. Earth Sci*, 6(3): 151-168.

Andrews, A. J., 1979. On the effect of low temperature seawater-basalt interaction on the distribution of sulfur in oceanic crust, layer 2. *Fall AGU EOS*, 60: 973.

Ariskin, A. A., Frenkel, M. Y., Barmina, G. S. and Nielsen, R. L., 1993. COMAGMAT: A FORTRAN program to model magma differentiation processes. *Computers and Geosciences*, 19: 1155-1170.

Arthur, M. A., Kump, L. R., Dean, W. E. and Larson, R. L., 1991. Superplume, supergreenhouse? *EOS*, 72: 301.

Aspden, J. A. and McCourt, W. J., 1986. Mesozoic oceanic terrane in the central Andes of Colombia. *Geology*, 14: 415-418.

Azéma, J. and Tournon, J., 1980. La Péninsule de Santa Elena, Costa Rica: Un massif ultrabasic charrié en marge pacifique de l'amerique centrale. *Compte Rendu Hebdomadaire des Séances de l'Academie des Sciences, Paris*, 290: 9-12.

Baker, E. T., 1994. A 6-year time series of hydrothermal plumes over the Cleft segment of the Juan de Fuca ridge. *J. Geophys. Res.*, 99: 4889-4904.

Barrero, D., 1979. *Geology of the Central Western Cordillera, West of Buga and Roldanillo, Colombia*, 4: (Publ. Esp. INGEOMINAS), 75.

Baumgartner, P. O., Mora, C. R., Butterlin, J., Sigal, J., Glaçon, G., Azéma, J. and Bourgois, J., 1984. Sedimentación y paleografía del Cretácico y Cenozoico del litoral pacífico de Costa Rica. *Revista Geológica de America Central*, 1: 57-136.

Beets, D. J., Klaver, G., Beunk, F. F., Kieft, C. and Maaskant, P., 1982. Picrites as parental magma of MORB-type tholeiites. *Nature*, 296: 341-343.

Bence, A. E., Papike, J. J. and Ayuso, R. A., 1975. Petrology of submarine basalts from the central Caribbean. *J. Geophys. Res.*, 80: 4775-4804.

Bender, J. F., Hodges, F. N. and Bence, A. E., 1978. Petrogenesis of basalts from the project FAMOUS area: experimental study from 0 to 15 kbars. *Earth Plan. Sci. Lett.*, 41: 277-302.

Bercovici, D. and Mahoney, J., 1995. Double flood basalts and plume head separation at the 660-kilometer discontinuity. *Science*, 266: 1367-1369.

Berggren, W. A., Kent, D. V., Flynn, J. J., and Van Couvering, J. A., 1985. Cenezoic geochronology. *J. Geophys. Res.*, 96: 1407-1418.

Berggren, W. A., Kent, D. V., Swisher, C. C., and Aubrey, M.-P., in press. A revised Cenezoic geochronology and chronostratigraphy. *In* Berggren, W. A., Kent, D. V. and Hardenbol, J. (Eds.), *Geochronology, Time Scales and Global Stratigraphic Correlations: A Unified Temporal Framework for an Historical Geology:* (Society of Economic Paleontologists and Mineralogists).

Berrange, J. P. and Thorpe, R. S., 1988. The geology, geochemistry, and emplacement of the Cretaceous-Tertiary ophiolitic rocks of the Nicoya Complex of the Osa Peninsula, southern Costa Rica. *Tectonophys.*, 147: 193-220.

Berrangé, J. P., Bradley, D. R. and Snelling, N. J., 1989. K/Ar dating of the ophiolitic Nicoya Complex of the Osa Peninsula. *J. South Am. Earth Sci*, 2(1): 49-59.

Besairie, H. and Collignon, M., 1972. Géologie de Madagascar: Les terrains sédimentaires. *Ann. Géol. Madagascar*, 35: 1-105.

Bienvenu, P., Bougault, H., Joron, J. L., Reuil, M. and Dmitriev, L., 1990. MORB alteration: rare-earth element/non-rare-earth hygromagmaphile element fractionation. *Chemical Geology*, 82: 1-14.

Boulter, M. C. and Mancum, S. B., 1989. The Brito-Arctic igneous province flora around the Paleocene/Eocene boundary. *In* Eldholm, O., Thiede, J. and Taylor, E. et al., *Proc. ODP, Sci. Results 104:* College Station, Texas (Ocean Drilling Program), 663-680.

Bourgois, J., Azema, J., Baumgartner, P. O., Tournon, J., Desmet, A. and Auboin, J., 1984. The geologic history of the Caribbean-Cocos plate boundary with special reference to the Nicoya ophiolite complex (Costa Rica) and DSDP results (Legs 67 and 84 off Guatemala): a synthesis. *Tectonophys.*, 108: 1-32.

Bowland, C. L. and Rosencrantz, E., 1988. Upper crustal structure of the western Colombian Basin, Caribbean Sea. *G.S.A. Bull.*, 100: 534-546.

Brasier, M. D., 1988. Foraminiferal extinction and ecological colapse during global biological events. *In* Larwood, G. P. (Eds.), *Extinction and Survival in the Fossil Record:* Oxford (Clarendon Press), 37-64.

Brass, G. W., Southam, J. R. and Peterson, W. H., 1982. Warm saline bottom water in the ancient ocean. *Nature*, 296: 620-623.

Bridgewater, D., Keto, L., McGregor, V. R., and Myers, J. S., 1976. Archean gneiss complex of Greenland. *In* Escher, A. and Watt, W. S. (Eds.), *Geology of Greenland:* Copenhagen (Geological Survey of Greenland), 18-75.

Brown, S. and Downie, C., 1984. Dinoflagellate cyst biostratigraphy of late Paleocene/early Eocene sediments from 552, 553A, 555, leg 81. *In* Roberts, D. G. and Schnitker, D. (Eds.), *Init. Repts. DSDP:* Washington (U.S. Govt. Printing Office), 565-579.

Burke, K. P., Fox, P. J. and Sengör, A. M. C., 1978. Buoyant ocean floor and the evolution of the Caribbean. *J. Geophys. Res.*, 83: 3949-3954.

Campbell, I. H. and Griffiths, R. W., 1990. Implications of mantle plume structure for the evolution of flood basalts. *Earth Plan. Sci. Lett.*, 99: 79-93.

Chalmers, J. A., 1991. New evidence on the structure of the Labrador Sea/Greenland continental margin. *J. Geol. Soc. London*, 148: 899-908.

Chase, C. G., 1972. The N plate problem of plate tectonics. *Geophys. J. Royal Astr. Soc.*, 29: 117-122.

Coffin, M. F. and Eldholm, O., 1994. Large igneous provinces: crustal structure, dimensions, and external consequences. *Rev. Geophys.*, 32(1): 1-36.

Courtillot, V. and Besse, J., 1987. Magnetic reversals, polar wander, and core- mantle coupling. *Science*, 237: 1140-1147.

Dagley, P. and Mussett, A. E., 1986. Paleomagnetism and radiometric dating of the British Tertiary Igneous province: Muck and Eigg. *Geophys. J. Roy. Astron. Soc.*, 85: 221-242.

Dalrymple, G. B., Clague, D. A., Vallier, T. L. and Menard, H. W., 1988. ^{40}Ar-^{39}Ar age, petrology, and tectonic significance of some seamounts in the Gulf of Alaska. *In* Keating, B. H., Fryer, P., Batiza, R. and Boehlert, G. W. (Eds.), *Seamounts, Islands, and Atolls:* (Am. Geophys. Union Monograph), 297-315.

de Boer, J., 1979. The outer arc of the Costa Rican orogen (oceanic basement complexes of the Nicoya and Santa Elena Peninsulas). *Tectonophys.*, 56: 221-259.

Deer, W. A., Howie, R. A. and Zussman, J., 1992. *An Introduction to the Rock Forming Minerals*, Essex, England (Longman Group), 696.

Dengo, G., 1962. Tectonic igneous sequence in Costa Rica. *In* Engel, A. E. J., James, H. L. and Leonard, B. F. (Eds.), *Petrologic studies: a volume to honor A.F. Buddington:* Boulder, Colorado (Geological Society of America), 133-161.

Denyer, P. and Arias, O., 1993. Geologia del norte de la Peninsula de Nicoya, Costa Rica. *Revista Geológica de America Central*, 16: 69-84.

De Souza, H. A. F., Espinosa, A. and Delaloye, M., 1984. K-Ar ages of basic rocks in the Patia Valley, southwest Colombia. *Tectonophys.*, 107: 135-145.

Dickin, A. P., 1988. The North Atlantic Tertiary Province. *In* Macdougall, J. D. (Eds.), *Continental Flood Basalts:* Dordrecht, Netherlands (Kluwer Academic Publishers), 111-149.

Diebold, J. B., Driscoll, N. W., Abrams, L., Buhl, P., Donnelly, T. W., Laine, E. P. and Leroy, S. A., 1995. A regional geophysical survey of the Venezuelan Basin and Beata Ridge; implications for interpretations of stratigraphy and tectonics. *EOS*, 76: F614.

Diebold, J. B., Stoffa, P. L., Buhl, P. and Truchan, M., 1981. Venezuela basin crustal structure. *J. Geophys. Res.*, 86: 7901-7923.

Doe, B. R., 1970. *Lead Isotopes*, Berlin (Springer-Verlag), 137.

Donnelly, T. W., 1973. Late Cretaceous basalts from the Caribbean, a possible flood basalt province of vast size. *EOS*, 54: 1004.

Donnelly, T. W., 1985. Mesozoic and Cenezoic plate evolution of the Caribbean region. *In* Stehli, F. G. and Webb, S. D. (Eds.), *The Great American Biotic Interchange:* New York-London (Plenum Press),

Donnelly, T. W., 1994. The Caribbean Creataceous basalt association: a vast igneous province that includes the Nicoya Complex of Costa Rica. *Profil* , (University of Stuttgart), 7: 17-45

Donnelly, T. W., and ten others, 1990. History and tectonic setting of Caribbean magmatism. *In* Dengo, G. and Case, J. E. (Eds.), *The Caribbean Region:* Boulder, CO (Geological Society of America), 339-374.

Donnelly, T. W., Melson, K., Kay, R. and Rogers, J. J. W., 1973. Basalts and dolerites of Late Cretaceous age from the central Caribbean. *In* Edgar, N. T. and Saunders, J. B. (Eds.), *Initial Reports of the Deep Sea Drilling Project:* Washington D.C. (U.S. Govt. printing office), 989-1012.

Duncan, R. A. and Hargraves, 1990. $^{40}Ar/^{39}Ar$ geochronology of basement rocks from the Mascarene Plateau, Chagos Bank, and Maldives Ridge. *In* Duncan, R. A., Backman, J. and Peterson, L. C. (Eds.), *Proc. ODP, Sci. Results:* College Station, Texas (Ocean Drilling Program), 43-52.

Duncan, R. A. and Hargraves, R. B., 1984. Plate tectonic evolution of the Caribbean region in the mantle reference frame. *In* Bonini, W. E., Hargraves, R. B. and Shagam, R. (Eds.), *The Caribbean-South American Plate Boundary and Regional Tectonics:* Boulder (Geological Society of America Memoir),

Duncan, R. A. and Hogan, L. G., 1994. Radiometric dating of young MORB using the ^{40}Ar-^{39}Ar incremental heating method. *Geophys. Res. Lett.*, 21(18): 1927-1930.

Duncan, R. A. and Pyle, D., 1988. Rapid eruption of the Deccan flood basalts at the Cretaceous/Tertiary boundary. *Nature*, 333: 841-843.

Duncan, R. A. and Richards, M. A., 1991. Hotspots, mantle plumes, flood basalts, and true polar wander. *Rev. Geophys.*, 29: 31-50.

Dupre, B. and Echeverria, L.N., 1984. Pb isotopes of Gorgona Island (Colombia): isotopic variations correlated with magma type. *Earth Planet. Sci. Lett.*, 67: 186-190.

Echeverria, L. N., 1980. Tertiary or Mesozoic komatiites from Gorgona Island, Colombia; Field relations and geochemistry. *Contrib. Min. Pet.*, 73: 253-266.

Edgar, N. T. and Saunders, J. B., 1973. *Initial Reports of the Deep Sea Drilling Project*, 15: Washington D.C (U.S. Govt. printing office), 1135.

Edgar, N. T., Ewing, J. I. and Hennion, J., 1971. Seismic refraction and reflection in the Caribbean Sea. *Am. Assoc. Pet. Geol. Bull*, 55: 833-870.

Elder, W. P., 1989. Molluscan extinction patterns across the Cenomanian-Turonian stage boundary in the Western Interior of the United States. *Paleobiology*, 15: 299-320.

Eldholm, O. and Grue, K., 1995. North Atlantic volcanic margins: Dimensions and production rates. *J. Geophys. Res.*, 99: 2955-2968.

Eldholm, O., Theide, J., Taylor, E. et al., 1987. *Proc. ODP, Init. Repts.*, 104: (College Station, TX (Ocean Drilling Program).

Escalante, G., 1990. The geology of southern Central America and western Colombia. *In* Dengo, G. and Case, J. E. (Eds.), *The Caribbean Region:* Boulder, CO (Geological Society of America), 201-230.

Ewing, J., Antoine, J. and Ewing, M., 1960. Geophysical measurements inthe western Caribbean Sea and in the Gulf of Mexico. *J. Geophys. Res.*, 65: 4087-4126.

Ewing, J., Talwani, M., Ewing, M. and Edgar, T., 1967. *Sediments of the Caribbean.* International Conference on Tropical Oceanography Proceedings, University of Miami, 51.

Faure, G., 1986. *Principles of Isotope Geology*, New York (John Wiley and Sons), 589.

Forsyth, D. W., 1992. Geophysical constraints on mantle flow and melt generation beneath mid-ocean ridges. *In* Phipps Morgan, J., Blackman, D. K. and Sinton, J. M. (Eds.), *Mantle Flow and Melt Generation at Mid-Ocean Ridges:* Washington DC (American Geophysical Union), 1-65.

Forsythe, L. M., Nielsen, R. L. and Fisk, M. R., 1994. High-field-strength element partitioning between pyroxene and basaltic to dacitic magmas. *Chem. Geol.*, 117: 107-125.

Fram, M. S. and Lesher, C. E., 1993. Geochemical constraints on mantle melting during creation of the North Atlantic basin. *Nature*, 363: 712-715.

Frey, F. A., 1983. Rare earth element abundances in upper mantle rocks. *In* Henderson, P. (Eds.), *Rare Earth Element Geochemistry, Developments in Geochemistry:* Amsterdam (Elsevier), 153-203.

Frey, F. A., Green, D. H. and Roy, S. D., 1978. Integrated models of basalt petrogenesis: A study of quartz tholeiites to olivine melilites from south Eastern Australia utilizing geochemical and experimental petrological data. *J. Petrology*, 19: 463-513.

Frisch, W., Meschede, M. and Sick, M., 1992. Origin of the Central American ophiolites: Evidence from paleomagnetic results. *G.S.A. Bull.*, 104: 1301-1314.

Galli-Olivier, C., 1979. Ophiolite and island arc volcanism in Costa Rica. *G.S.A. Bull.*, 90: 444-452.

Gansser, A., Dietrich, V. J. and Cameron, W. E., 1979. Paleogene komatiites from Gorgona Island. *Nature*, 278: 545-546.

Goosens, P. J., Rose, W. I. and Flores, D., 1977. Geochemistry of tholeiites of the Basic Igneous Complex of northwestern South America. *G.S.A. Bull.*, 88: 1711-1720.

Gradstein, F. M., Agterberg, F. P., Ogg, J. G., Hardenbol, J., van Veer, P., Thierry, J. and Hunag, Z., 1994. A Mesozoic timescale. *J. Geophys. Res.*, 99: 24051-24074.

Graham, D. W., Christie, D. M., Harpp, K. S. and Lupton, J. E., 1993. Mantle plume helium in submarine basalts from the Galapagos Platform. *Science*, 262: 2023-2026.

Green, T. H., Sie, S. H., Ryan, C. G. and Cousens, D. R., 1989. Proton microprobe-determined partitioning of Nb, Ta, Zr, Sr and Y between garnet, clinopyroxene and basaltic magma at high pressure and temperature. *Chem. Geol.*, 74: 201-216.

Grove, T. L., Kinzler, R. J. and Bryan, W. B., 1992. Fractionation of mid-ocena Ridge basalt (MORB). *In* Phipps Morgan, J., Blackman, D. K. and Sinton, J. M. (Eds.), *Mantle Flow and Melt Generation at Mid-Ocean Ridges:* Washington DC (American Geophysical Union), 71, ed. 281-310.

Gursky, H.-J., Gursky, M., Schmidt-Effing, R. and Wildberg, H., 1984. Karten zur Geologie von Nordwest Costa Rica (Mittelamerika) mit Erläuten. *Geol. und Paläontol.*, 18: 173-182.

Hall, S., 1995. Oeanic basement of the Caribbean basins. *Geol. Soc. Am. Annual Meeting Abst. Progr.*, New Orleans.

Hansen, H., Rex, D. C., Guise, P. G., and Brooks, C. K., 1993. $^{40}Ar/^{39}Ar$ ages on Tertiary East Greenland basalts from the Scoresby Sund area. *EOS*, 74: 625.

Harpp, K. S., 1995. Magmatic evolution of mid-ocean ridges and hotspots: isotopic and trace element studies of the East Pacific Rise, Mid-Atlantic Ridge, and Galapagos Islands. unpublished Ph.D. thesis, Cornell University.

Harries, P. J., 1995. Onshore-offshore trends in macrofaunal repopulation data from the Cenomanian-Turonian (mid-Cretaceous) mass extinction. *Geol. Soc. Am. Annual Meeting Abst. Progr.* New Orleans.

Harrison, R. K. and Merriman, R. J., 1984. Petrology, mineralogy, and chemistry of basaltic rocks: Leg 81. *In* Roberts, D. G., Schnitker, D. et al., *Init. Repts. DSDP 81:* Washington (U.S. Govt. Printing Office), 743-774.

Hart, M. B. and Ball, K. C., 1986. Late Cretaceous anoxic events, sea-level changes, and the evolution of planktonic foraminifera. *In* Summerhayes, C. P. and Shackleton, N. J. (Eds.), *North Atlantic Paleoceanography:* Oxford (Blackwell), 67-78.

Hart, M. B. and Leary, P. N., 1989. The stratigraphic and paleogeographic setting of the late Cenomanian 'anoxic' event. *J. Geol. Soc. London*, 146: 305-310.

Herbin, J. P., Montadert, L., Müller, R., Gomez, R., Thurow, J. and Wiedmann, J., 1986. Organic-rich sedimentation at the Cenomananian-Turonian boundary in oceanic and coastal basins in the North Atlantic and Tethys. *In* Summerhayes, C. P. and Shackleton, N. J. (Eds.), *North Atlantic Paleoceanography:* Oxford (Blackwell), 389-422.

Hess, P. C., 1992. Phase equilibria constraints on the origin of ocean floor basalts. *In* Morgan, J. P., Blackman, D. K. and Sinton, J. M. (Eds.), *Mantle Flow and Melt Generation at Mid-Ocean Ridges:* Washington DC (American Geophysical Union), 67-102.

Hey, R., Johnson, G. L. and Lowrie, A., 1977. Recent plate motions in the Galápagos area. *G.S.A. Bull.*, 88: 1385-1403.

Hinz, K., 1981. A hypothesis on terrestrial catastophes: wedges of very thick oceanward diping layers beneath passive continental margins. *Geologische Jahrbuch*, E22: 3-28.

Hurfurd, A. J. and Hammerschmidt, K., 1985. $^{40}Ar/^{39}Ar$ and K-Ar dating of the Bishop and Fish Canyon Tuffs: Calibration ages for fission-track dating standards. *Chem. Geol.*, 58: 23-32.

Ingram, B. L., Coccioni, R., Montanari, A. and Richter, F. M., 1994. Strontium isotopic composition of mid-Cretaceous seawater. *Science*, 264: 546-550.

Jarvis, I., et al., 1988. Microfossil assemblages and the Cenomanian-Turonian (late Cretaceous) ocean anoxic event. *Cret. Res.*, 9: 3-103.

Jenner, G. A., Longerich, H. P., Jackson, S. E. and Fryer, B. J., 1990. ICP-MS - A powerful tool for high-precision trace-element analysis in earth sciences: evidence from selected USGS reference samples. *Chem. Geol.*, 83: 133-148.

Jochum, K. P., Seufert, H. M. and Thirlwall, M. F., 1990. High-sensitivity Nb analyses by spark-source mass spectrometry (SSMS) and calibration of XRF Nb and Zr. *Chem. Geol.*, 81: 1-16.

Joron, J. L., Bougault, H., Maury, R. C., Bohn, M., and Desprairies, A., 1984. Strongly depleted tholeiites from the Rockall Plateau margin, North Atlantic: Geochemistry and mineralogy. *In* Roberts, D. G., Schnitker, D. et al., *Init. Repts. DSDP 81:* Washington (U.S. Govt. Printing Office), 783-794.

Jürgensen, T. and Mikkelsen, N., 1974. Coccoliths from volcanic sediments (Danian) in Nugssuaq, West Greenland. *Bull.of the Geol.Soc. Denmark*, 23: 225-230.

Kaufmann, E. G., 1986. High resolution event stratigraphy: Regional and global Cretaceous bio-events. *In* Walliser, O. H. (Eds.), *Global Bio-Events: A Critical Approach:* Berlin (Springer-Verlag), 279-335.

Keppler, H., 1996. Constraints from partitioning experiments on the composition of subduction-zone fluids. *Nature*, 380: 237-240.

Kerr, A. C., Marriner, G.F., Arndt, N.T., Tarrney, J., Nivia, A., Saunders, A.D., Stoery, M., and Duncan, R.A., 1996. The petrogenesis of Gorgona komatiites, picrites andbasalts: new field, petrographic and geochemical constraints. *Chem. Geol.*, : in press.

Kerr, A. C., Tarney, J., Marriner, G. F., Klaver, G. T., Saunders, A. D. and Thirlwall, M. F., in press. The geochemistry and petrogenesis of the late Cretaceous picrites and basalts of Curaçao, Netherlands Antilles: remnant of an oceanic plateau. *Large Igneous Provinces* AGU Monograph.

Kerr, A. C., Tarney, J., Marriner, G. F., Klaver, G. T., Saunders, A. D. and Thirlwall, M. F., in press. The geochemistry and petrogenesis of the late Cretaceous picrites and basalts of Curaçao, Netherlands Antilles: remnant of an oceanic plateau. *Lithos* , in press.

Kharin, G. N., et al., 1976. K-Ar age of the basalts of the Norwegian-Greenland Sea Glomar Challenger leg 38 DSDP. *In* Talwani, M., Udintsev, G. et al., *Init. Repts. DSDP 38:* Washington (U.S. Govt. Printing Office), 755-760.

Klaver, G., 1987. *The Curaçao Lava Formation; an ophiolitic analogue of the anomalous thick layer 2B of the mid-Cretaceous oceanic plateaus in the western Pacific and central Caribbean.* GUA papers. Univ. of Amstersdam. 168.

Klein, E. M. and Langmuir, C. H., 1987. Global correlations of ocean basalt chemistry with axial depth and crustal thickness. *J. Geophys. Res.*, 92: 8089-8115.

Knox, R. W. and Morton, A. C., 1988. The record of early Tertiary N Atlantic volcanism in sediments of the North Sea Basin. *In* Morton, A. C. and Parson, L. M. (Eds.), *Early Tertiary Volcanism and the Opening of the NE Atlantic:* (Geol. Soc. London Sp. Publ.), 407-419.

Kuhnt, W., Thurow, J., Wiedmann, J. and Herbin, J. P., 1986. Oceanic anoxic conditions around the Cenomanian/Turonian boundary and the response of biota.*SCOPE/UNEP report:* Hamburg, 205-246.

Kuijpers, E. P., 1980. The geologic history of the Nicoya Ophiolite Complex, Costa Rica and its geotectonic significance. *Tectonophys.*, 68: 233-255.

Kurz, M. D., Kammer, D. P., Kenna, T. C. and Geist, D., 1993. Dynamics and evolution of the Galápagos hotspot from helium isotopes. *Eos* , 74(43): 632.

Langmuir, C. H., Klein, E. M. and Plank, T., 1992. Petrological systematics of mid-ocean ridge basalts: constraints on melt generation beneath ocean ridges. *In* Phipps Morgan, J., Blackman, D. K. and Sinton, J. M. (Eds.), *Mantle Flow and Melt Generation at Mid-Ocean Ridges:* Washington DC (American Geophysical Union), 71: 183-280.

Lanphere, M. A. and Dalrymple, G. B., 1976. Identification of excess ^{40}Ar by the $^{40}Ar/^{39}Ar$ age spectrum technique. *Earth Plan. Sci. Lett.*, 32: 141-148.

Lanphere, M. A. and Dalrymple, G. B., 1978. The use of $^{40}Ar/^{39}Ar$ data in evaluation of disturbed K-Ar systems. *In* Zartmano, R. E. (Ed.), *Short Papers of the Fourth International Conference, Geochronology, Isotope Geology:* (U.S. Geol. Surv. Open-File Rep.), 241-243.

Lanphere, M. A., Dalrymple, G. B., Fleck, R. J. and Pringle, M. S., 1990. Intercalibration of mineral standards for K-Ar and ^{40}Ar-^{39}Ar age measurements. *EOS*, 71: 1658.

Larsen, H. C. and Jakobsdóttir, S., 1988. Distribution, crustal properties and significance of seawards-dipping sub-basement reflectors off E Greenland. *In* Morton, A. C. and Parson, L. M. (Eds.), *Early Tertiary Volcanism and the Opening of the NE Atlantic:* London (Geol. Soc. London Sp. Publ.), 95-114.

Larsen, H. C., Saunders, A. D. , Clift, P. D., et al., 1995. *Proc. ODP, Init. Res.*, 152: College Station, TX (Ocean Drilling Program).

Larsen, L. M., Pedersen, A. K., Pedersen, G. K., and Piasecki, S., 1992. Timing and duration of early Tertiary volcanism in the North Atlantic: new evidence from West Greenland. *In* Storey, B. C., Alabaster, T. and Pankhurst, R. J. (Eds.), *Magmatism and the Causes of Continental Breakup:* London (The Geological Society), 321-334.

Larson, R. L. and Olson, P., 1991. Mantle plumes control magnetic reversal frequency. *Earth Plan. Sci. Lett.*, 107: 437-447.

Larson, R. L., 1991. Geological consequences of superplumes. *Geology*, 19: 547-550.

Lawver, L. A. and Müller, R. D., 1994. Iceland hotspot track. *Geology*, 22: 311-314.

LeHuray, A. P. and Johnson, E. S., 1989. Rb-Sr systematics of Site 642 volcanic rocks and alteration materials. *In* Eldholm, O., Thiede, J., Taylor, E. et al., *Proc. ODP, Sci. Results 104:* College Station, Texas (Ocean Drilling Program), 437-448.

Lindsley, D. H., 1983. Pyroxene thermometry. *Am. Min.*, 68: 477-493.

Ludwig, W. J., Houtz, R. E. and Ewing, J. I., 1975. Profiler-sonobuoy measurements in the Colombia and Venezuela Basins, Caribbean Sea. *Am. Assoc. Pet. Geol. Bull*, 59: 115-123.

Macintyre, R. M. and Hamilton, P. J., 1984. Isotopic geochemistry of lavas from Site 553 and 555. *In* Roberts, D. G. and Schnitker, D. et al., *Init. Repts. DSDP:* Washington (U.S. Govt. Printing Office), 775-782.

Mahoney, J. J. and Spencer, K. J., 1991. Isotopic evidence for the origin of the Manihiki and Ontong-Java oceanic plateaus. *Earth Plan. Sci. Lett.*, 104: 196-210.

Mahoney, J. J., Storey, M., Duncan, R. A., Spencer, K. J. and Pringle, M., 1993. Geochemistry and age of the Ontong Java Plateau. *In* Pringle, M., Sager, W. W., Sliter, W. V. and Stein, S. (Eds.), *The Mesozoic Pacific Geology, Tectonics, and Volcanism:* Washington D.C. (American Geophysical Union), 233-261.

Mason, B., 1966. *Principles of Geochemistry*, New York (John Wiley and Sons),

Mattson, P. H. and Pessagno, E. A. J., 1979. Jurassic and Early Cretaceous radiolarian in Puerto Rico ophiolites - tectonic implications. *Geology*, 7: 440-444.

Maurasse, F., Husler, J., Georges, G., Schmitt, R. and Damond, P., 1979. Upraised Caribbean seafloor below acoustic reflector B" at the southern Peninsula of Haiti. *Geol. en Mijnbouw*, 58: 71-83.

McCourt, W. J., Aspden, J. A. and Brook, M., 1984. New geological and geochronological data from the Colombian Andes: Continental growth by multiple accretion. *J. Geol. Soc. London*, 141: 831-845.

McDonough, W. F. and Sun, S.-s., 1995. The composition of the Earth. *Chem. Geol.*, 120: 223-253.

McKenzie, D. and O'Nions, R. K., 1995. The source regions of ocean island basalts. *J. Petrology*, : 133-159.

Merriman, R. J., Taylor, P. N., and Morton, A. C., 1988. Petrochemistry and isotope geochemistry of early Palaeogene basalts forming the dipping reflector sequence SW of Rockall Plateau, North east Atlantic. *In* Morton, A. C. and Parson, L. M. (Eds.), *Early Tertiary Volcanism and the Opening of the NE Atlantic:* London (Geol. Soc. London Sp. Publ.), 123-135.

Millward, D., Marriner, G. F. and Saunders, A. D., 1984. Cretaceous tholeiite volcanic rocks from the Western Cordillera of Colombia. *J. Geol. Soc. London*, 141: 847-860.

Montgomery, H., Pessagno, E. A. J., Lewis, J. F. and Schellekens, J., 1994. Paleogeography of Jurassic fragments in the Caribbean. *Tectonics*, 13: 725-732.

Morton, A. C., Evans, D., Harland, R., King, C. and Ritchie, D. K., 1988. Volcanic ash in a cored borehole W of the Shetland Islands: evidence for Selandian (late Paleocene) volcanism in the Faeroes region. *In* Morton, A. C. and Parson, L. M. (Eds.), *Early Tertiary Volcanism and the Opening of the NE Atlantic:* London (Geol. Soc. London Sp. Publ.), 263-269.

Mussett, A. E., 1986. ^{40}Ar-^{39}Ar step-heating ages of the Tertiary igneous rocks of Mull, Scotland. *J. Geol. Soc. London*, 143: 887-896.

Mussett, A. E., Dagley, P., and Skelhorn, R. R., 1988. Time and duration of activity in the British Tertiary Igneous Province. *In* Morton, A. C. and Parson, L. M. (Eds.), *Early Tertiary Volcanism and the Opening of the NE Atlantic:* London (Geol. Soc. London Sp. Publ.), 337-348.

Noble, R. H., Macintyre, R. M., and Brown, P. E., 1988. Age constraints on Atlantic evolution: timing of magmatic activity along the E Greenland continental margin. *In* Morton, A. C. and Parson, L. M. (Eds.), *Early Tertiary Volcanism and the Opening of the North Atlantic:* London (Geol. Soc. London Sp. Publ.), 201-214.

Obradovich, J. D., 1993. A Cretaceous time scale. *In* Caldwell, W. G. E. and Kauffman, E. G. (Eds.), *Evolution of the Western Interior Basin:* (Geological Association of Canada Special Paper), 379-396.

Officer, C. B., Ewing, J. I., Edwards, R. S. and Johnson, H. R., 1957. Geophysical investigations in the eastern Caribbean: Venezuelan basin, Antilles island arc, and Puerto Rico outer trench. *G.S.A. Bull.*, 68: 359-378.

Orth, C. J., Attrep, M. J., Quintana, L. R., Elder, W. P., Kauffman, E. G., Diner, R. and Villamil, T., 1993. Elemental abundance anomalies in the late Cenomanian extinction interval: a search for the source(s). *Earth Plan. Sci. Lett.*, 117: 189-204.

Perch-Nielsen, K., 1973. Danian and Campanian/Maastrichtian coccoliths in a volcanic province, West Greenland. *Bull. Geol.Soc. Denmark*, 22(79-82):

Peucker-Ehrenbrink, B., Hofmann, A. W. and Hart, S. R., 1994. Hydrothermal lead transfer from mantle to continental crust: the role of metalliferous sediments. *Earth Plan. Sci. Lett.*, 125: 129-142.

Pindell, J. L. and Barrett, S. F., 1990. Geological evolution of the Caribbean region; A plate tectonic perspective. *In* Dengo, G. and Case, J. E. (Eds.), *The Caribbean Region:* Boulder, CO (Geological Society of America), 405-433.

Pringle, M. S., 1993. Age progressive volcanism in the Musicians Seamounts: A test of the hotspot hypothesis. *In* Pringle, M., Sager, W. W., Sliter, W. V. and Stein, S. (Eds.), *The Mesozoic Pacific Geology, Tectonics, and Volcanism:* Washington D.C. (American Geophysical Union), 187-215.

Raup, D. M. and Sepkoski, J. J., Jr., 1984. Periodicity of extinctions in the geologic past. *Proc. Natl. Acad. Sci.*, 81: 801-805.

Raup, D. M. and Sepkoski, J. J., Jr., 1986. Periodic extinction of family and genera. *Science*, 231: 833-836.

Richards, M. A. and Griffiths, R. W., 1989. Thermal entrainment by deflected plumes. *Nature*, 342: 900-902.

Richards, M. A., Duncan, R. A., and Courtillot, V. E., 1989. Flood basalts and hotspot tracks: Plume heads and tails. *Science*, 246: 103-107.

Richardson, C., Oakley, P. J., and Cann, J. R., 1984. Trace and major element chemistry of basalts from Leg 81. *In* Roberts, D. G. and Schnitker, D. et al., *Init. Repts. DSDP 81:* Washington (U.S. Govt. Printing Office), 795-806.

Ringwood, A. E., 1975. *Comoposition and Petrology of the Earth's Mantle*, New York (McGraw Hill), 265.

Roberts, D. G. and Schnitker, D. et al., 1984. *Init. Repts. DSDP, 81*: Washington (U.S. Govt. Printing Office), 923.

Santamaria, F. and Schubert, C., 1974. Geochemistry and geochronology of the southern Caribbean-northern Venezuela plate boundary. *G.S.A. Bull.*, 85: 1085-1098.

Sarmiento, J. L., Herbert, T. D. and Toggweiler, J. R., 1988. Causes of anoxia in the world oceans. *Global Geochemical Cycle*, 2: 115-128.

Sayeed, V., Maurasse, F., Husler, J. and Schmitt, R., 1978. Geochemistry and petrology of some mafic rocks from Dumisseau, southern Haiti. *EOS Trans. Am. Geophys. Union*, 59: 403.

Schlanger, S. O. and Jenkyns, H. C., 1976. Cretaceous oceanic anoxic events: Causes and consequences. *Geologie en Mijnbouw*, 55: 179-184.

Schlanger, S. O., Arthur, M. A., Jenkyns, H. C. and Scholle, P. A., 1987. The Cenomanian-Turonian Ocean Anoxic Event, I. Stratigraphy and distribution of carbon rich beds and the marine $d^{23}C$ excursion. *In* Brooks, J. and Fleet, A. J. (Eds.), *Marine Petroleum Source Rocks.*

Schmidt-Effing, R., 1979. Alter und genese des Nicoya-Komplexes einer ozeanischen Päleokruste (Oberjura bis Eozän) im südlichen Zentralamerika. *Geol. Rund.*, 68: 457-494.

Scholle, P. A. and Arthur, M. A., 1980. Carbon isotope fluctuations in Cretaceous pelagic limestones; potential stratigraphic and petroleum exploration tool. *Am. Assoc. Pet. Geol. Bull*, 64: 67-87.

Schönharting, G. and Abrahamsen, N., 1989. Paleomagnetism of the volcanic sequence in Hole 642E, ODP Leg 104, Vøring Plateau, and correlation with early tertiary basalts in the North Atlantic. *In* Eldholm, O., Thiede, J. and Taylor, E. et al., *Proc. ODP, Sci. Results 104:* College Station, Texas (Ocean Drilling Program), 911-920.

Scotese, C. R., 1989. Plate tectonic reconstructions of the Cretaceous and Cenezoic ocean basins. *In* Scotese, C. R. and Sager, W. W. (Eds.), *Mesozoic and Cenezoic Plate Reconstructions:* 27-48.

Sen, G., Hickey-Vargas, R., Waggoner, D. G. and Maurasse, F., 1988. Geochemistry of basalts from the Dumisseau Formation, southern Haiti; Implications for the origin of the Caribbean Sea crust. *Earth Plan. Sci. Lett.*, 87: 423-437.

Spadea, P., Espinosa, A. and Orrego, A., 1989. High-MgO extrusive rocks from the Romeral zone ophiolites in the southwestern Colombian Andes. *Chem. Geol.*, 77: 303-321.

Staudigal, H. and Hart, S. R., 1983. Alteration of basaltic glass: Mechanism and significance for the oceanic crust-seawater budget. *Geochim. Cosmochim. Acta*, 47: 337-350.

Storey, M., Mahoney, J. J., Kroenke, L. W. and Saunders, A. D., 1991. Are oceanic plateaus site of komatiite formation? *Geology*, 19: 376-379.

Storey, M., Mahoney, J. J., Saunders, A. D., Duncan, R. A., Kelley, S. P. and Coffin, M. F., 1995. Timing of hot spot-related volcanism and the breakup of Madagascar and India. *Science*, 267: 852-855.

Swanson, D. A. and al, e., 1975. Linear vent systems and estimated rates of magma production and eruption for the Yakima basalt on the Colombia Plateau. *American Journal of Science*, 275: 877-905.

Talwani, M. and Eldholm, O., 1977. Evolution of the Norwegian-Greenland Sea. *G.S.A. Bull.*, 88: 969-999.

Talwani, M. and Udintsev, G. et al., 1976. *Init. Repts. DSDP*, 38: Washington (U.S. Govt. Printing Office), 1256.

Taras, B. D. and Hart, S. R., 1987. Geochemical evolution of the New England seamount chain: Isotopic and trace element constraints. *Chem. Geol.*, 64: 35-54.

Tarduno, J. A., et al., 1991. Rapid formation of the Ontong-Java plateau by Aptian mantle plume volcanism. *Science*, 254: 399-403.

Taylor, P. N. and Morton, A. C., 1989. Sr, Nd, and Pb isotope geochemistry of the upper and lower volcanic series at site 642. *In* Eldholm, O., Thiede, J., Taylor, E. et al., *Proc. ODP, Sci. Results 104:* College Station, Texas (Ocean Drilling Program), 429-435.

Tejada, M. L. G., Mahoney, J. J., Duncan, R. A. and Hawkins, M. P., in press. Age and geochemistry of basement and alkalic rocks of Malaita and Santa Isabel, Solomon Islands, southern margin of Ontong Java Plateau. *J. Petrology.*

Thompson, R. N. and Gibson, S. A., 1991. Subcontinental mantle plumes, hotspots and pre-existing thinspots. *J. Geol. Soc. London*, 148: 973-977.

Toussant, J. F., Botero, G. and Restrepo, J. J., 1978. Datación K-Ar de batolito de Buga. *Publ. Esp. Geol. Univ. Nat. Colombia ed.*, 13: 1-3.

Upton, B. G. J., Emeleus, C.H., Rex, D.C., and Thirlwall, M.F., 1995. Early Tertiary magmatism in NE Greenland. *J. Geol. Soc. London*, 152: 959-964.

VanDecar, J. C., James, D. E. and Assumpção, M., 1995. Seismic evidence for a fossil mantle plume beneath South America and implications for plate driving forces. *Nature*, 378: 25-31.

Vogt, P. R. and Avery, O. E., 1974. Detailed magnetic surveys in the northeast Atlantic and Labrador Sea. *J. Geophys. Res.*, 79: 363-389.

Vogt, P. R., 1989. Volcanogenic upwelling of anoxic, nutrient-rich water: A possible factor in carbonate-bank/reef demise and benthic faunal extinctions? *G.S.A. Bull.*, : 1225-1245.

Von Damm, K. L., 1990. Seafloor hydrothermal activity: Black smoker chemistry and chimneys. *An. Rev. Earth Planet. Sci.*, 18: 173-204.

Walker, J. C. G., 1986. Global geochemical cycles of carbon, sulfur and oxygen. *Marine Geology*, 70: 159-174.

Walker, R. J., Echeverria, L. M., Shirey, S. B. and Horan, M. F., 1991. Re-Os isotopic constraints on the origin of volcanic rocks, Gorgona Island, Colombia: Os isotopic evidence for ancient heterogeneities in the mantle. *Contrib. Min. Pet.*, 107: 150-162.

Wallace, P. and Carmichael, I. S. E., 1992. Sulfur in basaltic magmas. *Geochimica et Cosmochimica Acta*, 56: 1863-1874.

Weaver, B. L., 1991. The origin of ocean island basalt end-member compositions: trace element and isotopic constraints. *Earth Plan. Sci. Lett.*, 104(1991):

White, R. S. and McKenzie, D., 1989. Magmatism at Rift zones: The generation of volcanic continental margins and flood basalts. *J. Geophys. Res.*, 94: 7,685-7,729.

White, R. S., 1992. Magmatism during and after continental breakup. *In* Storey, B. C., Alabaster, T. and Pankhurst, R. J. (Eds.), *Magmatism and the Causes of Continental Breakup:* London (The Geological Society), 1-16.

White, W. M., 1985. Sources of oceanic basalts: Radiogenic isotope evidence. *Geology*, 13: 115-118.

White, W. M., McBirney, A. R. and Duncan, R. A., 1993. Petrology and geochemistry of the Galápagos Islands: Portrait of a pathological mantle plume. *J. Geophys. Res.*, 98: 19533-19563.

Wiedmann, J., 1978. Ammonites from the Curaçao Lava Formation, Curaçao, Caribbean. *Geol. Mijnbouw*, 57: 361-364.

Wignall, P. B., 1994. *Black Shales*, Oxford (Oxford University Press), 127.

Wildberg, H. G. H., 1987. High level and low level plagiogranites from the Nicoya ophiolite complex, Costa Rica, Central America. *Geol. Rund.*, 76(1): 285-301.

Wildberg, H., 1984. Der Nicoya-Komplex, Costa Rica, Zentralamerika: Magmatisme und Genese polygenetischen Ophiolith-Komplexes. Münsterisches Forschungen zur Geologie und Paläontologie. 62: 123.

Zindler, A. and Hart, S. R., 1986. Chemical geodynamics. *An. Rev. Earth Planet. Sci.*, 14: 493-571.

Appendices

Appendix 1

The following are the step heating data for all of the 40Ar-39Ar analyses reported in Chapter II. All measurements have been corrected for decay (37Ar) and mass fractionation. The start number refers to the analysis number of the first heating step

ODP 152-915A-24R-2 plagioclase

J = 1.651 e-3

°C	Age	1σ	36Ar	σ36	37Ar	σ37	39Ar	σ39	40Ar	σ40
600	344.2	23.4	6.60E-04	7.1E-06	0.0320	0.0003	0.0003	5.3E-06	0.2245	2.3E-04
800	71.4	3.1	1.86E-03	2.4E-05	2.3350	0.0023	0.0085	3.7E-05	0.5328	3.4E-04
900	96.1	5.1	1.13E-03	1.9E-05	1.7100	0.0170	0.0045	3.2E-05	0.3095	2.9E-04
1025	75.9	3.6	1.45E-03	1.9E-05	2.8130	0.0280	0.0069	3.5E-05	0.3355	3.1E-04
1100	88.6	6.5	1.37E-03	2.0E-05	1.3490	0.0130	0.0036	2.4E-05	0.3788	3.2E-04
1175	93.6	8.3	9.20E-04	1.6E-05	0.8217	0.0082	0.0023	2.0E-05	0.2622	2.3E-04
1250	168.7	9.2	5.90E-04	7.3E-06	0.2780	0.0028	0.0009	1.4E-05	0.1951	2.8E-04
1350	91.2	5.9	8.10E-04	1.7E-05	0.6700	0.0067	0.0030	2.7E-05	0.2625	2.6E-04

ODP 152-915A-24R-2 phenocryst-free groundmass (2E7) irr 5-20-94 start 94-249

J = 1.746 e-3

°C	Age	1σ	36Ar	σ36	37Ar	σ37	39Ar	σ39	40Ar	σ40
525	46.9	3.4	4.65E-03	3.5E-05	0.0630	0.0006	0.0191	6.2E-05	1.6720	1.4E-03
625	54.3	2.2	7.81E-03	3.9E-05	0.1240	0.0012	0.0317	7.8E-05	2.8850	1.0E-03
725	41.2	2.0	8.90E-03	5.5E-05	2.0390	0.0200	0.1635	2.4E-04	4.7400	2.5E-03
825	49.3	1.2	1.92E-03	2.1E-05	1.9070	0.0190	0.0870	1.6E-04	1.8350	1.0E-03
950	52.3	1.4	2.13E-03	2.5E-05	2.4870	0.0250	0.0854	1.4E-04	1.8840	2.3E-03
110	39.0	2.8	2.50E-03	2.8E-05	0.7970	0.0080	0.0199	9.3E-05	0.9320	1.9E-03
1400	32.1	2.2	6.70E-03	4.2E-05	8.2390	0.0820	0.0448	9.3E-05	1.7350	1.0E-03

ODP 152-915A-25R-1 phenocryst-free groundmass (2E7) irr 10-2-94 start 94-477

J = 1.551 e-3

°C	Age	1σ	36Ar	σ36	37Ar	σ37	39Ar	σ39	40Ar	σ40
650	41.0	5.4	6.45E-03	3.6E-05	0.0857	0.0009	0.0113	4.8E-05	2.0636	1.2E-03
800	48.5	1.8	1.72E-03	2.7E-05	1.1180	0.0110	0.0709	1.3E-04	1.6289	7.3E-04
950	52.1	1.8	2.31E-03	2.8E-05	2.3430	0.0230	0.1114	1.4E-04	2.5253	1.1E-03
1050	44.6	2.2	9.60E-04	2.1E-05	0.5340	0.0053	0.0212	5.5E-05	0.5669	4.0E-04
1200	37.0	1.6	1.05E-02	5.0E-05	13.2400	0.1300	0.1026	1.4E-04	3.0456	1.1E-03
1400	35.7	4.0	2.73E-03	3.3E-05	3.1780	0.0320	0.0168	2.3E-05	0.6853	2.0E-04

ODP 152-917A-17R-4 groundmass plagioclase (2E6) irr 5-20-94 start 94-242

J = 1.669 e-3

°C	Age	1σ	36Ar	σ36	37Ar	σ37	39Ar	σ39	40Ar	σ40
550	7.6	18.1	7.98E-03	5.0E-05	0.0280	0.0000	0.0025	1.1E-05	2.3620	1.0E-03
675	17.7	6.4	1.49E-02	6.0E-05	0.2340	0.0020	0.0170	5.9E-05	4.4840	2.0E-03
825	38.1	3.6	2.71E-04	5.3E-06	0.0085	0.0001	0.0028	2.5E-05	0.1106	1.1E-04
975	33.1	1.0	9.33E-03	3.9E-05	0.2680	0.0027	0.1278	1.5E-04	4.0040	2.9E-03
1100	27.4	0.6	5.88E-03	3.7E-05	4.0770	0.0410	0.2167	2.7E-04	3.3560	1.8E-03
1250	34.1	1.6	5.63E-03	4.0E-05	7.4240	0.0740	0.0609	1.1E-04	1.6920	8.0E-04
1400	70.5	4.0	5.22E-04	7.0E-06	0.4330	0.0043	0.0039	2.8E-05	0.2053	3.0E-04

ODP 152-917A-23R-1A basalt (2E13) irr 5-20-94 start 94-281

J = 1.563 e-3

°C	Age	1σ	36Ar	σ36	37Ar	σ37	39Ar	σ39	40Ar	σ40
525	90.6	6.7	1.28E-03	2.4E-05	0.0046	0.0001	0.0030	2.9E-04	0.4764	2.1E-04
650	65.7	3.2	1.97E-02	2.5E-04	0.2730	0.0003	0.2020	1.1E-04	10.0620	2.2E-03
725	62.1	2.2	4.64E-03	3.8E-05	0.3430	0.0034	0.1608	1.8E-04	4.9490	5.4E-03
800	61.5	2.2	2.15E-03	2.7E-05	0.4200	0.0042	0.1615	1.8E-04	4.1830	3.2E-03
875	60.0	2.0	1.49E-03	2.4E-05	0.4990	0.0050	0.1933	2.2E-04	4.5760	5.5E-03
925	58.0	2.0	1.04E-03	9.0E-06	0.4710	0.0050	0.1059	1.6E-04	2.4790	2.0E-03
1050	61.0	2.2	6.46E-04	8.1E-06	0.6750	0.0070	0.1024	3.6E-04	2.3840	4.1E-03
1200	56.4	2.0	4.69E-03	3.9E-05	6.5700	0.0660	0.2394	2.3E-04	5.6360	4.7E-03
1400	59.3	2.2	1.45E-03	2.6E-05	1.2400	0.0120	0.0694	1.8E-04	1.7960	1.7E-03

ODP 152-917A-23R-1B basalt (4G2) irr 10-20-94 start B5450

J = 1.674 e-3

RF	Age	1σ	36Ar	σ36	37Ar	σ37	39Ar	σ39	40Ar	σ40
220	61.2	2.1	1.21E-02	1.8E-04	0.4200	0.0040	0.1587	3.6E-04	6.7991	2.9E-03
260	60.8	2.2	6.09E-04	1.1E-04	0.2980	0.0030	0.0906	2.7E-04	2.0102	7.5E-04
300	59.8	3.2	2.00E-03	1.5E-04	0.1430	0.0010	0.0357	6.8E-04	1.2984	7.6E-04
350	60.6	3.4	6.00E-04	1.8E-04	0.1570	0.0020	0.0338	1.0E-04	0.8423	5.0E-04
425	49.1	7.6	5.70E-04	1.2E-04	0.2780	0.0030	0.0299	3.1E-04	0.6360	4.7E-04
fusion	60.0	1.6	9.10E-04	2.0E-04	1.7730	0.0170	0.0450	1.9E-04	0.9792	1.2E-03

ODP 152-917A-23R-3 altered tuff feldspar (1D3) irr start

J = 1.740 e-3

°C	Age	1σ	36Ar	σ36	37Ar	σ37	39Ar	σ39	40Ar	σ40
550	57.2	2.4	1.65E-03	1.7E-05	0.0219	0.0002	0.0154	4.6E-05	0.7755	5.0E-04
650	36.0	6.2	7.40E-04	7.6E-06	0.0076	0.0001	0.0023	2.2E-05	0.2443	2.2E-04
800	50.1	10.0	1.28E-03	1.7E-05	0.4240	0.0042	0.1052	1.2E-04	2.0730	7.0E-04
900	56.4	1.2	1.04E-03	1.8E-05	0.7000	0.0070	0.1262	1.5E-04	2.5930	7.7E-04
975	55.4	1.4	3.50E-04	1.3E-05	0.2107	0.0021	0.0312	6.9E-05	0.6551	4.5E-04
1075	57.8	1.1	2.20E-03	2.4E-05	1.3350	0.0130	0.2120	1.7E-04	4.5580	1.2E-03
1150	58.0	1.1	1.08E-03	8.6E-06	1.0560	0.0110	0.1752	1.8E-04	3.5720	9.7E-04
1250	59.6	1.1	2.10E-03	2.2E-05	2.7090	0.0270	0.4137	2.7E-04	8.5000	2.3E-03

ODP 152-917A-24R-1 feldspar (1D4) irr start 94-108

J = 1.721 e-3

°C	Age	1σ	36Ar	σ36	37Ar	σ37	39Ar	σ39	40Ar	σ40
650	83.6	2.4	3.11E-03	2.9E-05	0.0172	0.0002	0.0296	6.7E-05	1.7359	7.6E-04
800	62.8	1.4	8.06E-03	4.3E-05	0.1830	0.0018	0.3782	2.8E-04	10.1590	2.3E-03
875	61.1	1.4	8.80E-04	6.5E-06	0.2420	0.0024	0.4722	2.7E-04	9.7010	1.6E-03
925	61.2	1.4	8.50E-04	7.6E-06	0.1210	0.0012	0.2393	2.0E-04	5.0410	1.4E-03
975	61.1	1.4	7.10E-04	7.1E-06	0.1900	0.0019	0.4037	2.5E-04	8.2890	2.0E-03
1025	61.8	1.4	1.16E-03	1.5E-05	0.2850	0.0029	0.6019	4.4E-04	12.5280	2.4E-03
1050	60.6	1.2	6.68E-04	1.5E-05	0.2240	0.0022	0.4841	2.7E-04	9.8010	2.6E-03
1075	61.1	1.2	1.62E-03	9.0E-06	0.2080	0.0021	0.4536	2.5E-04	9.5480	2.5E-03
1100	63.1	1.4	7.80E-04	1.6E-05	0.2110	0.0021	0.4663	2.6E-04	9.8720	2.2E-03
1125	63.1	1.4	7.60E-04	7.5E-06	0.2290	0.0023	0.5110	2.7E-04	10.7840	2.5E-03
1150	63.0	1.4	9.60E-04	6.9E-06	0.3400	0.0034	0.7528	2.8E-04	15.8190	4.1E-03
1175	62.4	1.4	1.48E-03	8.4E-06	0.3390	0.0034	0.7279	3.0E-04	15.3050	3.5E-03
1200	63.5	1.4	9.40E-04	1.6E-05	0.2510	0.0025	0.5394	3.2E-04	11.5070	2.4E-03
1225	63.3	1.4	9.10E-04	8.3E-06	0.1900	0.0019	0.4052	2.5E-04	8.6690	2.7E-03
1250	62.0	1.4	1.04E-03	8.3E-06	0.1510	0.0015	0.3279	2.2E-04	6.9580	2.1E-03
1300	63.4	1.4	8.80E-04	1.9E-05	0.2790	0.0028	0.5604	4.6E-04	11.9060	3.6E-03

ODP 152-917A-40R-4, 15-20 cm basalt (2E12) irr start

J = 1.559 e-3

°C	Age	1σ	36Ar	σ36	37Ar	σ37	39Ar	σ39	40Ar	σ40
550	97.6	3.4	1.12E-02	5.7E-05	0.1300	0.0013	0.0872	1.7E-04	6.4020	2.5E-03
650	76.5	2.6	5.39E-03	3.5E-05	0.2780	0.0028	0.1094	1.6E-04	4.6070	2.0E-03
750	66.9	2.2	1.68E-03	2.2E-05	0.3910	0.0039	0.1234	1.3E-04	3.4500	4.1E-03
850	66.4	2.2	2.11E-04	6.1E-06	0.1720	0.0017	0.0426	1.4E-04	1.0714	2.9E-03
925	62.5	2.0	1.11E-03	2.1E-05	0.9810	0.0098	0.3350	6.2E-04	7.8120	5.1E-03
1000	61.0	2.0	6.23E-04	8.2E-06	0.6065	0.0061	0.2232	4.9E-04	5.0570	1.1E-03
1075	58.5	2.0	5.35E-04	7.7E-06	0.3050	0.0031	0.1296	1.6E-04	2.8730	1.3E-03
1200	53.4	1.8	2.48E-03	2.8E-05	2.9080	0.0290	0.1711	1.9E-04	3.7520	6.4E-03
1325	57.7	2.0	2.63E-03	3.1E-05	3.5670	0.0360	0.1194	3.8E-04	2.9360	9.4E-03
1400	59.0	6.0	4.58E-04	1.6E-05	0.2280	0.0023	0.0051	3.6E-05	0.2237	4.0E-04

ODP 152-917A-52R-1 dacite (2E4) irr 5-20-94 start B5269

J = 1.696 e-3

RF	Age	1σ	36Ar	σ36	37Ar	σ37	39Ar	σ39	40Ar	σ40
	95.5	12.4	6.74E-02	1.8E-04	0.0340	0.0003	0.0256	1.6E-04	20.7150	8.5E-03
	68.2	4.2	1.21E-02	1.2E-04	0.0585	0.0006	0.0548	1.7E-04	4.7970	4.9E-03
	62.8	1.4	1.02E-02	1.1E-04	0.1380	0.0014	0.1721	4.0E-04	6.5960	4.6E-03
	61.4	1.2	2.07E-02	1.7E-04	0.2060	0.0021	0.3383	3.0E-04	13.0030	5.0E-03
	61.4	1.4	8.38E-03	1.1E-04	0.1230	0.0012	0.1967	2.0E-04	6.4800	2.1E-03
	61.2	1.2	6.98E-03	1.0E-04	0.1250	0.0013	0.1942	2.2E-04	6.0030	1.2E-03
	61.6	1.2	3.73E-03	5.0E-05	0.1090	0.0011	0.1170	4.2E-04	3.4870	6.2E-04
	61.6	1.8	3.01E-03	9.0E-05	0.1120	0.0011	0.1048	1.6E-04	3.0270	1.2E-03
	61.6	5.2	1.70E-03	1.4E-04	0.1770	0.0018	0.0302	1.4E-04	1.1050	4.7E-04

ODP 152-917A-55R-4 plagioclase (1D5) irr start 94-132

J = 1.725 e-3

°C	Age	1σ	36Ar	σ36	37Ar	σ37	39Ar	σ39	40Ar	σ40
650	85.3	3.4	1.60E-03	1.8E-05	0.7704	0.0077	0.0055	2.9E-05	0.5520	4.0E-04
80	77.3	1.9	2.31E-03	2.2E-05	1.9740	0.0190	0.0128	3.9E-05	0.8211	4.9E-04
950	87.3	1.8	1.66E-03	2.1E-05	2.1420	0.0210	0.0142	4.9E-05	0.6933	6.1E-04
1100	105.7	3.4	1.45E-03	2.2E-05	0.6738	0.0067	0.0066	3.2E-05	0.5945	4.0E-04
1200	81.4	2.5	1.20E-03	1.9E-05	0.9958	0.0010	0.0080	3.7E-05	0.4738	4.4E-04
1300	87.4	6.5	9.00E-04	1.7E-05	0.4663	0.0047	0.0027	2.3E-05	0.2950	2.9E-04
1450	101.1	2.7	1.09E-03	7.8E-06	0.6437	0.0064	0.0035	2.5E-05	0.3690	2.7E-04

ODP 152-917A-64R-2 plagioclase (1D6) irr start 94-139

J = 1.705 e-3

°C	Age	1σ	36Ar	σ36	37Ar	σ37	39Ar	σ39	40Ar	σ40
650	69.7	3.8	4.85E-03	3.3E-05	1.7550	0.0180	0.0188	5.2E-05	1.7080	6.4E-04
800	64.1	3.4	4.11E-03	3.0E-05	2.5960	0.0260	0.0200	5.8E-05	1.4010	5.1E-04
950	62.6	2.2	1.39E-02	4.9E-05	5.2820	0.0530	0.0642	9.9E-05	4.9590	1.4E-03
1025	68.6	4.2	4.28E-03	3.3E-05	0.7991	0.0080	0.0164	5.9E-05	1.5700	6.4E-04
1125	58.2	3.2	3.17E-03	2.9E-05	0.9015	0.0090	0.0185	5.5E-05	1.2160	5.4E-04
1250	72.4	3.6	1.58E-03	2.2E-05	1.1580	0.0120	0.0139	4.9E-05	0.6966	3.1E-04
1350	89.6	4.0	1.06E-03	8.1E-06	0.5508	0.0055	0.0054	2.9E-05	0.4140	3.3E-04
1450	125.3	17.8	8.90E-04	1.7E-05	0.2998	0.0030	0.0019	2.2E-05	0.3109	2.5E-04

ODP 152-917A-69R-2 groundmass plagioclase (2E10) irr 5-20-94 start 94-234

J = 1.582 e-3

°C	Age	1σ	36Ar	σ36	37Ar	σ37	39Ar	σ39	40Ar	σ40
600	41.2	2.6	2.09E-02	6.9E-05	0.2550	0.0023	0.0397	5.2E-05	6.7390	3.5E-03
750	62.0	2.2	2.88E-03	3.0E-05	0.3690	0.0037	0.0480	5.8E-05	1.8806	2.0E-03
850	61.0	1.8	8.95E-03	4.3E-05	1.8270	0.0180	0.2992	9.9E-05	8.9900	5.6E-03
925	60.9	1.8	3.12E-03	2.8E-05	2.2431	0.0220	0.3248	5.9E-05	7.7600	5.7E-03
975	60.8	1.8	1.65E-03	2.0E-05	0.7250	0.0070	0.1133	5.5E-05	2.8700	2.1E-03
1050	59.9	1.8	3.48E-03	2.9E-05	0.8580	0.0086	0.1908	4.9E-05	5.0200	2.7E-03
1150	58.9	2.0	1.99E-03	2.5E-05	0.8350	0.0084	0.0507	2.9E-05	1.5730	1.2E-03
1400	59.4	2.0	3.14E-03	3.0E-05	3.0670	0.0310	0.0731	2.2E-05	2.1850	1.1E-03

ODP 152-917A-83R-2 basalt (5D2) irr 11-15-95 start B5570

J = 1.633 e-3

RF	Age	1σ	36Ar	σ36	37Ar	σ37	39Ar	σ39	40Ar	σ40
200	88.5	17.6	3.00E-03	6.0E-05	0.0899	0.0009	0.0067	5.0E-05	1.0351	7.1E-04
260	82.2	5.4	1.22E-03	6.3E-05	0.2780	0.0028	0.0222	1.8E-04	0.9570	4.3E-04
320	68.6	2.3	1.35E-03	9.0E-05	0.8720	0.0087	0.0862	2.9E-04	2.3576	1.8E-04
380	68.3	2.2	1.88E-03	1.0E-04	0.8970	0.0090	0.1005	4.0E-04	2.8400	1.3E-04
450	73.5	6.3	8.00E-04	1.0E-04	0.1610	0.0016	0.0277	1.1E-04	0.9215	3.8E-04
fusion	106.3	9.6	8.50E-04	6.0E-05	0.6110	0.0061	0.0165	4.2E-04	0.7976	5.2E-04

ODP 152-917A-88R-8 basalt (5D3) irr 11-15-95 start B5581

J = 1.596 e-3

RF	Age	1σ	36Ar	σ36	37Ar	σ37	39Ar	σ39	40Ar	σ40
210	118.0	55.0	4.28E-03	1.0E-04	0.0943	0.0009	0.0043	7.0E-05	1.4530	6.2E-04
265	64.3	9.0	1.10E-03	1.0E-04	0.2770	0.0028	0.0186	7.0E-05	0.7236	4.6E-04
340	64.0	3.1	2.23E-03	1.8E-04	1.1540	0.0120	0.1035	1.4E-04	2.8911	1.8E-03
420	64.2	3.3	9.00E-04	1.0E-04	0.4370	0.0044	0.0547	1.6E-04	1.4674	2.0E-04
500	66.4	4.0	1.00E-03	8.0E-05	0.4720	0.0047	0.0361	7.0E-05	1.0992	2.5E-04
fusion	97.0	14.2	5.00E-04	9.0E-05	0.2750	0.0028	0.0107	1.0E-04	0.4892	5.0E-04

ODP 152-918D-94R-2 basalt ( ) irr start B5249

J = 1.389 e-3

°C	Age	1σ	36Ar	σ36	37Ar	σ37	39Ar	σ39	40Ar	σ40
	47.4	12.2	1.83E-02	5.5E-05	0.0180	0.0020	0.0108	5.3E-06	5.6124	3.3E-03
	51.8	4.2	1.48E-02	9.0E-05	0.0846	0.0008	0.0312	3.7E-05	5.0463	2.3E-03
	51.2	1.2	6.50E-03	9.0E-05	0.4580	0.0046	0.1382	3.2E-05	4.7440	2.2E-03
	52.4	1.4	1.16E-03	5.0E-05	0.2250	0.0023	0.0699	3.5E-05	1.8040	1.5E-03
	51.7	2.8	9.00E-04	9.0E-05	0.0868	0.0009	0.0364	2.4E-05	1.0193	2.0E-03
	53.3	2.8	2.10E-03	1.4E-04	0.2690	0.0027	0.0546	2.0E-05	1.7740	1.7E-03
	52.0	1.8	2.70E-03	8.0E-05	1.5740	0.0150	0.0690	1.4E-05	2.1050	1.3E-03

ODP 152-918D-106R-2 basalt (1D17) irr start

J = 1.640 e-3

°C	Age	1σ	36Ar	σ36	37Ar	σ37	39Ar	σ39	40Ar	σ40
600	163.3	18.6	5.59E-03	3.1E-05	0.0196	0.0002	0.0014	1.6E-05	1.7300	6.5E-04
800	78.3	8.4	6.66E-02	6.8E-05	1.5370	0.0150	0.0589	1.7E-04	21.1400	5.6E-03
950	78.7	5.8	1.74E-02	7.0E-05	1.0990	0.0110	0.0309	7.2E-05	5.8860	1.3E-03
1100	85.5	7.2	4.13E-03	2.6E-05	0.5020	0.0050	0.0081	3.7E-05	1.4150	5.5E-04
1250	73.4	7.2	5.70E-03	3.9E-05	3.4650	0.0350	0.0132	4.4E-05	1.6710	6.7E-04

ODP 152-918D-106R-2 groundmass plagioclase (2E8) irr start 94-262

J = 1.625 e-3

°C	Age	1σ	36Ar	σ36	37Ar	σ37	39Ar	σ39	40Ar	σ40
900	60.4	30.0	6.81E-03	5.3E-05	0.1090	0.0011	0.0031	2.7E-05	2.0660	3.7E-03
1000	46.1	6.6	2.80E-02	8.6E-05	1.4240	0.0140	0.0239	6.5E-05	8.5200	3.6E-03
1100	46.8	9.8	6.47E-03	4.3E-05	2.3440	0.0230	0.0093	4.7E-05	1.8500	1.7E-03
1400	44.5	12.2	3.54E-03	2.9E-05	3.3900	0.0340	0.0065	3.9E-05	0.8418	9.2E-04

ODP 152-918D-110R-4 groundmass plagioclase (2E9) irr start 94-256

J = 1.600 e-3

°C	Age	1σ	36Ar	σ36	37Ar	σ37	39Ar	σ39	40Ar	σ40
550	85.2	7.6	4.51E-03	3.5E-05	0.1170	0.0012	0.0081	4.0E-05	1.5650	1.1E-03
850	52.6	2.0	6.16E-03	4.4E-05	2.0280	0.0200	0.0565	1.4E-04	2.6800	1.3E-03
1000	49.1	2.0	2.21E-03	2.5E-05	1.3900	0.0140	0.0317	7.6E-05	1.0760	7.5E-04
1200	33.3	3.0	5.33E-03	3.7E-05	6.0800	0.0610	0.0271	8.1E-05	1.3570	7.8E-04
1400	55.6	8.0	2.62E-03	2.8E-05	2.5750	0.0260	0.0079	3.9E-05	0.6851	6.2E-04

Appendix 2

The following are the step heating data for all of the 40Ar-39Ar analyses reported in Chapter III. All measurements have been corrected for decay (37Ar) and mass fractionation. The start number refers to the analysis number of the first heating step

NC93-2 Nicoya basalt (B-1) irr 8-18-93 start B4825

J = 1.530 e-3

RF	Age	1σ	36Ar	σ36	37Ar	σ37	39Ar	σ39	40Ar	σ40
200	91.0	28.0	1.42E-02	1.0E-04	0.110	0.0011	0.0702	0.00008	4.4220	0.0027
250	91.9	6.1	3.80E-03	5.0E-05	0.170	0.0017	0.0713	0.00003	1.3490	0.0009
450	89.9	4.0	7.10E-03	4.0E-05	0.832	0.0083	0.1863	0.00014	2.6366	0.0015
fusion	89.5	7.2	6.15E-03	5.0E-05	2.030	0.002	0.1341	0.00016	2.0594	0.0027

NC93-3 Nicoya basalt (B-4) irr 7-9-93 start B4753

J = 1.500 e-3

RF	Age	1σ	36Ar	σ36	37Ar	σ37	39Ar	σ39	40Ar	σ40
195	90.4	12.0	2.50E-03	1.0E-04	0.114	0.0011	6.07E-03	5.00E-05	0.9360	0.0003
235	88.7	9.6	1.69E-03	1.0E-04	0.473	0.0047	1.00E-02	1.00E-04	0.7930	0.0076
300	93.0	10.1	3.90E-03	8.0E-05	0.484	0.0048	9.81E-03	1.60E-04	1.4500	0.0003
400	108.0	15.7	6.35E-03	1.0E-04	0.373	0.0037	7.73E-03	6.00E-05	2.1570	0.0031
fusion	86.6	11.7	4.43E-03	8.0E-05	1.380	0.014	5.32E-03	9.00E-05	1.3460	0.0003

NC93-9 Nicoya plagioclase (B-4) irr 2-7-94 start B5190

J = 1.688 e-3

RF	Age	1σ	36Ar	σ36	37Ar	σ37	39Ar	σ39	40Ar	σ40
210	51.9	5.5	3.10E-03	1.3E-04	0.339	0.003	2.14E-02	1.10E-04	1.2640	0.0003
275	86.8	3.5	1.90E-03	1.6E-04	1.450	0.015	4.06E-02	5.50E-05	1.5760	0.0010
330	117.4	2.9	2.20E-03	7.0E-05	0.906	0.009	3.24E-02	1.70E-04	1.8570	0.0010
400	121.9	7.2	1.70E-03	1.8E-04	0.458	0.005	2.45E-02	8.00E-05	1.3550	0.0004
460	139.2	5.9	1.28E-03	1.0E-04	0.319	0.003	1.62E-02	1.20E-04	1.1100	0.0008
fusion	152.5	7.4	2.00E-03	1.4E-04	0.530	0.005	1.79E-02	1.70E-04	1.4690	0.0009

NC93-11 Nicoya basalt (1D19) irr start 94-94

J = 1.626 e-3

°C	Age	1σ	36Ar	σ36	37Ar	σ37	39Ar	σ39	40Ar	σ40
550	87.9	3.5	1.15E-03	2.1E-05	0.072	0.0007	7.21E-03	3.30E-05	0.6622	0.0004
650	74.4	4.4	1.13E-03	1.8E-05	0.050	0.0005	3.94E-03	2.40E-05	0.4302	0.0004
800	73.7	2.3	3.41E-03	2.3E-05	0.484	0.0048	2.27E-02	5.80E-05	1.5440	0.0006
1000	84.1	2.5	3.67E-03	3.1E-05	0.900	0.009	4.54E-02	8.10E-05	2.3310	0.0008
1200	82.0	2.5	5.96E-03	3.5E-05	5.267	0.052	5.19E-02	8.40E-05	2.7280	0.0008

NC93-14B Nicoya basalt ( ) irr 6-17-93 start 93-381

J = 5.30 e-4

°C	Age	1σ	36Ar	σ36	37Ar	σ37	39Ar	σ39	40Ar	σ40
600	88.6	5.9	2.53E-02	2.1E-04	0.180	0.0018	1.04E-02	7.50E-05	8.4260	0.0039
750	86.3	3.5	7.67E-03	9.9E-05	0.242	0.0024	9.05E-03	7.00E-05	3.0560	0.0015
900	83.4	1.8	4.36E-03	6.4E-05	0.462	0.0046	1.94E-02	1.30E-04	2.9670	0.0013
1050	81.4	3.2	1.67E-03	1.1E-05	0.193	0.0019	1.50E-02	1.00E-04	1.7510	0.0012
1200	82.2	3.6	1.66E-03	1.2E-05	0.136	0.0014	8.16E-03	1.00E-04	1.1800	0.0008
1350	84.5	1.9	5.20E-03	2.2E-05	0.273	0.0027	1.05E-02	1.00E-04	2.4480	0.0015
1600	81.9	5	6.37E-03	1.0E-04	0.300	0.003	6.00E-03	6.00E-05	2.3720	0.0012

NC93-18 Nicoya basalt (C-5) irr 2-7-94 start B5213

J = 5.30 e-4

RF	Age	1σ	36Ar	σ36	37Ar	σ37	39Ar	σ39	40Ar	σ40
190	90.3	12.7	5.70E-03	2.7E-05	0.103	0.001	5.18E-03	5.50E-04	1.8330	0.0005
250	89.1	6.1	4.07E-03	8.0E-05	0.275	0.003	1.20E-02	4.50E-05	1.5360	0.0004
325	94.5	5.6	7.70E-03	8.0E-05	0.449	0.004	1.42E-02	9.00E-04	2.6840	0.0007
425	92.4	2.9	6.50E-03	5.0E-05	0.445	0.004	2.04E-02	2.20E-05	2.5130	0.0020
fusion	88.5	2.7	9.90E-03	4.0E-05	2.272	0.022	2.01E-02	1.80E-04	3.2970	0.0034

NC93-20 Nicoya basalt (B-4) irr 7-9-93 start B4753

J = 1.520 e-3

RF	Age	1σ	36Ar	σ36	37Ar	σ37	39Ar	σ39	40Ar	σ40
195	91.7	17	5.10E-03	8.0E-05	0.062	0.0006	4.40E-03	7.00E-05	1.6700	0.0013
235	90.5	10.7	2.73E-03	8.0E-05	0.182	0.0018	5.88E-03	4.20E-05	0.9970	0.0009
300	91.1	10	2.66E-03	5.0E-05	0.305	0.0031	6.00E-03	1.20E-04	0.9620	0.0046
400	89.3	4.2	4.40E-03	5.0E-05	0.312	0.0031	1.10E-02	5.20E-05	1.6390	0.0011
fusion	90	4.6	8.30E-03	7.0E-05	1.770	0.018	1.41E-02	6.00E-05	2.7460	0.0100

NC93-24 Nicoya basalt (C-4) irr 2-7-94 start B5202

J = 1.688 e-3

RF	Age	1σ	36Ar	σ36	37Ar	σ37	39Ar	σ39	40Ar	σ40
200	30.7	11.1	1.40E-02	2.0E-04	0.069	0.0007	1.58E-02	1.70E-04	4.2880	0.0010
270	58.5	3	1.36E-02	1.1E-04	0.243	0.002	3.66E-02	5.60E-04	4.6970	0.0004
330	68.1	1.5	8.50E-03	2.5E-05	0.360	0.004	2.94E-02	1.00E-04	3.1620	0.0015
390	94.1	5.1	3.30E-03	1.0E-04	0.451	0.005	1.94E-02	1.30E-04	1.5460	0.0003
470	99.8	4.5	2.50E-03	8.0E-05	0.868	0.009	1.84E-02	1.90E-04	1.2700	0.0003
fusion	114.6	5.5	4.00E-03	8.0E-05	1.450	0.015	1.70E-02	3.00E-04	1.6930	0.0002

NC93-32 Nicoya basalt (C-3) irr 2-7-94 start B5196

J = 1.688 e-3

RF	Age	1σ	36Ar	σ36	37Ar	σ37	39Ar	σ39	40Ar	σ40
210	61.8	4.2	3.03E-03	1.1E-04	0.197	0.002	2.16E-02	7.00E-05	1.3230	0.0009
275	85.3	3.2	1.71E-03	7.0E-05	0.470	0.005	2.26E-02	1.60E-04	1.1100	0.0005
340	88.7	2.5	4.07E-03	9.0E-05	0.946	0.009	4.32E-02	1.00E-04	2.4090	0.0005
400	99.6	3.7	1.91E-03	8.0E-05	0.255	0.003	2.26E-02	2.20E-04	1.3010	0.0008
470	118.9	11.4	1.26E-03	1.7E-04	0.201	0.002	1.22E-02	5.00E-05	0.8440	0.0007
fusion	130	2.8	5.00E-03	4.6E-05	0.760	0.008	2.95E-02	1.70E-04	2.7020	0.0007

NC93-34 Nicoya basalt (B-4) irr 8-18-93 start B4806

J = 1.520 e-3

RF	Age	1σ	36Ar	σ36	37Ar	σ37	39Ar	σ39	40Ar	σ40
200	71.7	2.9	7.60E-03	8.7E-05	0.145	0.0015	7.00E-03	3.20E-04	2.9160	0.0008
250	91.7	2.7	4.21E-03	1.0E-04	0.185	0.0018	3.20E-02	7.60E-05	2.3110	0.0007
290	92.1	1.8	4.40E-03	5.0E-05	0.254	0.0025	2.58E-02	2.40E-05	2.1550	0.0015
345	87.7	1.9	3.80E-03	1.0E-04	0.323	0.0032	4.51E-02	1.40E-04	2.5530	0.0012
400	88.1	1.3	3.10E-03	1.0E-04	0.268	0.0027	7.57E-02	2.00E-05	3.3550	0.0052
fusion	85.1	1.3	1.06E-02	2.0E-04	2.030	0.02	1.60E-01	2.20E-04	7.9590	0.0038

NC93-36 Nicoya plagioclase (C-1) irr 2-7-94 start B5182

J = 1.688 e-3

RF	Age	1σ	36Ar	σ36	37Ar	σ37	39Ar	σ39	40Ar	σ40
190	43.6	13.7	3.37E-03	8.5E-05	0.126	0.001	5.50E-03	7.90E-05	1.0640	0.0007
260	87.9	10.3	2.64E-03	9.0E-05	0.413	0.004	7.90E-03	5.80E-05	1.0050	0.0005
300	104.0	7.2	3.70E-03	8.0E-05	0.707	0.007	1.11E-02	1.50E-04	1.4710	0.0013
360	128.4	10.7	4.26E-03	1.0E-04	0.713	0.007	1.50E-02	1.10E-04	1.8370	0.0015
410	131.3	4.6	2.40E-03	6.0E-05	0.476	0.005	1.50E-02	1.90E-04	1.3290	0.0001
470	151.2	5.1	1.68E-03	8.0E-05	0.483	0.005	1.82E-02	2.50E-04	1.3840	0.0011
fusion	179.2	3.6	4.45E-03	8.5E-05	1.407	0.014	4.99E-02	9.50E-05	4.2320	0.0030

NC93-38 Nicoya basalt (1D20) irr start 94-83

J = 1.619 e-3

°C	Age	1σ	36Ar	σ36	37Ar	σ37	39Ar	σ39	40Ar	σ40
500	41.6	14.3	2.42E-03	2.2E-05	0.015	0.0001	1.32E-03	1.50E-05	0.7317	0.0004
650	66.1	4.1	7.50E-03	4.1E-05	0.122	0.0012	9.62E-03	4.30E-05	2.4250	0.0008
800	81.8	3.4	1.78E-02	6.3E-05	0.682	0.0068	2.22E-02	5.10E-05	5.8160	0.0012
950	105.9	3.7	9.32E-03	4.7E-05	0.662	0.0066	1.96E-02	5.70E-05	3.4160	0.0008
1100	64.1	2.3	4.18E-03	3.1E-05	0.875	0.0088	2.23E-02	6.20E-05	1.6520	0.0010

JC93-1 Jacó basalt (1D21) irr start 94-89

J = 1.612 e-3

°C	Age	1σ	36Ar	σ36	37Ar	σ37	39Ar	σ39	40Ar	σ40
650	48.1	3.6	3.26E-03	2.6E-05	0.237	0.0024	6.70E-03	3.66E-05	1.0556	0.0005
800	83.4	3.5	1.66E-03	2.0E-05	0.330	0.0033	7.21E-03	3.00E-05	0.6698	0.0005
1000	83.6	2.8	1.94E-03	2.1E-05	0.838	0.0084	2.01E-02	5.08E-05	1.0820	0.0006
1200	85.5	2.9	1.12E-02	5.4E-05	6.850	0.069	4.78E-02	8.60E-05	4.0430	0.0001

JC93-3 Jacó basalt (B-7) irr 2-7-94 start B5233

J = 1.550 e-3

RF	Age	1σ	36Ar	σ36	37Ar	σ37	39Ar	σ39	40Ar	σ40
200	66.4	5.1	3.50E-03	1.0E-04	0.069	0.001	7.90E-03	5.00E-05	1.2170	0.0003
250	77.8	9.4	1.54E-03	7.0E-05	0.169	0.002	9.35E-03	1.00E-04	0.6925	0.0003
350	35.4	4.6	2.39E-03	6.0E-05	0.288	0.003	1.02E-02	1.50E-04	0.8128	0.0006
475	38.4	4.2	1.85E-03	9.0E-05	0.523	0.005	1.87E-02	1.20E-04	0.7617	0.0001
fusion	61.7	8.5	2.01E-03	1.0E-04	1.650	0.017	1.38E-02	1.60E-04	0.7531	0.0004

QP93-1 Quepos basalt (B-6) irr 2-7-94 start B5227

J = 1.550 e-3

RF	Age	1σ	36Ar	σ36	37Ar	σ37	39Ar	σ39	40Ar	σ40
190	41.2	1.4	3.62E-03	8.0E-05	0.087	0.0009	4.72E-02	1.00E-04	1.7680	0.0008
250	65.3	0.8	2.20E-03	5.6E-05	0.246	0.0025	8.71E-02	1.60E-04	2.7090	0.0008
300	65.3	1.1	2.90E-03	1.3E-04	0.219	0.0022	1.16E-01	7.80E-05	3.5860	0.0009
350	62.3	0.7	1.50E-03	4.9E-05	0.168	0.0017	1.24E-01	1.50E-04	3.2540	0.0023
400	59.1	0.9	9.00E-04	7.5E-05	0.203	0.002	9.05E-02	2.00E-04	2.1920	0.0007
fusion	51.7	1.3	2.80E-03	1.0E-04	1.440	0.014	1.77E-01	1.30E-03	4.1450	0.0010

Appendix 3

The following are the step heating data for all of the 40Ar-39Ar analyses reported in Chapter IV. All measurements have been corrected for decay (37Ar) and mass fractionation. The start number refers to the analysis number of the first heating step

DSDP 15-146-42-2, 62-65 cm (B-3) start B4303 irr. 10-9-92

J = 1.550 e-3

RF	Age	1σ	36Ar	σ36	37Ar	σ37	39Ar	σ39	40Ar	σ40
210	120.9	4.3	2.21E-02	4.30E-05	0.220	0.002	8.69E-03	1.19E-05	6.9090	3.00E-03
255	110.0	4.1	6.37E-03	5.70E-05	0.346	0.004	1.02E-02	1.80E-04	2.3070	1.10E-03
315	127.1	7.4	3.40E-03	9.00E-05	0.390	0.004	4.90E-03	5.70E-05	1.1910	7.30E-04
415	96.7	13.1	2.65E-03	6.40E-05	0.245	0.003	4.18E-03	7.80E-05	0.9031	2.40E-04
fusion	82.3	5.0	2.96E-03	4.20E-05	1.317	0.013	8.20E-03	6.10E-05	0.9916	1.40E-04

DSDP 15-146-42-3, 103-106 cm (C-6) start B5208 irr. 2-7-94

J = 1.688 e-3

RF	Age	1σ	36Ar	σ36	37Ar	σ37	39Ar	σ39	40Ar	σ40
210	133.6	10.7	2.38E-02	5.00E-05	0.113	0.001	4.18E-03	5.00E-05	7.2110	4.10E-03
260	90.5	3.6	1.50E-02	5.00E-05	0.668	0.007	1.56E-02	1.00E-04	4.8260	7.60E-04
325	90.8	6.7	6.05E-03	5.00E-05	0.570	0.006	7.05E-03	5.00E-05	1.9470	7.20E-04
400	95.6	4.9	3.40E-03	5.00E-05	0.647	0.007	1.04E-02	8.00E-05	1.2730	6.60E-04
fusion	118.4	5.3	5.35E-03	1.00E-04	3.056	0.031	1.97E-02	4.00E-05	2.0500	1.70E-03

DSDP 15-146-43-1, 131-125 cm (B-4) start B4308 irr. 10-9-92

J = 1.550 e-3

RF	Age	1σ	36Ar	σ36	37Ar	σ37	39Ar	σ39	40Ar	σ40
200	119.4	5.6	2.22E-02	5.60E-05	0.168	0.002	0.0065	1.40E-04	6.81E+00	6.60E-03
240	116.0	2.9	7.10E-03	5.20E-05	0.336	0.003	0.0103	1.70E-04	2.50E+00	1.30E-03
280	114.9	7.3	4.90E-03	7.40E-05	0.503	0.005	0.0066	6.10E-05	1.68E+00	8.30E-04
325	109.7	7.2	4.01E-03	4.40E-05	0.352	0.004	0.0052	2.70E-05	1.37E+00	7.90E-04
365	118.8	5.5	2.90E-03	4.40E-05	0.206	0.002	0.0040	4.80E-05	1.01E+00	8.20E-04
fusion	117.1	3.9	5.17E-03	3.70E-05	0.930	0.009	0.0087	2.40E-05	1.81E+00	2.80E-04

DSDP 15-146-43-4, 94-96 cm (C-7) start B5218 irr. 2-7-94

J = 1.688 e-3

RF	Age	1σ	36Ar	σ36	37Ar	σ37	39Ar	σ39	40Ar	σ40
210	46.7	40.8	2.28E-02	5.00E-05	0.121	0.001	0.0042	5.30E-04	6.80E+00	5.60E-04
255	94.5	5.5	1.23E-02	5.00E-05	0.338	0.003	0.0087	1.00E-04	3.85E+00	7.80E-04
315	85.5	9.2	9.60E-03	5.00E-05	0.331	0.003	0.0052	6.00E-05	2.93E+00	7.60E-04
415	127.6	7.9	9.00E-03	5.00E-05	0.348	0.004	0.0061	5.00E-05	2.86E+00	1.40E-03
fusion	89.0	14.0	8.45E-03	1.00E-04	1.200	0.012	0.0074	2.40E-04	2.51E+00	1.80E-03

DSDP 15-150-11-2, 11-13 cm (B-5) start B4314 irr. 10-9-92

J = 1.55 e-3

RF	Age	1σ	36Ar	σ36	37Ar	σ37	39Ar	σ39	40Ar	σ40
165	98.9	5.4	3.01E-02	8.00E-05	0.160	0.002	0.0108	4.80E-05	9.27E+00	4.10E-03
200	92.7	3.2	1.06E-02	5.00E-05	0.428	0.004	0.0136	2.70E-05	3.55E+00	2.90E-03
240	111.4	6.5	6.45E-03	4.20E-05	0.352	0.004	0.0055	5.00E-05	2.09E+00	1.30E-03
285	91.9	11.7	3.40E-03	8.00E-05	0.340	0.003	0.0056	7.00E-05	1.16E+00	1.60E-04
335	102.5	3.3	2.07E-03	3.00E-05	0.178	0.002	0.0041	5.00E-05	7.48E-01	6.80E-04
fusion	105.2	9.3	1.60E-03	4.00E-05	0.861	0.009	0.0040	3.50E-05	5.37E-01	2.50E-04

DSDP 15-153-20-1, 39-41 cm (B-6) start B4320 irr. 10-9-92

J = 1.55 e-3

RF	Age	1σ	36Ar	σ36	37Ar	σ37	39Ar	σ39	40Ar	σ40
200	127.7	4.2	5.11E-03	5.00E-05	0.086	0.001	0.0103	3.00E-05	1.99E+00	1.30E-03
240	98.3	2.6	1.81E-03	3.50E-05	0.243	0.002	0.0138	5.50E-05	1.01E+00	4.00E-04
280	99.5	6.4	3.50E-03	5.70E-05	0.415	0.004	0.0075	8.50E-05	1.27E+00	6.30E-04
335	101.9	4.3	6.40E-03	4.20E-05	0.646	0.007	0.0090	7.80E-05	2.15E+00	1.80E-03
fusion	103.4	4.3	6.85E-03	4.60E-05	1.583	0.016	0.0101	2.60E-05	2.24E+00	2.30E-03

DSDP 15-153-20-1, 39-41 cm plagioclase (3C4) start 96-128 irr. 9-7-95

J = 1.615 e-3

°C	Age	1σ	36Ar	σ36	37Ar	σ37	39Ar	σ39	40Ar	σ40
600	238.1	8.2	3.33E-03	3.50E-05	0.124	0.001	0.0037	1.90E-05	1.28E+00	5.20E-04
750	116.8	2.2	4.48E-03	3.10E-05	1.272	0.013	0.0157	5.40E-05	1.83E+00	6.20E-04
900	121.8	1.7	2.25E-03	3.00E-05	2.277	0.023	0.0207	4.80E-05	1.32E+00	5.90E-04
1050	95.3	1.5	1.67E-03	1.70E-05	2.400	0.024	0.0181	5.20E-05	8.59E-01	7.40E-04
1200	105.8	1.3	1.56E-03	1.70E-05	2.394	0.024	0.0141	4.00E-05	7.35E-01	4.20E-04
1400	110.8	3.8	4.20E-03	2.80E-05	8.931	0.089	0.0143	2.80E-05	8.56E-01	4.90E-04

HA74-24 Haiti basalt (5E4) irr 11-15-95 start 95-373

J =1.577 e-3

°C	Age	1σ	36Ar	σ36	37Ar	σ37	39Ar	σ39	40Ar	σ40
	144.1	4.6	1.67E-02	8.40E-05	1.927	0.0190	0.0209	8.40E-05	5.8220	2.00E-03
	108.3	1.7	1.96E-02	9.00E-05	2.085	0.0210	0.0126	8.00E-05	10.5117	3.00E-03
	91.0	1.2	1.61E-02	7.70E-05	3.980	0.0400	0.0977	1.90E-04	7.5643	2.30E-03
	91.8	1.3	6.22E-03	6.10E-05	3.509	0.0350	0.0650	1.60E-04	3.6387	1.30E-03
	92.0	1.5	2.62E-03	4.40E-05	1.881	0.0190	0.0333	9.00E-05	1.6879	9.20E-04
	90.2	1.4	1.86E-03	3.90E-05	1.689	0.0170	0.0317	1.00E-04	1.4100	1.00E-03
	91.2	1.4	8.33E-03	6.20E-05	14.717	0.1470	0.0544	1.10E-04	2.7795	1.10E-03
	126.6	9.4	2.00E-03	4.50E-05	3.089	0.0310	0.0068	5.50E-05	0.5536	6.10E-04

HA74-25 Haiti basalt (5E5) irr 11-15-94 start

J =1.537 e-3

°C	Age	1σ	36Ar	σ36	37Ar	σ37	39Ar	σ39	40Ar	σ40
	412.9	51.4	0.0	0.00026	0.128	0.001	0.004	0.000119	13.575	0.0120
	109.1	4.5	0.0	0.00012	1.28	0.013	0.019	0.00021	5.7403	0.0032
	90.4	8.7	0.0	0.00014	0.489	0.005	0.010	0.00023	0.669	0.0003
	97.5	8.4	0.0	0.000074	1.397	0.014	0.011	0.00034	0.7258	0.0007
	88.6	7.7	0.0	0.000045	0.696	0.007	0.006	0.00028	0.4359	0.0005

HA76-120 Haiti basalt (B2) irr 6-4-92 start B4044

J =1.490 e-3

RF	Age	1σ	36Ar	σ36	37Ar	σ37	39Ar	σ39	40Ar	σ40
	106.0	4.2	1.90E-03	3.79E-05	0.0176	0.0002	0.0107	1.19E-04	0.9459	4.25E-04
	97.5	1.4	1.02E-03	4.40E-05	0.1080	0.0011	0.0352	1.00E-04	1.6010	2.05E-03
	89.3	2.0	1.76E-03	3.50E-05	0.4170	0.0042	0.0508	2.60E-04	2.2090	2.50E-03
	84.5	2.9	1.27E-03	5.40E-05	0.2720	0.0027	0.0236	1.20E-04	1.0920	2.00E-03
	89.2	3.9	3.00E-03	9.10E-05	1.3700	0.0140	0.0241	1.55E-04	1.5540	9.80E-04

HA76-165 Haiti basalt (B2) irr 11-12-92 start B4200

J =1.550 e-3

RF	Age	1σ	36Ar	σ36	37Ar	σ37	39Ar	σ39	40Ar	σ40
	96.4	3.2	0.00425	0.000068	0.034	0.000	0.0216	0.0003	2.0270	0.0065
	92.3	1.9	0.0009	0.0001	0.168	0.002	0.0681	0.00019	2.5900	0.0066
	89.2	1.7	0.00251	0.00005	0.273	0.003	0.0352	0.0001	1.8760	0.00049
	85.4	2.8	0.0033	0.00005	0.292	0.003	0.0183	0.00015	1.5260	0.00079
	94.4	6.0	0.00615	0.0002	1.390	0.014	0.0285	0.00041	2.6790	0.0014

HA76-173 Haiti basalt (B1) irr 6-4-92 start B4038

J =1.521 e-3

RF	Age	1σ	36Ar	σ36	37Ar	σ37	39Ar	σ39	40Ar	σ40
	45.6	6.7	0.0043	0.0000623	0.021	0.000	0.01416	0.000301	1.5160	0.0008
	68.0	3.6	0.00408	0.0000532	0.144	0.001	0.0314	0.000109	1.9840	0.00092
	79.9	4.4	0.00456	0.0000623	0.183	0.002	0.0146	0.0001	1.7660	0.00013
	78.9	4.3	0.0042	0.0000528	1.406	0.014	0.0303	0.0001	1.9850	0.0017

HA76-173B Haiti basalt (C-3) irr 11-15-92 start B4480

J =1.820 e-3

°C	Age	1σ	36Ar	σ36	37Ar	σ37	39Ar	σ39	40Ar	σ40
	51.1	2.3	3.90E-03	5.00E-05	0.0325	0.0003	0.0214	1.00E-04	1.4920	4.40E-04
	74.9	4.3	1.70E-03	1.00E-04	0.0877	0.0009	0.0222	1.50E-04	1.0100	2.00E-04
	87.7	5.6	1.10E-03	1.00E-04	0.1350	0.0001	0.0170	2.30E-04	0.7719	1.50E-04
	73.8	5.8	2.70E-03	1.00E-04	0.2180	0.0002	0.0170	3.10E-04	1.1490	8.50E-03
	78.8	6.3	2.50E-03	1.00E-04	0.4310	0.0043	0.0156	1.70E-04	1.0380	5.70E-04
	84.1	5.1	2.60E-03	1.00E-04	0.9730	0.0097	0.0201	1.30E-04	1.0960	9.10E-03

HA77-28 Haiti basalt (B1) irr 10-9-92 start B4195

J =1.550 e-3

RF	Age	1σ	36Ar	σ36	37Ar	σ37	39Ar	σ39	40Ar	σ40
	97.4	3.5	0.00245	0.000058	0.052	0.001	0.0153	0.00006	1.2700	0.0042
	95.1	3.6	0.0021	0.0001	0.161	0.002	0.025	0.00029	1.4800	0.00116
	89.6	2.8	0.00385	0.00005	0.272	0.003	0.0171	0.00017	1.6750	0.0013
	89.2	3.0	0.00385	0.00005	0.279	0.003	0.0145	0.000024	1.5870	0.0033
	87.9	2.2	0.00645	0.00005	1.540	0.015	0.0231	0.00012	2.5000	0.0012

GOR92-1 Gorgona basalt (B-6) start irr 10-16-92

J =

RF	Age	1σ	36Ar	σ36	37Ar	σ37	39Ar	σ39	40Ar	σ40
	117.1	18.1	3.55E-03	1.00E-04	0.0460	0.0046	0.0047	1.00E-04	4.7610	3.80E-03
	86.3	4.8	2.73E-03	1.40E-04	0.2030	0.0020	0.0187	1.80E-04	1.2670	9.80E-03
	79.5	16.0	4.60E-03	2.40E-04	0.4900	0.0049	0.0142	9.96E-05	1.5440	5.50E-03

GOR92-14 Gorgona basalt (B-7) start B4501 irr 10-16-92

J =

RF	Age	1σ	36Ar	σ36	37Ar	σ37	39Ar	σ39	40Ar	σ40
	73.0	7.4	9.50E-03	8.80E-05	0.0490	0.0049	0.0104	3.10E-04	3.0510	3.90E-03
	88.3	1.9	5.50E-03	5.00E-05	0.2930	0.0029	0.0338	3.40E-04	2.5480	2.07E-02
	76.8	5.3	2.30E-04	1.00E-04	0.2720	0.0027	0.0167	1.30E-04	1.0250	1.10E-03

GOR92-18 Gorgona basalt (C-1) start irr 10-16-92

J =

RF	Age	1σ	36Ar	σ36	37Ar	σ37	39Ar	σ39	40Ar	σ40
	60.5	18.5	1.95E-03	1.00E-04	0.0393	0.0039	0.0051	1.00E-04	0.6575	3.60E-03
	87.1	3.2	2.90E-03	1.00E-04	0.1020	0.0010	0.0286	1.00E-04	1.6010	9.60E-03
	68.3	7.9	9.50E-03	1.80E-04	0.5470	0.0055	0.0254	1.70E-04	3.1260	3.10E-03

GOR92-27 Gorgona basalt (C-2) start B4498 irr 10-16-92

J =

RF	Age	1σ	36Ar	σ36	37Ar	σ37	39Ar	σ39	40Ar	σ40
	85.3	13.5	9.17E-03	3.90E-05	0.0097	0.0001	0.0041	3.01E-04	2.6970	4.40E-04
	88.4	3.2	5.31E-03	1.00E-04	0.1260	0.0013	0.0317	1.09E-04	2.4210	2.46E-03
	87.7	2.8	4.06E-04	5.00E-05	0.2710	0.0027	0.0205	1.00E-04	0.6110	7.00E-04

GOR92-37 Gorgona basalt (C-5) start irr 10-16-92

J =

RF	Age	1σ	36Ar	σ36	37Ar	σ37	39Ar	σ39	40Ar	σ40
	132.1	33.5	2.20E-03	4.20E-05	0.0425	0.0004	0.0018	1.40E-04	0.7046	1.40E-03
	64.3	6.9	1.01E-02	1.40E-04	0.1246	0.0012	0.0188	2.60E-04	3.3190	1.50E-03
	126.8	7.4	4.70E-03	1.30E-04	0.4450	0.0045	0.0139	2.90E-04	1.7960	9.30E-04

BE79-249 Curaçao basalt (B-4) irr 11-15-92 B4055

J =1.521 e-3

RF	Age	1σ	36Ar	σ36	37Ar	σ37	39Ar	σ39	40Ar	σ40
	89.0	1.9	0.00244	0.000104	0.080	0.001	0.0506	0.00024	2.3940	0.00165
	89.7	1.1	0.00499	0.0000623	0.301	0.003	0.0747	0.00011	3.9440	0.0034
	69.6	2.0	0.003	0.0001	0.573	0.006	0.0567	0.0005	2.3000	0.005
	75.1	1.4	0.00357	0.00013	0.506	0.005	0.232	0.00018	7.4800	0.0039
	76.6	1.3	0.00468	0.00012	2.080	0.021	0.243	0.00013	8.1100	0.00376

BK79-118 Curaçao basalt (B-3) irr 11-15-92 B4049

J =1.521 e-3

RF	Age	1σ	36Ar	σ36	37Ar	σ37	39Ar	σ39	40Ar	σ40
	25.0	20.0	3.61E-03	4.94E-05	0.0260	0.0003	0.0015	4.50E-05	1.0780	1.30E-03
	52.8	18.6	2.48E-02	5.50E-05	0.2830	0.0028	0.0062	7.80E-05	7.4110	1.80E-02
	75.5	30.5	1.04E-02	4.80E-05	0.2000	0.0020	0.0052	1.10E-04	3.1770	1.90E-03
	80.6	5.9	1.32E-02	4.00E-05	0.2060	0.0021	0.0157	8.70E-05	4.3550	6.90E-03
	66.0	3.6	4.17E-02	8.80E-05	2.7400	0.0270	0.0551	1.00E-04	13.4000	1.10E-02

BK79-262 Curaçao basalt (A-6) irr 11-15-92

J =1.725 e-3

RF	Age	1σ	36Ar	σ36	37Ar	σ37	39Ar	σ39	40Ar	σ40
	61.6	16.1	0.0115	0.00012	0.057	0.001	0.00688	0.00012	3.5200	0.000374
	90.0	5.6	0.0042	0.0001	0.065	0.001	0.0156	0.0001	1.6990	0.0022
	79.7	4.7	0.0042	0.00011	0.106	0.001	0.0224	0.0004	1.8220	0.0024
	88.5	5.3	0.0029	0.00005	0.099	0.001	0.0085	0.00005	1.0970	0.0014
	82.4	4.7	0.0034	0.00005	0.138	0.001	0.00968	0.000063	1.2540	0.0014
	88.4	1.3	0.01655	0.000048	2.263	0.023	0.0458	0.00012	6.0080	0.0021

79BE-73 Curaçao basalt (A-) irr 11-15-92

J =1.725 e-3

RF	Age	1σ	36Ar	σ36	37Ar	σ37	39Ar	σ39	40Ar	σ40
	48.8	12.2	2.51E-03	5.70E-05	0.0685	0.0007	0.0042	1.00E-04	0.8017	2.90E-04
	89.2	7.2	6.11E-03	1.00E-04	0.2460	0.0025	0.0125	8.70E-05	2.1490	3.00E-03
	88.7	5.0	3.80E-03	7.00E-05	0.2220	0.0022	0.0152	1.00E-04	1.5480	3.60E-03
	91.9	1.5	5.16E-03	8.70E-05	0.2390	0.0024	0.0657	2.50E-04	3.5760	1.10E-03
	88.6	2.5	4.60E-03	5.00E-05	0.1860	0.0019	0.0190	1.10E-04	1.8980	2.40E-04
	87.1	1.6	1.98E-02	2.00E-05	3.9500	0.0400	0.0723	2.80E-05	7.5370	6.50E-03

79KV-9 Curaçao Koraal Tabak sill (5A8) irr 11-15-94 start 95-381

J =1.355 e-3

°C	Age	1σ	36Ar	σ36	37Ar	σ37	39Ar	σ39	40Ar	σ40
	98.9	8.3	7.29E-03	5.70E-05	0.0999	0.0010	0.0063	5.50E-05	0.2405	1.40E-03
	75.2	3.5	5.52E-02	1.10E-04	2.6760	0.0270	0.1136	1.20E-04	19.6150	3.20E-03
	77.1	3.4	3.14E-02	7.70E-05	1.7930	0.0180	0.1355	1.30E-04	13.4540	2.40E-03
	75.0	3.3	4.15E-02	8.80E-05	5.3710	0.0537	0.1803	2.10E-04	17.3630	2.80E-03
	93.1	6.1	7.71E-03	6.20E-05	3.0330	0.0303	0.0229	7.70E-05	5.1180	1.20E-03

Appendix 4: Standard Analyses

Microprobe Standard Analyses

	KANO feldspar		KAUG augite	
	run	std. value	run	std. value
SiO_2	67.33	66.44	50.05	50.73
Al_2O_3	20.07	20.12	8.46	8.73
TiO_2			0.77	0.74
FeO	0.11	0.2	6.28	6.34
MnO			0.11	0.13
CaO	0.54	0.87	15.78	15.82
MgO			16.31	16.65
K_2O	2.35	2.35		0
Na_2O	9.35	9.31	1.31	1.27
NiO				
Cr_2O_3			0.45	
Total	99.75	99.29	99.07	100.41

ICP-MS Standard Analyses

	Standard Values			Run 2-17-95	
	W-1[1]	W-1[2]	W-1[3]	W-1A	W-1B
Rb	21.4	21.6		21.5	21.8
Y	26	22.6		23.5	24.0
Zr	99		98.6	97.6	98.2
Nb	9.5	7.9	7.67	8.1	8.1
Ba	161			158	163
La	11	10.9		10.76	11.01
Ce	23.5	24		23.65	23.52
Pr	3.2	3.27		3.10	3.19
Nd	14.6	14.4		13.2	13.6
Sm	3.68	3.65		3.30	3.36
Eu	1.12	1.14		1.09	1.13
Gd	4.01	4.24		3.81	4.03
Tb	0.63	0.645		0.64	0.66
Dy	3.99	4.18		3.76	3.89
Ho	0.81	0.803		0.79	0.82
Er	2.3	2.25		2.2	2.4
Tm	0.34	0.333		0.32	0.34
Yb	2.03	2.17		1.99	2.08
Lu	0.32	0.34		0.31	0.33
Hf	2.5			2.58	2.59
Ta	0.48			0.52	0.51
Pb	7.5	7.83		6.60	6.60
Th	2.4	2.65		2.68	2.72
U	0.57	0.605		0.61	0.65

1 Govindaraju (1994)
2 Jochum et al. (1990)
3 Jenner et al. (1990)